Application of Perturbation Theory Methods to Nuclear Data Uncertainty Propagation using the Collision Probability Method

Pouya Sabouri

UNIVERSITÉ DE GRENOBLE

THÈSE

Pour obtenir le grade de

DOCTEUR DE L'UNIVERSITÉ DE GRENOBLE

Spécialité : **Mécanique des Fluides, Energétique, Procédés**

Arrêté ministériel :

Présentée par

Pouya Sabouri

Thèse dirigée par **Ivan KODELI**

préparée au sein du **Laboratoire de Physique Subatomique et de Cosmologie (LPSC Grenoble)**
et de **l'Ecole Doctorale Ingénierie - Matériaux, Mécanique, Environnement, Energétique, Procédés, Production**

Application of Perturbation Theory Methods to Nuclear Data Uncertainty Propagation using the Collision Probability Method

Thèse soutenue publiquement le 28 Octobre 2013 ,
devant le jury composé de :

Gérald Rimpault
CEA, Cadarache, Président
Barry Ganapol
University of Arizona, Rapporteur
Guy Marleau
École Polytechnique de Montréal, Rapporteur
Philippe Dessagne
Institut Pluridisciplinaire Hubert Curien, Examinateur
David Lecarpentier
Electricité de France, Examinateur
Dimitri Rochman
Nuclear Research and Consultancy Group, Examinateur
Elsa Merle-Lucotte
LPSC Grenoble, Invitée
Ivan Kodeli
Jozef Stefan Institute, Directeur de thèse
Adrien Bidaud
LPSC Grenoble, Encadrant

"Sois satisfait des fleurs, des fruits, même des feuilles,
Si c'est dans ton jardin à toi que tu les cueilles !
Puis, s'il advient d'un peu triompher, par hasard,
Ne pas être obligé d'en rien rendre à César,
Vis-à-vis de soi-même en garder le mérite,
Bref, dédaignant d'être le lierre parasite,
Lors même qu'on n'est pas le chêne ou le tilleul,
Ne pas monter bien haut, peut-être, mais tout seul !"

— Edmond Rostand – Cyrano de Bergerac

Acknowledgements

I am indebted to my friends and mentors Dr. Sebastien Chabod, and Henry-Emmanuel Thyébault, and Shahab Dabiran for their support and confidence in me.

I wish to express my gratitude to my thesis director Professor Ivan Kodeli (IJS) and the International Expert at CEA Cadarache Dr. Gérald Rimpault for the highly valuable and irreplaceable support and guidance that they constantly provided me in the course of this study. A special thanks goes out to the kind Dr. Barry Ganapol at the University of Arizona, not only for his wonderful course on neutron transport but also for his valuable corrections and feedback; and I am equally grateful to Dr. Guy Marleau (EPM) for his corrections and editing. My gratitude also goes to Dr. David Lecarpentier (EDF) and Dr. Dimitri Rochman (NRG) for all their valuable advice and support throughout my entire studies. I am also very grateful to Dr. Victor Mastrangelo (IPN Orsay) for his many valuable comments and suggestions regarding my defence presentation and for the editing of this document. A special thanks to Dr. Elsa Merle-Lucotte for all her support, and to Dr. Alexis Nuttin and Dr. Tomas Jezo for their technical support and valuable corrections.

In the course of this study, I had the great opportunity to spend some time at the SINETICS department at EDF Clamart. I thank David Lecarpentier, Dr. Helene Ourly, Ansar Calloo and Sandra Poumerouly for their warm welcome, irreplaceable help and advice.

I am deeply thankful to the secretaries at LPSC Christine Servoz-Gavin, Sonia Benaissa, Colette Deslorieux, and Audrey Colas for the tremendous amount of help that they provided me during my stay in France. I am also grateful to the librarian Emmanuelle Vernay, Thierry Descombes, and Christine Gondrand at informatics. It was a pleasure knowing Mahfoud Yamouni, Nicolas Capellan, and Gregoire Kessedjian.

Finally, I am deeply thankful to my family and friends.

Pouya Sabouri
December, 2013

To my mother

Contents

*

Introduction

With the advent of modern computing power, the use of mock-up experiments for reactor design is now extensively completed by computer simulations and numerical modeling. However, even the best models can only be as accurate as their input parameters. As a result, there is an increasing demand from the nuclear industry, research and safety authorities for best estimates of design and performance parameters (for instance, the k_{eff}), as well as the confidence interval where the computed estimates are reliable.

In reactor physics, we are confronted with the problem of neutron transport over long distances involving strong attenuations of the flux. The evolution and transport of the neutrons are governed by the Boltzmann equation. From a neutronics point of view, the medium in which the neutron is emerged and interacts with is defined by its dimensions, composition, geometrical layout of its diverse components and its initial conditions. It is therefore clear that to model correctly the reactor behavior, one must have a good understanding of the properties of neutron interactions, over the large range of energies concerned (some thirteen orders of magnitude), with the medium where the interaction takes place. Here emerges the need for a deep verification and validation of the nuclear data used and the treatment methodology that awaits it to become usable by the transport code. Of course, the data format used varies with the transport code used, due to different treatments of the resonances, treatments for anisotropy, and the nature of the transport solution (deterministic or Monte Carlo). With each such treatments, the base data is transformed into another format, while at the same time, an error is introduced.

For transport computations, there exists a number of various cross section evaluations prepared by various laboratories across the world: ENDF (United States), JEFF (European Union), JENDL (Japan), BROND (Russia), CENDL (China), etc. What has been often suggested is that a user should not combine different evaluations in the same computation. Implicitly included in this advice is the admittance of the important role that error treatment, propagation and compensation play, and that all the present evaluations are, to a certain measure, only approximations. Accordingly, for a viable determination of performance parameters (such as the k_{eff}) that are representative of the physical environment, it is not only sufficient to uniquely perform computations and simulations of the system under question, but also required is the validation of the computational tools and the underlying base data. This point is imperative in industrial projects where a knowledge of the associated uncertainties in the neutronics calculation is vital.

This study involves the problems of modeling of physical systems, solving the neutron transport equation, cross section treatments, and error propagation, with a focus

on sensitivity (and uncertainty) analysis using deterministic codes, multi-group libraries and nuclear data. This study has required the development of methods and tools, that are applied to, and validated with integral experiments (benchmarks). Complementary to differential measurements, integral experiments are used in particular, for studying critical configurations, with the primary goal of validating the coherence between the microscopic and the integral data. Comparing the predictions given by a method or a simulation tool with results of an integral experiment not only permits the verification of the code and the base data, but also provides an evaluation of the coherence with the cross section library, the estimated nuclear data uncertainties and the accuracy of the transport solution.

The analysis of sensitivities using perturbation theory is one of the tools that has proven its efficiency to quantify the importance/weight of the physical phenomena at play in the reactor. Such a study permits for a better understanding of the various approximations that are inherently accompanied with the applied physical models. Perturbation theory methods, as applied to neutron transport for sensitivity analysis, allow expressing in a systematic way the effects from a variation in the operators of the Boltzmann equation originating from an uncertainty in the base data, on an integral parameter such as k_{eff}, reactor power, reaction rates, source worth, fuel burn-up, etc. Starting from a sensitivity computation, the process of the propagation of uncertainties offers a powerful means to link the uncertainty in the base data, usually expressed in terms of covariance matrices, to variations in integral parameters.

Amongst other applications, a sensitivity/uncertainty analysis permits to identify the nuclear reactions and their energy domains most relevant to an integral parameter. Such an analysis also allows for the identification of the corresponding uncertainties and permits for multiple applications in the process of design and validation. Effectively, a sensitivity and uncertainty analysis can be used to track the nuclear data, whose improvement can bring an increased precision to the computation. In this way, a sensitivity and uncertainty analysis provides a rational guide for the conception of future experiments aimed at further improvement of the data.

This thesis is structured as follows: in chapter 1, nuclear data, with an emphasis on covariance matrices, is described and a theoretical overview of the process involved in neutron transport, modeling and the sensitivity approach to nuclear data uncertainty propagation is provided. Next, chapter 2 provides a brief presentation of the currently available methodology and codes as well as the developments that have been necessary for performing nuclear data uncertainty propagation with the code DRAGON. Chapter 3 presents the conceptual developments that were required to perform an accurate computation of the sensitivity and uncertainty in the transport computation. Finally, chapter 4 provides a validation for the methodology and developments presented in chapters 2 and 3 by applying the developed tools to the three problems outlined by the OECD in the framework of Uncertainty Analysis and Criticality Safety Assessment (UACSA) benchmark.

Chapter 1

Theoretical Foundations

This chapter provides a theoretical overview of the process involved in the sensitivity approach to nuclear data uncertainty propagation as applied to transport computations. It serves to familiarize the reader with the notions, theory and terminology that are necessary for the remainder of this work.

We begin with a discussion of nuclear data, and the uncertainties that are inherently associated with it. Here, we discuss the concept of covariances, as related to nuclear data uncertainty propagation, followed with a discussion on the data currently available in the form of cross section evaluation files. The data contained in these evaluations is the backbone of any physics computation. It can be thought of as the first step of the physics computation.

Having introduced the concept of nuclear data and its uncertainties, the remainder of the chapter progresses to illustrate how one can relate the nuclear data uncertainties, associated with and available in cross section evaluation files, to integral parameters (such as the k_{eff}, or a reaction rate) computed by the transport code. To do this, we proceed as follows:

- Starting with the transport equation, we will derive the integral form of the transport equation.

- We will then advance to discretize the obtained equations and arrive at the concep of the collision probability.

- Subsequently, we will introduce the concept of adjoint operators, and derive the adjoint form of the transport equation. Here, we reach the concept of the adjoint flux, a quantity that is essential to performing sensitivity and uncertainty analysis for reactivity (k_{eff}).

- We will then introduce the concept of generalized adjoints, and the equations associated with them, which are fundamental for deriving perturbation expressions

corresponding to integral responses such as reaction rates and breeding ratios.

- Having introduced the adjoint formulation of the Boltzmann equation, we proceed to derive perturbation expressions for reactivity and linear ratios of the flux.

- Using the perturbation expressions for performance parameters such as reactivity and linear ratios of the flux, we define the concept of sensitivity functions and present sensitivity formulas which relate the sensitivity of these performance parameters to the base data.

- We then present the law of propagation of errors, used to propagate the uncertainties in the base data to the uncertainty on a performance parameter of interest.

1.1 Nuclear Data

A good knowledge of nuclear data is essential in reactor physics computations. In this work, we will focus on data regarding the interaction of neutrons with nuclei. This data, presented under the form of nuclear cross sections, describes the possible modes of interaction of the neutron with the target nuclei. Amongst these reactions, we can distinguish two types of interactions, interactions through scattering in which the final state after the interaction between the two particles is composed of the same two particles, and absorption which results in the disappearance of the incident neutron. Absorption, additionally, can be divided into other reactions which may result in fission or emission of secondary particles (gamma, proton, alpha).

It is of course without doubt that one must resort to quantum mechanics in order to describe the underlying behaviours which govern the interaction of the neutron with the medium. However, an exact solution to the general N body Schrodinger equation is still beyond our reach, notably due to our poor understanding of the nuclear forces and the internal structure of the neutron. Therefore, we cannot address the process of neutron-nuclei interaction without resorting to various approximations and physical models, each of which is only valid within a specific range of conditions. Examples of such models is the R-matrix collision theory in the resolved resonance range, the Lane-Lynn approach in the unresolved range, the optical model, etc. These models are used to establish the systematic behaviours of the neutron-nuclei interaction, per reaction and for various families of isotopes. These behaviours are then in turn generalized and applied to nuclei for which experimental data does not exist.

To determine the numerical value of cross sections, with the precision which is essential in reactor computations, only measurements can assure the quality of the data. Since the 1960s numerous experiences, both differential and integral, have been performed, as an answer to the needs of the nuclear community. After the 1980s, a decline of efforts is witnessed due to the the general disinterest in reactor technology that followed the

Chernobyl and TMI nuclear accidents. Since some years now does one find a new interest for nuclear applications. We can therefore expect new demands for nuclear data, required to answer the needs which will arise during the design process of new reactors.

1.2 Covariances and Covariance Matrices

A physical value is characterized by its average $< q >$ and its distribution function around its mean $P(q)$, which determines its uncertainty. In the case where the variable q is discrete, with only a finite number of possible values q_i and a respective probability distribution function $P(q)$ (which by definition satisfies the normalization condition $\sum_i P(q_i) = 1$), then the mean value of q is defined by:

$$\langle q \rangle = \sum_i q_i P(q_i) \tag{1.1}$$

The accuracy/precision of q is judged by the difference between its mean and the distribution of its associated probability, i.e. the square root of the *variance*:

$$\sigma_q^2 = var(q) = (\Delta q)^2 = \left\langle (q - < q >)^2 \right\rangle = \sum_i (\delta q_i)^2 \frac{1}{N} \tag{1.2}$$

where $\delta q_i \equiv q_i - \langle q \rangle$, and N is the number of possible values q_i. The value Δq is called the *standard deviation*.

Some examples of probability distribution functions $P(q)$ are:

- Normal Distribution:

$$P(q) = \frac{1}{(\Delta q)\sqrt{2\pi}} \exp\left(\frac{-1}{2}\frac{(\delta q)^2}{\Delta q}\right) \tag{1.3}$$

- Uniform Distribution:

$$P(q) = \begin{cases} \frac{1}{2a} \text{ for } a > q > -a \\ 0 \text{ else} \end{cases} \tag{1.4}$$

- Log-Normal Distribution:

$$P(q) = \frac{1}{q\Delta q\sqrt{2\pi}} \exp\left(\frac{-ln(q) - \langle q \rangle}{2\Delta q^2}\right) \tag{1.5}$$

It is clear that for practical reasons, we cannot discuss all distributions in great details. To explicitly propagate all possible distributions would be cumbersome, even for today's computers. However, the Central Limit theorem states that a distribution of a great number of random and independent variables tends towards a normal Gaussian [1]. In most cases, this convergence is rapid. We note that applying a normal (Gaussian) distribution $P(q)$ may not always be appropriate. In particular, for the case of a small number of

samples, a Gaussian is not an accurate representation of the real statistical distribution. However, the advantage of this practice is considerable, since it permits us to represent the entire distribution with only two values, the mean and the standard deviation.

In the case of multi-variables, characterizing the multi-variate probability distribution function $P(\vec{q})$ requires not only knowledge of the deviation and the mean, but also of the correlations between the obtained samples. Here $\vec{q} = (q_i)_{i=1}^{N}$ is a vector composed of the N variables q_i. We note that it is possible for the different variables q_i to have correlations between them, which is normally represented in matrix notation by the *covariance matrix* $\mathbf{V} = (V_{ij})$:

$$\mathbf{V} = \left\langle (\vec{q} - \langle \vec{q} \rangle) \cdot (\vec{q} - \langle \vec{q} \rangle)^T \right\rangle \tag{1.6}$$

where $^{\mathbf{T}}$ stands for vector transposition and with the matrix elements V_{ij} defined as:

$$V_{ij} = \langle (q_i - \langle q_i \rangle) \cdot (q_j - \langle q_j \rangle) \rangle = \langle \delta q_i \cdot \delta q_j \rangle \tag{1.7}$$

Note that the diagonal elements of the matrix reduce to the variances:

$$V_{ii} = \left\langle {\delta q_i}^2 \right\rangle = var(q_i) \tag{1.8}$$

The *correlation matrix* $\mathbf{C}$ is defined to have the elements given by:

$$C_{ij} = \frac{V_{ij}}{\sqrt{V_{ii} V_{jj}}} = \frac{\langle \delta q_i \cdot \delta q_j \rangle}{\Delta q_i \Delta q_j} \tag{1.9}$$

where $\Delta q_i = \sqrt{V_{ii}}$ is the standard deviation. We see that the quantities on the diagonal of the correlation matrix always equal to unity, i.e. $C_{ii} = 1$, and that the non-diagonal terms lie between being completely anti-correlated and completely correlated, i.e. $-1 \leq C_{ij} \leq 1$.

Some useful mathematical properties of the covariance matrix are:

- The covariance matrix is symmetric, i.e. $V_{ij} = V_{ji}$

- Covariance matrices corresponding to independent physical observables are positive definite, i.e. $(\forall \vec{x} \in \mathbb{R}^{dim(\mathbf{V})}$ and $\vec{x} \neq \vec{0})$ then $\vec{x}^T \cdot \mathbf{V} \vec{x} > 0$ where ^{T} stands for vector transposition.

The covariance matrix takes into account both the uncertainties in the data as well as the correlations that exist between them. The correlations may originate from the nature of the experiment through which the cross sections were measured (for example, using the same equipment will propagate the uncertainties associated with the calibration of the instrument to the different measured parameters), or through the use of *integral measurements* where many parameters are measured simultaneously, or the subsequent analysis of the experimental data such as the normalization that was used in the measurement (for example using a reference reaction rate as normalization). It should be noted that

these correlations often play an important role in the computed overall uncertainty (see chapter 4).

Finally, we should note that while in reactor physics we typically interest ourselves to integral quantities (such as k_{eff}, or a reaction rate), due to the complexity of the system, the large energy range that is encountered, and the aggregate composition of the system, different reactions play different roles at different energies due to differences in the underlying physical processes. As a consequence, a complete evaluation of covariances should take into account all the diverse correlation terms, which vary as a function of energy, reaction, and material.

1.2.1 Cross Section Libraries and Corresponding Covariance Files

The cross section values originate from physical measurements as well as physical models. However, before they can be used with confidence in computations, they must be validated. The goal of the validation process is to show that the obtained results from the measurement or model are coherent and complete. It is also crucial to present the obtained data in a standard format, this of course is essential for facilitating communication between the various laboratories involved, and use by the users. This process of the evaluation and validation of the ensemble of nuclear data, and their placing in the standard format involves many steps.

Firstly, we have seen that evaluations are based on experimental measurements, which are subjected to a critical analysis. The results of the measurements, accompanied with reports of evaluations are public in the form of an international experimental database called EXFOR. The evaluation report specifies the details of the experiment, and should include a complete estimation of the uncertainties due to the experimental technique used. However, this practice is often not followed or incomplete. In the EXFOR data base for example, we often find that only the statistical errors are being reported and systematic uncertainties are rarely reported, and as a result, the correlations between the measured nuclear data are neglected. This makes often the construction of the variance-covariance matrices difficult, sometimes requiring some detective work.

The experimental data can not cover the entire range of energies, reactions and isotopes. This missing information is completed by using various physical models. Finally, they are put in a prescribed format called the Evaluated Nuclear Data File (ENDF format [2]). These data files, called evaluations, are then validated with the help of criticality experiments.

The evaluation of cross sections are performed by many organisms in the world and are proposed under the format of a cross section library evaluation, updated periodically. Amongst the recent evaluations, prepared at different laboratories in the world, we can cite a few such as: ENDF/B-VII (United States), JEFF 3.1 (EU), JENDL 4.0 (Japan), BROND (Russia), CENDL (China), and TENDL (Holland). To be able to use the different evaluations in the same computational code with the goal of comparison, it

is convenient to present the data under a standardized format.

The Evaluated Nuclear Data File (ENDF), is the standard digital format under which these files are provided. Today, we can reproach some historical faults associated with this format; the fact that the base structure was defined in the 1960s - an epoch where computing power was much less powerful than today. To note a few: the limitation of 80 columns (characters) per line, the numbering of the lines appearing in the evaluation, the limitation of the precision of the values presented. The main reason that we still use this format today, which other than a few cosmetic modifications remains relatively the same today, is the enormous cost that a complete change in format would require. We have therefore learned to live with these inconveniences, with the hope that some day the inconveniences associated with the format become constraining to a level where we are obligated to redefine it.[1]

At present however, this format fulfils its role sufficiently well. The most limiting constraint is the precision of the stored values, 12 characters maximum, including the exponential and its sign. The advantage of the format is that all the evaluations mentioned above give their data in this format, which allows their treatment with the same code, an advantage which is essential to spread use and compare differences in obtained results.

Covariance Matrices

The area of covariance matrix generation was for a long time and in particular since the Three-Mile Island accident neglected. In recent years, the situation is improving rapidly and important efforts are being invested in the development of mathematical methods for error propagation aimed at producing more reliable, complete and consistent cross-section covariance matrices. Modern mathematical techniques are applied based on Bayesian error propagation approach for combining the uncertainties of different origins involved in the nuclear data evaluation process. In particular, since the evaluation of cross-sections combines experimental measurements (differential, but in some cases also integral measurements) and nuclear model calculations, the covariance matrices must reflect the uncertainties coming from both measurement and nuclear models. Uncertainties from measurements can be found in the EXFOR database [4] (although the data are sometimes considered as incomplete, particularly with regard to the correlations).

Except for a few cases (for example, the Watt-spectra [5]), most nuclear models are non-linear, therefore Monte Carlo methods have been proposed to account for their parameter uncertainties [6], [1]. Monte Carlo methods can, in principle, reach an arbitrary level of accuracy and are particularly suitable for the study of error propagation in complex nuclear reaction systems, due to their easy implementation and their generality. However, the main problem that still remains is that the error propagation calculation necessitates knowledge of the input errors of model parameters and their probability distribution function *prior* to the Monte Carlo computation itself.

[1]Indeed, in 2012, an activity on defining a new format was initiated within the OECD/NEA WPEC Subgroup 38 on "A modern nuclear database structure beyond the ENDF format" [3].

Examples of recent modern covariance matrices include the data included in the JENDL-4.0, TENDL, ENDF/B-VII and JEFF-3.1 cross-section evaluations.

1.3 Computational Neutron Transport

Neutron transport in a reactor is a diffusive process. A neutron is born at high energies, travels throughout the reactor while being slowed down by elastic and inelastic scattering collisions. During this process, it can be lost due to leakage or captured either by interaction through parasitic capture reactions, or interact in a neutron producing reaction such as $(n, 2n)$, $(n, 3n)$, etc. or the more probable case of fission (n, f). This process is called the neutron life *cycle* [7], defined as the period starting with the emission of the fission neutron and ending with the capture or escape of these neutrons.[2] The parameter of interest in describing this system is the neutron population density $N(\bar{\rho})$ in (cm^{-3} sr^{-1} eV^{-1}) or the more common neutron flux $\phi(\bar{\rho})$ (in cm^{-2} s^{-1} sr^{-1} eV^{-1}). The Boltzmann equation, also called the neutron transport equation, is an equation of conservation characterizing the neutron population for a relatively small number of neutrons colliding in a vast sea of nuclei that compose the domain D with the boundary ∂D.

1.3.1 The Boltzmann Equation

In its integro-differential form [8], assuming that neutrons are emitted isotropically from fission and that interaction probabilities are invariant under rotations, the time- independent neutron transport equation takes the form:

$$\hat{\Omega} \cdot \vec{\nabla}\phi(\vec{r}, \hat{\Omega}, E) + \Sigma(\vec{r}, E)\phi(\vec{r}, \hat{\Omega}, E) = Q(\vec{r}, E, \hat{\Omega}) + Q_e(\vec{r}, \hat{\Omega}, E) \tag{1.10}$$

with the *collision source* $Q(\vec{r}, E, \hat{\Omega})$ defined as:

$$Q(\vec{r}, E, \hat{\Omega}) = \int_{\hat{\Omega}'} d\hat{\Omega}' \int_{E'} dE' q(\vec{r}, \hat{\Omega}' \to \hat{\Omega}, E' \to E) \tag{1.11}$$

and the *collision density* $q(\vec{r}, \hat{\Omega}' \to \hat{\Omega}, E' \to E)$ defined such that:

$$q(\vec{r}, \hat{\Omega}' \to \hat{\Omega}, E' \to E) = \overbrace{\frac{\chi(\vec{r}, E)}{4\pi k_{eff}} \nu(E') \Sigma_f(\vec{r}, E') \phi(\vec{r}, \hat{\Omega}', E')}^{\text{Fission density}} + \overbrace{\Sigma_s(\vec{r}, \hat{\Omega}' \to \hat{\Omega}, E' \to E) \phi(\vec{r}, \hat{\Omega}', E')}^{\text{Scattering density}} \tag{1.12}$$

where :

- $\phi(\vec{r}, \hat{\Omega}, E)$: the neutron angular flux at the point $\vec{r}$, in the direction $\hat{\Omega}$ and at the energy E.

[2] In deterministic calculations, one could think of the average neutron cycle

- $\Sigma(\vec{r}, E)$: the total macroscopic cross section at point $\vec{r}$ and energy E.

- $\Sigma_f(\vec{r}, E')$: the macroscopic fission cross section at point $\vec{r}$ and energy E'.

- ν: the average number of neutrons produced by fission.

- $\chi(\vec{r}, E)$: the neutron fission spectrum at point $\vec{r}$ and energy E; note that we have assumed fission neutrons to be emitted isotropically, and all fissile isotopes have the same spectrum.

- $\Sigma_s(\vec{r}, \hat{\Omega}' \rightarrow \hat{\Omega}, E' \rightarrow E)$: the differential scattering cross section for a neutron of energy E' and in direction $\hat{\Omega}'$ to be scattered to a neutron at energy $E + dE$ and direction $\hat{\Omega} + d\hat{\Omega}$.

- k_{eff}: the multiplication factor.

- $Q_e(\vec{r}, \hat{\Omega}, E)$: the steady state neutron source

Equation 1.10 is an equation of conservation with the term on the left representing the neutrons lost due to leakage and collisions, and the term on the right representing the neutron source such as neutrons released during the the fission process or the down scattered from higher energies[3], or emitted from a physical fixed source Q_e. When the physical fixed source Q_e of the equation 1.10 is non-zero, imposing a steady state condition $k_{eff} = 1$ is implied. In the case where Q_e is zero, equation 1.10 represents an eigenvalue problem with the eigenvalue $\lambda = \frac{1}{k_{eff}}$ corresponding to the fundamental mode. The k_{eff} value in this case provides a measure of balance between neutrons lost from the system (due to leakage, and absorption) and the neutrons entering the system or produced by fission. For the rest of this work, we will assume that the source Q_e is equal to zero. This assumption is consistent with the typical k_{eff} search in lattice computation.

Boundary Conditions

In order to solve equation 1.10, boundary conditions quantifying the flux behaviour at the boundary ∂D are required. Assuming that no neutron sources exist on the boundary ∂D, we can take the incoming flux at the surface ∂D to have the form [9]:

$$\phi(\vec{\rho}_-) = \beta[\phi] = \int_{\partial D_+} \beta(\vec{\rho'}_+ \rightarrow \vec{\rho}_-)\phi(\vec{\rho'}_+) d\bar{\rho'}_+ \tag{1.13}$$

where $\bar{\rho}_- = (\vec{r}, \hat{\Omega}, E) \in \partial D_-$ and $\bar{\rho}_+ = (\vec{r'}, \hat{\Omega}', E') \in \partial D_+$ are points in the phase space located on the boundary ∂D, with $\hat{\Omega}$ and $\hat{\Omega}'$ correspond to the incoming and out going directions respectively. Here, $\phi(\bar{\rho}_-)$ refers to the neutron flux entering the volume at the

[3]Note that at thermal energies, up-scattering can be possible.

boundary ∂D, and $\phi(\bar{\rho}_+)$ refers to the neutron flux leaving the surface boundary ∂D. The five-dimensional surface element $d\vec{\rho}'_+ = dA' d\hat{\Omega}' dE'$ involves the surface element dA' on the boundary ∂D, the solid angle $d\hat{\Omega}'$ and the energy differential dE'. The kernel $\beta(\vec{\rho}'_+ \rightarrow \vec{\rho}_-)$ of the integral equation 1.13 relates the incoming and out going neutron fluxes; a variety of conditions can be represented including void, isotropic reflection, and specular/mirror reflection. The most common conditions used in practical calculations are representative of local reflection, or void, for which the kernel $\beta(\vec{\rho}'_+ \rightarrow \vec{\rho}_-)$ takes the form [9]:

$$\beta(\vec{\rho}'_+ \rightarrow \vec{\rho}_-) = \begin{cases} 0 & \text{void condition} \\ \frac{1}{\pi}\beta(\vec{r}, E' \rightarrow E)(\hat{\Omega}' \cdot \hat{n})\delta_A(\vec{r'} - \vec{r}) & \text{isotropic reflection} \\ \beta(\vec{r}, E' \rightarrow E)\delta(\hat{\Omega}' \cdot \hat{\Omega}_R - 1)\delta_A(\vec{r'} - \vec{r}) & \text{specular reflection} \end{cases} \quad (1.14)$$

where :

- $\beta(\vec{r}, E' \rightarrow E)$: local albedo matrix
- δ_A: the delta function that reduces volume integration to an integral over the surface ∂D
- $\hat{\Omega}_R = \hat{\Omega} - 2(\hat{\Omega} \cdot n)\hat{n}$ corresponding to the mirror reflection angle

Numerical Solutions

Except for the simplest cases [10], equation 1.10 cannot be solved analytically so that a numerical formalism must be used. Several numerical methods exist for the resolution of the above equations, some of which include [11] :

- The S_N method involving the discretization in angle and energy of equation 1.10
- The P_N method involving the expansion of the angular flux in its spherical harmonics.
- The B_N method using the spatial and energy separability of the flux with the buckling approximation, and a spherical harmonics treatment for the angular flux.
- The Method of Characteristics (MOC) involving the solution of the integral Boltzmann equation on its characteristic lines.
- The Method of Collision Probabilities (CP) involving volume discretization of the integral equation.
- Monte Carlo methods.

The Method of Characteristics and the method of Collision Probabilities are available in the code DRAGON [12] which is the main code used in this work. The remainder work will be limited to the method of Collision Probabilities; this is concurrent with the current methodology used in the French and Canadian industries.

1.3.2 Anisotropy and the Transport Correction

In the absence of a fixed source (i.e. $Q_e = 0$), the left hand side of equation 1.10 becomes:

$$\begin{aligned}\hat{\Omega}\cdot\vec{\nabla}\phi(\vec{r},\hat{\Omega},E)+\Sigma(\vec{r},E)\phi(\vec{r},\hat{\Omega},E) &= Q(\vec{r},E,\hat{\Omega})\\ &= \int_{E'}dE'\int_{\hat{\Omega}'\in 4\pi}d\hat{\Omega}' q(\vec{r},\hat{\Omega}'\rightarrow\hat{\Omega},E'\rightarrow E)\end{aligned} \tag{1.15}$$

As seen, the collision source $Q(\vec{r},E,\hat{\Omega})$ appearing on the right hand-side of equation 1.15 has a dependence on the angular component $\hat{\Omega}$. Since most observables in reactor physics can be reduced in terms of reaction rates, the main component of interest is the angle integrated scalar flux $\phi(\vec{r},E) = \int_{\hat{\Omega}\in 4\pi}\phi(\vec{r},E,\hat{\Omega})d\hat{\Omega}$. The common assumption [12] is to assume that the collision source appearing in equation 1.15 is isotropic. While this is certainly true for the case of fission[4] at the energies encountered in reactor physics (E< 20 MeV), scattering anisotropy must somehow be accounted for. This is typically done by modifying the total and scattering cross sections into their transport corrected form according to the procedure presented below.

The Transport Correction

Assuming rotational invariance, and representing the differential scattering cross section in its Legendre Polynomial form we have [13, 14] :

$$\Sigma_s(\vec{r},\hat{\Omega}\cdot\hat{\Omega}',E'\rightarrow E) = \frac{1}{2\pi}\Sigma_s(\vec{r},\overbrace{\hat{\Omega}\cdot\hat{\Omega}'}^{\mu},E'\rightarrow E) = \frac{1}{2\pi}\Sigma_s(\vec{r},\mu,E'\rightarrow E) \tag{1.16}$$

$$\Sigma_s(\vec{r},\mu,E'\rightarrow E) = \overbrace{\frac{1}{2}\Sigma_{s,0}(\vec{r},E'\rightarrow E)}^{\text{zeroth term}} + \overbrace{\frac{3}{2}\Sigma_{s,1}(\vec{r},E'\rightarrow E)\,\mu}^{\text{first term}} \tag{1.17}$$

where we have limited ourselves to a first order expansion (P_1) to derive the P_0 transport corrected form of the scattering source (this is consistent to what is computed in DRAGON). Here, $\mu = \hat{\Omega}\cdot\hat{\Omega}'$ is the cosine of the scattering angle. The zeroth order coefficient $\Sigma_{s,0}$ and the first order coefficient $\Sigma_{s,1}$ are defined as:

$$\Sigma_{s,0}(\vec{r},E'\rightarrow E) = \int_{\mu=-1}^{1}d\mu\Sigma_s(\vec{r},\mu,E'\rightarrow E) \tag{1.18}$$

$$\Sigma_{s,1}(\vec{r},E'\rightarrow E) = \int_{\mu=-1}^{1}d\mu\mu\Sigma_s(\vec{r},\mu,E'\rightarrow E) \tag{1.19}$$

The goal is to modify the P_0 component in order to account for the anisotropy introduced by the P_1 term. We therefore add a forward peak component to the zeroth order Legendre Expansion so that

$$\Sigma_s(\vec{r},\hat{\Omega}\cdot\hat{\Omega}',E'\rightarrow E) = \frac{1}{2}\bar{\Sigma}_{s,0} + \Delta\Sigma_{tr}\delta(\mu-1) \tag{1.20}$$

[4]Note that at high neutron incident energies, the angular distribution for the neutrons emitted from fission is slightly anisotropic.

where $\bar{\Sigma}_{s,0}$ is the modified P_0 coefficient and the additional term $\Delta\Sigma_{tr}\delta(\mu-1)$ accounts for the forward peak in the scattering angle associated with anisotropic scattering. Multiplying equation 1.20 by the Legendre Polynomials ($P_0(\mu)=1$ and $P_1(\mu)=\mu$), integrating over μ and comparing with equation 1.17 we see that [14]:

$$\text{for l=0 } \bar{\Sigma}_{s,0}(\vec{r},E'\to E)+\Delta\Sigma_{tr}(\vec{r},E'\to E)=\Sigma_{s,0}(\vec{r},E\to E') \tag{1.21}$$

$$\text{for l=1 } \Delta\Sigma_{tr}(\vec{r},E'\to E)=\Sigma_{s,1}(\vec{r},E'\to E) \tag{1.22}$$

so that equation 1.20 reduces to:

$$\begin{aligned}\Sigma_s(\vec{r},E'\to E,\mu)=&\frac{1}{2}\left(\Sigma_{s,0}(\vec{r},E'\to E)-\Sigma_{s,1}(\vec{r},E'\to E)\right)\\&+\Sigma_{s,1}(\vec{r},E'\to E)\delta(\mu-1)\end{aligned} \tag{1.23}$$

substituting the scattering cross section defined by equation 1.23 into the transport equation given by equation 1.15, we have [14]:

$$\begin{aligned}\hat{\Omega}\cdot\nabla\phi(\vec{r},E,\hat{\Omega})+\Sigma(\vec{r},E)\phi(\vec{r},E,\hat{\Omega})-\int_0^\infty dE'\Sigma_{s,1}(\vec{r},E'\to E)\phi(\vec{r},E'\hat{\Omega})\\=\bar{Q}(\vec{r},E)\end{aligned} \tag{1.24}$$

where the *transport corrected* collision source is defined as:

$$\begin{aligned}\bar{Q}(\vec{r},E)&=\int_0^\infty dE'q(\vec{r},E'\to E)\\&=\frac{1}{4\pi}\int_0^\infty dE'\left(\Sigma_{s,0}(\vec{r},E'\to E)-\Sigma_{s,1}(\vec{r},E'\to E)\right)\phi(\vec{r},E')\\&+\frac{\chi(\vec{r},E)}{4\pi k_{eff}}\int_0^\infty dE'\nu\Sigma_f(\vec{r},E')\phi(\vec{r},E')\end{aligned} \tag{1.25}$$

where the $1/4\pi$ coefficient appearing in the first term is due to the definition given in equation 1.16. Simplifying the term $\int_0^\infty dE'\ \Sigma_{s,1}(\vec{r},E'\to E)\phi(\vec{r},E'\hat{\Omega})$ appearing on the right hand side of equation 1.24 requires an additional approximation. The *micro-reversibility* approximation, valid in the thermal domain, states that the neutrons are in quasi-equilibrium with the nucleus [14], so that:

$$\Sigma_{s,1}(\vec{r},E'\to E)\phi(\vec{r},E',\hat{\Omega})=\Sigma_{s,1}(\vec{r},E\to E')\phi(\vec{r},E,\hat{\Omega}) \tag{1.26}$$

from substitution of equation 1.26 into the transport equation 1.24, we have [14]:

$$\hat{\Omega}\cdot\nabla\phi(\vec{r},E,\hat{\Omega})+\bar{\Sigma}(\vec{r},E)\phi(\vec{r},E,\hat{\Omega})=\bar{Q}(\vec{r},E) \tag{1.27}$$

where [14]:

$$\bar{\Sigma}(\vec{r},E)=\Sigma(\vec{r},E)-\Delta\Sigma_{tr}(\vec{r},E) \tag{1.28}$$

$$\bar{\Sigma}_{s,0}(\vec{r},E'\to E)=\Sigma_{s,0}(\vec{r},E'\to E)-\delta(E'-E)\Delta\Sigma_{tr}(\vec{r},E) \tag{1.29}$$

$$\Delta\Sigma_{tr}(\vec{r},E)=\int_0^\infty dE'\Sigma_{s,1}(\vec{r},E\to E') \tag{1.30}$$

Equation 1.27, partially takes into account the effect from linearly anisotropy of the scattering cross section while removing the angular dependence of the collision source. By reducing the total cross section to the transport corrected cross section defined by equation 1.28, the diffusion length of the neutron is increased. This mimics the actual efffect from linear anisotropy of scattering; the scattered neutron, due to the linear anisotropy of the scattering cross section in the laboratory frame, has a higher chance of continuing in the forward direction (defined as the initial direction of the incident neutron). We note that in the sections that follow, we will assume that the total and scattering cross sections are transport corrected as defined by equations 1.29 and 1.28 without explicitly using the overhead bar notation. Similarly, the source Q will correspond to the transport corrected collision source (which is now isotropic) given by equation 1.25.

1.3.3 Integral formulation

The Green's function formalism for the Boltzmann equation is one of the most elegant representations of the transport equation. A good cover of the various formalisms that exist for the transport equation can be found in [10]. In this section, to arrive at the definition of the first flight kernel, we will mimic the derivation of the Green's function provided in [10]. In the Green's function formalism, first the domain of the transport equation is extended to the infinite plane. To do this, the collision source of equation 1.27 is modified by adding a surface source chosen so that the extended flux outside of the original domain vanishes. The extended flux can then be represented as a convolution of the Green's function with the modified collision source over the extended domain. By doing so, the integro-differential equation 1.27 is transformed into an integral equation corresponding to a Fredholm integral equation of the second kind [13, 10].

The Extended Flux

The extended flux $\tilde{\phi}(\bar{\rho}) = \Theta_D(\bar{\rho})\phi(\bar{\rho})$ can be thought of as the neutron flux over the domain extended to infinity. The characteristic function $\Theta_D(\vec{r})$ is defined as:

$$\Theta_D(\vec{r}) = \begin{cases} 1 & \vec{r} \in D \\ 0 & \text{else} \end{cases} \tag{1.31}$$

Multiplying the flux $\phi(\bar{\rho})$ by $\Theta_D(\vec{r})$ assures that the extended flux $\tilde{\phi}(\bar{\rho})$ vanishes to zero on the exterior of the domain D. Substituting the extended flux $\tilde{\phi}(\bar{\rho}) = \Theta_D(\vec{r})\phi(\bar{\rho})$ into the integro-differential transport equation 1.10 gives [10]:

$$\left[\hat{\Omega} \cdot \nabla + \Sigma(\vec{r}, E)\right] \tilde{\phi}(\vec{r}, E, \hat{\Omega}) = Q_m(\vec{r}, \hat{\Omega}, E) \tag{1.32}$$

with the modified collision source $Q_m(\vec{r}, \hat{\Omega}, E)$ is defined as [10]:

$$Q_m(\vec{r}, \hat{\Omega}, E) = \int_{E'} dE' q(\vec{r}, E' \to E) + \overbrace{\phi(\vec{r}, \hat{\Omega}, E)\hat{\Omega} \cdot \vec{\nabla}\Theta_D(\vec{r})}^{\text{Surface Source}} \tag{1.33}$$

note that the collision source $Q(\vec{r}, E)$ (or $q(\vec{r}, E' \to E)$) is defined by equation 1.25.

The last term of equation 1.33 involving the gradient of the characteristic function $\Theta_D(\vec{r})$ is obtained by invoking the Leibniz's differentiation rule for $\hat{\Omega}\cdot\nabla(\phi(\vec{r},\hat{\Omega},E)\Theta_D(\vec{r}))$ with the gradient of the characteristic function $\Theta_D(\vec{r})$ interpreted as a delta function. As will be seen in integral formulation given by equation 1.39, this term corresponds to the equivalent surface source required to have the modified flux $\tilde{\phi}$ vanish outside of the domain D [10].

The Green's Function

The Green's function (also called the first flight kernel) $\mathfrak{I}(E;\vec{r'}\to\vec{r})$ for the Boltzmann equation 1.10 satisfies [15] :

$$\begin{aligned}\left[\hat{\Omega}\cdot\vec{\nabla}+\Sigma(\vec{r},E)\right]\mathfrak{I}(E;\vec{r'}\to\vec{r}) \\ = \delta(\vec{r}-\vec{r'}) \end{aligned} \tag{1.34}$$

$$\text{with } \lim_{|\vec{r}|\to\infty}\mathfrak{I}(E;\vec{r'}\to\vec{r})=0 \text{ and } \lim_{|\vec{r'}|\to\infty}\mathfrak{I}(E;\vec{r'}\to\vec{r})=0 \tag{1.35}$$

We can convert equation 1.34 to an ordinary differential equation by tracing the neutron's trajectory along the direction $\hat{\Omega}=\frac{\vec{r'}-\vec{r}}{|\vec{r'}-\vec{r}|}$. Multiplying equation 1.34 by the delta function $\delta\left(\hat{\Omega}-\frac{\vec{r}-\vec{r'}}{|\vec{r}-\vec{r'}|}\right)$, we have:

$$\begin{aligned}\delta\left(\hat{\Omega}-\frac{\vec{r}-\vec{r'}}{|\vec{r}-\vec{r'}|}\right)\left[\hat{\Omega}\cdot\vec{\nabla}+\Sigma(\vec{r},E)\right]\mathfrak{I}(E;\vec{r'}\to\vec{r}) \\ = \delta\left(\hat{\Omega}-\frac{\vec{r}-\vec{r'}}{|\vec{r}-\vec{r'}|}\right)\delta\left(\vec{r}-\vec{r'}\right)\end{aligned} \tag{1.36}$$

The streaming term $\hat{\Omega}\cdot\nabla$ of equation 1.36 along the trajectory $\hat{\Omega}=\frac{\vec{r'}-\vec{r}}{|\vec{r}-\vec{r'}|}$ simplifies to:

$$\hat{\Omega}\cdot\vec{\nabla}=\frac{d}{ds}=\frac{\partial\vec{r'}}{\partial s}\cdot\vec{\nabla}_{\vec{r'}} \tag{1.37}$$

where we have used the parametrization $\vec{s}=s\hat{\Omega}=\vec{r'}-\vec{r}$ with $s=|\vec{r'}-\vec{r}|$. The left hand side of equation 1.37 can be inverted by multiplying both sides with the integrating factor $e^{-\tau(|\vec{r}-\vec{r'}|)}$. Here $\tau(|\vec{r}-\vec{r'}|)=\int_{\vec{r'}}^{\vec{r}}\Sigma(\vec{s})ds$ is the optical length of the neutron, appearing in the exponential integration factor to account for the attenuation of the neutron population along the trajectory $\vec{r'}=\vec{r}+s\hat{\Omega}$, resulting from interactions with the medium (hence the dependence on the total cross section). Inverting the operator $\frac{d}{ds}$ appearing in equation 1.36 gives [15]:

$$\mathfrak{I}(E;\vec{r'}\to\vec{r})=\frac{\exp\left[-\int_{\vec{r'}}^{\vec{r}}ds\Sigma(\vec{s},E)\delta\left(\frac{\vec{s}}{s}-\frac{\vec{r}-\vec{r'}}{|\vec{r}-\vec{r'}|}\right)\right]}{|\vec{r}-\vec{r'}|^2} \tag{1.38}$$

The first flight kernel $\mathfrak{I}(E;\vec{r'}\to\vec{r})$ represents the probability that a neutron leaving $\vec{r'}$

will reach, uncollided, the interval $d\vec{r}$ around $\vec{r}$. The neutron's trajectory is along the path $\vec{s} = s\hat{\Omega}$ where $\hat{\Omega} = \frac{\vec{r}-\vec{r'}}{|\vec{r}-\vec{r'}|}$ is the direction of the neutron.

By using the first flight kernel $\mathfrak{J}$, the integral equation for the extended neutron flux $\tilde{\phi}(\bar{\rho})$ appearing in equation 1.32 can be written as:

$$\phi(\vec{r}, E, \hat{\Omega}) \cdot \Theta_D(\vec{r}) = \int_{\vec{r'}} d\vec{r'} \int_{\Omega' \in 4\pi} d\hat{\Omega}' \mathfrak{J}(E; \vec{r'} \to \vec{r}) \delta(\hat{\Omega} - \frac{\vec{r}-\vec{r'}}{|\vec{r}-\vec{r'}|}) \cdot Q_m(\vec{r'}, \hat{\Omega}', E) \tag{1.39}$$

where the collision source $Q_m(\vec{r'}, \hat{\Omega}', E)$ was defined by equation 1.33. Equation 1.39, which can be verified from direct substitution of $\tilde{\phi}$ into equation 1.32, states that the contribution of the neutron flux at the point $\vec{r}$ is the contribution of the spatial sum of the neutrons emitted from the modified collision source Q_m at the point $\vec{r'}$ weighted by the Green's function $\mathfrak{J}(E; \vec{r'} \to \vec{r})$; the Green's function $\mathfrak{J}(E; \vec{r'} \to \vec{r})$ is the probability that a neutron at point $\vec{r'}$ will reach the point $\vec{r}$. The delta function $\delta(\hat{\Omega} - \frac{\vec{r}-\vec{r'}}{|\vec{r}-\vec{r'}|})$ assures that only those neutrons traveling towards the point $\vec{r}$ (i.e. in the direction $\hat{\Omega} = \frac{\vec{r'}-\vec{r}}{|\vec{r}-\vec{r'}|}$) contribute to the flux $\phi(\vec{r}, E, \hat{\Omega})$ at point $\vec{r}$.

Properties of the Green's function

An important property of the first flight kernel, which we will benefit from later in section 1.4.2 when discussing the theorem of reciprocity, is its symmetrical nature. In an infinite medium, it is clear that the first flight kernel $\mathfrak{J}(E; \vec{r'} \to \vec{r})$ is symmetric (since in this case $\mathfrak{J}(E; \vec{r'} \to \vec{r}) = \mathfrak{J}(E; |\vec{r'} - \vec{r}|)$). It is possible to show [16] that $\mathfrak{J}$ is symmetric for any system. This can be done as such; writing the Green's function for two points $\vec{r_1}, \vec{r_2} \in D$ in the domain D we have [16]:

$$\left[\hat{\Omega} \cdot \vec{\nabla} + \Sigma(\vec{r}, E)\right] \mathfrak{J}(E, \vec{r_1} \to \vec{r}) = \delta(\vec{r} - \vec{r_1}) \tag{1.40}$$

$$\left[\hat{\Omega} \cdot \vec{\nabla} + \Sigma(\vec{r}, E)\right] \mathfrak{J}(E, \vec{r_2} \to \vec{r}) = \delta(\vec{r} - \vec{r_2}) \tag{1.41}$$

multiplying equation 1.40 by $\mathfrak{J}(E, \vec{r_2} \to \vec{r})$ and equation 1.41 by $\mathfrak{J}(E, \vec{r_1} \to \vec{r})$, integrating over $\vec{r} \in D$ while noting that the terms containing the $\hat{\Omega} \cdot \nabla$ can be integrated by parts, and subtracting the two obtained equations, we see that the terms appearing on the left hand side of equations 1.40 and equations 1.41 will be identical and vanish by subtraction so that:

$$\int_{\vec{r}} \mathfrak{J}(E, \vec{r_2} \to r) \delta(\vec{r} - \vec{r_1}) d\vec{r} = \int_{\vec{r}} \mathfrak{J}(E, \vec{r_1} \to r) \delta(\vec{r} - \vec{r_2}) d\vec{r} \tag{1.42}$$

Integration over the remaining terms, which involve the delta functions gives [16]:

$$\mathfrak{J}(E, \vec{r_1} \to \vec{r_2}) = \mathfrak{J}(E, \vec{r_2} \to \vec{r_1}) \tag{1.43}$$

The relation given by equation 1.42 states that [17] the angular density at $\vec{r_2}$ due to an isotropic unit source at $\vec{r_1}$ is the same as the angular density at $\vec{r_1}$ due to an isotropic unit source at $\vec{r_2}$. A number of relations can be derived from expression 1.43 which are called

"reciprocity theorems". These relations use the symmetrical nature of the first flight kernel with respect to the spatial variables $\vec{r}$, and $\vec{r'}$ and make it possible (in mono-energetic cases) to solve a simpler problem than the original problem, and then relate the obtained solution to the solution of the original problem [17]. In the numerical computation of equation 1.34, the theorems are useful as they provide a closing relationship for the numerically computed first flight kernel. The interested user is referred to [17] for a more detailed discussion of the subject.

Boundary Conditions

It is beneficial at this point to integrate directly the flux boundary conditions into equation 1.39. We note that by using the divergence theorem, the term in the modified collision source Q_m, containing the gradient can be simplified to [10]:

$$\int_{\vec{r'}\in \text{all space}} d\vec{r'}\phi(\vec{r'},\hat{\Omega}',E')\mathfrak{I}(E;\vec{r'}\rightarrow\vec{r})\hat{\Omega}'\cdot\vec{\nabla}\Theta_D(\vec{r'}) = \tag{1.44}$$

$$\int_{S_\infty} dA_{S'}\hat{n}_{S'}\cdot\hat{\Omega}'\phi(\vec{r'},\hat{\Omega}',E')\mathfrak{I}(E;\vec{r'}\rightarrow\vec{r})\Theta_D(r_{\vec{S'}}) - \int_{\vec{r'}\in D} d\vec{r'}\hat{\Omega}'\cdot\nabla_{\vec{r'}}(\phi(\vec{r'},\hat{\Omega}',E')\mathfrak{I}(E;\vec{r'}\rightarrow\vec{r}))$$

$\int_{S_\infty} dA_{S'}\hat{n}_{S'}\cdot\hat{\Omega}'\phi(\vec{r'},\hat{\Omega}',E')\mathfrak{I}(E;\vec{r'}\rightarrow\vec{r})\Theta_D(r_{\vec{S'}})$ → 0

where $\hat{n}_S$ is the outward normal of the surface S'. Note that for a finite domain, the first integral appearing on the right hand side cancels to zero by the definition of the characteristic function (i.e. $\lim_{r_{S'}\rightarrow r_{S_\infty}}\Theta_D(\vec{r}_{S'}) = 0$) and for an infinite domain the integral renders to zero by the boundary condition given in equation 1.35. Applying once more the divergence theorem to the the second term of equation 1.31 gives [10]:

$$\int_{\vec{r'}\in D} d\vec{r'}\hat{\Omega}'\cdot\nabla_{\vec{r'}}(\phi(\vec{r'},\hat{\Omega}',E')\mathfrak{I}(E;\vec{r'}\rightarrow\vec{r})) = -\int_{\partial D} dA_s\hat{n}_S\cdot\hat{\Omega}'\phi(\vec{r'},\hat{\Omega}',E')\mathfrak{I}(E;\vec{r'}\rightarrow\vec{r}) \tag{1.45}$$

where dA_S is the surface element on the surface ∂D with the outward normal $\hat{n}_S$. Equation 1.39 can then be written as [10]:

$$\begin{aligned}
&\phi(\vec{r},E,\hat{\Omega})\cdot\Theta_D(\vec{r}) = \\
&\quad\int_{\vec{r'}} d\vec{r'}\int_{E'} dE'\int_{\Omega'\in 4\pi} d\hat{\Omega}'\mathfrak{I}(E;\vec{r'}\rightarrow\vec{r})\delta(\hat{\Omega}-\frac{\vec{r}-\vec{r'}}{|\vec{r}-\vec{r'}|})\ \cdot q(\vec{r'},E'\rightarrow E) \\
&+\int_{\hat{\Omega}'\in 4\pi} d\hat{\Omega}'\int_{\vec{r'}\in\partial D} dA_s\hat{n}_S\cdot\hat{\Omega}'\phi(\vec{r_S'},\hat{\Omega}',E)\mathfrak{I}(E;\vec{r_S'}\rightarrow\vec{r})\delta(\hat{\Omega}-\frac{\vec{r}-\vec{r_S'}}{|\vec{r}-\vec{r_S'}|})
\end{aligned} \tag{1.46}$$

where the incoming flux, $\phi(\vec{r_S},\hat{\Omega}',E')$ for $\hat{n_S}\cdot\hat{\Omega}<0$, is assumed to be known or related to the outgoing flux, $\phi(\vec{r_S},\hat{\Omega}',E')$ for $\hat{n_S}\cdot\hat{\Omega}>0$, by a boundary conditions such as equation 1.13. The unknown outgoing flux can be found by approaching the boundary from inside

the medium ($\vec{r} \to \vec{r}_{S,+}$). Setting $\vec{r} = \vec{r}_{S,+}$ in equation 1.46 gives [10]:

$$\begin{aligned}
&\phi(\vec{r}_{S,+}, E, \hat{\Omega}) \cdot \Theta_D(\vec{r}) = \\
&\int_{\vec{r'}} d\vec{r'} \int_{E'} dE' \int_{\Omega' \in 4\pi} d\hat{\Omega}' \mathfrak{I}(E; \vec{r'} \to \vec{r}_{S,+}) \delta(\hat{\Omega} - \frac{\vec{r_{S,+}} - \vec{r'}}{|\vec{r_{S,+}} - \vec{r'}|}) \cdot q(\vec{r'}, E' \to E) \\
&+ \int_{\hat{\Omega}' \in 4\pi} d\hat{\Omega}' \int_{\vec{r'} \in \partial D} dA_s \hat{n}_S \cdot \hat{\Omega}' \phi(\vec{r'_S}, \hat{\Omega}', E) \mathfrak{I}(E; \vec{r'_S} \to \vec{r}_{S,+}) \delta(\hat{\Omega} - \frac{\vec{r_{S,+}} - \vec{r'_S}}{|\vec{r_{S,+}} - \vec{r'_S}|})
\end{aligned} \tag{1.47}$$

Equations for the Scalar Flux

To obtain the scalar flux, we can integrate equation 1.46 over all angular directions $\hat{\Omega} \in 4\pi$. First, parameterizing the spatial vector $\vec{r'} = \vec{r} - s\hat{\Omega}''$, with $s = |\vec{r'} - \vec{r}|$ and noting that:

$$\text{inside the domain: } d\vec{r'} = s^2 ds d\hat{\Omega}'' \tag{1.48}$$

$$\text{on the surface: } (\hat{n}_S \cdot \hat{\Omega}'') dA_S = s_S^2 d\hat{\Omega}'' \tag{1.49}$$

equation 1.46 is simplified to:

$$\begin{aligned}
&\phi(\vec{r}, E, \hat{\Omega}) \cdot \Theta_D(\vec{r}) = \\
&= \int_{E'} dE' \int_{\Omega' \in 4\pi} d\hat{\Omega}' \int s^2 ds \mathfrak{I}(E; (\vec{r} - s\hat{\Omega}) \to \vec{r}) \cdot q(\vec{r'}, E' \to E) \\
&+ \int_{\hat{\Omega}' \in 4\pi} d\hat{\Omega}' \int_{\hat{\Omega} \in 4\pi} ds_S \; s_S^2 \phi(\vec{r} - s_S\hat{\Omega}, \hat{\Omega}', E) \mathfrak{I}(E; (\vec{r} - s_S\hat{\Omega}) \to \vec{r}) \delta(\hat{\Omega} - \hat{\Omega}')
\end{aligned} \tag{1.50}$$

where we have used the fact that the $\hat{\Omega}''$ integration over delta function $\delta(\hat{\Omega} - \frac{\vec{r} - \vec{r'}}{|\vec{r} - \vec{r'}|}) = \delta(\hat{\Omega} - \hat{\Omega}'')$, appearing in equation 1.47, collapses the $\hat{\Omega}'$ to $\hat{\Omega}$. To obtain the scalar flux $\phi(\vec{r}, E) = \int_{\hat{\Omega} \in 4\pi} d\hat{\Omega} \phi(\vec{r}, \hat{\Omega}, E)$, we integrate equation 1.50 over $\hat{\Omega} \in 4\pi$ and, once more, use equations 1.48 and 1.49 to arrive at [12]:

$$\begin{aligned}
\vec{\phi}(\vec{r}, E) = &\overbrace{\int_{\vec{r'} \in D} \frac{\exp(-\tau(s, E))}{s^2} q(\vec{r'}, E' \to E) d^3\vec{r'}}^{\text{Contribution from the collision source}} \\
&+ \overbrace{\int_{\vec{r'} \in \partial D} \frac{\exp(-\tau(s_s, E))}{s_S^2} \left(\hat{\Omega} \cdot \hat{n}_-\right) \phi_-(\vec{r}_S, E, \hat{\Omega}') d^2r'}^{\text{Contribution from the surface source}}
\end{aligned} \tag{1.51}$$

Here $\phi_-(\vec{r}, E, \hat{\Omega}')$ denotes the incoming angular flux at the surface ∂D with the inward normal $\hat{n}_-$, for the neutrons entering the volume D.

The first term of equation 1.51 represents the contribution from the collision source to the flux, convoluted with the exponential attenuation factor that appeared through the first flight kernel defined in equation 1.38; since the first flight kernel was interpreted as the probability that a neutron leaving $\vec{r'}$ will reach the interval $d\vec{r}$ around the point $\vec{r}$, the convolution appearing in the first integral represents the contribution of the collision

source q to the neutron flux at the point $\vec{r}$. Similarly, the second term is the contribution of all neutrons entering the surface ϕ_- to the flux at point $\vec{r}$. The second term has been obtained by noting that since the point $\vec{r}$ lies inside the surface, given the concavity of the surface, the only set of possible directions for which a neutron at the surface can contribute to the point $\vec{r}$ are those who are entering the volume at its boundary ∂D (i.e. $\hat{\Omega}\cdot\hat{n}_- > 0$ with $\hat{n}_-$ being the inward normal of the surface ∂D). This is taken into account during the integration by the delta function $\delta(\hat{\Omega} - \frac{\vec{r}-\vec{r'}}{|\vec{r}-\vec{r'}|}) = 0$ for $\hat{\Omega}\cdot\hat{n}_- < 0$ - neutrons that leave the volume do not contribute to the flux at $\vec{r}$.[5]

Through use of the first flight kernel $\mathfrak{I}(E;\vec{r'}\rightarrow\vec{r})$, equation 1.10 has been transformed into equation 1.39 which is a Fredholm equation of the second kind [13]. A great benefit of this integral approach is the flexibility for the types of geometries which can be modeled. The only requirement on the geometry type being the concavity of the boundary ∂D. The interested reader is referred to [10] for an in-depth discussion of the various formalisms associated with the Boltzmann equation.

1.4 Discretized Form

In this section, we will present the discretized form of the integral transport equation and arrive at the concept of the collision probability, which is used to derive the numerical form of the transport equation 1.51. To solve equation 1.51 numerically requires discretization in energy, angle and space. We will first use the multi-group approximation to discretize over energy, and arrive at the multi-group form of the transport equation 1.51. We will then proceed to discretize over angle and space. This gives rise to the concept of the Collision Probability. Using the collision probabilities, we will present the numerical form of the integral transport equation 1.51, referred to as the current-interface method, and used by the code DRAGON.

1.4.1 Energy discretization: the multi-group approximation

The multi-group approximation [18, 14, 10] begins with the partitioning of the total energy interval into G groups of interest with the energy interval $\Delta E_g = [E_g, E_{g-1}]$. Partitioning the energy integrals over the energy domain into sums of integrals, we have:

$$\int_{E'} dE' q(\vec{r}, E' \rightarrow E) = \sum_{g=1}^{G} \int_{\Delta E_g} dE' q(\vec{r}, E' \rightarrow E) \tag{1.52}$$

[5]Note that the boundary conditions enter the equations through the surface term appearing in equation 1.51

Integrating equation 1.27 over the energy group ΔE_g results in a system of equations of the form:

$$\hat{\Omega}\cdot\vec{\nabla}\int_{\Delta E_g} dE\phi(\vec{r},\hat{\Omega},E) + \int_{\Delta E_g} dE\Sigma(\vec{r},E)\phi(\vec{r},\hat{\Omega},E) = \sum_{g'=1}^{G}\int_{\Delta E_g} dE\int_{\Delta E_{g'}} dE' q(\vec{r},E'\rightarrow E) \text{ for } g=1,...,G \tag{1.53}$$

The multi-group approximation reduces to assuming that the flux is separable in terms of a fast varying fine flux $f(E)$, and a slow varying group flux $\phi_g(\vec{r},\hat{\Omega})$ (representing the asymptotic behavior of the flux), i.e.

$$\phi(\vec{r},\hat{\Omega},E) = f(E)\phi_g(\vec{r},\hat{\Omega}) \tag{1.54}$$

where $f(E)$ is assumed to be piecewise smooth and satisfies the normalization condition [10]:

$$\int_{\Delta E_g} f(E)dE = 1 \tag{1.55}$$

Using the multi-group approximation, equation 1.10 then becomes [10]:

$$\hat{\Omega}\cdot\vec{\nabla}\phi_g(\vec{r},\hat{\Omega}) + \Sigma_g(\vec{r})\phi_g(\vec{r},\hat{\Omega}) = \frac{1}{4\pi}\sum_{g'=1}^{G}\int d\hat{\Omega}'\Sigma_{s,g\rightarrow g'}(\vec{r})\phi_{g'}(\vec{r}) + \frac{1}{4\pi k_{eff}}\chi_g\sum_{g'=1}^{G}\nu_{g'}\Sigma_{fg'}(\vec{r})\phi_{g'}(\vec{r}) \tag{1.56}$$

with the group parameters defined as [10]:

$$\Sigma_g(\vec{r}) = \int_{\Delta E_g} dE f(E)\Sigma(\vec{r},E) \tag{1.57}$$

$$\Sigma_{s,g\rightarrow g'} = \int_{\Delta E_g} dE\int_{\Delta E_{g'}} dE'\Sigma_s(\vec{r},E'\rightarrow E)f(E') \tag{1.58}$$

$$\nu_g\Sigma_{fg}(\vec{r}) = \int_{\Delta E_g} dE f(E)\nu(E)\Sigma_f(\vec{r},E) \tag{1.59}$$

$$\chi_g = \int_{\Delta E_g} dE\chi(E) \tag{1.60}$$

Repeating the procedure of the previous section for the system of equations defined by equation 1.56, gives the multi-group form of equation 1.46:

$$\phi_g\left(\vec{r},\hat{\Omega}\right)\cdot\Theta_D\left(\vec{r}\right) = \sum_{g'=1}^{G}\int_{\vec{r'}} d\vec{r'}\int_{\Omega'\in 4\pi} d\hat{\Omega}'\Im_g\left(\vec{r'}\rightarrow\vec{r}\right)\delta\left(\hat{\Omega}-\frac{\vec{r}-\vec{r'}}{|\vec{r}-\vec{r'}|}\right)\cdot q^{g'\rightarrow g}(\vec{r}) + \int_{\hat{\Omega}'\in 4\pi} d\hat{\Omega}'\int_{\vec{r'}\in\partial D} dA_s\hat{n}_S\cdot\hat{\Omega}'\phi_g\left(\vec{r_S'},\hat{\Omega}'\right)\Im_g\left(\vec{r_S'}\rightarrow\vec{r}\right)\delta\left(\hat{\Omega}-\frac{\vec{r}-\vec{r'}}{|\vec{r}-\vec{r'}|}\right) \tag{1.61}$$

with the group to group collision source $q^{g'\to g}$ and the first flight kernel $\mathfrak{I}_g$ are defined as:

$$q^{g'\to g}(\vec{r})\phi_g(\vec{r}) = \frac{\chi_g(\vec{r})}{4\pi k_{eff}}\nu_{g'}\Sigma_{fg'}\left(\vec{r}\right)\phi_{g'}\left(\vec{r}\right)\Theta_D(\vec{r}) \tag{1.62}$$
$$+\frac{1}{4\pi}\Sigma_{s,g'\to g}\left(\vec{r}\right)\phi_{g'}\left(\vec{r}\right)\Theta_D\left(\vec{r}\right)$$

$$\mathfrak{I}_g\left(\vec{r'}\to\vec{r}\right) = \frac{\exp\left[-\int_{\vec{r'}}^{\vec{r}} ds\Sigma_g(\vec{s})\delta\left(\frac{\vec{s}}{s}-\frac{\vec{r}-\vec{r'}}{|\vec{r}-\vec{r'}|}\right)\right]}{|\vec{r}-\vec{r'}|^2} \tag{1.63}$$

Similarly, the multi-group form of equation 1.47 for the out-going flux is given by:

$$\phi_g(\vec{r}_{S,+},\hat{\Omega})\cdot\Theta_D(\vec{r}) = \sum_{g'=1}^{N_G}\int_{\vec{r'}} d\vec{r'}\int_{\hat{\Omega}'\in 4\pi} d\hat{\Omega}'\mathfrak{I}_g(\vec{r'}\to\vec{r}_{S,+})\cdot q^{g'\to g}(\vec{r'})$$
$$+\int_{\hat{\Omega}'\in 4\pi} d\hat{\Omega}'\int_{\vec{r'}_S\in\partial D} dA_s\hat{n}_S\cdot\hat{\Omega}'\phi_g(\vec{r'}_S,\hat{\Omega}')\mathfrak{J}_g(\vec{r'}_S\to\vec{r}_{S,+})\delta\left(\hat{\Omega}-\frac{\vec{r}-\vec{r'}}{|\vec{r}-\vec{r'}|}\right) \tag{1.64}$$

The multi-group approximation, as defined in equation 1.54, is the base of nearly all deterministic reactor codes [10]. However, due to the large domain in energy (from 10^{-5}eV to 20 MeV) and the non-regular behavior of the cross sections in the resonance region, the choice of the functions $f(E)$ is not evident. We will now discuss the choice for the function $f(E)$ in the frame work of the narrow resonance approximation.

Slowing Down in a Homogeneous Medium: the Narrow Resonance Approximation

Let us consider an infinite homogeneous mixture, composed of a single resonant nuclide of atomic density N_r and other non-resonant nuclides of density N_k for $k \neq r$. Let us further assume that the cross sections for the non-resonant nuclides are constant, and purely due to scattering (i.e. no absorption takes place). In this case the total cross section of a non-resonant isotope σ_k is equal to its scattering cross section $\sigma_{s,k}$. Furthermore, integrating over all angular directions, we have:

$$\Sigma_s(E'\to E) = \Sigma_s(E')P(E'\to E) \tag{1.65}$$

with:

$$P(E'\to E) = \begin{cases} \frac{1}{(1-\alpha)E'} & E \le E' \le E/\alpha \\ 0 & \text{else} \end{cases} \tag{1.66}$$

where $\alpha = \left(\frac{A-1}{A+1}\right)^2$, and A is the atomic number of the isotope in question. The Boltzmann equation 1.27 corresponding to the homogeneous mixture is written as [19, 20]:

$$\left(N_r\sigma_r(E) + \sum_{k\neq r} N_k\sigma_{s,k}\right)\phi(E) = \overbrace{\frac{1}{1-\alpha_r}\int_E^{E/\alpha_r} N_r\sigma_{s,r}(E')\phi(E')\frac{dE'}{E'}}^{\text{Scattering Source due to the resonant isotope}} + \underbrace{\sum_{k\neq r}\frac{1}{1-\alpha_k}\int_E^{E/\alpha_k} N_k\sigma_{s,k}\phi(E')\frac{dE'}{E'}}_{\text{Scattering Source due to the non-resonant moderator}} \tag{1.67}$$

The factor $\frac{1}{1-\alpha_k}$ with $\alpha_k = \left(\frac{A-1}{A+1}\right)^2$ appears due to the energy transfer function presented in equation 1.66. We note that in equation 1.67, only the cross section for the resonant isotope is assumed to have an energy dependence with the cross sections for the non-resonant isotopes assumed to be constant and equal to their potential cross section [19].

Simplifying the second term appearing on the right hand side of equation 1.67, requires additional assumptions. The narrow resonance approximation consists of assuming that the resonance width of the resonant nuclide r is narrow in comparison to the average energy loss of the neutron per collision. This implies that most neutrons that appear near the resonance peak energy are coming from outside of the resonance peak due to scattering from energies much higher than the resonance. If we assume that the neutron flux outside of the resonant region (the second integral on the right hand side of equation 1.67) has a $\frac{1}{E}$ shape, the sum in equation 1.67 simplifies to [20, 19]:

$$\begin{aligned}\sum_{k\neq r}\frac{1}{1-\alpha_k}\int_E^{E/\alpha_k} N_k\sigma_{s,k}\phi(E')\frac{dE'}{E'} &= \sum_{k\neq r}\frac{N_k\sigma_{s,k}}{1-\alpha_k}\int_E^{E/\alpha_k}\phi(E')\frac{dE'}{E'} \\ &\sim \sum_{k\neq r}\frac{N_k\sigma_{s,k}}{1-\alpha_k}\int_E^{E/\alpha_k}\frac{1}{E'}\frac{dE'}{E'} \\ &= \sum_{k\neq r} N_k\sigma_{s,k}\frac{1}{E}\end{aligned} \tag{1.68}$$

The first term appearing on the right hand side of equation 1.67 can be simplified by assuming that the scattering cross section of a resonant nuclide outside of its resonance is constant, and that the flux spectrum has a $1/E$ shape outside of this region. This term simplifies to:

$$\begin{aligned}\frac{1}{1-\alpha_r}\int_E^{E/\alpha_r} N_r\sigma_{s,r}(E')\phi(E')\frac{dE'}{E'} &\sim \frac{N_r\sigma_{s,r}}{1-\alpha_r}\int_E^{E/\alpha_r}\phi(E')\frac{dE;}{E'} \\ &\sim \frac{N_r\sigma_{s,r}}{1-\alpha_r}\int_E^{E/\alpha_r}\frac{1}{E'}\frac{dE'}{E'} = N_r\sigma_{s,r}\frac{1}{E}\end{aligned} \tag{1.69}$$

substitution of equations 1.69 and 1.68 into equation 1.67 gives:

$$\left(N_r\sigma_r(E) + \sum_{k\neq r} N_k\sigma_{s,k}\right)\phi(E) = \frac{N_r\sigma_{s,r} + \sum_{k\neq r} N_k\sigma_{s,k}}{E} \tag{1.70}$$

so that:

$$\begin{aligned}\phi(E) &= \frac{N_r\sigma_{s,r} + \sum_{k\neq r} N_k\sigma_{s,k}}{N_r\sigma_r(E) + \sum_{k\neq r} N_k\sigma_{s,k}}\frac{1}{E} \\ &= \frac{\sigma_{s,r} + \sigma_0}{\sigma_r(E) + \sigma_0}\frac{1}{E}\end{aligned} \tag{1.71}$$

where $\sigma_0 = \sum_{k\neq r}\frac{N_k}{N_r}\sigma_{s,k}$ is called the background/dilution cross section of the homogeneous mixture.

Equation 1.70 provides an analytical formulation for the form of the energy dependence of the neutron flux. We note that the absolute value of the neutron flux is not necessary as it enters equations 1.57 to 1.60 as a ratio ($f(E) = \phi(E)/\phi_g$). Finally, note that to arrive at the energy flux given by equation 1.71, we assumed that:

1. Only one resonant isotope is present (or more generally, no resonance overlap exists).
2. Scattering is elastic and the neutron energy is much higher than the thermal energy.
3. Non-resonant nuclide have a constant scattering cross section.
4. The resonant nuclide has a constant scattering cross section above the resonance.
5. The energy dependence of the neutron flux outside of the resonance has a $\frac{1}{E}$ shape (valid in the epithermal region).
6. The neutron source in the resonance region is due to neutrons coming from outside of the resonance (the resonance is narrow).

Slowing Down in a Heterogeneous Medium: Equivalence Theory

In heterogeneous systems, equivalence theory methods can be used to provide a relation between the slowing down flux in the heterogeneous medium and the slowing down flux in a homogeneous medium. This point will be further discussed in chapter 3. Typically, tabulated values of the group parameters defined in equations 1.57-1.60 are calculated using the fine flux function $f(E)$ of an infinite homogeneous medium for several different ratios of a dilution cross section σ_0 using the flux similar to that given in equation 1.71. Resonant self-shielding methods based on an equivalence principle [21] between a heterogeneous and a homogeneous geometry are then used during the lattice calculation to evaluate the equivalent group parameters corresponding to the homogeneous case. The methods usually involve expressing the fine flux (or the more useful resonance integral I) of the heterogeneous case $f^{HET}(E)$ as a linear combination of homogeneous fine-structure

functions f_n^{HOM} each corresponding to a specific concentration of the resonant isotope so that [21]: [6]

$$f(E) = \sum_{n=1}^{N} \alpha_n(E) f_n^{HOM}(E) \tag{1.72}$$

The treatment can be quite accurate, with [21] reporting an average error of 1.5% (using 22 groups over the resonance region) on the absorption rate when comparing against hyper fine (with 1561 groups over the resonance region) calculations.

1.4.2 Discretized Flux Equations

Discretization

To obtain a numerical solution for the transport equation 1.61, we divide the domain D into N_V regions with volume V_i, and the external boundary ∂D into N_S surfaces S_α. We first define the scalar flux $\phi_{i,g}$ for energy group g, inside the region i as the average of the flux $\phi_g(\vec{r})$ over the region so that:

$$\phi_{i,g} = \frac{1}{V_i} \int_{V_i} \phi_g(\vec{r}) d^3r \tag{1.73}$$

Next, we will assume that the cross sections and the collision source operator within each volume region are constant, so that [12]:

$$\Sigma_x^g(\vec{r}) = \Sigma_{x,j}^g \text{ for } \vec{r} \in V_j \text{ and reaction type } x \tag{1.74}$$

$$q^{g' \to g}(\vec{r}) = q_j^{g' \to g} = \sum_{g'} \left(\frac{\chi_{g,j}}{4\pi k_{eff}} \nu \Sigma_{f,j}^{g'} + \Sigma_{s,j}^{g' \to g} \right) \phi_{j,g'} \qquad \text{for } \vec{r} \in V_j \tag{1.75}$$

Next, the surface flux $\phi_{+,g}$ and $\phi_{-,g}$ which appear in equation 1.51 and 1.64 are approximated by a series expansion in terms of the half-range spherical harmonics $\psi^\nu(\hat{\Omega}, \hat{n}_\pm)$, so that [92, 12]:

$$\phi_{\pm,g}(\vec{r_S}, \hat{\Omega}) = \frac{1}{4\pi} \sum_{\nu=0}^{N_\nu} \phi_{\pm,g}^\nu(\vec{r_S}) \psi^\nu(\hat{\Omega}, \hat{N}_\pm) \tag{1.76}$$

where we have truncated the series at $N_\nu = 3$. The half-range spherical harmonics $\psi^\nu(\hat{\Omega}, \hat{N}_\pm)$ which appear in equation 1.76 are defined as [92, 12]:

$$\psi^\nu(\hat{\Omega}, \hat{N}_\pm) = \begin{cases} 1 & \text{for } \nu = 0 \\ \sqrt{2}(3\hat{\Omega} \cdot \hat{N}_\pm^1 - 2) & \text{for } \nu = 1 \\ 2\hat{\Omega} \cdot \hat{N}_\pm^2 & \text{for } \nu = 2 \\ 2\hat{\Omega} \cdot \hat{N}_\pm^3 & \text{for } \nu = 3 \end{cases} \tag{1.77}$$

with the normal vector $\hat{N}_\pm^1 = \hat{N}_\pm$ being the inward normal to the surface S_α, and the

[6] Usually the relation is given in terms of the Resonance integral $I_{(n,ABS)}^{HOM} = C \int_E dE \Sigma_{(n,ABS)}(E) \phi(E) \frac{1}{E}$, as in reality, this is the parameter available in the library and what is interpolated.

vectors $\hat{N}_{\pm}^2$, and $\hat{N}_{\pm}^3$ chosen such that $\left\{\hat{N}_{\pm}^1, \hat{N}_{\pm}^2, \hat{N}_{\pm}^3\right\}$ forms a three dimensional orthogonal bases on the surface S_α. The half-range spherical harmonics satisfy the orthogonality relation given by [92, 12]:

$$\int_{(\hat{\Omega}\cdot\hat{N}_{\pm})>0} (\hat{\Omega}\cdot\hat{N}_{\pm})\psi^{\nu}(\hat{\Omega},\hat{N}_{\pm})\psi^{\mu}(\hat{\Omega},\hat{N}_{\pm})d\hat{\Omega} = \pi\delta_{\mu}^{\nu} \tag{1.78}$$

where δ_{μ}^{ν} is the Kronecker delta function. Taking the inner product of equation 1.76 with the half range spherical harmonic $\psi^{\nu}(\hat{\Omega},\hat{N}_{\pm})$ over the surface element S_α, we can see that the average angular flux components $\phi_{\pm,g}^{\nu,\alpha}$ in the energy group g is defined as [12, 92]:

$$\phi_{\pm,g}^{\nu,\alpha} = \frac{4}{S_\alpha}\int_{S_\alpha} dA_{S_\alpha} \int_{(\hat{\Omega}\cdot\hat{N}_{\pm})>0} d\hat{\Omega}(\hat{\Omega}\cdot\hat{N}_{-})\psi^{\nu}(\hat{\Omega},\hat{N}_{\pm})\phi_{\pm,g}(\vec{r}_S,\hat{\Omega}) \tag{1.79}$$

where dA_{S_α} is the differential surface element on the surface S_α. Integrating the integral form of the transport equation given by equation 1.61, and using equation 1.73 and equation 1.79 for the average flux inside the region j and on the surface S_α respectively, we arrive at the discretized form of the integral transport equation [12]:

$$\begin{aligned} V_i\phi_{i,g} = &\sum_{\alpha=1}^{N_S}\sum_{\nu=0}^{N_\nu}\phi_{-,g}^{\nu,\alpha}\int_{\vec{r}\in V_i}\int_{\vec{r}_S\in S_\alpha}\frac{e^{-\tau^g(s_S)}}{4\pi s_S^2}(\hat{\Omega}\cdot\hat{N}_{-})\psi^{\nu}(\hat{\Omega},\hat{N}_{-})d\vec{r}dA_{S_\alpha} \\ &+\sum_{g'}\sum_{j=1}^{N_V} q_j^{g'\to g}\int_{\vec{r}\in V_i}\int_{\vec{r}'\in V_j}\frac{e^{-\tau^g(s)}}{s^2}d\vec{r}'d\vec{r} \end{aligned} \tag{1.80}$$

The discretized form of equation 1.64 can be obtained by taking the average of outgoing angular flux over the surface S_α; integrating over the surface S_α we have [12]:

$$\begin{aligned} \frac{S_\alpha}{4}\phi_{+,g}^{\nu} = &\sum_{\beta=1}^{N_S}\sum_{\mu=0}^{N_\nu}\phi_{-,g}^{\mu,\beta}\int_{S_\alpha}\int_{S_\beta}\frac{e^{-\tau^g(s_S)}}{4\pi s_S^2}(\hat{\Omega}\cdot\hat{N}_{+})\psi^{\nu}(\hat{\Omega}\cdot\hat{N}_{+})\psi^{\mu}(\hat{\Omega}\cdot\hat{N}_{-})\ dA_{S_\beta}\ dA_{S_\alpha} \\ &+\sum_{j=1}^{N_V} q_j^{g'\to g}\int_{S_\alpha}\int_{\vec{r}'\in V_j}\frac{e^{-\tau^g(s)}}{s^2}(\hat{\Omega}\cdot\hat{N}_{-})\psi^{\nu}(\hat{\Omega},\hat{N}_{+})\psi^{\nu}(\hat{\Omega},\hat{N}_{+})\ d\vec{r}'\ dA_{S_\alpha} \end{aligned} \tag{1.81}$$

Equations 1.80 and 1.81 are the discretized form of the integral transport equation given by equations 1.61 and 1.64. We will now proceed to put equations 1.80 and 1.81 in their matrix form by defining the concept of the collision probability.

Reduced Collision Probabilities

The reduced collision probability is the space or surface integrated form of the first flight kernel $\mathfrak{J}$ presented in equation 1.63. From equations 1.80 and equation 1.81, we see that we can separate four types of coefficients, all of which involve space or surface integrals of the first flight kernel $\mathfrak{J}$. These coefficients are called the reduced collision probabilities

and can be defined as [12]:

$$p_{ij}^{g} = \frac{1}{V_i}\int_{\vec{r}\in V_i}\int_{\vec{r'}\in V_j}\frac{e^{-\tau^g(s)}}{s^2}d\vec{r'}d\vec{r} \tag{1.82}$$

$$p_{i\alpha}^{\nu,g} = \frac{1}{V_i}\int_{\vec{r'}\in V_i}\int_{S_\alpha}\frac{e^{-\tau^g(s_S)}}{4\pi s_S^2}(\hat{\Omega}\cdot\hat{N}_-)\psi^\nu(\hat{\Omega},\hat{N}_-)d\vec{r'}dA_{S_\alpha} \tag{1.83}$$

$$p_{\alpha i}^{\nu,g} = \frac{4}{S_\alpha}\int_{S_\alpha}\int_{\vec{r}\in V_i}\frac{e^{-\tau^g(s)}}{s^2}(\hat{\Omega}\cdot\hat{N}_+)\psi^\nu(\hat{\Omega},\hat{N}_+)dA_{s_\alpha}d\vec{r} \tag{1.84}$$

$$p_{\alpha\beta}^{\nu\mu,g} = \frac{4}{S_\alpha}\int_{S_\alpha}\int_{S_\beta}\frac{e^{-\tau^g((s_S)}}{4\pi s_S^2}(\hat{\Omega}\cdot\hat{N}_-)(\hat{\Omega}\cdot\hat{N}_+)\psi^\nu(\hat{\Omega},\hat{N}_+)\psi^\mu(\hat{\Omega},\hat{N}_+)dA_{S_\alpha}dA_{S_\beta} \tag{1.85}$$

Rewriting equations 1.80 and equation 1.81 by using the definitions for the reduced collision probabilities defined in equations 1.82 to 1.85 gives [12]:

$$\phi_{i,g} = \sum_{\alpha=1}^{N_S}\sum_{\mu=0}^{N_\nu}p_{i\alpha}^{\mu,g}\phi_{-,g}^{\mu,\alpha} + \sum_{j=1}^{N_V}\sum_{g'=1}^{N_G}p_{ij}^{g}Q_{j,g} \tag{1.86}$$

$$\phi_{+,g}^{\nu,\alpha} = \sum_{\beta=1}^{N_S}\sum_{\mu=0}^{N_\nu}p_{\alpha\beta}^{\nu\mu,g}\phi_{-,g}^{\mu,\beta} + \sum_{g'=1}^{N_G}\sum_{j=1}^{N_V}p_{\alpha j}^{\nu,g}Q_{j,g} \tag{1.87}$$

where $Q_{j,g} = \sum_{g'} q_j^{g'\to g}$ is the neutron source in volume j and energy group g.

The reduced region to region collision probabilities p_{ij}^g represent the probability that a neutron in region i will reach region j. Similarly for the reduced region to surface, surface to region, and surface to surface collision probabilities $p_{i\alpha}^g$, $p_{\alpha j}^g$, and $p_{\alpha\beta}^g$ which represent the probability of the neutron at the region/surface denoted by the first index will reach the region/surface denoted by the second index.

Theorems of Reciprocity

From the symmetry principle of the first flight kernel given by equation 1.43 it is possible to derive directly the following reciprocity relations for the reduced collision probability [12]:

$$V_i p_{ij} = V_j p_{ji} \tag{1.88}$$

$$V_i p_{i\alpha}^{\nu} = S_\alpha p_{\alpha i}^{\nu} \tag{1.89}$$

$$S_\alpha p_{\alpha\beta}^{\nu\mu} = S_\beta p_{\beta\alpha}^{\mu\nu} \tag{1.90}$$

Multiplying equation 1.86 by the volume V_i, and equation 1.87 by the surface area S_α and using equations 1.94-1.90 we have:

$$V_i\phi_{i,g} = \overbrace{\sum_{\alpha=1}^{N_S}\sum_{\mu=0}^{N_\nu} S_\alpha p_{\alpha i}^{\mu,g}\phi_{-,g}^{\mu,\alpha}}^{\text{contribution from the incoming surface current}} + \overbrace{\sum_{j=1}^{N_V}\sum_{g'=1}^{N_G} V_j p_{ji}^{g} Q_{j,g}}^{\text{contribution from the collision source}} \tag{1.91}$$

$$S_\alpha\phi_{+,g}^{\nu,\alpha} = \underbrace{\sum_{\beta=1}^{N_S}\sum_{\mu=0}^{N_\nu} S_\beta p_{\beta\alpha}^{\nu\mu,g}\phi_{-,g}^{\mu,\beta}}_{\text{Contribution from the incoming surface current}} + \underbrace{\sum_{g'=1}^{N_G}\sum_{j=1}^{N_V} V_j p_{\alpha j}^{\nu,g} Q_{j,g}}_{\text{Contribution from the collision source}} \tag{1.92}$$

Noting that the volume D and the boundary ∂D were partitioned into the sub-volumes V_i and surfaces S_α (i.e. $D = \bigcup_{i=1}^{N_V}$ and $\partial D = \bigcup_{\alpha=1}^{N_S} S_\alpha$), we see that equation 1.91 and 1.92 represent conservation laws for the volume integrated flux and the surface integrated current. Equation 1.91 states that the volume integrated flux in volume i at group g is the sum of the surface integrated incoming current (weighted by the probability that the incoming neutron will reach volume i) and the volume integrated collision source (weighted by the probability that the neutron born from the collision source will reach volume i). Similarly, equations 1.92 states that the total surface integrated outgoing current at surface S_α is the sum of the neutron current entering volume D (weighted by the probability that these neutrons will reach the surface S_α) and the total volume integrated neutron source inside the volume D (weighted by the probability that these neutrons will reach the surface α).

Matrix Form

In matrix notation, equations 1.86 and 1.87 can be written as:

$$\vec{\phi} = \mathbf{P_{VS}}\vec{J}_- + \mathbf{P_{VV}}\vec{Q} \tag{1.93}$$

$$\vec{J}_+ = \mathbf{P_{SS}}\vec{J}_- + \mathbf{P_{SV}}\vec{Q} \tag{1.94}$$

Here, $\vec{J}_+$ and $\vec{J}_-$ refer to the vectors of the outgoing and incoming currents respectively, the flux vector $\vec{\phi}$ refers to the vector containing the region-energy flux components, and the source $\vec{Q} = (\sum_{g'} q_{j,g'\to g})$ is the vector containing the neutron source in region j and energy group g. The flux vector $\vec{\phi}$ and the collision source $\vec{Q}$ are therefore of the size $N_V \times N_G$ and the vectors $\vec{J}_-$ and $\vec{J}_+$ are of the size $(N_\nu+1)\times N_S \times N_G$. Here N_G refers to the number of energy groups available on the multi-group library. The matrix $\mathbf{P_{VV}}$ is then composed of N_G energy blocks of $(N_V \times N_V)$ matrices containing the volume to volume reduced collision probabilities p_{ij}^g. Similarly, the matrix $\mathbf{P_{SV}}$ is composed of N_G energy blocks of $(N_\nu + 1) \times N_S \times N_V$ matrices containing volume to surface reduced collision probabilities $(p_{\alpha j}^{\nu,g})$, $\mathbf{P_{SS}}$ is composed of N_G blocks of $((N_\nu+1)\times N_S)^2$ matrices containing the surface to surface reduced collision probabilities $p_{\alpha\beta}^{\mu\mu,g}$, and $\mathbf{P_{VS}}$ is composed of N_G energy blocks of $(N_V \times (N_\nu+1)\times N_S)^2$ matrices containing the surface to volume collision probabilities $p_{i\alpha}^{\mu,g}$.

Boundary Conditions

Associated with the transport equation 1.86 and 1.87 are boundary conditions of the form given by equation 1.13. In this work, we will cover the two most common boundary conditions when performing lattice computations: void boundary conditions and specular reflective boundary conditions. For both of these cases, the transport equation 1.86 and 1.87 can be greatly simplified.

- **Void BC** In the case of void boundary conditions, the incoming current $\vec{J}_- = 0$ at the surface boundary so that equation 1.93 reduces to:

$$\vec{\phi} = \cancelto{0}{\mathbf{P_{VS}}\vec{J}_-} + \mathbf{P_{VV}}\vec{Q} = \mathbf{P}\vec{Q} \tag{1.95}$$

  where the equivalent collision probability matrix $\mathbf{P}$ is defined as $\mathbf{P} = \mathbf{P}_{VV}$.

- **Specular Reflection** In the case of reflective boundary conditions, two options can be used:

  1. The incoming current $\vec{J}_-$ is equal to the outgoing current $\vec{J}_+$. Substituting $\vec{J}_+ = \vec{J}_-$ into equation 1.94 and solving for $\vec{J}_-$ we arrive at:

$$\vec{\phi} = \mathbf{P} \cdot \vec{Q} \tag{1.96}$$

     where the new collision probability matrix $\mathbf{P}$ is defined to as [12]:

$$\mathbf{P} = (\mathbf{P_{VV}} + \mathbf{P_{VS}} \cdot (\mathbf{I} - \mathbf{P_{SS}})^{-1} \cdot \mathbf{P_{SV}}) \tag{1.97}$$

  2. The more common (and more accurate) method which avoids the finite expansion for the angular flux in terms of the half range spherical harmonics given by equation 1.76 is to unfold the cell and compute the collision probability matrix $\mathbf{P} = \mathbf{P_{VV}}$ for the unfolded cell (infinite geometry). The flux then satisfies:

$$\vec{\phi} = \mathbf{P} \cdot \vec{Q} \tag{1.98}$$

The key point being that in both cases, the boundary conditions can be taken directly into account by defining an equivalent collision probability matrix $\mathbf{P}$ so that:

$$\vec{\phi} = \mathbf{P} \cdot \vec{Q} \tag{1.99}$$

Standard Form

The standard form of the transport equation refers to the eigenvalue problem usually written as:

$$(\mathbf{A} - \lambda\mathbf{B}) \cdot \vec{\phi} = 0 \tag{1.100}$$

where $\lambda = \frac{1}{k_{eff}}$ and $\mathbf{A}$ and $\mathbf{B}$ are the corresponding operators of the Boltzmann equation. Equation 1.100 is the difference between the net neutrons lost (due to leakage and net absorption), and the neutrons gained from fission. To write equation 1.99, we first note

that the collision source $\vec{Q}$ is by definition given as:

$$\vec{Q} = (\mathbf{S} + \lambda\mathbf{F}) \cdot \vec{\phi} \tag{1.101}$$

Here, $\mathbf{S}$ is the scattering matrix and $\mathbf{F}$ is the fission matrix. These matrices are composed of $N_V \times N_V$ blocks of $(N_G \times N_G)$ matrices and are dense in energy and diagonal in space, have components corresponding to the regional scattering matrix $\mathbf{S}_i = (\Sigma_{s,g'\to g})_i$ and the fission matrix $\mathbf{F}_i = (\overrightarrow{\chi^T} \cdot \overrightarrow{\nu\Sigma_F})_i = (\chi_g \nu\Sigma_{f,g'})_i$ for $i = 1, N_V$. The matrix equation satisfied by the flux is then:

$$\vec{\phi} = \mathbf{P}(\mathbf{\Sigma})\,(\mathbf{S} + \lambda\mathbf{F})\,\vec{\phi} \tag{1.102}$$

where $\mathbf{\Sigma} = (\Sigma_g)_i$ is the regional total cross section matrix (diagonal in energy and space) and has been included in the formula to note the explicit dependence of the collision probability matrix on the total cross section $\mathbf{\Sigma}$. We note that the total cross section and the scattering matrix $\mathbf{S}$ appearing in equation 1.102 are transport corrected according to procedure outlined in section 1.3.2. The standard form of the transport equation given by equation 1.102 is then:

$$(\mathbf{A} - \lambda\mathbf{B})\,\vec{\phi} = 0 \text{ where} \tag{1.103}$$

$$\mathbf{A} = \mathbf{I} - \mathbf{P}(\mathbf{\Sigma})\cdot\mathbf{S} \tag{1.104}$$

$$\mathbf{B} = \mathbf{P}(\mathbf{\Sigma}) \cdot \mathbf{F} \tag{1.105}$$

here $\mathbf{I}$ refers to the $(N_V \times N_G)^2$ identity matrix.

1.5 Adjoint Equations

The adjoint formalism is the basis for the sensitivity approach to uncertainty analysis. In this section, we begin with the definition of adjoint operators in infinite dimensional vector spaces, followed by the equivalent form of the operators in finite dimensional vector spaces. We will then present a discussion on the physical interpretation of the adjoint function, at which point we will proceed to derive the adjoint equations corresponding to the integral and integro-differential forms of the Boltzmann equation and the relationship between the two.

1.5.1 Adjoint Operators

In mathematics, an inner product space $\mathbb{V}$ [23] is a vector space equipped with an inner product $\langle \square, \square \rangle$ satisfying the conditions of symmetry (or conjugate symmetry if complex spaces are considered), linearity, and positive-definiteness. Given any two functions $f(\bar{\rho}) \in \mathbb{V}^\dagger$ and $g(\bar{\rho}) \in \mathbb{V}$, belonging to the vector spaces $\mathbb{V}^\dagger$, and $\mathbb{V}$ respectively, the inner product $\langle f(\bar{\rho}), g(\bar{\rho}) \rangle : \mathbb{V}^\dagger \times \mathbb{V} \to \mathbb{R}$ can be thought of as a mapping from the set of direct products $\mathbb{V}^\dagger \times \mathbb{V}$ to the real numbers. Here $\mathbb{V}^\dagger$ denotes the dual space of $\mathbb{V}$. The vector space of our interest is the space of all differentiable and uniformly bounded functions over the domain D.

Adjoint Operators in Infinite Dimensional Vector Spaces

In reactor physics, the principle observable is a detector reading which is usually expressed in terms of a reaction rate so that the inner product can be defined as:

$$\langle f(\bar{\rho}), g(\bar{\rho})\rangle = \int_{\bar{\rho}} d\bar{\rho} f(\bar{\rho}) g(\bar{\rho}) \tag{1.106}$$

where $\bar{\rho} = (\vec{r}, \hat{\Omega}, E)$ and the integration is over the region $\vec{r} \in D$, and all angular directions $\hat{\Omega} \in 4\pi$ and all energies $E \in [0, \infty)$. Considering a linear operator $\mathbf{A}$ acting on the function $g(\bar{\rho})$, we can think of a corresponding adjoint operator $\mathbf{A}^\dagger$ acting on the dual space $V^\dagger$ such that:

$$\langle f(\bar{\rho}), \mathbf{A} g(\bar{\rho})\rangle = \left\langle \mathbf{A}^\dagger f(\bar{\rho}), g(\bar{\rho})\right\rangle \tag{1.107}$$

Based on the definition 1.107, it is possible to derive expressions for adjoint operators. In particular, for the inner product defined in 1.106, provided that conditions at the boundary of domain ∂D are chosen so as to eliminate any surface terms that may appear, we can derive adjoints for various operators. For differential operators, the adjoint operator can be derived from integration by parts and satisfies:

$$\mathbf{A} g \equiv \nabla^\alpha g \rightarrow \mathbf{A}^\dagger f = (-1)^\alpha \nabla^\alpha f \tag{1.108}$$

where $\alpha \in \mathbb{N}$. From definition 1.107, adjoint of convolution operators can be obtained by a simple change in the order of the convolution, so that:

$$\mathbf{A} g(\bar{\rho}) = \int d\bar{\rho}' \mathfrak{J}(\bar{\rho}' \rightarrow \bar{\rho}) g(\bar{\rho}') \rightarrow \mathbf{A}^\dagger f(\bar{\rho}) = \int d\bar{\rho}' \mathfrak{J}(\bar{\rho} \rightarrow \bar{\rho}') f(\bar{\rho}') \tag{1.109}$$

The adjoint of scalar operators is identical to the original operator by merit of equation 1.107.

Adjoint Operators for Finite Dimensional Vector Spaces

In section 1.4.1, using the multi-group approximation, we discretized the energy domain into N_G energy groups. Similarly, in section 1.4.2 we discretized the spatial dimension into N_V volumes. Functions and distributions in space and energy (such as the cross section and the scalar flux) were then discretized as vectors of dimension $\mathbb{R}^{N_G \times N_V}$, and took the form:

$$\vec{F} = \overbrace{\left(\overbrace{F_1^1, ..., F_{N_V}^1}^{N_V}, ..., \overbrace{F_1^G, ..., F_{N_V}^G}^{N_V}\right)}^{N_G} \tag{1.110}$$

$$\vec{D} = \overbrace{\left(\overbrace{D_1^1, ..., D_{N_V}^1}^{N_V}, ..., \overbrace{D_1^G, ..., D_{N_V}^G}^{N_V}\right)}^{N_G} \tag{1.111}$$

The spatial and regional components of a distribution $D(\vec{r}, E)$ can be defined to be the integral of their values over the energy groups, and averages over regions, i.e.

$$D(\vec{r}, E) \rightarrow \frac{1}{V_i} \int_{\vec{r} \in V_i} d\vec{r} \int_{E_g}^{E_{g-1}} dE D(\vec{r}, E) \equiv D_i^g \tag{1.112}$$

for example, the flux represents such a distribution function.

Similar to the multi-group approximations, we note that a function $F(\vec{r}, E)$ (such as a cross section) can be discretized in space and in energy, using the weighting given by the distribution $D(\vec{r}, E)$:

$$F(\vec{r}, E) \rightarrow \frac{1}{D_i^g} \int_{E_g}^{E_{g-1}} dE F(\vec{r}, E) D(\vec{r}, E) \tag{1.113}$$

Integrals in energy can then be discretized as sums in energy, and integrals in space can be discretized into sums of the average value over the regional volume V_i. Using equations 1.112 and 1.113, the vector inner product corresponding to the reaction rate then becomes [24]:

$$\begin{aligned} \langle F(\vec{r}, E), D(\vec{r}, E) \rangle \equiv \int_{E'} dE' \int_{\vec{r'} \in D} d\vec{r} (F(\vec{r}, E) D(\vec{r}, E)) \\ \longrightarrow \sum_{g=1}^{N_G} \sum_{i=1}^{N_V} F_i^g V_i D_i^g = \vec{F}^T \cdot \mathbf{V} \cdot \vec{D} \equiv \left\langle \vec{F}, \vec{D} \right\rangle \end{aligned} \tag{1.114}$$

To preserve the inner product, we can then define the adjoint operator as [15, 24]:

$$\mathbf{A}^\dagger = \mathbf{V}^{-1} \cdot \mathbf{A}^\mathbf{T} \cdot \mathbf{V} \tag{1.115}$$

where $^\mathbf{T}$ refers to matrix transposition. It can be seen that with the adjoint $\mathbf{A}^\dagger$ of the operator $\mathbf{A}$ defined by 1.115 satisfies [24]:

$$\begin{aligned} \left\langle \mathbf{A}^\dagger \vec{F}, \vec{D} \right\rangle &= \left(\mathbf{V^{-1}} \cdot \mathbf{A^T} \cdot \mathbf{V} \cdot \vec{F} \right)^T \cdot \mathbf{V} \cdot \vec{D} \\ &= \vec{F^T} \cdot \left(\mathbf{V} \cdot \mathbf{A} \cdot \mathbf{V^{-1}} \right) \cdot \mathbf{V} \cdot \vec{D} \\ &= \vec{F^T} \cdot \mathbf{V} \cdot \mathbf{A} \cdot \vec{D} = \left\langle \vec{F}, \mathbf{A} \cdot \vec{D} \right\rangle \end{aligned} \tag{1.116}$$

where the second equality was obtained from the diagonal nature of the volume matrix ($\mathbf{V} = \mathbf{V^T}$).

1.5.2 The Classical Adjoint

Importance: the Adjoint Function

In describing physical observables, one must consider the fashion in which the experiment is conducted to measure the observable of interest (i.e. the nature and the configuration of the detectors used to measure the observable). For each observable - be it criticality, a detector reading, etc. we can think of a form of measurement/a hypothetical detector,

which can be used to measure the observable at a specific time t_f. We note that a neutron at earlier time $t < t_f$ can contribute to this detector reading either by interacting directly with the detector at time t_f or through its *progenies* who can also interact with the detector and contribute to the detector reading. The *progeny* of a neutron being defined as all those neutrons who trace back their life-cycle to the original neutron (i.e. the neutrons that are created from the interaction of the original neutron with the medium). We can define an importance function $\phi^\dagger$ (called a detector distribution function [25]) which provides a measure of the *importance*/contribution of a neutron to the detector reading [25]. A key principle in perturbation theory, introduced by Usachev [7] and discussed by Lewins [25], is the principle of the conservation of importance which states [7, 25]:

Axiom. Conservation of Importance: A neutron is as important as its progenies.

The axiom of conservation of importance ensures that a particle at time t contributes to the detector reading at the later time t_f only through its progenies, and that the importance of these neutrons is conserved [25].

The basic properties of this importance function $\phi^\dagger$ can then be derived from the properties under which the hypothetical experiment (or detector) operates. For example, since the detector reading depends on the population of the neutrons in the reactor (i.e. the neutron flux $\phi(\bar{\rho})$), we can expect the detector importance function $\phi^\dagger$ to depend solely on the same variables that the neutron flux $\phi(\bar{\rho})$ depends on. Also, since we should not expect to measure any observables other than those expressed in terms of the neutron flux, we should not expect the importance function $\phi^\dagger$ to depend on any variables other than those that the neutron flux depends on, so that $\phi^\dagger = \phi^\dagger(\bar{\rho})$. Similarly, our knowledge of the detector importance function $\phi^\dagger(\bar{\rho})$ is limited to the domain D in which the neutron population is computed (i.e. the region where the experiment takes place). A neutron outside of this domain does not contribute to the detector reading so that the importance function $\phi^\dagger(\bar{\rho})$ should vanish outside of D. The boundary conditions for the detector distribution can also be derived from the behavior of the neutron population at the boundary; if the conditions at the boundary are such that a neutron leaving the domain, will not enter (i.e. $\vec{J}_{-,\partial D} = 0$ where $\vec{J}_{-,\partial D}$ is the incoming current at the domain boundary ∂D), then the importance for the neutrons leaving the boundary ∂D vanishes so that $J^\dagger_{+,\partial D} = 0$. Here, $J^\dagger_{+,\partial D}$ denotes the net importance of the neutrons leaving the surface.

In his 1965 book [25], based on the variational principle, Lewins provides a comprehensive formulation that discusses the logical equality between the adjoint function and the detector importance function. The integro-differential adjoint function, which minimizes the energy density for the variational form of the Boltzmann equation, is interpreted as the importance of the neutron to the hypothetical detector reading/observable.

We will see in the following passages, that depending on the specific formalism used for the Boltzmann equation, the physical interpretation of the adjoint function will be somewhat different.

Integro-differential Formulation

The integro-differential form of the Boltzmann equation was presented earlier in equation 1.10. In the absence of the fixed source Q_e, and using the transport corrected form of the scattering and total cross sections so as to remove the angular dependence of the collision source we have:

$$\hat{\Omega} \cdot \vec{\nabla}\phi(\vec{r}, \hat{\Omega}, E) + \Sigma(\vec{r}, E)\phi(\vec{r}, \hat{\Omega}, E) = Q(\vec{r}, E) = \int dE' q(\vec{r}, E' \to E) \tag{1.117}$$

where q was defined as:

$$q(\vec{r}, E' \to E) = \frac{\chi(\vec{r}, E)\nu\Sigma_f(\vec{r}, E')}{4\pi k_{eff}}\phi(\vec{r}, E') + \frac{1}{4\pi}\Sigma_s(\vec{r}, E' \to E)\phi(\vec{r}, E') \tag{1.118}$$

by using the relations given by equations 1.108 and 1.109, the adjoint of equation 1.117 is derived to be [8]:

$$-\hat{\Omega} \cdot \nabla\phi^\dagger(\vec{r}, \hat{\Omega}, E) + \Sigma(\vec{r}, E)\phi^\dagger(\vec{r}, \hat{\Omega}, E) = \int_{E'} dE' q^\dagger(\vec{r}, E' \to E) \tag{1.119}$$

where:

$$q^\dagger(\vec{r}, E' \to E) = \frac{\chi(\vec{r}, E')\nu\Sigma_f(\vec{r}, E)}{4\pi k_{eff}}\phi(\vec{r}, E') + \frac{1}{4\pi}\Sigma_s(\vec{r}, E \to E')\phi(\vec{r}, E') \tag{1.120}$$

$\phi^\dagger(\vec{r}, \hat{\Omega}, E)$ is the adjoint flux pertaining to the solution of the integro-differential Boltzmann equation 1.117. Lewins [25] interprets the adjoint flux $\phi^\dagger(\vec{r}, \hat{\Omega}, E)$ as the total *number* of neutrons added ultimately to the critical reactor originating from one neutron source at the phase space position $\bar{\rho} = (\vec{r}, \hat{\Omega}, E)$, i.e. the sum of all the *progenies* of the neutron at the phase space $\bar{\rho}$; The function $\phi^\dagger$ is generally called [25, 15] the *source importance function*. Weighting the source importance function by the neutron flux, i.e. $\left\langle \phi^\dagger(\bar{\rho}), \phi(\bar{\rho}) \right\rangle$ gives the ultimate contribution of the neutron flux to the *total neutron density* [25].

Integral Formulation

The integral equation for the neutron flux was given by equation 1.39 and can be written as:

$$\phi(\vec{r}, E) = \int_{\vec{r'}} d\vec{r'} \int_{\hat{\Omega}\in 4\pi} d\hat{\Omega} \int_{E'} dE' \; \mathfrak{I}(E; \vec{r'} \to \vec{r})\delta(\hat{\Omega} - \frac{\vec{r} - \vec{r'}}{|\vec{r} - \vec{r'}|}) \cdot q(\vec{r}, E' \to E) \tag{1.121}$$

where for simplicity we have ignored the surface source appearing in equation 1.33. The neutron source appearing $q(\vec{r}, E' \to E)$ is defined by equation 1.118 and the first flight kernel $\mathfrak{I}(E; \vec{r'} \to \vec{r})$ was given in equation 1.38 as:

$$\mathfrak{I}(E; \vec{r'} \to \vec{r}) = \frac{\exp\left[-\int_{\vec{r'}}^{\vec{r}} ds \Sigma(\vec{s}, E)\delta\left(\frac{\vec{s}}{s} - \frac{\vec{r}-\vec{r'}}{|\vec{r}-\vec{r'}|}\right)\right]}{|\vec{r}-\vec{r'}|^2} \tag{1.122}$$

with the parameterization $\vec{s} = s\hat{\Omega}$. By using relations 1.108 and 1.109, it can be seen that the adjoint of the integral Boltzmann equation 1.121 satisfies [15]:

$$\psi^\dagger(\vec{r}, E) = \int_{\vec{r'}} d\vec{r'} \int_{\hat{\Omega}' \in 4\pi} d\hat{\Omega} \int_{E'} dE' \mathfrak{I}(E'; \vec{r} \to \vec{r'}) \delta(\hat{\Omega} - \frac{\vec{r}-\vec{r'}}{|\vec{r}-\vec{r'}|}) \cdot q^\dagger(\vec{r'}, E' \to E) \tag{1.123}$$

where $q^\dagger$ was defined in equation 1.120.

It has been noted by Lewins [25] that the adjoint of the integral Boltzmann equation has a different physical interpretation than the adjoint of the integro-differential Boltzmann equation. In particular, the adjoint of the integral equation, $\psi^\dagger(\vec{r}, E)$, also called the *flux importance function*, is interpreted to be the total *flux* of neutrons added to the critical reactor as a result of *a unit flux* of neutrons at the phase space $\bar{\rho}$ [26, 15]. Equation 1.123 is then an equation of conservation of importance. It states that the flux importance function at position $\bar{\rho}$ is the sum of the flux importances of all those neutrons which have scattered from energies E to energy groups E' and traveled from the point $\vec{r}$ to $\vec{r'}$ (i.e. the sum of all the progenies); this is represented as the product of the first flight kernel with the collision source. Weighting the flux importance function with the flux $\phi(\bar{\rho})$, i.e. $\left\langle \psi^\dagger(\vec{r}, E), \phi(\vec{r}, E) \right\rangle$, and using equation 1.123 gives the ultimate contribution of the *neutron source* to the *total neutron flux* in the reactor [15, 25].

Relation between the flux importance and the source importance function

The source importance function $\phi^\dagger(\vec{\rho})$ was interpreted as the contribution of a unit neutron source at the phase space $\bar{\rho}$ to the total neutron density. The flux importance function $\psi^\dagger$ was interpreted as the contribution of a unit flux at phase space $\bar{\rho}$ to the total flux density. Since the neutron flux $\phi(\bar{\rho})$ is the product of the neutron source $N(\bar{\rho})$ with the velocity, it is then clear that:

$$\frac{\left\langle 1, \phi^\dagger(\bar{\rho}) \right\rangle}{\langle 1, \psi^\dagger(\bar{\rho}) \rangle} = \frac{1}{\bar{v}} \tag{1.124}$$

where $\bar{v}$ is the average neutron velocity. The two importance functions then satisfy [15]:

$$\phi^\dagger(\vec{r}, E) = \frac{1}{\bar{v}} \int_{\hat{\Omega} \in 4\pi} d\hat{\Omega} \int_{\vec{r'} \in D} d\vec{r'} \mathfrak{I}(E; \vec{r} \to \vec{r'}) \delta\left(\hat{\Omega} - \frac{\vec{r'}-\vec{r}}{|\vec{r'}-\vec{r}|}\right) \psi^\dagger(\vec{r'}, E) \tag{1.125}$$

taking the inner product of 1.125 by the collision source $\int_{E'} dE' q(\vec{r}, E' \rightarrow E)$, and re-arranging some of the integrals, we have:

$$\left\langle \phi^\dagger(\vec{r}, E), \int_{E'} dE' q(\vec{r}, E' \rightarrow E) \right\rangle \tag{1.126}$$

$$= \frac{1}{\bar{v}} \left\langle \int_{\hat{\Omega} \in 4\pi} d\hat{\Omega} \int_{\vec{r'} \in D} d\vec{r'} \mathfrak{I}(E; \vec{r} \rightarrow \vec{r'}) \delta \left(\hat{\Omega} - \frac{\vec{r'} - \vec{r}}{|\vec{r'} - \vec{r}|} \right) \psi^\dagger(\vec{r'}, E'), \int_{E'} dE' q(\vec{r}, E' \rightarrow E) \phi(\vec{r}, E) \right\rangle$$

$$= \frac{1}{\bar{v}} \underbrace{\int_E dE \int d\vec{r'} \psi^\dagger(\vec{r'}, E) \overbrace{\int d\hat{\Omega} \int d\vec{r} \int_{E'} dE' \mathfrak{I}(E; \vec{r} \rightarrow \vec{r'}) \delta \left(\hat{\Omega} - \frac{\vec{r'} - \vec{r}}{|\vec{r'} - \vec{r}|} \right) q(\vec{r}, E' \rightarrow E) \phi(\vec{r}, E')}^{\phi(\vec{r'}, E) \text{ by equation 1.121}}}_{\text{total } \textbf{flux} \text{ contribution}}$$

$$= \left\langle \psi^\dagger(\vec{r}, E), \phi(\vec{r}, E) \right\rangle \frac{1}{\bar{v}}$$

where the spatial integrals are over the entire space $\vec{r} \in D$ and $\vec{r'} \in D$ and all solid angles $\hat{\Omega} \in 4\pi$.
Equation 1.126 can be interpreted as such: the first flight kernel $\mathfrak{I}(E, \vec{r'} \rightarrow \vec{r})$ transforms the collision source $q(\vec{r'}, E' \rightarrow E)$ into the flux $\phi(\vec{r'}, E)$. Weighting this by the flux importance function $\psi^\dagger$ gives the contribution of the neutron source to the total neutron *flux*. Dividing by the average neutron velocity gives the contribution of the neutron source to the total neutron *density* which was the interpretation given to $\phi^\dagger(\bar{\rho})$.

1.5.3 Discretized Form of the Adjoint Equations

We will now proceed to present the discretized form of the integral adjoint equation.

The Integral Adjoint- The Flux Importance Function

The matrix equation satisfied by the flux $\vec{\phi}$ was given in equation 1.102 as:

$$\vec{\phi} = \mathbf{P}(\mathbf{\Sigma}) \cdot (\mathbf{S} + \lambda \mathbf{F}) \cdot \vec{\phi} \tag{1.127}$$

where the matrices $\mathbf{S}$ and $\mathbf{F}$ are dense in energy and diagonal in space so that:

$$\mathbf{S} \cdot \mathbf{V} = \mathbf{V} \cdot \mathbf{S} \tag{1.128}$$

$$\mathbf{F} \cdot \mathbf{V} = \mathbf{V} \cdot \mathbf{F} \tag{1.129}$$

The collision probability matrix $\mathbf{P}$ was shown to be dense in space and diagonal in energy. Note that the reciprocity relation of equation 1.91 given as $V_i p_{ij}^g = V_j p_{ji}^g$ is written in matrix form as:

$$\mathbf{V} \cdot \mathbf{P} = \mathbf{P^T} \cdot \mathbf{V} \tag{1.130}$$

where we have used the diagonal nature of the regional volume matrix $\mathbf{V}$. Taking the adjoint of equation 1.127, with the discretized adjoint operator defined by equation 1.115,

gives [24]:

$$\begin{aligned}\vec{\psi}^{\dagger} &= \mathbf{V^{-1}} \cdot (\mathbf{S^T} + \lambda \mathbf{F^T}) \cdot \mathbf{P^T} \cdot \mathbf{V} \cdot \vec{\psi}^{\dagger} \\ &= \mathbf{V^{-1}} \cdot (\mathbf{S^T} + \lambda \mathbf{F^T}) \cdot \mathbf{V} \cdot \mathbf{P} \cdot \vec{\psi}^{\dagger} \\ &= (\mathbf{S^T} + \lambda \mathbf{F^T}) \cdot \mathbf{P} \cdot \vec{\psi}^{\dagger} \end{aligned} \tag{1.131}$$

where the second equality was obtained by merit of the reciprocity law given by equation 1.130. The third equality was obtained by virtue of the diagonal nature of the scattering operator $\mathbf{S}$ and the fission operator $\mathbf{F}$ in space as is presented in equations 1.128 and 1.129 respectively. We note that the transpose of the fission operator $\mathbf{F} = \overrightarrow{\chi^T} \cdot \nu\vec{\Sigma}_F$ is given by:

$$\mathbf{F^T} = \overrightarrow{(\nu\Sigma)^T} \cdot \overrightarrow{\chi} = (\nu_g \Sigma_g \chi_{g'}) \tag{1.132}$$

Standard Form for the Flux Importance Function

The standard form of the integral adjoint can be derived from equation 1.131 as:

$$(\mathbf{A}^{\dagger} - \lambda \mathbf{B}^{\dagger}) \cdot \vec{\psi}^{\dagger} = 0 \text{ where} \tag{1.133}$$

$$\mathbf{A}^{\dagger} = \mathbf{I} - \mathbf{S^T} \cdot \mathbf{P} \tag{1.134}$$

$$\mathbf{B}^{\dagger} = \mathbf{F^T} \cdot \mathbf{P} \tag{1.135}$$

Relation with the Source Importance

In equation 1.131, we obtained the equation for the flux importance to be given as:

$$\vec{\psi}^{\dagger} = (\mathbf{S^T} + \lambda \mathbf{F^T}) \cdot \mathbf{P} \cdot \vec{\psi}^{\dagger} \tag{1.136}$$

In equation 1.125 we saw that the source importance function (i.e. the adjoint of the integro-differential Boltzmann equation) was given as the convolution of the first flight kernel with the flux importance function. Multiplying equation 1.136 by the collision probability matrix $\mathbf{P}$ we have:

$$\mathbf{P} \cdot \vec{\psi}^{\dagger} = \mathbf{P} \cdot (\mathbf{S^T} + \lambda \mathbf{F^T}) \cdot \mathbf{P} \cdot \vec{\psi}^{\dagger} \tag{1.137}$$

defining $\vec{\phi}^{\dagger} = \mathbf{P}(\mathbf{\Sigma}) \cdot \vec{\psi}^{\dagger}$ then gives:

$$\phi^{\dagger} = \mathbf{P}(\mathbf{\Sigma}) \cdot (\mathbf{S^T} + \lambda \mathbf{F^T}) \cdot \vec{\phi}^{\dagger} \tag{1.138}$$

Equation 1.138 is the matrix equivalent to equation 1.125 (ignoring the normalization $\frac{1}{\bar{v}}$), which is satisfied by the adjoint of the integro-differential Boltzmann equation. It is also easier to solve for the adjoint $\phi^{\dagger}$, given the similarity of equation 1.138 to the flux equation 1.127. Indeed, the sole modification needed to be made to the code for solving the adjoint flux given by equation $\phi^{\dagger}$ is to transpose matrices $\mathbf{\Sigma_s} \rightarrow \mathbf{\Sigma_s^T}$ and $\mathbf{F} \rightarrow \mathbf{F^T}$, along with some additional book keeping, given the different form of the scattering matrix due to reversing the group orders [24].

1.6 Generalized Adjoints

The formalism that was presented in the previous section and the related interpretations were those corresponding to the classical adjoint. As discussed in the next section, the classical adjoint [8] can be used to derive a perturbation formula for reactivity. However, one of the main goals behind lattice computations is the generation of two group cross sections for use with a diffusion code. Perturbation expressions for two group cross sections involve the computation of the *generalized adjoint* [7] which will be presented in this section. These adjoints are the particular solution to the non-homogeneous Boltzmann equation, with the non-homogeneous source $S^\dagger$ chosen based on the response of interest. We will discuss some features about them below.

The Generalized Adjoint

Consider the response/functional of the form:

$$R[\phi] = \frac{\langle H_n, \phi \rangle}{\langle H_d, \phi \rangle} \tag{1.139}$$

where ϕ is the neutron flux that satisfies the Boltzmann equation:

$$(\mathbf{A} - \lambda \mathbf{B}) \cdot \phi = 0 \tag{1.140}$$

and the functions $H_n = H_n(\bar{\rho}, \bar{q})$, $H_d = H_d(\bar{\rho}, \bar{q})$ are functions which can have a dependence on phase space $\bar{\rho}$ as well as on other parameters $\bar{q}$. Examples of such functionals are reaction rates (normalized), or the breeding ratios or few group cross sections. For these responses/observables, the functions H_n and H_d will be cross sections. For example, a breeding ratio in a PWR would have: $H_n = \Sigma^{^{238}U}_{(n,capture)}$ as the ^{238}U capture cross section while $H_d = \sum_{I \in \text{fissile}} \Sigma^I_{(n,f)}$ as the sum of the fission cross sections for all fissile elements I present in the system.

The adjoint source $S^\dagger$, for which the non-homogeneous Boltzmann adjoint is solved, is chosen based on the response of interest R. For reasons which will be explained in the next section, it is defined as the functional derivative [13] of the response $R[\phi]$ with respect to the flux ϕ, so that:

$$S^\dagger = \frac{\partial R}{\partial \phi} = \frac{H_n}{\langle H_d, \phi \rangle} - R \frac{H_d}{\langle H_d, \phi \rangle} \tag{1.141}$$

The generalized adjoint corresponding for the integral form of the Boltzmann equation is then defined to satisfy [15, 24]:

$$\Gamma^\dagger = (\mathbf{S^T} + \lambda \mathbf{F^T}) \cdot \mathbf{P} \cdot \Gamma^\dagger + S^\dagger \tag{1.142}$$

or in standard form:

$$(\mathbf{A}^\dagger - \lambda \mathbf{B}^\dagger) \cdot \Gamma^\dagger = S^\dagger \text{ where} \tag{1.143}$$

$$\mathbf{A}^\dagger = \mathbf{I} - \mathbf{S}^\mathbf{T} \cdot \mathbf{P}(\mathbf{\Sigma}) \tag{1.144}$$

$$\mathbf{B}^\dagger = \mathbf{F}^\mathbf{T} \cdot \mathbf{P}(\mathbf{\Sigma}) \tag{1.145}$$

Some interesting observations can be noted about the generalized flux $\Gamma^\dagger$. First, note that the class of functions $\Gamma^\dagger$ represents the solution to a non-homogeneous Boltzmann equation, which has the singular operator $\mathbf{A}^\dagger - \lambda \mathbf{B}^\dagger$ (with $\psi^\dagger$ being its solution). Therefore, the class of sources for which equation 1.142 has a solution is limited. In particular, since the neutron flux is positive at all the phase space points $\bar{\rho}$ (i.e. there are no negative neutrons), a completely positive source would result in an ever increasing flux, while a negative source would result in an ever decreasing flux so that a steady state solution of equation 1.142 cannot exist. Taking the inner product of equation 1.141 with the neutron flux $\phi(\bar{\rho})$ we see that:

$$\left\langle S^\dagger, \phi \right\rangle = 0 \tag{1.146}$$

Equation 1.146, also known as the Fredholm alternative [27] restricts the possible set of sources $S^\dagger$ to those that are orthogonal to the flux ϕ. As seen, all responses of the form R given by equation 1.139 (ratios of linear functionals of ϕ) satisfy this condition. However, linear ratios of the flux such as an unnormalized reaction rate ($R \equiv \langle \Sigma, \phi \rangle$) do not satisfy this condition. The restriction is consistent with the physical property of the Boltzmann equation: in a reactor, described by the Boltzmann equation 1.140, the flux level that is measured by a detector can have in principle any value. A detector describes the physical state of the reactor only once it has been normalized by some factor (i.e. calibrated). Regardless of the normalization factor used for the detector, the ratios of two readings is always uniquely defined. The condition of the need for a flux normalization translates to the condition of having a response of the form given by equation 1.142, and therefore a source $S^\dagger$ that always satisfies equation 1.146. For such responses, a generalized adjoint $\Gamma^\dagger$ always exists [15, 28].

Next, note that the solution $\Gamma^\dagger$ to equation 1.142 is not unique. This is of course true for any non-homogeneous differential equation; If $\Gamma_p^\dagger$ is the particular solution of equation 1.142, then for all $\alpha \in \mathbb{R}$, we also have:

$$\Gamma^\dagger = \Gamma_p^\dagger + \alpha \psi^\dagger \tag{1.147}$$

as a solution. Here $\psi^\dagger$ refers to the flux importance function defined as the Homogeneous solution of the Boltzmann equation 1.142. It is important to eliminate most of the homogeneous component $\psi^\dagger$ from the function $\Gamma^\dagger$ so that it will not dominate the information related to the source $S^\dagger$ [74].

Numerical Solution

The method suggested by Usachev [7] to solve for the Generalized Adjoint is the Neumann Series Method. The convergence can always be speed up using an Euler-Knopp acceleration routine [28, 10]. A unique solution for the Generalized Adjoint can be obtained

from the series [7] :

$$\Gamma^\dagger = \sum_{n=0}^{\infty} \Gamma_n^\dagger \tag{1.148}$$

where:

$$\mathbf{A}^\dagger \Gamma_0^\dagger = S^\dagger \tag{1.149}$$

$$\mathbf{A}^\dagger \Gamma_n^\dagger = \lambda \mathbf{B}^\dagger \Gamma_{n-1}^\dagger \tag{1.150}$$

In the formalism of Usachev [7], the series given by equation 1.148 represents the sum of the importances over all generations[7] up to and including the present generation[8]. Taking the inner product of the first equation with the flux ϕ we see that the solutions Γ_n of these equations satisfy:

$$\begin{aligned} 0 = \left\langle S^\dagger, \phi \right\rangle &= \left\langle \mathbf{A}^\dagger \Gamma_0^\dagger, \phi \right\rangle = \left\langle \Gamma_0^\dagger, \mathbf{A}\phi \right\rangle = \left\langle \Gamma_0^\dagger, \lambda \mathbf{B} \phi \right\rangle \\ &= \left\langle \lambda \mathbf{B}^\dagger \Gamma_0^\dagger, \phi \right\rangle = \left\langle \mathbf{A}^\dagger \Gamma_1^\dagger, \phi \right\rangle = ... \\ &= \left\langle \mathbf{A}^\dagger \Gamma_n^\dagger, \phi \right\rangle = \left\langle \lambda \mathbf{B}^\dagger \Gamma_n^\dagger, \phi \right\rangle \end{aligned} \tag{1.151}$$

so that the solutions $\Gamma_n^\dagger$ are orthogonal to the fission source. The orthogonality conditions are equations of conservation of importance. $\mathbf{B}^\dagger \Gamma_n^\dagger$ is the response of the detector at n generations before the detector reading, weighted by the probability (per unit path) of the birth of neutrons from fission. However, the total detector response is zero by virtue of the orthogonality relation between the source $S^\dagger$ and the flux ϕ, so that by virtue of equation 1.146 and the equalities given in 1.151, the total importance is conserved [15]. The method suggested by Stacey [28, 24] is to remove the projection along the fission source from the function $\Gamma^\dagger$, i.e.

$$\Gamma^\dagger = \Gamma^\dagger - \frac{\left\langle \Gamma^\dagger, \mathbf{B} \cdot \phi \right\rangle}{\langle \phi^\dagger, \mathbf{B} \cdot \phi \rangle} \tag{1.152}$$

This method ensures that the generalized adjoint $\Gamma^\dagger$ will converge towards the unique generalized adjoint which is orthogonal to the fission source, i.e. satisfies the chain of equalities appearing in equation 1.151.

Generalized Adjoint for the Integro-Differential Boltzmann Equation

To obtain the generalized adjoint corresponding to the adjoint of the integro-differential non-homogeneous Boltzmann equation, we multiply equation 1.142 by the collision probability matrix $\mathbf{P}(\mathbf{\Sigma})$, so that:

$$\mathbf{P}(\mathbf{\Sigma}) \cdot \Gamma^\dagger = \mathbf{P}(\mathbf{\Sigma}) \cdot (\mathbf{S^T} + \lambda \mathbf{F^T}) \cdot \mathbf{P}(\mathbf{\Sigma}) \cdot \Gamma^\dagger + \mathbf{P}(\mathbf{\Sigma}) \cdot S^\dagger \tag{1.153}$$

defining $\Gamma^* = \mathbf{P}(\mathbf{\Sigma}) \cdot \Gamma^\dagger$, and $S^* = \mathbf{P}(\mathbf{\Sigma}) \cdot S^\dagger$ we arrive at the equation satisfied by the generalized adjoint Γ^* of the integro-differential Boltzmann equation which also satisfies

[7] Note that one is moving backwards in time.

[8] The first generation is defined as n=0.

[24]:

$$\Gamma^* = \mathbf{P}(\mathbf{\Sigma}) \cdot (\mathbf{S^T} + \lambda \mathbf{F^T}) \cdot \Gamma^* + S^* \tag{1.154}$$

1.7 Perturbation Theory

Perturbation theory in reactor physics is usually used and presented in terms of the integro-differential formulation of the transport equation. This use of perturbation theory is convenient for two reasons:

1. The integro-differential form of the transport equation is the more commonly encountered form of the transport equation when performing computations. Of the computational methods for resolving the transport which were mentioned in section 1.3.1, the integro-differential formulation of the transport equation corresponds to the S_N, the P_N and the B_N methods, which are the more widely used approaches for resolving the transport equation.

2. The perturbations in the operators appearing in the integro-differential form of the transport equation are linear in terms of perturbations in the underlying physical parameters (in our case, the nuclear data). This makes sensitivity expressions derived from perturbation formulas using the integro-differential form of the transport equation easier to use than their integral counter parts.

However, a perturbation theory formulated using the integral form of the transport equation is also of interest, principally for two reasons [15] :

1. First is the capacity of integral transport methods to compute accurate solutions in heterogeneous systems. This property, which is unique to integral transport methods, allows for an accurate computation of reactivity worths of small samples inserted within the core, or for an accurate account of the heterogeneity of the reactor system.

2. When using the integral formulation of the transport equation, perturbations in the operators appearing in the integral transport equation (see equations 1.103-1.105) become non-linear in terms of perturbations in the underlying physical parameters. It can be shown that use of the adjoint function for the unperturbed system is more accurate when using the integral formulation of the transport equation than its integro-differential formulation [26, 15].

Khairallah and Storrer [29] investigate this second property in application to computing Doppler reactivity coefficients for fast reactors. Their method is based on the collision-probability formulation of perturbation theory, which is also discussed in [26]. In [26], while discussing the features of perturbation theory using the collision probability method, McGrawth and Fischer also discuss the physical differences in the meaning/interpretation of the adjoint function which arise from the various formulations of integral transport theory. In the previous section, we provided their interpretation in relation to the collision probability method, which can also be found in [25], and [15]. In [15], Greenspan provides a survey of the collision probability method, the birth rate density formulation, and the

fission rate density formulations and discusses in detail the accuracy of each formulation.

In this section, we will first derive perturbation formulas expressing the resultant perturbation in R (in our case reactivity and two-group cross sections) in terms of perturbations in the operators of the Boltzmann equation. We then proceed to discuss kernel perturbations - a concept necessary in the integral formalism of the transport equation to relate perturbations in the operators of the integral form of the Boltzmann equation to perturbations in the base data.

1.7.1 Perturbation Expressions

There are three main approaches to derive perturbation expressions:

- The approaches based on physical considerations, such as that taken by Usachev [7], and Lewins [25]. In this approach, the importance functions are tracked in generations to derive a resultant perturbation (the perturbation affects all cycles).

- The standard approach [30, 15] is based on deriving perturbation expressions starting from the reference and perturbed Boltzmann equations.

- The variational approach, developed by Pomraning [31], with a comprehensive treatise is presented by Stacey in [28], starts with a functional related to the specific parameter of interest. Equations are then derived for the adjoint flux which minimizes this functional.

In this section we will review the standard approach for deriving perturbation formulas.

First Order Perturbation

Suppose that we have solved the Boltzmann equation 1.100 corresponding to a specific system and obtained the eigenvalue λ and the scalar flux ϕ. We shall refer to this system as our *reference system* whose values depend on a number of physical parameters q_i such as the moderator temperature, the fuel enrichment, the value of a microscopic cross section within a specific energy range, etc. We can now imagine a perturbation δq in one of the parameters $q \rightarrow q_p = q + \delta q$ where q is the parameter for the reference state, δq is the perturbation and q_p is the system parameter for the new *perturbed system*. Here, the subscript $_p$ refers to the perturbed system.

Next, we note that the perturbation in the base parameter q will result in perturbations $\delta\mathbf{A}$ and $\delta\mathbf{B}$ in the operators of the standard form of the transport equation (such as the operators appearing in equation 1.100). Similarly, the perturbation δq will result

in the perturbations $\delta\lambda$ and $\delta\phi$ in the eigenvalue and flux of the reference state, so that:

$$\mathbf{A} \rightarrow \mathbf{A_p} \equiv \mathbf{A} + \delta\mathbf{A} \tag{1.155}$$
$$\mathbf{B} \rightarrow \mathbf{B_p} \equiv \mathbf{B} + \delta\mathbf{B} \tag{1.156}$$
$$\phi \rightarrow \phi_p \equiv \phi + \delta\phi \tag{1.157}$$
$$\lambda \rightarrow \lambda_p \equiv \lambda + \delta\lambda \tag{1.158}$$

where the index p stands for the new *perturbed system*. In the rest of this work, we will assume that the perturbations are of *first order*. That is, we will ignore all second order terms such that $\delta X \delta Y = 0$ for $X, Y = \{\mathbf{A}, \mathbf{B}, \delta\phi, \delta\lambda\}$. This is a standard assumption [7, 30, 28, 15, 24] for problems encountered in reactor physics[9] as well as in many other research fields.

Perturbation Expressions for Reactivity

Suppose that a perturbation in the base system parameter $q \rightarrow q + \delta q$ results in the perturbations in the operators $\mathbf{A}$, $\mathbf{B}$, λ, and ϕ according to equations 1.155-1.158. The Boltzmann equations for the reference and perturbed system are then given by:

$$\text{reference}: \ \mathbf{A} \cdot \phi = \lambda \mathbf{B} \cdot \phi \tag{1.159}$$
$$\text{perturbed}: \ \mathbf{A_p} \cdot \phi_p = \lambda_p \mathbf{B}_p \cdot \phi_p \tag{1.160}$$
$$\text{reference adjoint}: \ \mathbf{A}^\dagger \cdot \phi^\dagger = \lambda \mathbf{B}^\dagger \cdot \phi^\dagger \tag{1.161}$$

Note that the adjoint flux $\phi^\dagger$ is the solution to the adjoint of equation 1.159 - we have not made any concrete statement or assumption regarding the specific formalism of the Boltzmann equation.

Expanding equation 1.160, ignoring all the second and higher order terms and subtracting from equation 1.159 we have:

$$(\mathbf{A} - \lambda\mathbf{B}) \cdot \delta\phi + (\delta\mathbf{A} - \lambda\delta\mathbf{B}) \cdot \phi = \delta\lambda \mathbf{B} \cdot \phi \tag{1.162}$$

Taking the inner product with the adjoint equation $\phi^\dagger$ and solving for $\delta\lambda$ we obtain:

$$\begin{aligned} \delta\lambda &= \frac{\cancelto{0}{\left\langle (\mathbf{A}^\dagger - \lambda\mathbf{B}^\dagger)\phi^\dagger, \delta\phi \right\rangle}}{\langle \phi^\dagger, \mathbf{B} \cdot \phi \rangle} + \frac{\left\langle \phi^\dagger, (\delta\mathbf{A} - \lambda\delta\mathbf{B}) \cdot \phi \right\rangle}{\langle \phi^\dagger, \mathbf{B} \cdot \phi \rangle} \\ &= \frac{\left\langle \phi^\dagger, (\delta\mathbf{A} - \lambda\delta\mathbf{B}) \cdot \phi \right\rangle}{\langle \phi^\dagger, \mathbf{B} \cdot \phi \rangle} \end{aligned} \tag{1.163}$$

where the first term was simplified by using the definition of the adjoint operator given by equation 1.107, so that:

$$\left\langle \phi^\dagger, (\mathbf{A} - \lambda\mathbf{B}) \cdot \delta\phi \right\rangle = \left\langle (\mathbf{A}^\dagger - \lambda\mathbf{B}^\dagger) \cdot \phi^\dagger, \delta\phi \right\rangle$$

[9] Stacey [28] suggests higher order perturbation theory for deep penetration and radiation shielding problems.

and by noting that the adjoint flux satisfies equation 1.161. Equation 1.163 presents the perturbation in the eigenvalue λ in terms of perturbations in the operators of the Boltzmann equation. To compute the perturbation in λ requires the flux ϕ, its adjoint $\phi^\dagger$ and the perturbations in the operators $\delta\mathbf{A}$ and $\delta\mathbf{B}$. In this way, we avoid the need for the computation of the perturbation $\delta\phi$ in the flux, which would otherwise require a new solution of the transport equation for each perturbation δq.

Perturbation Expressions for Linear Ratios of the Flux

We will now proceed to derive perturbation formulas for linear ratios of the flux. Let R be a linear ratio of the flux (see equation 1.139):

$$R[\phi] = \frac{\langle H_n, \phi \rangle}{\langle H_d, \phi \rangle} \tag{1.164}$$

where $H_n(\bar{\rho}, \bar{q})$ and $H_d(\bar{\rho}, \bar{q})$ are functions which may have a dependence on the phase space $\bar{\rho}$ and the base parameters $\bar{q}$. Here, $\bar{q}$ denotes the vector containing all parameters q. The distribution $\phi(\bar{r}, E)$ is the flux for our reference state. i.e.

$$(\mathbf{A} - \lambda\mathbf{B}) \cdot \phi = 0 \tag{1.165}$$

Let us also assume that we solved equation 1.142 for the generalized adjoint $\Gamma^\dagger$ which satisfies:

$$\Gamma^\dagger = (\mathbf{S^T} + \lambda\mathbf{B^T}) \cdot \mathbf{P} \cdot \Gamma^\dagger + S^\dagger \tag{1.166}$$

with the source $S^\dagger$ defined by equation 1.141 so that:

$$S^\dagger = \frac{\partial R}{\partial \phi} = \frac{H_n}{\langle H_d, \phi \rangle} - R\frac{H_d}{\langle H_d, \phi \rangle} \tag{1.167}$$

Given a perturbation in a base parameter $q \to q + \delta q$, we have the Boltzmann equation for the perturbed system:

$$(\mathbf{A_p} - \lambda\mathbf{B_p}) \cdot \phi_p = 0 \tag{1.168}$$

with the perturbed response R_p satisfying:

$$R_p[\phi_p] = \frac{\langle H_{n,p}, \phi_p \rangle}{\langle H_{d,p}, \phi_p \rangle} \tag{1.169}$$

where $H_{n,p} = H_n(\bar{\rho}, \bar{q} + \delta\bar{q})$ and $H_{d,p} = H_d(\bar{\rho}, \bar{q} + \delta\bar{q})$. To first order, the perturbation in δR of R is then given by:

$$\delta R = \left(\overbrace{\frac{\langle \delta H_n, \phi \rangle}{\langle H_d, \phi \rangle} - R \cdot \frac{\langle \delta H_d, \phi \rangle}{\langle H_d, \phi \rangle}}^{\text{Direct Perturbation in } R} \right) + \left(\overbrace{\frac{\langle H_n, \delta\phi \rangle}{\langle H_d, \phi \rangle} - R \cdot \frac{\langle H_d, \delta\phi \rangle}{\langle H_d, \phi \rangle}}^{\text{Resultant Perturbation from } \delta\phi} \right) \tag{1.170}$$

$$= \frac{\langle \delta H_n, \phi \rangle}{\langle H_d, \phi \rangle} - R \cdot \frac{\langle \delta H_d, \phi \rangle}{\langle H_d, \phi \rangle} + \left\langle S^\dagger, \delta\phi \right\rangle \tag{1.171}$$

where the last equality was obtained by merit of equation 1.168. Note that the first term appearing on the right hand side of equation 1.170 is the resultant perturbation in the functional R due to the direct dependence of the functions H_n and H_d on the parameter $\bar{q}$, and the second term appearing on the right hand side of equation 1.170 is the resultant perturbation in the functional R due to its implicit dependence on q through the explicit dependence of R on the neutron flux ϕ.

Expanding equation 1.166, and ignoring higher order terms, we have:

$$(\mathbf{A} - \lambda\mathbf{B}) \cdot \delta\phi = (\delta\lambda\mathbf{B} + \lambda\delta\mathbf{B} - \delta\mathbf{A}) \cdot \phi \tag{1.172}$$

Taking the inner product of equation 1.172 with the generalized adjoint given by equation 1.143, and noting the orthogonality relation given by equation 1.146 between the source $S^\dagger$ with the flux ϕ, we have:

$$\begin{aligned} \left\langle \Gamma^\dagger, (\mathbf{A} - \lambda\mathbf{B}) \cdot \phi \right\rangle &= \left\langle (\mathbf{A}^\dagger - \lambda\mathbf{B}^\dagger) \cdot \Gamma^\dagger, \delta\phi \right\rangle \\ &= \left\langle S^\dagger, \delta\phi \right\rangle = \left\langle \Gamma^\dagger, (\delta\lambda\mathbf{B} + \lambda\delta\mathbf{B} - \delta\mathbf{A}) \cdot \phi \right\rangle \end{aligned} \tag{1.173}$$

Substituting equation 1.173 into equation 1.171, we arrive at:

$$\delta R = \left(\overbrace{\frac{\langle \delta H_n, \phi \rangle}{\langle H_d, \phi \rangle} - R \cdot \frac{\langle \delta H_d, \phi \rangle}{\langle H_d, \phi \rangle}}^{\text{Direct Perturbation in } R} \right) + \overbrace{\left\langle \Gamma^\dagger, (\delta\lambda\mathbf{B} + \lambda\delta\mathbf{B} - \delta\mathbf{A}) \cdot \phi \right\rangle}^{\text{equivalent perturbation from } \delta\phi} \tag{1.174}$$

we could think that to compute δR requires knowledge of $\delta\lambda$ and thus knowledge of the adjoint flux $\phi^\dagger$. However, by virtue of the chain of equalities given by equation 1.151, we have:

$$\delta R = \left(\frac{\langle \delta H_n, \phi \rangle}{\langle H_d, \phi \rangle} - R \cdot \frac{\langle \delta H_d, \phi \rangle}{\langle H_d, \phi \rangle} \right) + \left\langle \Gamma^\dagger, (\lambda\delta\mathbf{B} - \delta\mathbf{A}) \cdot \phi \right\rangle \tag{1.175}$$

The above equation provides a convenient formulation for calculating the effects of a given perturbation in the input parameter q on the response R. We note that for each perturbation in the input parameter q, the parameters which appear in equation 1.170 could be computed directly. However, most analysis usually involves calculating effects that come from all sorts of system alterations in the input data, so that a direct approach for each parameter would require a direct calculation for each input parameter, thereby making such an approach very costly in computer power and simulation time.

By using the generalized adjoint function $\Gamma^\dagger$, we have removed the need for the computation of the flux perturbation $\delta\phi$ (which would otherwise have to be computed for each perturbation in $\bar{q}$). Thus the computation of δR requires only the computation of the function $\Gamma^\dagger$, the flux ϕ, and the perturbation in the operators $\delta\mathbf{A}$ and $\delta\mathbf{B}$.

1.7.2 Kernel Perturbations

The operators in the perturbation expressions using the integral formalism of the Boltzmann equations are different than their counterparts which appear in the integro-differential formalism. In particular, perturbations in the operators of the integro-differential formalism can always be expressed in terms of linear perturbations in the underlying nuclear data (the operators are linear with respect to the cross sections). This is not the case when the integral formulation of the Boltzmann equation is used so that the perturbations in the operators must be somehow accounted for. In [32, 26, 29], due to the one-dimensional nature of the geometries considered, an analytical formula for the CP could be obtained so that the perturbations can be computed. Another approach is to provide an approximation accounting for the perturbation in the first flight kernel in terms of a perturbation in the total cross section [24]. These two options will be discussed in this section.

Perturbations in the First Flight Kernel

The operators $\mathbf{A}$ and $\mathbf{B}$ for the integral formulation are given by equations 1.104 and equations 1.105 as:

$$\mathbf{A} = \mathbf{I} - \mathbf{P}(\mathbf{\Sigma})\cdot\mathbf{S} \tag{1.176}$$

$$\mathbf{B} = \mathbf{P}(\mathbf{\Sigma}) \cdot (\overrightarrow{\chi^T} \cdot \overrightarrow{\nu\Sigma_F}) \tag{1.177}$$

To use equation 1.163 (or equation 1.175) with the integral adjoint $\psi^\dagger$ (or the generalized integral adjoint $\Gamma^\dagger$) requires knowledge of the perturbations in the operators $\mathbf{A}$ and $\mathbf{B}$. To first order, these perturbations are given by:

$$\delta\mathbf{A} = -(\delta\mathbf{P}\cdot\mathbf{S} + \mathbf{P}\cdot\delta\mathbf{S}) \tag{1.178}$$

$$\delta\mathbf{B} = (\delta\mathbf{P}\cdot\mathbf{F} + \mathbf{P}\cdot\delta\mathbf{F}) \tag{1.179}$$

As observed from equation 1.178, the perturbation in $\delta\mathbf{A}$ depends on the perturbation in the CP matrix $\delta\mathbf{P}$ which depends on the perturbation in the first flight kernel $\mathfrak{I}$.

In equation 1.38, we defined the first flight kernel $\mathfrak{I}$ to be:

$$\mathfrak{I}(E;\vec{r'}\rightarrow\vec{r}) = \frac{\exp\left[-\int_{\vec{r'}}^{\vec{r}} ds\Sigma(\vec{s},E)\delta\left(\frac{\vec{s}}{s} - \frac{\vec{r}-\vec{r'}}{|\vec{r}-\vec{r'}|}\right)\right]}{|\vec{r}-\vec{r'}|^2} \tag{1.180}$$

where $\vec{s} = s\hat{\Omega}$. The perturbation in this kernel due to a perturbation $\delta\Sigma$ in the total cross section is then given as [32, 15]:

$$\delta\mathfrak{I}(E;\vec{r'}\rightarrow\vec{r}) \equiv \mathfrak{I}(E;\vec{r'}\rightarrow\vec{r})\left\{\exp\left[-\int_{\vec{r'}}^{\vec{r}} ds\delta\Sigma(\vec{s},E)\delta\left(\frac{\vec{s}}{s} - \frac{\vec{r}-\vec{r'}}{|\vec{r}-\vec{r'}|}\right)\right] - 1\right\} \tag{1.181}$$

Equation 1.181 shows that the perturbation in the first flight kernel $\mathfrak{I}$ depends on the perturbation in the total cross section. Integrating equation 1.181 over the volumes V_j

and V_i we see that the resultant perturbation in the reduced collision probability p_{ij} is given by:

$$\delta p_{ij}^g = \frac{1}{V_i} \int_{\vec{r} \in V_i} \int_{\vec{r'} \in V_j} \int_{\hat{\Omega} \in 4\pi} d\vec{r} d\vec{r'} d\hat{\Omega}$$
$$\mathfrak{I}(E_g; \vec{r'} \to \vec{r}) \cdot \left\{ \exp\left[- \int_{\vec{r'}}^{\vec{r}} ds \delta\Sigma_T^g(\vec{s}, E) \delta\left(\frac{\vec{s}}{s} - \frac{\vec{r} - \vec{r'}}{|\vec{r} - \vec{r'}|} \right) \right] - 1 \right\} \tag{1.182}$$

Computation of this integral is difficult, and requires modification in the integration subroutines of DRAGON. We note that performing this integration would also be computationally expensive, considering the time consuming nature of the collision probability integration and the need to perform the integration for each $\delta\Sigma_T^g$ - per group and per mixtures, and would somewhat defeat the purpose of using perturbation theory. Therefore, we have not investigated this option. We will now present a solution introduced by Takahashi [33] to compute the perturbation in the collision probability $\delta\mathbf{P}$.

The $\mathbf{P}_0$ Approximation for the Kernel Perturbation

The approximation suggested by Takahashi [33] and implemented in DRAGON by T. Courau consists in replacing the perturbation in the total cross section which appears on the left hand side of the integro-differential Boltzmann equation by an equivalent source in the in-group scattering term.

Let us consider the integro-differential form of the transport equation:

$$\left(\hat{\Omega} \cdot \nabla + \mathbf{\Sigma} \right) \phi(\vec{r}, \hat{\Omega}, E) = (\mathbf{S} + \lambda \mathbf{F}) \cdot \phi(\vec{r}, E) \tag{1.183}$$

the integral equation for the flux is then:

$$\vec{\phi} = \mathbf{P}(\mathbf{\Sigma}) \cdot (\mathbf{S} + \lambda \mathbf{F}) \cdot \vec{\phi} \tag{1.184}$$

let us now add $\delta\mathbf{\Sigma}$ to both sides of equation 1.183 so that the integro-differential and the integral equation will now satisfy:

$$\left(\hat{\Omega} \cdot \nabla + \mathbf{\Sigma} + \delta\mathbf{\Sigma} \right) \phi(\vec{r}, \hat{\Omega}, E) = (\mathbf{S} + \lambda \mathbf{F}) \cdot \phi(\vec{r}, E) + \delta\mathbf{\Sigma} \cdot \phi(\vec{r}, \hat{\Omega}, E) \tag{1.185}$$
$$\vec{\phi}(\vec{r}, E) = \mathbf{P}(\mathbf{\Sigma} + \delta\mathbf{\Sigma}) \cdot (\mathbf{S} + \lambda \mathbf{F}) \, \phi(\vec{r}, E) + \mathbf{P}(\mathbf{\Sigma} + \delta\mathbf{\Sigma}) \cdot \delta\mathbf{\Sigma} \cdot \phi(\vec{r}, E) \tag{1.186}$$

we note that the flux remains unchanged since we have added the operator $\delta\mathbf{\Sigma}$ to both sides of the equation. If the flux is now isotropic, so that $\phi(\vec{r}, \hat{\Omega}, E) \simeq \frac{1}{4\pi} \phi(\vec{r}, E)$, then we see that [34]:

$$\phi(\vec{r}, E) \simeq \mathbf{P}(\mathbf{\Sigma} + \delta\mathbf{\Sigma}) \cdot [\mathbf{S} + \lambda \mathbf{F} + \delta\mathbf{\Sigma}] \cdot \phi(\vec{r}, E) \tag{1.187}$$

Expanding $\mathbf{P}(\mathbf{\Sigma} + \delta\mathbf{\Sigma}) \simeq \mathbf{P}(\mathbf{\Sigma}) + \delta\mathbf{P}$ and substituting in 1.187 while ignoring the second order term $\delta\mathbf{P} \cdot \delta\mathbf{\Sigma}$, we have [34]:

$$-\mathbf{P} \cdot \delta\mathbf{\Sigma} \cdot \phi = \delta\mathbf{P} \cdot (\mathbf{S} + \lambda \mathbf{F}) \cdot \phi \tag{1.188}$$

Let us now consider the perturbation expression appearing in equation 1.163 for the eigenvalue λ:

$$\delta\lambda = \frac{\left\langle \psi^\dagger, (\delta\mathbf{A} - \lambda\delta\mathbf{B})\phi \right\rangle}{\langle \psi^\dagger, \mathbf{B}\phi \rangle} \tag{1.189}$$

Substituting equations 1.178 and 1.179 into equation 1.189 and using the approximation given by equation 1.188 for $\delta\mathbf{P}\cdot(\mathbf{S}+\lambda\mathbf{F})$ we have:

$$\begin{aligned}
\delta\lambda &= -\frac{\left\langle \psi^\dagger, \{\mathbf{P}\cdot(\delta\mathbf{S}+\lambda\delta\mathbf{F}) + \delta\mathbf{P}\cdot(\lambda\mathbf{F}+\mathbf{S})\}\cdot\phi \right\rangle}{\langle \psi^\dagger, \mathbf{P}(\boldsymbol{\Sigma})\cdot\mathbf{F}\phi \rangle} \\
&= -\frac{\left\langle \mathbf{P^T}(\boldsymbol{\Sigma})\cdot\psi^\dagger, \{-\delta\boldsymbol{\Sigma}+\lambda\delta\mathbf{F}+\delta\mathbf{S}\}\cdot\phi \right\rangle}{\langle \mathbf{P^T}(\boldsymbol{\Sigma})\cdot\psi^\dagger, \mathbf{F}\phi \rangle} \\
&= \frac{\left\langle \phi^\dagger, (\delta\boldsymbol{\Sigma}-\delta\mathbf{S}-\lambda\delta\mathbf{F})\phi \right\rangle}{\langle \phi^\dagger, \mathbf{F}\phi \rangle}
\end{aligned} \tag{1.190}$$

where the last equality was obtained by using the relation between the integral and the differential adjoint (i.e. $\phi^\dagger = \mathbf{P}\cdot\psi^\dagger$). We see from equation 1.190 that by expressing the resulting perturbation $\delta\mathbf{P}$ in the collision probability matrix in terms of the change in the total cross section, and by assuming that the flux is isotropic, we arrive at the equivalent sensitivity expression corresponding to the integro-differential form of the perturbation formulas.

1.8 Sensitivity Functions

In nuclear data uncertainty propagation, a sensitivity function can be thought of as a linear transformation that represents the relative change in the reactor performance parameter R resulting from a relative change in the nuclear data q. These sensitivity functions provide the basis to the sensitivity approach of uncertainty propagation. The sensitivity function can be thought of as the first order derivative or slope of the response R with respect to a relative change $\delta q/q$ in the input variable q:

$$S_R^q(\bar{\rho}) = \frac{\delta R}{R} \Big/ \frac{\delta q(\bar{\rho})}{q(\bar{\rho})} \tag{1.191}$$

where $\bar{\rho}$ stands for the phase space variables $(\bar{r}, E, \hat{\Omega})$. R is usually a functional of the flux with a dependence on q that could be (and in most cases is) non-linear (see equation 1.164). Therefore, the sensitivity function S_R^q (expressed in %/%) represents the relative change in R due to small relative changes in q.

In this section, we derive sensitivity formulas for reactivity and linear functionals of the flux, which were presented in equation 1.164. The sensitivities formulas that we

present here express the sensitivity of the response (criticality or a linear ratio of the flux) to the multi-group cross sections that appear in the multi-group form of the transport equation. These sensitivities are typically referred to as *explicit* sensitivity as they ignore any additional feedback from the perturbation in the fine flux. We mentioned in section 1.4.1 that to compute the multi-group cross sections which appear in the transport equation requires a self shielding computation, whose goal is the computation of the fine flux $f(E)$ appearing as the weighting function in equations 1.57 to 1.60. A change in the nuclear data (such as a resonance parameter), can be expected to result in a perturbation in the fine flux $f(E) \rightarrow f(E) + \delta f(E)$. In chapter 3, we will show that this resulting perturbation (which is ignored when computing the explicit sensitivity) can be accounted for by an additional sensitivity. This additional sensitivity is called the *implicit sensitivity* as it originates from the implicit dependence of multi-group cross sections (and therefore the computed flux) on the fine flux function $f(E)$.

1.8.1 Sensitivity Formulas for Reactivity

In the case where the flux is isotropic (we will discuss flux anisotropy in chapter 3), replacing $\lambda = \frac{1}{k_{eff}}$ in equation 1.190 gives:

$$\delta(\frac{1}{k_{eff}}) = \frac{\left\langle \phi^{\dagger}, (\delta\mathbf{\Sigma} - \delta\mathbf{S} - \frac{1}{k_{eff}}\delta\mathbf{F}) \cdot \phi \right\rangle}{\langle \phi^{\dagger}, \mathbf{F}\phi \rangle} \tag{1.192}$$

noting that $\delta(\frac{1}{k_{eff}}) = \frac{-\delta k_{eff}}{k_{eff}} \cdot \frac{1}{k_{eff}}$ we have:

$$\frac{\delta k_{eff}}{k_{eff}} = \frac{\left\langle \phi^{\dagger}, (k_{eff}\delta\mathbf{S} + \delta\mathbf{F} - k_{eff}\delta\mathbf{\Sigma}) \cdot \phi \right\rangle}{\langle \phi^{\dagger}, \mathbf{F}\phi \rangle} \tag{1.193}$$

multiplying equation 1.193 by $q/\delta q$ we obtain the sensitivity $S^q_{k_{eff}}$ of the k_{eff} to the parameter q, given by:

$$S^q_{keff} = \frac{q}{k_{eff}}\frac{\delta k_{eff}}{\delta q} = \frac{\left\langle \phi^{\dagger}, (\overbrace{qk_{eff}\delta_q\mathbf{S} + q\delta_q\mathbf{F}}^{\text{GAIN}} - \overbrace{qk_{eff}\delta_q\mathbf{\Sigma}}^{\text{LOSS}}) \cdot \phi \right\rangle}{\langle \phi^{\dagger}, \mathbf{F}\phi \rangle} \tag{1.194}$$

where $q \in \left\{\nu_g, \chi_g, \sigma_{(n,el),g}, \sigma_{(n,inel),g}, \sigma_{(n,f),g}, ...\right\}$ is a multi-group parameter and $\delta_q \equiv \frac{\partial}{\partial q}$.

Computation of S^q_{keff} using equation 1.194 requires computation of the inner products appearing in the nominator and the fission source normalization factor appearing in the denominator. Computation of the latter can be avoided by noting the sum of the sensitivities of the fission yields will reduce to identity. What is usually done is to compute the unnormalized sensitivities appearing in the nominator of equation 1.194 for the various multi-group parameters and then normalize by the total sum of the $\bar{\nu}$ sensitivities [37].

1.8.2 Sensitivity Formulas for Linear Functionals of the Flux

For a response $R[\phi]$ of the form given by equation 1.139:

$$R[\phi] = \frac{\langle H_n, \phi \rangle}{\langle H_d, \phi \rangle} \tag{1.195}$$

we have from equation 1.175:

$$\delta R = \left(\frac{\langle \delta H_n, \phi \rangle}{\langle H_d, \phi \rangle} - R \cdot \frac{\langle \delta H_d, \phi \rangle}{\langle H_d, \phi \rangle} \right) + \left\langle \Gamma^\dagger, (\lambda \delta \mathbf{B} - \delta \mathbf{A}) \cdot \phi \right\rangle \tag{1.196}$$

where $\Gamma^\dagger$ was the generalized adjoint to the integral form of the non-homogeneous Boltzmann equation given by equation 1.166. In the case where the flux is isotropic, and using the relation between the integral adjoint $\Gamma^\dagger$ and the differential adjoint Γ^* along with equations 1.178-1.179 and 1.188 for the Kernel perturbation, we have:

$$\delta R = \left(\frac{\langle \delta H_n, \phi \rangle}{\langle H_d, \phi \rangle} - R \cdot \frac{\langle \delta H_d, \phi \rangle}{\langle H_d, \phi \rangle} \right) + \langle \Gamma^*, (\lambda \delta \mathbf{F} + \mathbf{S} - \delta \mathbf{\Sigma}) \cdot \phi \rangle \tag{1.197}$$

The sensitivity S_R^q of the response R to the nuclear data q can then be computed by:

$$S_R^q \equiv \frac{q}{R} \frac{\delta R}{\delta q} = \frac{q}{R} \left\{ \left(\frac{\langle \delta_q H_n, \phi \rangle}{\langle H_d, \phi \rangle} - R \cdot \frac{\langle \delta_q H_d, \phi \rangle}{\langle H_d, \phi \rangle} \right) + \langle \Gamma^*, (\lambda \delta_q \mathbf{F} + \delta_q \mathbf{S} - \delta_q \mathbf{\Sigma}) \cdot \phi \rangle \right\} \tag{1.198}$$

1.9 Uncertainty Propagation

In this work, we assume that the nuclear data q is with uncertainties and correlations supplied under the form of a covariance matrix $\mathbf{V}$, where $\mathbf{V}$ is in relative units (i.e. in $(\%)^2$). We can thus propagate the uncertainties of the base data to compute the uncertainties on the integral parameter R. This work can be done using *law of propagation of errors*:

$$\left(\frac{\Delta R}{R} \right)^2 = \vec{S^T} \cdot \mathbf{V} \cdot \vec{S} = \sum_i \sum_j S_R^{q_i} V_{ij} S_R^{q_j} \tag{1.199}$$

where the sensitivities $S_R^{q_i}$ represent the variation of the response R to a variation in the base nuclear data q_i. The ensemble of sensitivity coefficients as a function of nuclear reaction and energy are denoted by the vector $\vec{S}$. Here, ^{T} refers to matrix transposition. In the case where we are interested in more than one response R_i, the sensitivities are expressed in matrix form with elements S_{ij} given by [1]:

$$S_{ij} = S_{R_j}^{q_i} = \frac{q_i}{R_j} \frac{\partial R_j}{\partial q_i} \tag{1.200}$$

Chapter 2

Methodology: Part I
Codes used and General Development

In this section, we provide a quick overview of the codes we have used in our analysis, as well as the general developments that we have made both in data processing and related to performing the sensitivity analysis. The computations related to this work which lies in the domain of the sensitivity approach to nuclear data uncertainty propagation can be divided into two major tasks. First, while the idea of supplying covariance matrices along with evaluations dates back to the 1960s, it is only recently that we are seeing an effort by evaluators to systematically include covariance matrices in their evaluated data files. Even where matrices are available, the task of arriving at the data that is in accordance with the needs of the transport or the sensitivity code is not evident. The second task is performing the sensitivity computation and uncertainty analysis itself. Currently, the capacity to perform such a computation today exists in few codes and outside of this work, is not available in DRAGON.

2.1 DATA & DATA Processing

We present in this section the NJOY nuclear data processing code, which we use to generate continuous energy and multi-group cross section data for use with the WIMS libraries [38]. We then proceed to describe the WIMS format.

2.1.1 NJOY

Before the nuclear data provided in the Evaluated Nuclear Data File can be used by codes such as DRAGON, the data must be processed by a nuclear data processing code. The code NJOY [39] is used in our work for this purpose.

The NJOY program has a modular approach, with the output of one module (called an NJOY tape) being the input for the next module. A typical NJOY computation relevant to this work is as follows:

- The RECONR module of NJOY is used to represent the cross section data in continuous energy form for the temperature available on the Evaluated Nuclear Data File (usually the cross section data is provided at 293° K).
- The BROADR module is used to Doppler Broaden the resonances at temperatures corresponding to those requested by the user in the input file.
- The UNRESR module produces average cross section values in the unresolved resonance region as a function of a background/dilution cross section σ_0 which is requested by the user in the input file (see equation 1.71).
- The GROUPR module is used to calculate the slowing down flux as a function of energy in an infinite homogeneous medium for the background dilution cross section σ_0 requested by the user in the input file. It then uses the computed slowing down flux as the weighting function to generate the multi-group cross sections given by equations 1.57 to 1.60.
- The module WIMSR produces multi-group parameters in a format compatible with the WIMS code. This format is described in the next section.

The NJOY outputs containing the continuous spectrum energy cross section files is called PENDF (outputs of RECONR, BROADR, UNRESR), and the GROUPR output which contains the multi-group cross sections is called GENDF.

ERRORR

The module ERRORR of NJOY [40] is the incorporation of the covariance processing code ERRORRJ in NJOY [41] and can be used to process nuclear data covariance files available in the ENDF to covariances in multi-group format for:

- resonance parameters (provided under mt 32 in the ENDF)
- multi-group cross sections (under mt 33 in the ENDF)
- secondary angular and energy distributions (under mt 34 & 35 in the ENDF)

In order to propagate covariances from resonance parameters to covariances for group-wise cross sections, the derivative $\frac{\partial \sigma_g}{\partial \Gamma_i}$ of the group wise cross section $\sigma_g(E;\vec{\Gamma})$ with respect to the resonance parameter Γ_i must be computed. The derivative is computed in ERRORR by using a direct perturbation approach; for example, if N resonance parameters $(\Gamma_i)_{i=1}^N$ are provided in the ENDF, then N derivatives must be computed. The derivative $\frac{\partial \sigma_g}{\partial \Gamma_i}$ is computed as the average over the continuous energy interval of the continuous energy cross section $\sigma(E;\vec{\Gamma})$ (note that in NJOY, energy increases with increasing group number). Here, we have explicitly included the vector of resonance parameters $\vec{\Gamma} = (\Gamma_i)_{i=1}^N$ in our notation for the continuous cross section $\sigma(E;\vec{\Gamma})$ to emphasize its dependence on the N

resonance parameters. The derivative of the continuous energy cross section is computed by direct perturbation using a central difference scheme so that [40]:

$$\begin{aligned}\frac{\partial \sigma_g}{\partial \Gamma_i} &= \frac{1}{\Delta E}\int_{E_g}^{E_{g+1}} dE \frac{\partial \sigma(E;\vec{\Gamma})}{\partial \Gamma_i} \\ &= \frac{1}{\Delta E}\int_{E_g}^{E_{g+1}} dE \frac{\sigma(E;\Gamma_1,..,\Gamma_{i-1},\Gamma_i+\Delta\Gamma_i,\Gamma_{i+1},..) - \sigma(E;\Gamma_1,..,\Gamma_{-1},\Gamma_i-\Delta\Gamma_i,\Gamma_{i+1},..)}{2\Delta\Gamma_i}\end{aligned} \tag{2.1}$$

Once the derivatives $\frac{\partial \sigma_g}{\partial \Gamma_i}$ for all the N resonance parameters are computed, the covariance matrix for the multi-group cross sections can be computed using the law of propagation of errors given by equation 1.199.

2.1.2 ANGELO & LAMBDA

In computing the response uncertainty contributions using the sandwich rule given by equation 1.199, the covariance matrices that we use must be consistent in energy meshing and in reaction definition with the sensitivities that we have computed. The reaction definition requires additional treatment and is discussed in chapter 3. The collapse/expansion of the energy mesh can be performed by the code ANGELO [43]. For example, the covariances provided with the SCALE 5/6 code [42], hence referred to as SCALE 5/6 covariances, are given in a 44 energy group format and correspond to covariances for individual channel reactions/partial cross sections (i.e. (n,elastic), (n,inelastic), (n,2n), ...). In this work, we use ANGELO to transform the SCALE 44 group matrices to the WIMS 172-group grid. ANGELO constructs a union grid and uses a flat flux interpolation routine to extend the uncertainties and the correlation matrices to the union grid.[1] The uncertainty vectors and correlation matrices are then collapsed to the WIMS 172-group grid, defined as their lethargy average over each group. The produced covariances correspond to individual channel/partial reaction covariances given in 172×172 format.

Once the covariances are processed by ANGELO, the program LAMBDA [43] is used to check the mathematical properties of the multi-group covariance matrices. The correlation matrices are tested to determine if any element exceeds unity. Furthermore, the number of positive, negative and zero eigenvalues are computed and the matrix is classified on this basis [43].

2.2 WIMS Libraries

WIMS-D (Winfrith Improved Multi-group Scheme-D) is a lattice physics cell code released by Winfrith Technology Center in the UK [44, 45]. At its time, WIMS was one of the few codes available to the public on non-commercial terms and was widely used in many laboratories for thermal research reactor and power reactor computations [38]. Before the 1990s, the libraries associated with WIMS was the 69 group library generated

[1] Note that the energy meshing between the new grid and the original grid should not be drastically different.

in the United Kingdom based on evaluations dating back to the 1960s.

In the 2001, in collaboration with the Jozef Stefan Institute, the IAEA released a new version of libraries, in (a slightly modified) WIMS format, which were based on the most recent nuclear data files available at the time. Today, the libraries exist in 69 group and 172 group format and are freely available at [46, 38].

ENERGY Meshing

In this work, we use the 172 group WIMS libraries released by the IAEA [46]. The energy meshing corresponds to the XMAS-172 group energy grid [47] and contains:

- 45 fast groups (E= $1.11378 * 10^4$ eV to $1.96403 * 10^7$ eV)
- 47 resonance groups (E= 4.12925 eV to $1.11378 * 10^4$ eV)
- 80 thermal groups (E=$1.0 * 10^{-5}$ to 4.12925 eV)

2.2.1 WIMS-D Format

WIMS uses the collision probability method to solve the Boltzmann equation in lattice configurations. It therefore requires the group-wise transport cross section, the fission cross section $\sigma_{f,g}$, the absorption cross section $\sigma_{ABS,g}$, the group to group transfer scattering matrix $\sigma_{s,g'\to g}$, the fission yield $\bar{\nu}_g$, and the fission spectrum $\bar{\chi}_g$. We note that for thermal neutrons, the bound atom scattering matrices must be provided as a function of temperature. Self shielded cross sections are provided in terms of the resonance integral, defined using the intermediate resonance approximation with the intermediate resonance (Goldstein-Cohen) factor λ (provided for each group) as input for NJOY.

Absorption and Scattering Cross Sections

Except for a few isotopes (namely ^{1}H, ^{2}H, ^{12}C, and ^{16}O) only the P_0 component for scattering matrices are provided on the WIMS library so that we will limit our discussion to isotropic scattering.

The group to group $\Sigma^{g'\to g}_{(n,SCAT)}$ of the lumped scattering transfer matrix available in the WIMS libraries (one matrix per isotope) is defined as [38]:

$$\Sigma^{g'\to g}_{(n,SCAT)} = \sigma^{g'}_{(n,el)} P^{g'\to g}_{(n,el)} + \sigma^{g'}_{(n,inel)} P^{g'\to g}_{(n,inel)} + 2\sigma^{g'}_{(n,2n)} P^{g'\to g}_{(n,2n)} + 3\sigma^{g'}_{(n,3n)} P^{g'\to g}_{(n,3n)} \tag{2.2}$$

where $\sigma^{g'}_{(n,x)}$ refers to the microscopic cross section in the energy group g' for the channel/partial reaction (n,x) with $x \in \{(n,el),(n,inel),(n,2n),(n,3n)\}$. Here, $P^{g'\to g}_{(n,x)}$ refers to the secondary energy distribution for reaction (n,x) and presents the probability that an incoming neutron at energy group g', which interacts with the nuclei via the channel (n,x), results in a neutron at energy g. The lumped scattering cross section in the WIMS library is reconstructed from the scattering matrix by summing over the out-going

neutron energies g of the group to group transfer matrix $\mathbf{S} = (\Sigma^{g' \to g})$ whose components were defined by equation 2.2. i.e. [38]

$$\sigma^{g'}_{(n,SCAT)} = \sum_{g=1}^{N_G} \Sigma^{g' \to g}_{(n,SCAT)} \tag{2.3}$$

Similarly, a lumped absorption cross section is defined as the sum of all reactions which result in the capture of a neutron. To preserve the total cross section $\sigma = \sigma_{(n,ABS)} + \sigma_{(n,SCAT)}$, the $\sigma_{(n,2n)}$ cross section and $2\sigma_{(n,3n)}$ cross sections are subtracted from the lumped absorption cross section. i.e. [38]

$$\sigma^{g}_{(n,ABS)} = \sum_{x \in (n,abs)} \sigma^{g}_{(n,x)} - \sigma^{g}_{(n,2n)} - 2\sigma^{g}_{(n,3n)} \tag{2.4}$$

where the summation index x appearing in equation 2.4 refers to all neutron absorbing reactions $x \in \{(n,\gamma),(n,p),(n,\alpha),(n,f),...\}$.[2] This is an intelligent way to store the data required by the transport code;[3] by storing the matrix $\Sigma^{g' \to g}_{n,SCAT}$, defined by equation 2.2, and the cross sections defined by equations 2.3 and 2.4, one avoids storing unnecessary data and performing redundant computations, that would otherwise, in the case where individual channel reactions had been provided, have to be performed.

Self Shielded Cross Sections

WIMS uses equivalence theory and the intermediate resonance approximation to compute the effective dilution factor σ_b representative of the heterogeneous geometry (see chapter 3.1). In the case of a homogeneous mixture composed of one resonant isotope with density N_r, and a moderator of density N_m, the dilution cross section is defined as [38]:

$$\sigma_b = \lambda_r \sigma^r_p + \sigma_0 \tag{2.5}$$

where λ_r (provided as input in the NJOY WIMSR module) is the intermediate resonance factor for the resonant isotope, σ^r_p is the potential scattering cross section for the resonant isotope, $\sigma_0 = \frac{N_m}{N_r}\sigma^m_p$ is the potential scattering cross section of the moderator per resonant atom.

The self-shielding data available on the WIMS libraries is tabulated as a function of temperature and the dilution factor σ_b given by equation 2.5. The choice for the dilution cross section σ_b is provided as user input for the NJOY WIMSR module. The "resonance integral" in terms of which the self shielding data is provided in the WIMS libraries is defined as [38]:

$$I_x(T,\sigma_b) \sim \frac{\sigma_b \sigma_x(\sigma_b)}{\sigma_b + \sigma_a(\sigma_b)} \tag{2.6}$$

where I_x is the resonance integral for reaction $x \in \{(n,ABS),(n,f)\}$, and σ_b is the dilution cross section of the corresponding homogeneous mixture. The resonance integral

[2] These correspond to the reactions under the mt number mt=102, .., 150 on the NJOY GENDF tape

[3] For example, the JEFF 3.1 evaluation of ^{238}U, processed by NJOY to WIMS 172 group mesh, the GENDF tape has a size of 5.0 Mb while the WIMSR output has a size of 335 Kb

$I(T, \sigma_b)$ provides a monotone increasing function (as a function of σ_b) for which interpolation over σ_b is both easy and accurate. The cross section $\sigma_x(\sigma_b)$ can be recovered from the resonance integral by [38]:

$$\sigma_x(\sigma_b) \sim \frac{\sigma_b I_x(T, \sigma_b)}{\sigma_b - I_a(T, \sigma_b)} \tag{2.7}$$

Transport Correction

In the WIMS libraries, a row transport correction is used for the thermal groups and a column transport correction is used for the fast groups. For the 172 group energy grid, the group transport correction is defined as [38]:[4]

$$\sigma^g_{s,1} = \begin{cases} \sum_{h=1}^{172} \sigma_{s,1}^{g \to h} & \text{, for the thermal groups } h \in [80, 172] \cap \mathbb{N} \\ \frac{\sum_{h=1}^{172} \sigma_{s,1}^{h \to g} J_h}{\sum_{h=1}^{172} J_h} & \text{, for the epithermal and fast groups } h \in [1, 80] \cap \mathbb{N} \end{cases} \tag{2.8}$$

where J_h is the neutron current in group h, and the $\sigma_{s,1}^{g \to h}$ refers to the g to h^{th} term of the P_1 (first Legendre coefficient) group to group scattering matrix. Here the first index refers to the incident neutron energy and the second index refers to the outgoing neutron energy. During the construction of the WIMS libraries, J_h is taken to be the current $\vec{J}$ of a "typical" PWR [38] cell and is provided as input for the NJOY WIMSR module.

2.2.2 WILLIE

WILLIE [38] is a program coded in FORTRAN 77 that can be used to create, modify, and compile WIMS libraries. In this work, we use WILLIE for converting WIMS libraries from ASCII format to binary format, and PYTHON modules that we have developed for the manipulation of the library.

2.3 SCALE/TSUNAMI

The Standard Computer Analyses for Licensing Evaluation (SCALE) [48, 49, 50] is a system code which functions in a modular fashion (SCA 2006). SCALE is composed of approximately 76 completely integrated modules which allow a large variety of computations, from treatment of cross sections to criticality safety applications and radiation shielding experiments.

Accompanying with the SCALE package is the Tools for Sensitivity and Uncertainty Analysis Methodology Implementation (TSUNAMI) [51, 52, 53]. TSUNAMI is a leading, state-of-the-art tool-set for nuclear data sensitivity and uncertainty analysis. At present, the code TSUNAMI is the natural choice for developers to benchmark against and from

[4]Note that the order of energy groups inverses in multi-group libraries with energy decreasing with increasing group number.

which the performance of developed tools can be compared [54, 55, 56].

The SAMS module [57] of TSUNAMI uses adjoint perturbation theory to compute sensitivities and perform nuclear data uncertainty propagation. The XSDRNPM module [49] in TSUNAMI-1D is a deterministic flux solver which solves the S_N form of the transport equation in 1-D geometries. For 2-D geometries, the module NEWT [50] of TSUNAMI-2D can be used to compute a deterministic solution for the flux and adjoint using the S_N form of the transport equation. Computation for three dimensional geometries is performed by the KENO module of TSUNAMI-3D that provides multi-group Monte Carlo flux and adjoint solutions which can be used to compute k_{eff} sensitivities. In 2011 [58], the perturbation theory applications of TSUNAMI-1D and TSUNAMI-2D were extended to include the capacity for sensitivity computation using Generalized Perturbation Theory (with user defined responses at input). GPT capabilities do not currently exist in TSUNAMI-3D.

2.4 DRAGON

The code DRAGON [12, 59] is an open source, deterministic transport code developed and freely available at the Institut de Génie Nucléaire (IGN) of the Ecole Polytechnique de Montréal (EPM). It includes all functions that characterize a lattice cell code, such as interpolation of microscopic cross sections supplied from standard libraries, resonance self shielding computations, multi-group and multi-dimensional neutron flux computations which can also take into account neutron leakage, as well as computation and editing of condensed and homogenized cross sections, and evolution/burn-up computations. The version of DRAGON used in this work is DRAGON 3.06J which was the most recent version at the start of this study.

DRAGON is a modular code, composed of twenty six modules each responsible for a specific type of computation. The modules are called in a sequential format with custom types of data stored in the memory (called LINKED LIST) and passed from one module to another. Behind the source code of DRAGON is the GANLIB driver [60] - a large collection of modules in FORTRAN 77 which are responsible for initializing the program, reading and checking the input file, memory allocation, handling advanced data (LINKED LIST), interpreting the input supplied by the user, starting and terminating one module after the other, and writing output data in several formats, etc. Use of the GANLIB drivers alleviates many of the set-backs that are typically accompanied with FORTRAN 77, most notably dynamic memory allocation and the unavoidable need for common blocks, and allows for a more developer friendly environment. Using the GANLIB driver also provides the user with an environment where complex simulations and pseudo-code (logical *if* and iterative *DO* loops, variable assigning, etc) can be written in the input file, thereby answering many needs which would otherwise involve source modification. The modular calculation associated with the GANLIB strategy also ensures that subsequent developments are easily implemented in a fully-integrated computation environment, and makes maintenance of the code easier [60].

A typical computation in DRAGON

DRAGON is capable of solving the Boltzmann equation using the Method of Characteristics (MOC) or the Collision Probability method (CP). We note that if the CP option is used, the flux solution is the scalar flux obtained from a CP solution with a transport corrected isotropic source (see section 1.3.2). This study relies on the CP method; a typical computation relevant to this work in DRAGON is as follows:

- The module **LIB:** is used to create or modify a library. It takes in as input the supplied library (in our case WIMS 172-group libraries) along with the mixture identification numbers, the isotopic densities and the corresponding temperatures. A library LINKED LIST structure is then created containing the multi-group parameters at the default dilution factor σ_b available on the reference library.[5]

- The module **GEO:** is then used to define a geometry. As a benefit of using Integral Transport Methods, a large range of geometries (with non-centered spatial meshing permitted) are available in 1D, 2D and 3D.

- Amongst a handful of tracking modules, the modules **EXCELT:** or **NXT:** can be used to set up the integration lines for the computation of the reduced CPs that is to follow. Defined by the user are the number of integration lines and number of angles which are then used to discretize the space.

- The module **SHI:** is responsible for performing the resonance self shielding computation. The module uses the Generalized Stamm'ler method [21] to compute the equivalent dilution factor (per group for the 47 resonance groups in the WIMS 172 group library) representative of the input heterogeneous geometry. The library is then updated with the group parameters interpolated over this dilution factor (i.e. self shielded cross sections). A Lagrange polynomial interpolation scheme [61, 62] is used to interpolate over the logarithm of the dilution factor.

- The module **ASM:** takes as input the self-shielded library generated by **SHI:** and the tracking data produced by **NXT:** /**EXCELT:**. Using a Gaussian quadrature integration routine [12, 61], **ASM:** performs the integrations of the reduced collision probabilities given by equations 1.82 to 1.85. The integration of the CP matrix is the most time consuming process during the computation.

- The module **FLU:** or **SAD:** can then be used to compute the forward and adjoint fluxes given by equations 1.102 and 1.138 [24, 34]. If the module **SAD:** is used, then the Generalized source $S^{\dagger}$ given by equation 1.141 and the corresponding generalized adjoint Γ^{*} given by equation 1.154 are also computed for multi-group cross section and reaction rate responses.

- The module **SNS:**, developed during the course of this study, takes as input the **FLU:** or **SAD:** output to compute sensitivities for reactivity, two group cross sections and a number of other responses.

[5] For example, for ^{238}U, the default dilution factor available on the WIMS libraries is $\sigma_b = 28.$ barns.

Once the sensitivities are computed by **SNS:**, uncertainty propagation can be performed using the sandwich rule given by equation 1.199. The covariance matrices, appearing in equation 1.199 are processed by the codes NJOY ERRORR or ANGELO and correspond to the WIMS 172 group energy grid. The process of uncertainty propagation will be discussed in more detail in chapter 3.

2.5 SUSD3D

SUSD3D [71, 37, 66, 67] is a sensitivity and uncertainty analysis code, originating from the code SUSD [64], and further developed by I. Kodeli at IJS [65, 66, 67]. The code uses first order perturbation theory, with the assumption that the sensitivities are constant to variations in base parameters within the domain associated with their uncertainties. This tends to be a general assumption when performing sensitivity analysis for nuclear data uncertainty propagation.

SUSD3D presents a modular fashion for development by allowing the integration of results from other codes to compute effectively sensitivities and propagate nuclear data uncertainties. In this fashion, it is possible to use already available work and avoid redundant development of tools for transport computation and cross section generation. At the same time, this approach allows the capacity to update the system of codes, as one version of this ensemble of codes can be more recent than the rest. SUSD3D was our first experience in sensitivity analysis. At the start of this work, we successfully coupled SUSD3D with DRAGON to perform nuclear data uncertainty propagation [63]. Indeed, much of the methodology that we have since coded in the more recent and object oriented language PYTHON, as well as the underlying algorithms that we have coded in FORTRAN 77 in the DRAGON module **SNS:**, result from our study of the SUSD3D code, so that we present a detailed description of SUSD3D here.

2.5.1 Methodology

Figure 2.1 presents the schematic of the sequences of codes/modules and data used in the code SUSD3D. The flux and adjoint fluxes used by the code are supplied generally from Discrete Ordinates S_N codes such as DOORS [68], DANTSYS [69] and TORT [70]. The cross sections and covariance matrices that are used by SUSD3D are prepared by the code NJOY. The covariance matrices can be from the code ANGELO as well. The codes GROUPR, ERROR34/SEADR (included in SUSD3D) and ERROR-J (which is now a part of NJOY under ERRORR) are required for the treatment of microscopic group-wise cross sections and covariance matrices which are used by SUSD3D during the computation of the sensitivity.

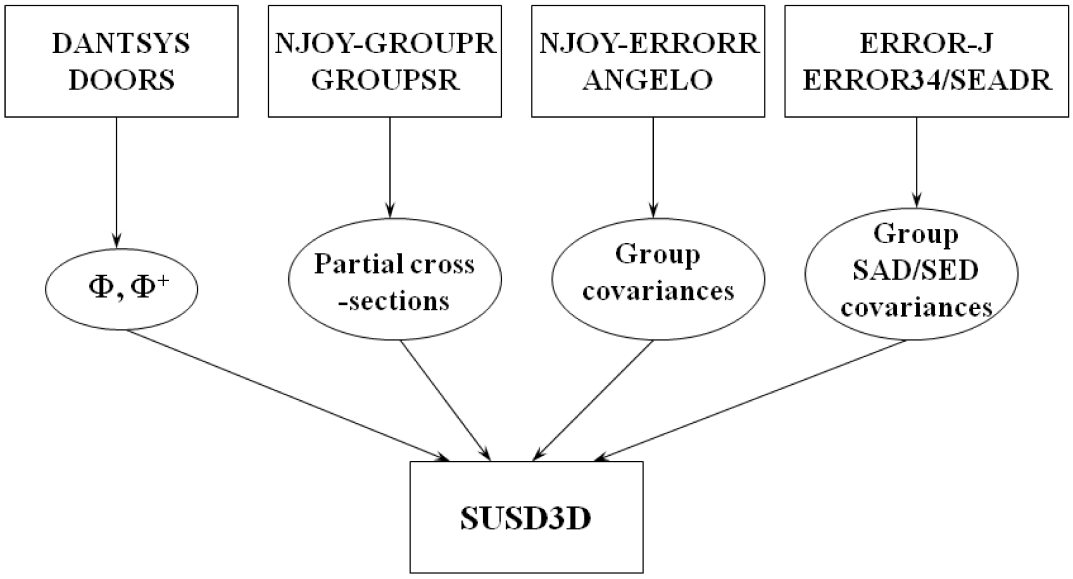

Figure 2.1: Schematic of the code SUSD3D. The codes DOORS and DANTSYS supply the forward and adjoint fluxes, the cross sections are computed by NJOY GROUPR, and the covariance matrices are processed by the code ANGELO or NJOY ERRORR or the older ERRORJ module. Reproduced from reference [65].

Theory-Review

In the discrete ordinates S_N formalism for the transport equation, what is normally computed by the code is the angular flux. The sensitivity $S_R^x(E)$ of the response R to the cross section Σ^x of reaction x at energy E is then given as [71]:

$$\begin{aligned} S_R^x(E) = & \overbrace{\frac{1}{R}\int_{\vec{r}} d\vec{r} \int_{\hat{\Omega}} d\hat{\Omega} - \Sigma^x(\vec{r},E)\cdot\phi(\vec{r},\hat{\Omega},E)\cdot\phi^\dagger(\vec{r},\hat{\Omega},E)}^{\text{LOSS}} \\ & + \frac{1}{R}\overbrace{\int d\vec{r}\int_{\hat{\Omega}} d\hat{\Omega}\int_{\hat{\Omega}'} d\hat{\Omega}'\int_{E'} dE'\ \Sigma_s^x(\vec{r},\hat{\Omega}\to\hat{\Omega}',E\to E')\cdot\phi(\vec{r},\hat{\Omega},E)\cdot\phi^\dagger(\vec{r},\hat{\Omega}',E')}^{\text{GAIN}} \\ & + \frac{1}{R}\overbrace{\int d\vec{r}\int_{\hat{\Omega}} d\hat{\Omega}\Sigma_D(\vec{r},E)\cdot\phi(\vec{r},\hat{\Omega},E)}^{\text{DIRECT}} \end{aligned} \tag{2.9}$$

where the response R is defined as [71]:

$$R = \int_{\vec{r}} d\vec{r}\int_{\hat{\Omega}} d\hat{\Omega}\int_E dE\ \Sigma_D(\vec{r},E)\cdot\phi(\vec{r},\hat{\Omega},E) \tag{2.10}$$

$\Sigma^x(\vec{r},E)$ = Total macroscopic cross section for reaction type x, at position $\vec{r}$, and energy E.

$\Sigma_s^x(\vec{r}, \hat{\Omega} \to \hat{\Omega}', E \to E')$= the (n,x) partial scattering macroscopic transfer function from angle $\hat{\Omega}$ to angle $\hat{\Omega}' + d\hat{\Omega}'$, and energy E to energy $E' + dE'$

$\Sigma_D(\vec{r}, E)$ = detector response function and source in adjoint calculation (eg. reaction cross sections, Kerma, damage functions, dose factors, etc)

$\phi(\vec{r}, \hat{\Omega}, E)$ = angular flux

$\phi^\dagger(\vec{r}, \hat{\Omega}, E)$ = adjoint flux or generalized adjoint flux (if detector response function $\Sigma_D \neq 0$).

Discretized Equations

In S_N codes, the solid angle $\hat{\Omega} \in 4\pi$ is divided into N partitions. The angular dependence of the scattering cross section is represented in terms of the cosine of the scattering angle $\mu_0 = \hat{\Omega} \cdot \hat{\Omega}' \in [-1, 1]$ and expanded in terms of Legendre polynomials so that [72, 71]:

$$\Sigma_S(\vec{r}, \mu_0, E \to E') = \frac{1}{4\pi} \sum_{l=0}^{L} \Sigma_S^l(\vec{r}, E \to E') \cdot P_l(\mu_0) \tag{2.11}$$

where the coefficients $\Sigma_s^l(\vec{r}, E \to E')$ are defined by:

$$\Sigma_S^l(\vec{r}, E \to E') = 2\pi \cdot (2l+1) \int_{-1}^{1} \Sigma_s(\vec{r}, \mu_0, E \to E') \cdot P_l(\mu_0) d\mu_0 \tag{2.12}$$

In practice the series appearing in equation 2.11 is truncated after a finite number of terms with L representing the largest term that is taken into account.

The direct and adjoint flux appearing in equation 2.9 and 2.10 are in reality represented in their multi-group form using the multi-group approximation, and expanded in terms of spherical harmonics $Y_{l,m}(\hat{\Omega})$ with the solid angle $\hat{\Omega}$ discretized the angles Ω_m such that $\cup_{m=1}^{N} \Omega_m = 4\pi$. The discretized form of the forward and adjoint fluxes are given as:

$$\phi_{g,i,m} = \sum_{l=0}^{L} \sum_{n=-l}^{l} Y_{l,n}(\Omega_m) \cdot M_{g,i}^{l,n} \tag{2.13}$$

$$\phi_{g,i,m}^\dagger = \sum_{l=0}^{L} \sum_{n=-l}^{l} Y_{l,n}(\Omega_m) \cdot M^{\dagger l,n}_{g,i} \tag{2.14}$$

Here g is the group index, i the region, and $\phi_{g,i,m}$ corresponds to the angular flux over the angular direction Ω_m. The flux and adjoint moments $M_{g,i}^{l,n}$ and $M^{\dagger l,n}_{g,i}$ are defined as:

$$M_{g,i}^{l,n} = \sum_{m} Y_{l,n}(\Omega_m) \cdot \phi_{g,i,m} \cdot \Delta\Omega_m \tag{2.15}$$

$$M^{\dagger l,n}_{g,i} = \sum_{m} \cdot \bar{Y}_{l,n}(\Omega_m) \cdot \phi_{g,i,m} \cdot \Delta\Omega_m \tag{2.16}$$

The discretized form of equation 2.9 is then given as [71]:

$$S^x_{R,g} = \frac{1}{R}\sum_i \Delta V_i \{\, \rho_i \,(\, - \sigma^x_{g,i} \sum_m \phi_{g,i,m} \cdot \phi^\dagger_{g,i,m} \cdot \Delta\Omega_m + \sum_{g'} \sum_{l=0}^{L} \sigma^x_{l,g\to g'} \sum_{n=-l}^{l} M^{l,n}_{g,i} \cdot M^{\dagger\, l,n}_{g',i} \Big) + \Sigma^i_{D,g} \sum_m \phi_{g,i,m} \Delta\Omega_m \Big\} \tag{2.17}$$

where

$\sigma^x_{g,i}$ = total microscopic cross section for reaction type x, in the space interval i and energy group g.

$\sigma_{l,g\to g'}$= l^{th} Legendre coefficient of the scattering microscopic cross section from energy group g to g'.

V_i= volume of the space mesh interval i.

ρ_i is the isotope's density in the region V_i.

$\phi_{g,i,m}$ and $\phi^\dagger_{g,i,m}$: forward and adjoint fluxes given by equations 2.13 and 2.14.

We finally note that both the flux moments $\phi_{i,m,g}$ and the angular moments $M^{l,n}_{g,i}$ appear in equation 2.17. Whereas in one- and two-dimensional calculations this is an acceptable approach, in three-dimensional computations, this approach can be unpractical due to the large number of direct and adjoint angular flux terms [71]. The alternative approach of the code SUSD3D is to use the flux moments which are given by equations 2.13 and 2.14. This approach tends to considerably reduce the required storage space and slightly reduce the CPU time as a result of the lower number of arithmetic involved by the code (the index n appearing in equation 2.17 is removed with this approach), while preserving the accuracy of the calculation.

Codes Structure

The SUSD3D code computes sensitivities and uncertainties in three sequential steps, called OVERLAYS:

OVERLAY 1 This is the most computationally demanding part of the calculation. Here, the flux-adjoint product $\phi_{g,i,k} \cdot \phi^\dagger_{g',i,k}$ for $k \in \{0,..,L\}$ and $g, g' \in \{1,..,N_G\}$, appearing in equation 2.17 is computed. The flux moment product is then integrated over regions composed of the same mixture (with $NMIX$ being the number of mixtures). This volume integrated moment product is called the SUFLUX and contains: the $g \times NMIX$ flux elements required for the computation of the direct term, the $g \times NMIX$ moment products required for the computation of the loss term, and the $g \times g \times (2L+1) \times NMIX$ moment products required for the computation of the scattering gain term. The SUFLUX is then written as a FORTRAN

Direct Access file (this tends to speed-up access by future modules greatly) at which point the OVERLAY 1 is terminated.

OVERLAY 2 In this step, the unnormalized sensitivities given by equation 2.17 are computed for each of the requested isotopes. The cross sections for the isotopes are read by SUSD3D from the NJOY GENDF tape that is supplied as input, along with the isotopic densities ρ_i which appear in equation 2.17. The unnormalized loss and gain terms are then computed according to equation 2.17 and are written in NJOY GENDF format to an output file.

OVERLAY 3 The unnormalized sensitivity is computed as the difference between the gain and loss terms which were computed in OVERLAY 2. If the sensitivity to k_{eff} is desired, then the fission normalization $\left\langle \phi^{\dagger}, \mathbf{F} \cdot \phi \right\rangle$ appearing in equation 1.194 must be computed. This can be avoided by instead dividing by the sum of all the unnormalized $\bar{\nu}$ sensitivities calculated in OVERLAY 2, i.e. dividing by the sum $\sum_g \sum_{I \in \text{fissile}} S^{\bar{\nu}}_{k_{eff},g}$ given by equation 2.17. Once the unnormalized sensitivities are normalized in this way, the uncertainty is computed using the Sandwich rule given by equation 1.199.

2.6 DINASOUR

The code DINASOUR has been developed [54] at McMaster University [54] with the goal of performing nuclear data uncertainty propagation with DRAGON. To perform uncertainty propagation, DINASOUR performs direct DRAGON simulations based on WIMS libraries that it generates by sampling the IAEA released WIMS libraries based on the covariance data (this usually requires several hundred direct simulations for each isotope). A benefit of the code is that it modifies the WIMS libraries (before the heterogeneous self-shielding computation) so that implicit sensitivities can be accounted for. Outside of our work, DINASOUR is one of the only current tool we know of for performing nuclear data uncertainty propagation using DRAGON. [6]

2.7 CASMO-4

CASMO-4 [89] is a standard tool for lattice physics calculation and solves the neutron transport equation using the Method of Characteristics [11]. Recently, developments have been performed at VTT in order to incorporate a sensitivity and uncertainty functionalities in the code [55, 56]. The approach taken at VTT also uses the WIMS libraries and perturbation theory. In this work, we will provide some comparisons regarding the differences in our methodology and that of CASMO-4.

2.8 Developments

In this section, we present a brief overview of some of the general tools that we have developed over the course of this study.

[6] The only other currently available tool is the Total Monte-Carlo method developed at NRG.

2.8.1 SAD: and General Developments

Introduction to SAD:

SAD: (Sources Adjoints/Directs) is a module in DRAGON composed of a collection of subroutines developed by T. Courau in the early 2000s at EPM [24]. The module is responsible for setting up the source functions of the form given by equation 1.141, and computing the Generalized adjoints Γ^* given by equation 1.154. The algorithm of the module **SAD:** is as follows:

- After allocation of memory and interpretation of the input geometries and library, which is performed in the subroutine *SAD*, the subroutine *SADGET* is called to read and interpret the input file.
- The subroutine *SADINI* is then called to compute the forward and adjoint fluxes by calling DRAGON's flux solver *FLUDRV* [7] to solve equations 1.102 and 1.138.
- Next, the subroutine *SADGAS* is called, which after allocating the necessary memory, calls *SADDTX* to compute the reaction rates (response values) appearing in equation 1.139. Scattering cross sections, defined as the difference between the total with the absorption cross section, are computed by *SADSCT*. Once the reaction rates are computed, the subroutine *SADPSA* is called to compute the generalized source $S^\dagger$, given by equation 1.141, and to write this source to the LINKEDLIST that is provided as input for **SAD:**.
- The subroutine *SADFLU* is then called to compute the generalized adjoint functions Γ^*, appearing in equation 1.154, for each source computed by *SADPSA* and writes the results to the flux LINKEDLIST, which is provided as input for **SAD:**.

Adjoint Sources

While the module **SAD:** offers a powerful tool for the computation of generalized adjoint functions, it is not currently functional in versions 3.06x of DRAGON. In version 3.05, the module is functional. Therefore, our starting point was to adapt the 3.05 source to the 3.06. After arriving at a functional version, a second set of developments were made by reprogramming most of *SADDTX*, *SADSCT* and *SADPSA* to allow for simpler definitions of sources, as well as defining new sources such as breeding ratios, normalized reaction rates, etc. Note that minor parts of **FLU:** also needed to be modified for this purpose.

Flux Re-balancing and Convergence

When solving for the flux given by equation 1.102, the convergence rate is dependent on the spatial and energy meshing. The first is effectively treated by using variational

[7] Note that this corresponds to computation using the Collision Probability method.

acceleration methods [36, 24, 95]. Convergence[8] in energy is usually accelerated using *flux re-balancing* [24, 35, 14]. Flux rebalancing consists of modifying the obtained regional flux during the iterative process to ensure the conservation of the total reaction rate in group g (i.e. the total reaction rate in group g should be equal to the collision source). When computing the flux, re-balancing tends to speed up the acceleration process. However, when computing Generalized adjoint flux given by equation 1.154, we see that re-balancing tends to slow down the convergence rate (this problem was also encountered during the original development of the module [24]). This is due to the fact that the generalized adjoint tends to change signs during the convergence process given the fact that the source is both positive and negative. We note that the positive and negative nature of the source is dictated by equation 1.146, i.e. the source is orthogonal to the flux which is non-negative throughout the entire energy range. Since flux re-balancing does not take into account the sign of the adjoint flux, use of re-balancing tends to slow down convergence (and sometimes no convergence is reached). Our attempt to answer this problem was what is recommended in [28, 76]: divide the source in two parts (one negative and one positive), solve the adjoint corresponding to each source, and recombine the source and the obtained adjoint fluxes at each outer iteration.

However, while this approach tends to slightly speed up the acceleration for each source function and ensures convergence with re-balancing, it tends to double the number of flux solutions so that the final computation time is longer than when not using re-balancing.

The solution implemented by T. Courau during the original development was to begin with a slightly contaminated source [24]:

$$\Gamma_0^\dagger = \alpha\phi^\dagger \text{ where } \alpha = \alpha_0 \frac{|S^\dagger|}{\phi^\dagger} \tag{2.18}$$

with the factor α chosen as the ratio of the vector norm of the source to the vector norm of the adjoint flux and $\alpha_0 = 10^{-2}$ by default. Convergence with this method is almost always reached if the initial source is contaminated according to equation 2.18, but it is still slower than when not using re-balancing.

Therefore, regardless of splitting the source in two, or contaminating the flux in the first few iterations, convergence is usually slower when using flux re-balancing. Finally, we note that the convergence criteria must be somewhat relaxed (usually two orders of magnitude than that desired for the flux) when solving for the generalized adjoint Γ^* [24]. We note that this does not seem to have an effect on the computed sensitivities.

2.8.2 SNS:

The module **SNS:**, developed in DRAGON as a part of this work, allows for the computation of sensitivity coefficients to the cross section data available in the WIMS libraries (independent of the specific evaluation or energy group meshing). Sensitivities for reac-

[8] Convergence in energy is performed in the inner iterations

tivity, two group cross sections, reaction rates and breeding ratios to multi-group cross sections, secondary particle energy distributions and fission yields can be computed using **SNS:**. In this section, we provide a brief overview of the structure of **SNS:**. Our development of **SNS:** is similar to the algorithm used by SUSD3D, so that we will only provide a short description here and present the additional development in the next chapter. A typical **SNS:** computation is as follows:

- After memory allocation and reading the tracking data provided from **EXCELT:** or **NXT:** the subroutine *SNSDRV* is called to compute the sensitivities.

- The subroutine *FLUGFL* is then called to read the forward and adjoint flux for all the responses available on the **SAD:** output. For each response, once the forward and adjoint flux have been computed, the subroutine *SENSFLX* is called to compute the SUFLUX which is then stored in a DRAGON binary file.

- Once the SUFLUX has been computed, the subroutine *SNSEIG* computes the k_{eff} sensitivities using an algorithm similar to the one used by SUSD3D to compute the reactivity sensitivities given by equation 1.194.

- The subroutine *SNSGPT* is then called to compute the sensitivities given by equation 1.198 for the responses available in the **SAD:** output.

Once the sensitivities are computed, their profiles, loss and gain terms, gain matrices, and direct terms are stored in DRAGON format in the **SNS:** output to be used for uncertainty analysis. This process will be discussed in further detail in the next chapter.

2.8.3 Data Processing with PYTHON

Behind the developments provided in chapter 3, and our results which are presented in chapter 4, there is a large collection of PYTHON modules that we have developed, in an object oriented style, and based on the Numerical PYTHON (NumPy) [96] and Scientific PYTHON (SciPy)[97] libraries. These modules permit the study and manipulation of the nuclear data encountered in its various formats and definitions. An Object Oriented approach in programming is crucial when handling the large quantity of data that is typically involved in nuclear data uncertainty propagation. The modules that have been developed, allow one to access and manipulate the nuclear data in its many formats and definitions, starting with the Evaluated Nuclear Data File, until the two group cross section data generated by DRAGON for use with a diffusion code. The developed modules allow one to establish a link between NJOY's continuous energy spectrum outputs (PENDF files output by RECONR, BROADR, and RECONR), multi-group cross section files (GENDF files), multi-group covariance files (ERRORR format), the data available in the WIMS library (WIMS format), and DRAGON outputs (LCM objects/XSM files). We note that the concepts being addressed here are not just a question of the difference

in format, but rather a difference in the definition of what constitutes a cross section. We provide here a brief description of the developed modules:

GANLIB in PYTHON

As mentioned earlier, the GANLIB driver is a large collection (26 thousand lines of code) of modules in FORTRAN 77 which perform many tasks including handling (reading and storing in memory, as well as writing) complex data structures which are used by the code DRAGON to store its output data. DRAGON output format is very complex [98]; the data is stored as a LCM object in LCM format [60]. The format allows for the data structure to be stored in terms of directories that can possess data and further subdirectories. While it is a very efficient approach to storing data, to read stored data without having access to the GANLIB drivers (i.e. outside of FORTRAN 77) is difficult. Indeed, a large part of the GANLIB driver is dedicated to read and write this complex format. As a result, accessing the DRAGON generated data necessary for performing sensitivity analysis and uncertainty propagation becomes a difficult task.

One way to overcome this problem is to rewrite new modules in the new programming language which would allow for the manipulation of the files. For example, such is the approach taken by the newly released (2011) graphical LCM object viewer available for use with DRAGON-4 [99, 100]- a collection of PYTHON modules have been written which are capable of reading LCM objects in ASCII format and permit graphical manipulation of the data.

To resolve the problem of manipulation of DRAGON's output data, we chose to compile the complete GANLIB drivers as a dynamic library (using the publicly available GFORTRAN compiler) that can then be imported into PYTHON using the *ctypes* class [101]. In this way, every module available in the GANLIB drivers can be called and used (so long as proper memory access is treated). The FORTRAN modules in GANLIB relevant to this work are:

- *LCMOP*: open an LCM object data structure

- *LCMSIX*: move up and down a directory

- *LCMGET*: get information contained in a subdirectory of an LCM object data structure

- *LCMPUT*: put information in a specified subdirectory

- *LCMCL*: close an LCM object data structure

To ease use of these modules (which are now imported into PYTHON using the compiled dynamic library and PYTHON's *ctypes* libraries), we have written interface functions for each of the listed FORTRAN modules. The primary form of data we use is our exported DRAGON outputs in DRAGON XSM [60] format (this is a compact binary form of the data), and then use the interface modules with the compiled dynamic library to access the desired data. Reading and writing files in this way tends to be extremely fast because the work is being done by the compiled FORTRAN code rather than in PYTHON (which tends to be slow, particularly at reading ASCII format). It also allows for a more developer friendly approach where hundreds of files can be manipulated by writing a simple *for loop* with a few lines of code.[9] The strategy for manipulating the files is identical to the GANLIB driver. We use the PYTHON equivalent of each of the modules listed above in the same way (open XSM files, move up and down the directories, get the data, put the data and close files). This approach also avoids a lot of redundant coding.

NJOY's GENDF, PENDF and ERRORR formats

Another type of data that is essential for a proper computation of reaction uncertainty contributions, when performing nuclear data uncertainty propagation is NJOY's GROUPR outputs. The continuous spectrum format is also useful for performing uncertainty propagation using NRG's Total Monte Carlo method (see appendix) and TALYS [102] generated ENDFs. We can not emphasize the importance of verifying the NJOY outputs when performing this type of computation; the NJOY processed data should be checked, to ensure proper processing before being used for uncertainty analysis. NJOY's outputs are similar to the ENDF output; each line is limited to 80 columns (characters), including the numbering of the lines, and contains six words (values) of 12 characters including the exponential and its sign.

Unlike the DRAGON format, the particular difficulty with GENDF and PENDF files is not their format but rather the quantity of data available in the files; GENDF format contains the dilution factors, energy meshing, multi-group cross sections including the Legendre Polynomial coefficients for the scattering cross sections and transfer matrices, fission yields, fission spectrum, the slowing down flux, bound atom thermal scattering data, etc. tabulated as a function of dilution and temperature. The PENDF contains similar data in continuous energy form.

As a part of this work we have developed, in an object oriented approach in PYTHON, a set of modules which allow for NJOY outputs to be read into memory, as well as to be written in the original format, with interface functions that allow easy access to a specific data type. Similarly, subroutines exist for interpolation over dilution and temperature. This is done by first constructing the resonance integral given by equation 2.6, performing a spline interpolation of the resonance integral over the logarithm of the dilution factor, and then transforming the interpolated resonance integral to the cross section by using equation 2.7. The interpolation in temperature is linear. A good example of application

[9] See the appendix for an application to uncertainty propagation for evolution computations using NRG's Total Monte Carlo method.

of subroutines is the construction of multi-group self-shielded covariances, which we perform by computing the covariances between the NJOY generated GENDF's using NRG's TALYS generated Evaluated Nuclear Data Files (see Appendix A). Another application is our treatment of the implicit effect presented in the next chapter.

ERRORR format in PYTHON

In performing uncertainty analysis, the multi-group cross section data (either in GENDF format or WIMS) are used in the process of computing the sensitivities which appear in the sandwich formula 1.199. An equally necessary quantity is the covariance matrix $\mathbf{V}$ which appears in the same equation. Therefore, we have developed another set of modules which allow us to manipulate the cross section covariance files (processed either by NJOY ERRORR or ANGELO). This set of modules can be used to read and write covariances in NJOY's ERRORR format. Other than computing the uncertainty using the sandwich rule 1.199, another possible application of these libraries is the construction of lumped covariances, corresponding in reaction definition to the cross sections that are contained in the WIMS libraries (see chapter 3).

WIMS in PYTHON

Another existing format encountered when performing nuclear data uncertainty propagation with DRAGON is the format of the WIMS library. This is essential if one is interested in manipulating the library directly (adding or removing cross sections), or performing direct perturbations - which is a valuable validation tool for the computation of sensitivities.[10] Therefore, another set of modules that we have built are object oriented modules capable of reading, writing, and manipulating entire WIMS libraries, as well as NJOY WIMSR outputs. Details of the WIMS format can be found in the FORTRAN 77 source code of the WILLIE [38] program.

PSUSD in PYTHON

PSUSD was our first attempt to develop a sensitivity and uncertainty analysis code for use with DRAGON. At the time of the development, SUSD3D suffered from two problems:

- The sensitivity computation in SUSD3D was done in single precision (this can have an important effect when computing heavy isotope (n,el) sensitivities).

- The code used a single dilution factor for all energy groups.

The question of precision, which is important for applications such as β_{eff} sensitivities, has since been addressed in SUSD3D by I. Kodeli, with the source has been changed to perform its arithmetics in double precision when using PARTISN as the computed flux

[10] Indeed, for the principle part of this work, we have used direct perturbations as a means to validate my obtained results and continue my developments.

and the adjoint are written in double precision. The second point has been partially addressed by I. Kodeli; the code now permits for cross section interpolation (for absorption cross sections), using a single dilution factor for all groups. Note that if the interpolation is performed over the cross sections (this is what is being done in SUSD3D currently) rather than the resonance integrals then it is difficult to obtain realistic values for the scattering cross section.

In all the PYTHON libraries that are described above, all of the arithmetic is performed in double precision. PSUSD uses our PYTHON modules for GENDF files to interpolate the cross sections at the appropriate temperature and dilution (contained in the DRAGON output library). It then computes, in a similar fashion to SUSD3D (three OVERLAYS), the sensitivities in double precision.

2.8.4 Uncertainty Analysis

Once the sensitivities have been computed (either by **SNS:** or PSUSD), the covariances are read using our PYTHON module and the related uncertainties are computed using equation 1.199. This process is discussed in more detail in chapter 3.

2.9 Problem Statement

We have now arrived at a point where we can produce explicit sensitivities similar to what is currently computed by our colleagues (SUSD3D, CASMO-4, DINASOUR). However, the sensitivities that we calculate are computed using the scalar flux and adjoint from a CP solution with a transport corrected source (what is available in DRAGON with a CP computation). The sensitivities that we compute also differ from SUSD3D (but similar to what is done in CASMO-4 and DINASOUR) in the sense that they are response sensitivities to the lumped reactions available in the WIMS libraries.

Limitations of our Computed Sensitivities

Our computed sensitivities with **SNS:** suffer from two major drawbacks:

- The implicit component of the sensitivity is ignored. This is also true for the methodology of SUSD3D and CASMO-4; *a priori*, this sensitivity should always be considered.
- The computed sensitivities are valid only for the case where the flux is isotropic. For scattering reactions, this computed sensitivity is accurate for reflected lattices (the reflective boundary condition promotes flux isotropy) but will be very inaccurate for problems involving anisotropy (such as problems involving leakage, larger assembly or full core computations). Scattering sensitivities are most affected from this approximation.

Limitations of our Computed Uncertainty Contributions

It will be shown in chapter 3 that even when the sensitivity is computed accurately, the task of uncertainty analysis is not a straight-forward application of equation 1.199 due to differences that exist in the definition between the reactions available in the WIMS libraries (lumped reactions given by equations 3.55-3.57), and the reactions in the covariance files (partial reaction cross sections such as (n,n), (n,inel),...). This limitation does not just apply to the sensitivities computed with **SNS:** but to all the codes that compute sensitivities with respect to lumped cross sections such as those computed by CASMO-4 [55, 56] and DINASOUR [54].[11]

For absorption, this problem can be overcome by constructing covariances for a covariance matrix corresponding in definition to lumped absorption cross section (this is done in chapter 3). However, as it will be further shown in chapter 3, with results provided in chapter 4, this methodology is not applicable to scattering sensitivities. As a result, the uncertainty contribution for heavy isotope scattering that is currently being computed by codes such as CASMO-4 and DINASOUR is not exact. This is quite unfortunate as heavy isotope (n,inel) reactions are reported to have high uncertainties and can contribute greatly to the overall response uncertainty.[12]

Problem Statement

The remainder of this work, we will progress towards a more accurate computation of the sensitivity and uncertainty by introducing further developments to account for:

- the implicit sensitivity.
- leakage and anisotropy.
- accurate computation of the uncertainty contribution from heavy isotope scattering reactions.

[11] While not discussed here, the ERANOS code also computes sensitivities to such reactions

[12] For the cases considered in chapter 4, we will see that that uncertainties for ^{238}U (n,inel) cross section is the dominant contributor to the k_{eff} uncertainty originating from ^{238}U.

Chapter 3

Methodology: Part II
Sensitivity Analysis with DRAGON

This chapter presents some of the more conceptual developments which were made, over the course of this study, with the code DRAGON in order to respond to the benchmarks presented in chapter 4. We concentrate on three effects. First, we will introduce an approximation that permits us to compute the perturbation in the spectral fine flux due to an underlying perturbation in the nuclear data. This allows us to compute the implicit sensitivity. Next, we will consider the problem of neutron leakage. By invoking the buckling formalism, and treating leakage as a standard cross section, we obtain a sensitivity expression that includes a correction term accounting for neutron leakage. This permits for an accurate computation of the scattering sensitivity. Finally, we present our methodology for computing uncertainties using sensitivities obtained in terms of the data available in the WIMS libraries and the uncertainty data currently available in the form of covariance matrices.

3.1 Spectral Fine Structure Effects

Sensitivity and uncertainty analysis in reactor physics usually begins with neutron transport computations at the group level, with a multi-group library that has been obtained through the necessary assumptions applicable to the system. But, as we discussed it when presenting the narrow resonance approximation introduced in section 1.4.1, a flux solution can be performed only after the multi-group cross sections corresponding to the geometry are computed. This is usually done through a self shielding calculation. The self shielding calculation uses the available information in the multi-group library to produce multi-group cross sections best representative of the system. In the case where equivalence methods are used, the self shielding calculation uses various simplifications to arrive at an equivalence principle between the slowing down flux in an infinite homogeneous medium and the slowing down flux in the heterogeneous geometry [73, 21]. The computed flux and adjoint solutions correspond to the system with these self shielded cross sections. The sensitivity expressions of equations 1.194 or 1.198 are then calculated in terms of these cross sections. They represent the % change in the response with respect to a 1% uniform change in the self shielded cross section.

However, it should be noted that a change in a nuclear data such as a resonance parameter can have a non-negligible effect on the group constants by affecting the weighting flux spectrum $f(E)$ appearing in equations 1.57 to 1.60. Within the resonance region where the weighting flux usually has a strong dependence on cross section parameters, the effect is a concern. This effect is usually accounted for [74, 75] as an additional sensitivity of the multi-group cross section to a change in the continuous spectrum cross section. However, it is difficult to compute this change due to the nonlinearity of the self shielding phenomena and the fact that we do not have access to continuous spectrum cross sections during the transport calculation.

In this section we proceed to compute the sensitivity of the self-shielded group parameter to the nuclear data parameter q. This computed sensitivity is comparable to what is called the implicit sensitivity [74, 75] in the system code SCALE [48, 49]. To compute the implicit sensitivity, we will first present a review of equivalence theory methods in application to the Wigner Cell - an isolated rod, emergent in a sea of moderator.

While this is one of the simpler heterogeneous geometries, it will allow the reader to become familiar with the notions involved in a self-shielding calculation. We will then proceed to present the chain rule approach introduced by Greenspan [15], which relates the perturbation in the self-shielded group parameter of the resonant isotope with the resultant perturbations in the group parameters of all the constituents of the geometry. We will then proceed to provide an analytical expression for the perturbation in the fine flux, which can be used with the chain rule approach of Greenspan to compute accurately the implicit sensitivity in homogeneous geometries. The approximation is more constraining in heterogeneous geometries and can only be used to predict the implicit sensitivity of a resonant isotope due to a perturbation in its nuclear data.

3.1.1 Self-shielding and Equivalence Theory

Self shielding calculations involving homogeneous-heterogeneous equivalence theory [77, 21, 73] usually begin with cross sections tabulated as a function of temperature and a dilution factor σ_0. The dilution factor σ_0 (barns) provides a measure of the moderator's ability to thermalize neutrons past the resonant isotope's many resonances. The definition of the dilution factor, depends on the specific approximation formalism that was used to generate the weighting flux. Each approximation (narrow resonance, intermediate resonance, etc.) [19] will result in a slightly different definition of the dilution factor σ_0.

In this section we will review the homogeneous-heterogeneous equivalence formalism in application to a simple heterogeneous system: the Wigner cell, using the Narrow Resonance Approximation (NRA) [78]. The approximation that we use in our implementation is the Intermediate Resonance Approximation (IRA). As will be seen in section 3.1.3, the NRA formulas can be adapted to the IRA by a change in notation and definition of the dilution factor.

In the framework of the Narrow Resonance Approximation, the dilution factor in a

homogeneous mixture with one resonant isotope is defined as [19] :

$$\sigma_0 = \sum_{k \neq r} \frac{N_k}{N_r} \sigma_{p,k} \tag{3.1}$$

where N_k is the atomic density of the non resonant isotope having the potential scattering cross section $\sigma_{p,k}$, and N_r is the atomic density of the resonant isotope (atms/cm-barns). As was discussed in Chapter 1, group parameters are generated by using the weighting flux corresponding to neutron thermalization/slowing down in an infinite homogeneous mixture composed of the resonant isotope with a moderator. In the case of the NRA, the fine flux in the homogeneous medium was defined in equation 1.71 to be [38, 19]:

$$\phi^{HOM}(E) = \frac{\sigma_{p,r} + \sigma_0}{\sigma_r(E) + \sigma_0} \frac{1}{E} \tag{3.2}$$

where σ_r and $\sigma_{p,r}$ are the resonant isotope's total and potential cross sections respectively. Note that in equation 3.2 we assumed the scattering cross section to be dominated by potential scattering.

In equivalence theory methods, flux expressions for a heterogeneous geometry often involve linear combinations of homogeneous fluxes given by equation 3.2. The goal of the equivalence method in self shielding computations is then to calculate a dilution factor σ_0 "best" representative of the geometry. This principle is well illustrated by using the Wigner Cell example - a single rod in a sea of moderator.

The Wigner Cell

We can imagine a two volume system, composed of an isolated fuel rod F immersed in a moderator region M. The total collision rate in the fuel is given as [19, 20]:

$$\begin{aligned} \Sigma_F(E)\phi_F(E)V_F = {} & P_{F\to F}(E)V_F \int_0^\infty dE' \Sigma_{s,F}(E' \to E)\phi_F(E') \\ & + P_{M\to F}(E)V_M \int_0^\infty dE' \Sigma_{s,M}(E' \to E)\phi_M(E') \end{aligned} \tag{3.3}$$

where $\Sigma_F = \Sigma_r + \sum_{k \in F} \Sigma_k$ is the fuel macroscopic total cross section, Σ_r is the macroscopic total cross section of the resonant isotope r, Σ_k is the macroscopic total cross section of the non-resonant isotope $k \neq r$, $\phi_F(E)$ is the flux in the fuel region, V_F is the volume of the fuel region, $\Sigma_{s,F}$ is the macroscopic scattering cross section in the fuel, $\Sigma_{s,M}$ is the macroscopic scattering cross section of the moderator, $P_{F\to F}$ and $P_{M\to F}$ are the fuel to fuel and moderator to fuel collision probabilities respectively.

Assuming scattering to be only possible by elastic collisions, so that the energy transfer probabilities can be effectively represented by the form presented in equation 1.66 and

integrating over the differential scattering cross sections leads to [19, 20]:

$$\Sigma_F(E)\phi_F(E)V_F = P_{F\to F}(E)V_F \sum_{k\in F}\int_E^{E/\alpha_k} \frac{N_k\sigma_{s,k}(E')\phi_F(E')}{(1-\alpha_k)E'}dE' + P_{M\to F}(E)V_M \sum_{i\in M}\int_E^{E/\alpha_i} \frac{N_k\sigma_{s,i}(E')\phi_M(E')}{(1-\alpha_i)E'}dE' \tag{3.4}$$

where the index $k \in F$ refers to isotopes in the fuel and the index $i \in M$ refers to isotopes in the moderator. Here, $\sigma_{s,k}$ and $\sigma_{s,i}$ are the microscopic scattering cross section of isotope k and i with density N_k and N_i, and $\alpha_k = \left(\frac{A_k-1}{A_k+1}\right)^2$, and A_k is the ratio of the mass number of isotope k to the neutron mass. Equation 3.4 can be greatly simplified if resonances are assumed to be narrow and well separated, so that they do not overlap. In this case they will have a small contribution to the integrals appearing in equation 3.4. If a resonance width is small, the neutrons that fall inside the resonant region come from outside of the resonance where interaction is dominated by the potential cross section. Outside the resonance, the flux $\phi(E)$ has the asymptotic shape of $\frac{C}{E'}$ (where with the proper normalization, C can be taken to be unity) and the scattering cross section of the resonant isotope is its potential/background cross section $\sigma_{r,p}$. We can also assume that the moderator cross section is constant and dominated by potential scattering so that $\sigma_{s,k} = \sigma_{p,k}$. Ignoring the contribution of the flux under the resonance to the energy integral of equation 3.4, we have [19, 20]:

$$\frac{1}{1-\alpha_k}\int_E^{E/\alpha_k} N_k\sigma_{p,k}\phi(E')\frac{dE'}{E'} = N_k\sigma_{p,k}\frac{1}{E} \text{ for } k \neq r \tag{3.5}$$

$$\frac{1}{1-\alpha_k}\int_E^{E/\alpha_r} N_r\sigma_{s,k}(E')\phi(E')\frac{dE'}{E'} = N_k\sigma_{p,k}\frac{1}{E} \text{ for for } k = r \tag{3.6}$$

In the case where only a single resonant isotope is considered, equation 3.4 simplifies to [20]:

$$\Sigma_F(E)\phi_F(E)V_F = \frac{1}{E}\left(P_{F\to F}(E)V_F\Sigma_{p,F} + P_{M\to F}(E)V_M\Sigma_{p,M}\right) \tag{3.7}$$

where $\Sigma_{p,F} = N_r\sigma_{p,r} + \sum_{k\neq r} N_k\sigma_{p,k}$ is the macroscopic potential scattering cross section of the fuel, and $\Sigma_{p,M} = \sum_{i\in M} N_i\sigma_{p,i}$ is the macroscopic potential scattering cross section of the moderator.

In the case where only two regions are considered, the reciprocity relation given by equation 1.88 becomes:

$$\frac{P_{M\to F}(E)}{V_F\Sigma_F(E)} = \frac{P_{F\to M}(E)}{V_M\Sigma_M} \tag{3.8}$$

Using the above reciprocity law, equation 3.7 reduces to [20]:

$$\phi_F(E) = \frac{1}{E}\left((1-P_{F\to M}(E))\frac{\Sigma_{p,F}}{\Sigma_M(E)} + P_{F\to M}(E)\right) \tag{3.9}$$

We note that equation 3.9 requires knowledge of the collision probability $P_{F\to M}(E)$. For

the Wigner cell, the fuel to moderator collision probability $P_{F\to M}$ can be expressed as [78, 20]:

$$\begin{aligned} P_{F\to M}(E) &= \frac{1}{\Sigma_F(E)\bar{l}} \int_0^\infty (1 - \exp(-\Sigma_F(E)l))\, dl \\ &= \frac{1}{\Sigma_F(E)\bar{l} + 1} \end{aligned} \tag{3.10}$$

where $\bar{l} = \frac{4V}{S}$ is the average chord length of the fuel geometry of volume V and surface area S. By merit of equation 3.9 the flux $\phi(E)$ of the Wigner cell simplifies to [20]:

$$\phi_F(E) = \frac{1}{E} \frac{\Sigma_{p,F} + 1/\bar{l}}{\Sigma_F(E) + 1/\bar{l}} \tag{3.11}$$

$$= \frac{1}{E} \frac{N_r\sigma_{p,r} + \sum_{k\neq r} N_k\sigma_{p,k} + \Sigma_e}{N_r\sigma_r(E) + \sum_{k\neq r} N_k\sigma_{p,k} + \Sigma_e} \tag{3.12}$$

$$= \frac{1}{E} \frac{\sigma_{p,r} + \overbrace{(\sigma_{0,F} + \Sigma_e/N_r)}^{\sigma_0}}{\sigma_r(E) + \underbrace{(\sigma_{0,F} + \Sigma_e/N_r)}_{\sigma_0}} \tag{3.13}$$

with $\sigma_{0,F} = \sum_{k\neq r} \frac{N_k}{N_r}\sigma_{p,k}$ and the escape cross section $\Sigma_e = \frac{1}{\bar{l}}$ defined as the inverse of the average chord length $\bar{l}$.

Equation 3.13 is remarkably similar to the slowing down flux given by equation 3.2 for an infinite homogeneous medium with the dilution factor $\sigma_0 = \sigma_{0,F} + \Sigma_e/N_r$. When the mean average chord length $\bar{l}$ is small (i.e. a large escape cross section Σ_e), as would be the case for a small rod, neutrons from the moderator can easily reach any point inside the rod and have a large chance of escaping from the fuel. Therefore, the flux depression due to the resonant isotope is minimal (the self-shielding effect is small).

Most equivalence theory based methods involve representing the fuel to moderator collision probability as rational expressions similar to equation 3.10. For complicated heterogeneous geometries, each formalism uses a number of assumptions regarding the form of the fine flux structure $\phi_F(E)$ to arrive at a representation of the escape probability $P_{F\to M}(E)$, and Σ_e which involve sums of rational expressions similar to equation 3.9.

During the computation of $P_{F\to M}(E)$, the choice of the nuclear data available is limited to the data available in the library. Relevant to the self shielding calculation, this data includes the constant potential cross section $\sigma_{p,r}$, and the temperature dependent resonance integral tabulated in terms of the dilution factor σ_0. The resonance integral was defined by equation 2.6 as [38]:

$$I = \frac{\sigma(T, \sigma_0)\sigma_0}{\sigma(T, \sigma_0) + \sigma_0} \tag{3.14}$$

Given the flux depressions under the resonance, the resonance integral I provides a mono-

tone increasing function (as a function of dilution) for which interpolation over the dilution and temperature can be performed.[1] If the intermediate resonance approximation is used, an intermediate resonance factor $\lambda \in [0, 1]$ is also provided [79, 80]. The intermediate resonance factor λ provides a measure of the width of the resonance with $\lambda = 0.0$ if the resonance is large, and $\lambda = 1.0$ if the resonance is narrow. The group cross sections can then be computed by inverting equation 3.14. An iterative procedure over the dilution factor σ_0 is performed to arrive at a set of cross sections that satisfy a representation of equation 3.4 for all resonant isotopes that are present in the system.

3.1.2 Spectral Fine Structure Effects: Chain Rule Approach of Greenspan

Returning to the Wigner cell problem and equation 3.13, it can be seen that a change in the nuclear data q that results in the changes $\delta\sigma_{p,r}$, $\delta\sigma_r$ in the cross sections and $\delta\sigma_0$ will cause a change $\delta\phi$ in the weighting flux of equation 3.13 given by:

$$\delta\phi(E) = \frac{\partial\phi(E)}{\partial\sigma_{p,r}}\delta\sigma_{p,r} + \frac{\partial\phi(E)}{\partial\sigma_r}\delta\sigma_r + \frac{\partial\phi(E)}{\partial\sigma_0}\delta\sigma_0 \tag{3.15}$$

The first two terms are perturbations in the weighting spectrum $\phi(E)$ from its explicit dependence on the potential and total cross sections $\sigma_{p,r}$ and σ_r. The third term containing $\delta\sigma_0$ takes into account the implicit perturbation [75] in the weighting spectrum due to the change in the dilution factor σ_0. It should be noted that σ_0 depends on all the cross sections of the other constituents of the assembly. This dependence comes from the collision probability term $P_{F\to M}$ which appears in equation 3.9 and the term $\sigma_{0,F} = \sum_{k\neq r}\frac{N_k}{N_r}\sigma_{p,k}$ which depends on the scattering cross sections of all isotopes present other than that of the resonant isotope. A change in the parameters of one isotope may therefore induce a change in the parameters of another isotope, thereby adding new correlations. A good example of this is the correlation between ^{238}U capture and hydrogen scattering in a LWR where an increase in the hydrogen atomic density will increase the moderation (increasing the dilution factor), thereby lowering the flux depression and thus increasing the value for the multi-group absorption cross section.

The group parameter $\left\langle\sigma_{x,I}^{HET}\right\rangle$ of isotope I for the heterogeneous geometry can then be expressed as:

$$\left\langle\sigma_{x,I}^{HET}\right\rangle = f_{x,I}(\sigma_0, \sigma_x(E))\sigma_{x,I}^{\infty} \tag{3.16}$$

where $\sigma_{x,I}^{\infty}$ is the group parameter available in the multi-group library generated using a $1/E$ weighting spectrum ($\sigma_0 = \infty$), and the f-factor [74] accounts for the neutron spectrum effect on the group constants in the continuous energy region. The f-factor is a representative correction due to heterogeneity effects and composition. It contains all information regarding the cross section, the isotopic composition of the geometry and the heterogeneity of the geometry. In many simple codes, the self shielding problem is handled from tabulated values of f-factors representing various geometries with interpolation

[1] Computationally, a simple linear interpolation will suffice, although Lagrange interpolation [62] is used in DRAGON. We use quadratic splines in our PYTHON codes

over geometric parameters used to generate the case dependent f-factors. In principle, the self-shielding f-factor of isotope I depends on all the other constituents of the assembly. The dependence comes from the weighting flux function that was used to generate the group parameters.

The change in the group constant $\left\langle \sigma_{x,I}^{HET} \right\rangle$ due to a change in the nuclear data q is then given by:

$$\frac{\partial \left\langle \sigma_{x,I}^{HET} \right\rangle}{\partial q} = f_{x,I} \frac{\partial \sigma_{x,I}^{\infty}}{\partial q} + \sigma_{x,I}^{\infty} \frac{df_{x,I}}{dq} \tag{3.17}$$

If $\left| f_{x,I} \frac{\partial \sigma_{x,I}^{\infty}}{\partial q} \right| >> \left| \sigma_{x,I}^{\infty} \frac{df_{x,I}}{dq} \right|$, then spectral fine structure effects are negligible and can be ignored so that there is a linear relationship between a change in the cross section σ_x^{∞} and the self shielded cross section $\left\langle \sigma_{x,I}^{HET} \right\rangle$. However, in the case where $\left| \sigma_{x,I}^{\infty} \frac{df_{x,I}}{dq} \right|$ is not negligible, the relation between the self shielded cross section and the nuclear data q becomes more complicated. In particular, since the f-factor $f_{x,I}$ depends on all the constituents of the assembly, we have [74]:

$$\frac{df_{x,I}}{dq} = \frac{\partial f_{x,I}}{\partial \sigma_x^I} \frac{\partial \sigma_x^I}{\partial q} + \sum_{J \neq I} \sum_y \frac{\partial f_{x,I}}{\partial \sigma_y^J} \frac{\partial \sigma_y^J}{\partial q} \tag{3.18}$$

with J changing over all isotopes other than I and all reactions y. We note that a change in the nuclear data parameter q can affect many different f-factors.

Next consider the sensitivity of the response R, due to a perturbation in the input parameter q. The contribution to the resulting change in the performance parameter R from a perturbation in q can be via many different channels, including all group constants. Therefore, $\frac{df}{dq}$ may no longer be negligible. Taking into account the possible contribution from all channels we arrive at the chain-rule form of the sensitivity given by Greenspan as [74]:

$$\begin{aligned} S_{Rq} &\equiv \frac{\delta R}{R} / \frac{\delta q}{q} \\ &= \sum_I \sum_x \overbrace{\left[\frac{\delta R}{R} / \frac{\delta \left\langle \sigma_{x,I}^{HET} \right\rangle}{\left\langle \sigma_{x,I}^{HET} \right\rangle} \right]}^{G_{R,x}^I} \overbrace{\left[\frac{\delta \left\langle \sigma_{x,I}^{HET} \right\rangle}{\left\langle \sigma_{x,I}^{HET} \right\rangle} / \frac{\delta q}{q} \right]}^{P_{x,q}^I} = \sum_I \sum_x G_{R,x}^I P_{x,q}^I \end{aligned} \tag{3.19}$$

Here, $G_{R,x}^I$ is the sensitivity coefficient of the performance parameter to the group constant; it is precisely what is being calculated in formulas such as equations 1.194 or 1.198 and is often referred to as the explicit sensitivity since it does not take into account any change in the fine flux due to the perturbation in the base parameter q. $P_{x,q}^I$ is the group constant sensitivity coefficient (to the base parameter q) and can be expressed from

equation 3.17 as [74]:

$$P^I_{x,q} \equiv \frac{\delta\left\langle\sigma^{HET}_{x,I}\right\rangle}{\left\langle\sigma^{HET}_{x,I}\right\rangle}\Big/\frac{\delta q}{q} = \overbrace{\left(f^I_x\frac{\delta\sigma^{\infty}_{x,I}}{\sigma^{HET}_{x,I}}\right)/\left(\frac{\delta q}{q}\right)}^{D^I_{x,q}} + \overbrace{\left(\frac{\delta f^I_x}{f^I_x}\right)/\left(\frac{\delta q}{q}\right)}^{Q^I_{x,q}}$$
$$= D^I_{x,q} + Q^I_{x,q} \tag{3.20}$$

The first term $D^I_{x,q}$ accounts for the direct change in the tabulated group cross section available in the multi-group library due to a change in the nuclear data q. The second term $Q^I_{x,q}$ accounts for the perturbation in the spectral fine structure which is taken into account through the change in the self shielding factor δf^I_x.

Equation 3.20 represents the sensitivity in (%/%) of the group cross section after self shielding $\left\langle\sigma^{HET}_{x,I}\right\rangle$ to a perturbation in the tabulated homogenized cross sections before self shielding $\left\langle\sigma^{\infty}_{x,I}\right\rangle$. If covariance matrices for group constants are calculated at each dilution factor appearing in the library (normally, this data is only provided at infinite dilution), then the uncertainty due to nuclear data q may be calculated in a straight forward manner.

When $q = \sigma^{\infty}_x$, the sensitivities $\left(\frac{\delta f^I_x}{f^I_x}\right)/\left(\frac{\delta\sigma^{\infty}_x}{\sigma^{\infty}_x}\right)$ that appear in equation 3.20 are difficult to calculate given the complexity of the self shielding problem. If equivalence theory methods are used, the computational time spent on the self shielding calculation is usually a small fraction of the total computation time of the transport calculation. This is particularly true for large cases. For core or assembly cases, representative sub-geometries are chosen for which a self shielding calculation is performed for 3x3 or 4x4 sub-cells with a different fuel mixture number assigned to each sub-geometry.[2] Flux computations for large cases are then performed using the computed self-shielded cross sections computed for the sub-geometries. Additionally, the sensitivity $\frac{df^I_x}{d\sigma^{\infty}_x}$ is non-negligible for only a few isotopes and reactions.[3] This suggests that computation of the expression $\frac{df^I_x}{d\sigma^{\infty}_{x,I}}$ by direct simulations (i.e. performing a self shielding calculation) is feasible. This option has been implemented using our PYTHON modules described in the previous chapter: the multi-group library is modified, a self shielding computation is performed, and the resultant implicit sensitivity is computed using equation 3.19. In homogeneous systems however, a simple analytic expression can be used to compute the resultant perturbation in the group parameter. In heterogeneous systems, as will be shown in the next section, an analytical expression can be used to estimate the direct component appearing in the summation rule given by equation 3.20 (the effect of an isotope on itself). The key point being that in both cases (a homogeneous system, or the effect of an isotope on itself in a heterogeneous system), a direct simulation approach can be avoided.

[2]The reader can imagine the necessity of modeling cells near the reflector, or control rod devices separately.

[3]eg. at BOL, for LWRs, the effect is only noticeable for ^{238}U and ^{1}H

3.1.3 Implementation

As far as computation is concerned, the only "nuclear data" parameters that appear on the WIMS multi-group libraries are group constants computed at inifnite dilution, the fission and absorption resonance integrals $I(T, \sigma_0)$,[4] and the dilution factor $\sigma_{p,I}$. An option implemented is then to perturb the group parameters and the resonance integrals and perform a self-shielding computation with DRAGON. Once the cross section sensitivities of equation 3.20 are calculated, the sensitivity of the response R defined in equation 3.19 can be calculated using classical perturbation theory for the sensitivity coefficient $G^I_{R,x}$. However, this approach requires several self shielding calculations for each isotope and each reaction. We will now proceed to derive an analytical expression for the perturbation in the fine flux that can be effectively applied to compute the implicit sensitivity in homogeneous geometries.

WIMSD4 uses the intermediate resonance approximation so that the slowing down flux for a given dilution factor σ_0 is defined as [38]:

$$\phi(E, \sigma_0) = \frac{\lambda\sigma_{p,r} + \sigma_0}{\sigma_a(E) + \lambda\sigma_{s,r}(E) + \lambda\sigma_{p,r} + \sigma_0}\frac{1}{E} \tag{3.21}$$

where $\sigma_a(E)$ is the resonant isotope's absorption cross section and λ is the Golden-Cohenstein factor used in the intermediate resonance approximation [79]. Since the scattering cross section is proportional to the potential cross section, an ϵ % uniform change in the cross section implies an ϵ % change in the potential cross section. We can imagine a uniform change in the scattering cross section, so that:

$$\sigma_{p,r} \rightarrow (1+\epsilon)\sigma_{p,r} \;\Rightarrow\; \sigma_{s,r}(E) \rightarrow (1+\epsilon)\sigma_{s,r}(E) \tag{3.22}$$

by merit of equation 3.21 the resulting change in the flux is given by:

$$\begin{aligned}\phi' &= \frac{\lambda\sigma_{p,r} + \sigma_0(1+\epsilon)^{-1}}{(1+\epsilon)^{-1}\sigma_0 + \lambda_r\sigma_{s,r} + \lambda_r\sigma_{p,r} + \sigma_a(1+\epsilon)^{-1}}\frac{1}{E} \\ &\sim \phi(E, \sigma_0') \cdot (1 + \frac{\epsilon\sigma_a}{\sigma_a(E) + \lambda\sigma_{s,r}(E) + \lambda\sigma_{p,r} + \sigma_0'})\end{aligned} \tag{3.23}$$

where $\sigma_0' \equiv (1+\epsilon)^{-1}\sigma_0$. The absorption resonance integral $I_{a,r}$ is stored in the multi-group library, tabulated as a function of the dilution factor $\sigma_b = \lambda\sigma_{p,r} + \sigma_0$. The ϵ % uniform perturbation in the scattering cross section is then equivalent to interpolating the resonance integrals at the new values of the background cross section:

$$\sigma_b' = \frac{\sigma_0}{1+\epsilon} + \lambda\sigma_{p,r} \tag{3.24}$$

and multiplying the obtained value by the term in the bracket appearing in equation 3.23.

[4] Only one set of scattering cross sections are provided at the "typical" dilution of a PWR.

Homogeneous Medium

In a homogeneous system, equation 3.21 provides an analytical approximation for the fine flux. Similarly, equation 3.23 provide an analytical expression for the change in the fine flux due to a uniform perturbation in the potential scattering cross section $\sigma_{p,r}$, and thus the scattering cross section $\sigma_{s,r}$ of the same isotope. Equation 3.24 expresses this perturbation in terms of an effective perturbation in the dilution factor. In a similar manner, a perturbation in the cross sections of an other isotope $k \neq r$ in the system can be accounted for by modifying the dilution cross section. If the Intermediate Resonance Approximation is used (IRA), the dilution factor defined in equation 3.13 is written as: $\sigma_{0,F} = \Sigma_{k \in m} \lambda_k \frac{N_k}{N_r} \sigma_{p,k}$ (computationally, the total cross section of isotope $k \neq r$ is assumed to be equal to $\sigma_{p,k}$). Therefore, a perturbation in the cross section of isotope $k \neq r$ will perturb the dilution cross section of isotope r as:

$$\sigma_b^r \rightarrow \sigma_b^r + \lambda_k \frac{N_k}{N_r} \delta\sigma_{p,k} \tag{3.25}$$

In a homogeneous medium, equations 3.24 and 3.25 can be used to provide an estimate for the perturbation in the group parameter $\delta \left\langle \sigma_{x,I}^{HET} \right\rangle / \left\langle \sigma_{x,I}^{HET} \right\rangle$. This approximation is as accurate as the value obtained by direct simulations (this is true to the limit of the IRA).

Heterogeneous Medium

Glancing back at equation 3.17, we may wonder how much does the heterogeneity of the system influence the sensitivity $\delta f_x^I / f_x^I$? The effect of the heterogeneity of the system is taken into account through the collision probability term of equation 3.7. For the Wigner cell, the simple expression for the collision probability resulted in the energy independent escape cross section Σ_e in equation 3.13. In general, the expressions for the collision probability are more complicated and require an iterative solution over all isotopes. In [21], Hebert and Marleau approximate the collision probability as a three term rational expansion of the fine flux for a homogeneous medium. The resulting expression is shown to be [21]:

$$\phi^{HET}(E) = \sum_{n=1}^{3} \alpha_n^g \frac{\lambda_r \Sigma_{p,r} + \Sigma_{0,n}^g}{\Sigma_{a,r}(E) + \lambda_r \Sigma_{s,r} + \Sigma_{0,r}^g} \frac{1}{E} \tag{3.26}$$

with:

$$\Sigma_{0,n}^g = N_r \sigma_{0,n}^g \tag{3.27}$$

$$\sum_{n=1}^{3} \alpha_n^g = 1 \tag{3.28}$$

for $n = 1, .., 3$. The dilution cross sections $\Sigma_{0,n}$, along with the coefficients α_n, which satisfy the summation rule given by equation 3.28, provide five degrees of freedom for approximating the collision probability (or the resulting expression for the heterogeneous fine flux) using the rational expansion given in equation 3.26. During the self shielding

computation, a system of equations is solved iteratively to obtain the coefficients α_n and the dilution cross sections $\sigma_{0,n}$ for each resonant isotope (iterating over the resonant isotopes). An equivalent dilution factor is then defined as [21]:

$$\Sigma^g_{eff} = N_r\sigma_{eff} = \left(\alpha_1(\Sigma^g_{0,1})^{\frac{1}{2}} + \alpha_2(\Sigma^g_{0,2})^{\frac{1}{2}} + \alpha_3(\Sigma^g_{0,3})^{\frac{1}{2}}\right)^2 \tag{3.29}$$

which is equivalent to the heterogeneous flux having the shape:

$$\phi^{HET}(E) = \frac{\lambda_r\Sigma_{p,r} + \Sigma^g_{eff}}{\Sigma_{a,r}(E) + \lambda_r\Sigma_{s,r} + \Sigma^g_{eff}}\frac{1}{E} \tag{3.30}$$

We can now imagine a uniform ϵ % increase the scattering and potential cross sections of the resonant isotope, and resulting in a perturbation of $\delta\Sigma^g_e$ in the equivalent group dependent dilution factor. The fine flux of the perturbed system is then given as:

$$\phi'^{HET}(E) = \frac{\lambda_r\Sigma_{p,r} + \Sigma^g_{eff}(1+\epsilon)^{-1}(1+\delta\Sigma_{eff}/\Sigma_{eff})}{(1+\epsilon)^{-1}\Sigma_{eff}(1+\delta\Sigma_{eff}/\Sigma_{eff}) + \lambda\Sigma_{s,r} + \lambda\Sigma_{p,r}}\frac{1}{E} \tag{3.31}$$

Equation 3.31 expresses the perturbed fine flux $\phi'^{HET}(E)$ as a change in the equivalent dilution factor, i.e.:

$$\Sigma^g_{eff} \rightarrow \Sigma_{eff}(1+\epsilon)^{-1}(1+\delta\Sigma_{eff}/\Sigma_{eff}) \tag{3.32}$$

The term in the first brackets accounts for the direct dependence of the fine flux on the cross section $\sigma_{p,r}$. The second term $\delta\Sigma_{eff}/\Sigma_{eff}$ is due to the resulting perturbation in the collision probability of the system (which would result in perturbations $(\delta\alpha_n)_3^{i=1}$ and $(\delta\sigma_{0,i})_3^{i=1}$ appearing in equations 3.27-3.29). If $|\delta\Sigma_{eff}/\Sigma_{eff}| << 1.0$, then the second bracket can be ignored with equation 3.31 reducing to equation 3.23. This rule can be expected whenever one attempts to predict the effect of an isotope on itself (i.e. a direct effect in the self shielding) and the resonances are narrow. In this case, the heavy isotope scattering reaction is efficient in removing neutrons from under the resonances, so that the direct term dominates the sensitivity and the second bracket of equation 3.31 can be effectively ignored. For the benchmarks presented in chapter 4, equation 3.23 is applied to accurately compute the effect from a perturbation in the ^{238}U(n,el) cross section on the ^{238}U(n, γ) group parameter which is used compute the implicit sensitivity of ^{238}U(n,el) from equation 3.19.

3.1.4 Verification

In chapter 4, we verify our methodology for computing scattering implicit sensitivities by comparing them with reference results obtained from SCALE/TSUNAMI-1D and SCALE/TSUNAMI-3D. Our library is the IAEA released WIMS library [38] based on the 172-group XMAS energy mesh [47] while the SCALE/TSUNAMI [51] package uses a 238-group energy mesh. Therefore, comparison of implicit sensitivity profiles is difficult due to the differences in meshing and the numerous resonances that are associated with heavy isotopes responsible for the implicit effect. Therefore, when comparing profiles, we average the SCALE sensitivity profiles over the WIMS 172-group structure, by first

constructing a union grid E^{383}_{UNION}:

$$E^{383}_{UNION} = E^{172}_{DRAGON} \cup E^{238}_{SCALE} \tag{3.33}$$

composed of the union of the SCALE 238-energy grid E^{238}_{SCALE} and the DRAGON/WIMS 172-group energy structure E^{172}_{DRAGON}. The union grid is observed to have 383 energy groups. The lethargy normalized SCALE sensitivity profile S^{SCALE}_{238g}/du is then expanded to this grid. We then perform a flat-flux energy integration of this sensitivity to collapse to the DRAGON/WIMS 172-group mesh.

3.2 Leakage and Anisotropy

When performing transport computations with lattice codes, the most commonly encountered geometries are infinite configurations of cells or assemblies. This corresponds to the k_{eff} solution that was discussed earlier in chapter 2 with reflective boundary conditions. Naturally, since the modeled geometry ignores the loss of neutrons due to leakage, the k_∞ value for such geometries is super-critical. In reality however, the core as well as the lattices within the core are at critical conditions due to the presence of leakage so that the leakage rate must be accounted for during the transport computation. The leakage rate depends on scattering anisotropy and neutron streaming [14]. In LWRs, scattering anisotropy must always be accounted for due to the hydrogen moderator. The streaming effect is caused by the presence of strong heterogeneity in the core or the presence of regions where the total cross section is low (such as for example a voided zone in the core) [14]. The streaming effect can also be anisotropic if the leakage is in a specific direction rather than identical in all three spatial directions or if the lattice properties are not identical over all spatial directions. In sensitivity analysis, we can expect a strong link between neutron scattering, neutron streaming, and leakage.

In section 1.7.2, we noted that for problems where the neutron flux is anisotropic, the approximation for the CP matrix given by equation 1.188 is inadequate. This is particularly true for scattering reactions due to the angular dependence of the scattering sensitivity gain term $\left\langle \phi^\dagger, \mathbf{S}\phi \right\rangle$ which appears in the sensitivity formulas (equations 1.194 and 1.198). Courau and Marleau [34] attempted to account for this by introducing a correction matrix $\mathbf{C}(\mathbf{\Sigma})$, whose elements were computed by direct perturbations (per mixture). However, as we will shortly see, the problem of the approximation for the CP matrix can be greatly simpled by reformulating the problem in terms the Buckling approximation, i.e. by treating leakage as a standard cross section. This approach not only greatly simplifies the task of approximating the resultant perturbation in the CP matrix, but also allows for the modeling of critical geometries in 1-D or 2-D, that would otherwise require 3-D transport solutions, thereby cutting greatly computational costs.

In this section, we will give a short review of the Buckling approximation and the method *SIGMA*. We will then derive a correction term in the sensitivity formulas which results from reformulating the problem in terms of its equivalent leakage problem. Finally, we will present our algorithm, as implemented in DRAGON, to effectively compute the sensitivity for critical geometries that can involve flux anisotropy induced by neutron

leakage.

3.2.1 The Buckling approximation

For a finite size reactor, there exists inside of the reactor a large region where the spatial variation of the flux is the same for all neutron energies [83]. This is the basis behind the buckling concept. In the buckling approximation, the spatial dependent flux $\phi(\vec{r}, \hat{\Omega}, E)$ is assumed to be separable and has the spatial decomposition given by [81]:

$$\phi(\vec{r}, \hat{\Omega}, E) = e^{i\vec{B}\cdot\vec{r}}\phi(E, \hat{\Omega}) \tag{3.34}$$

In equation 3.34, the spatial component $e^{i\vec{B}\cdot\vec{r}}$ accounts for the attenuation in the flux as $\vec{r}$ approaches the boundary of the geometry. The spectral component $\phi(\hat{\Omega}, E)$ can be thought of as the flux in the corresponding homogeneous infinite medium. Finally, the buckling coefficient B^2 provides a measure of the reactor size. It is inversely proportional to the size of the reactor and therefore the leakage, i.e. a small reactor will have a large buckling B^2 and therefore a large leakage rate.

Defining $\mu = \hat{\Omega}\cdot\hat{k}$ as the cosine of the direction $\hat{\Omega}$ along the z-axis (with unit vector $\hat{k}$), expanding the flux $\phi(E, \hat{\Omega})$ appearing in equation 3.34 in terms of Legendre Polynomials and substituting into the transport equation 1.10 gives [83]:

$$\phi(E, \mu) \sim \sum_l \phi_l(E) P_l(\mu) \tag{3.35}$$

$$\begin{aligned}\phi_l(E) = \frac{1}{4\pi}\sum_{n=0}^{\infty}\int_{E'=0}^{\infty} dE' \Sigma_{s,n}(E' \to E)\phi_n(E')\int_{\hat{\Omega}\in 4\pi} d\hat{\Omega}\frac{P_n(\mu)P_l(\mu)}{\Sigma(E) + iB\mu} \\ + \frac{\chi(E)}{4\pi k_{eff}}\int_{E'=0}^{\infty} dE'\nu(E')\Sigma_f(E')\phi_0(E')\int_{4\pi} d\hat{\Omega}\frac{P_l(\mu)}{\Sigma(E) + iB\mu}\end{aligned} \tag{3.36}$$

where $\Sigma(E)$ is the total cross section at energy E, $\Sigma_{s,n}(E' \to E)$ is the n^{th} Legendre coefficient of the scattering matrix, and $P_l(\mu)$ refers to the l^{th} Legendre Polynomial [13]. The flux moments $\phi_l(E)$ for $l \in \mathbb{N}$ are defined as:

$$\phi_l(E) = \frac{1}{4\pi}\int_{\hat{\Omega}\in 4\pi} d\hat{\Omega}\phi(E, \mu)P_l(\mu) \tag{3.37}$$

The system of equations 3.35-3.36 is called the B_N equations. In practice, the series appearing in equation 3.36 is truncated for values $n > N$, allowing equation 3.36 to be solved numerically to obtain the moment flux ϕ_l with $l = 0, .., N$.

An important property of the system 3.36 is the type of coupling that exists between the moments ϕ_l [83]. The flux moments ϕ_l are coupled through the scattering source of the series on the right hand side of equation 3.36. If the higher moments $\Sigma_{s,n}$ of the scattering cross section vanish for $n > N$, then the computed solution of the first N values of the moment flux are independent of the $(N+1)^{th}$ solution (i.e. the system is a lower diagonal matrix). This property of the B_N equations makes the computed flux $\phi(\mu, E)$ fairly accurate even when the series is truncated at the zeroth term (i.e. B_0 equations) or

the first term (i.e. B_1 equations). We note that this is not the case with the P_N equations where evaluating the values of the higher moments ($l > N$) alters the components found by a lower computation ($l \leq N$).

The B_0 approximation corresponds to truncating the series term in equation 3.36 at $N = 0$. In this case, an analytical expression [83] can be derived for the flux and the current of the system [83]:

$$\vec{J}^g = -id_0^g \vec{B}\phi^g = -d_0^g \nabla \cdot \phi^g(\vec{r}, \hat{\Omega}) \tag{3.38}$$

where $\vec{J}^g$ is the neutron current in group g, and ϕ^g is the average over group g of the flux $\phi(\vec{r}, \hat{\Omega})$ appearing in equation 3.34. The diffusion coefficient d_0^g is defined as [81, 83]:

$$d_0^g = \frac{1}{B}\left(\frac{1 - \frac{\Sigma^g}{B}\tan^{-1}\frac{B}{\Sigma^g}}{\tan^{-1}\frac{B}{\Sigma^g}}\right) = \frac{1}{3\Sigma^g}\left(1 - \frac{4}{15}\left(\frac{B}{\Sigma^g}\right)^2 + ...\right) \tag{3.39}$$

In the case where only the first term appearing in equation 3.39 is used to define the diffusion coefficient d_0^g, equation 3.38 reduces to the familiar Fick's law of diffusion [81].

Equation 3.38 can be used to obtain/derive an expression for the flux in a critical system with leakage. A group dependent leakage cross section $d^g B^2$ is added to the absorption cross section to account for the neutrons lost due to leakage. The transport equation to be solved is then given by [24, 82]:

$$\phi = \mathbf{P}(\mathbf{\Sigma} + \mathbf{dB^2})\left[\mathbf{S} + \overbrace{\lambda}^{\lambda=1}\mathbf{F}\right]\phi \tag{3.40}$$

The above equation is usually solved in an iterative fashion. For a heterogeneous system, cross sections for the equivalent homogeneous geometry are defined by weighting the cross sections of the heterogeneous system by the flux of the reflected heterogeneous geometry. The leakage term $\mathbf{dB^2}$ is then added to the absorption cross section to make the homogeneous system critical (i.e. $\lambda = 1$). However, the obtained buckling coefficient is not the critical buckling since the homogenized cross sections were calculated using the weighting flux for the reflected system (no leakage). Therefore, a new flux computation of the heterogeneous system must be performed with the additional leakage term $\mathbf{dB^2}$ added to the absorption cross section. The process is repeated until convergence for criticality (k_{eff}=1.0) and flux is reached. The interested reader is referred to [83] for a rigorous discussion of the subject.

If equation 3.40 is to be solved iteratively, a new computation of the collision probability matrix $\mathbf{P}(\mathbf{\Sigma} + \mathbf{dB^2})$ must be performed at each iteration. This is computationally demanding due to the time consuming nature of the collision probability integration. The method *SIGMA* [82, 24] consists of replacing the leakage term appearing in the collision probability matrix by a negative term in the in-group scattering matrix:

$$\Sigma_s^{g\to g} \to \Sigma_s^{g\to g} - d_0^g B^2 \tag{3.41}$$

The transport equation to be solved is then [24]:

$$\phi = \mathbf{P}(\mathbf{\Sigma}) \left[\mathbf{S} + \overbrace{\lambda}^{\lambda=1} \mathbf{F} - \mathbf{dB^2} \right] \phi \tag{3.42}$$

for the eigenvalue $\lambda = 1$. In the case where the flux is isotrpic, and the leakage source is constant per region, then it can be seen that equations 3.40 and 3.42 are equivalent. This approach eliminates the necessity of computing the CP matrix at each iteration.

3.2.2 Correction for Leakage

The integral adjoint $\psi^\dagger$ satisfies the adjoint of equation 3.42, given by:

$$\psi^\dagger = \left[\mathbf{S}^\dagger + \mathbf{F}^\dagger - \mathbf{dB^2} \right] \mathbf{P}^\dagger(\mathbf{\Sigma}) \psi^\dagger \tag{3.43}$$

with the differential adjoint satisfying $\phi^\dagger = \mathbf{P}^\dagger(\Sigma) \cdot \psi^\dagger$. If the leakage term $d^g B^2$ is treated as a standard cross section, equations 3.42 and 3.43 can be used to derive a corrected sensitivity expression accounting for the perturbation in the collision probability $\mathbf{P}(\mathbf{\Sigma})$ from neutron streaming and leakage. In a similar fashion to equation 1.188 of chapter 2, the perturbation in the collision probability operator due to a perturbation $\delta\mathbf{\Sigma}$ in the total cross section can be approximated as:

$$\delta\mathbf{P}(\mathbf{\Sigma}) \cdot (\mathbf{S} + \lambda\mathbf{F} - \mathbf{dB^2})\phi = -\mathbf{P}(\mathbf{\Sigma}) \cdot \delta\mathbf{\Sigma}\phi + \mathcal{O}(\delta^2 \mathbf{P}(\mathbf{\Sigma})) \tag{3.44}$$

Ignoring second order terms, and using the relation between the integral and the differential adjoint, the relative change $\delta k/k$ can then be expressed as:

$$\frac{\delta k_{eff}}{k_{eff}} = k_{eff} \frac{\left\langle \psi^\dagger, \left[\delta\mathbf{P} \cdot (\lambda\mathbf{F} + \mathbf{S} - \mathbf{dB^2}) + \mathbf{P} \cdot (\lambda\delta\mathbf{F} + \delta\mathbf{S} - \delta(\mathbf{dB^2})) \right] \phi \right\rangle}{\langle \phi^\dagger, \mathbf{F}\phi \rangle} \tag{3.45}$$

$$= \frac{\left\langle \phi^\dagger, \left[-k_{eff}\delta\mathbf{\Sigma} + k_{eff}\delta\mathbf{S} + \delta\mathbf{F} - k_{eff} \overbrace{\delta(\mathbf{dB^2})}^{\text{LEAKAGE TERM}} \right] \phi \right\rangle}{\langle \phi^\dagger, \mathbf{F}\phi \rangle} \tag{3.46}$$

with the additional term $\delta(d_0^g B^2)$ subtracted from the in-group gain term of scattering $\delta\mathbf{S}$. The sensitivity (in %/%) of k_{eff} to the nuclear data q is then given as:

$$\frac{q}{k_{eff}} \frac{\delta k_{eff}}{\delta q} = \frac{\left\langle \phi^\dagger, \left[-qk_{eff}\delta_q\mathbf{\Sigma} + qk_{eff}\delta_q\mathbf{S} + q\delta_q\mathbf{F} - qk_{eff}\delta_q(\mathbf{dB^2}) \right] \phi \right\rangle}{\langle \phi^\dagger, \mathbf{F}\phi \rangle} \tag{3.47}$$

where $\delta_q \mathbf{X} \equiv \frac{\delta \mathbf{X}}{\delta q}$.

The benefit of equation 3.46 is that the change in the leakage (which is related to the current $\vec{J}$ by equation 3.38) is now taken into account explicitly through the leakage term $\delta(\mathbf{dB^2})$. We can think of the forward and adjoint flux of a critical homogeneous

system with a void boundary condition. The flux and adjoint flux for this system should be identical to the flux and adjoint flux[5] given by equations 3.42 and 3.43 with the proper buckling vector $\mathbf{B}$.[6] Comparing equations 1.194 and 3.40, we see that the leakage term $\delta(d_0^g B^2)$ of equation 3.40 can be thought of as a correction term accounting for the resulting perturbation in leakage due to a perturbation δq in the nuclear data q.

The correction term can be computed from direct differentiation of equation 3.39, i.e.

$$\delta(d_0^g B^2) \sim \delta(\frac{1}{3\Sigma^g})B^2 = -B^2 \frac{1}{3\Sigma^g}\frac{\delta\Sigma^g}{\Sigma^g} \tag{3.48}$$

where we have ignored the higher order terms which appear in the diffusion coefficient defined by equation 3.39. [7] The effect of including the higher order terms appearing in equation 3.39 was studied for the benchmarks that are presented in chapter 4, and was found to have little effect (lower than 0.1% on the integrated sensitivity) so that the approximation given by equation 3.48 is sufficient. In the case where the nuclear data $q = \sigma_{x,I}^g$ is the group cross section for reaction $x \in \{(n, scat), (n, f), (n, abs)\}$ of isotope $I \in M$ of mixture M, the leakage term of equation 3.47 reduces to:

$$k_{eff}\sigma_{x,I}^g \delta_q(d_0^g B^2) \sim -\frac{k_{eff}B^2}{3\Sigma_M^g}\frac{N_I\sigma_{x,I}^g}{\Sigma_M^g} \tag{3.49}$$

where Σ_M is the total cross section of the mixture M.

We note that the diffusion coefficient given by equation 3.39 is exact only for the case where the flux and scattering are isotropic (the base assumption behind B_0 theory). More involved leakage models often yield more complex expressions for the diffusion coefficient in comparison to equation 3.39. In such cases, equation 3.49 can be thought of as an estimate for the sensitivity of the diffusion coefficient d^g to the multi group parameter $\sigma_{x,I}^g$.

Scattering Anisotropy

If conditions are such that anisotropic scattering is important, the transport corrected [81] total cross section $\Sigma - \Sigma_{s,1}$ may be used in equation 3.39. Here $\Sigma_{s,1} = \Delta_{tr}$ corresponds to the transport correction as given in equation 1.22 (or available in the library). The transport corrected diffusion coefficient is given by [81]:[8]

$$d_1^g = \frac{1}{3(\Sigma^g - \Sigma_{s,1}^g)} \tag{3.50}$$

[5] For 2D or 3D problems, we can think of the flux and adjoint averaged over the extra dimension

[6] This is true away from the reflector and for isotropic scattering

[7] For heterogeneous geometries, equation 3.48 ignores all indirect terms that arise from the heterogeneity of the system. As observed in the next chapter, contribution of this latter term is negligible in thermal systems with equation 3.48 providing an accurate estimate for the perturbation in the leakage rate.

[8] We note that d_1^g is the transport corrected form of d_0^g and not the diffusion coefficient corresponding to a B_1 leakage model.

The perturbation of the leakage term $\delta(d_1^g B^2)$ which appears in equation 3.46 can then be defined as:

$$\delta(d_1^g B^2) = -\frac{1}{3(\Sigma^g - \Sigma_{s,1}^g)} \frac{\delta\Sigma^g - \delta\Sigma_{s,1}^g}{\Sigma^g - \Sigma_{s,1}^g} B^2 \tag{3.51}$$

Similar to equation 3.49, in the case where the diffusion coefficient d_1^g, as defined in 3.50 is used, the leakage term appearing in equation 3.47 reduces to:

$$k_{eff}\sigma_{x,I}^g \delta_q(d_1^g B^2) = \begin{cases} -\frac{k_{eff}B^2}{3(\Sigma_M^g - \Sigma_{s,1,M}^g)} \frac{N_I\sigma_{x,I}^g - N_I\sigma_{s,1,I}^g}{\Sigma_M^g - \Sigma_{s,1;M}^g} & , x = (n, scat) \\ -\frac{k_{eff}B^2}{3(\Sigma_M^g - \Sigma_{s,1;M}^g)} \frac{N_I\sigma_{x,I}^g}{\Sigma_M^g - \Sigma_{s,1;M}^g} & , x \in \{(n, abs), (n, fiss)\} \end{cases} \tag{3.52}$$

An interesting observation is the appearance of the transport correction term $\Sigma_{s,1;I} = N_I\sigma_{s,1;I}$ (defined by equation 2.8) which now enters the sensitivity expression 3.46 through the term $\delta_q(d_1^g B^2)$ defined in equation 3.51 (or equation 3.52). For the case where only the isotropic component of the flux and adjoint are available (which is practically always the case in DRAGON), use of a transport correction in the sensitivity expression given by equation 1.194 is redundant. In this case, correcting the total and the in-group scattering cross section by the transport correction reduces to subtracting and adding the same term in the sensitivity expression of equation 1.194, with no net effect on the computed sensitivity:

$$\frac{q}{k_{eff}}\frac{\delta k_{eff}}{\delta q} = \frac{\left\langle \phi^\dagger, \left[-qk_{eff}\delta_q\left(\mathbf{\Sigma} - \mathbf{\Sigma_{s,1}}\right) + qk_{eff}\delta_q\mathbf{S} - qk_{eff}\delta_q\mathbf{\Sigma_{s,1}} + q\delta_q\mathbf{F}\right]\phi\right\rangle}{\langle \phi^\dagger, \mathbf{F}\phi\rangle} \tag{3.53}$$

$$= \frac{\left\langle \phi^\dagger, \left[-qk_{eff}\delta_q\mathbf{\Sigma} + qk_{eff}\delta_q\mathbf{S} + q\delta_q\mathbf{F} \cancelto{0}{-qk_{eff}\delta_q\mathbf{\Sigma_{s,1}} + qk_{eff}\delta_q\mathbf{\Sigma_{s,1}}}\right]\phi\right\rangle}{\langle \phi^\dagger, \mathbf{F}\phi\rangle}$$

The transport correction affects the resultant sensitivity in two ways;

- An isotropic computation (such as B_0 with no transport correction) tends to underestimate the effective leakage of the geometry [83]. By increasing the diffusion length $\lambda^g = 3d^g$, where the diffusion coefficient d^g was defined by equation 3.50, the transport correction $\Sigma_{s,1}$ of equation 2.8 presents a correction for anisotropic scattering with the preferential scattering in the forward direction, the initial neutron direction before the collision. For neutrons at high energies (which are most prone to leakage), scattering reactions compete with leakage. Since leakage is increased by taking into account the anisotropy, the effect is a net increase in the sensitivity of the scattering reaction competing with leakage. This can be seen from equation 3.52. A transport correction reduces the denominator of the leakage sensitivity $\delta_q(d_1^g B^2)$ defined by equation 3.52. As a result, use of equation 3.52 results in an increase in the magnitude of the sensitivity $\delta_x(d^g B^2)/\delta\Sigma_x$. We note that the sign of $\delta_x(d^g B^2)/\delta\Sigma_x$ appearing in equation 3.52 is negative for $x \in \{(n, abs), (n, scat), (n, f)\}$ so that the resultant change in the k_{eff} sensitivity is positive.

- Next, we note that the ratio $\delta k_{eff}/\delta\Sigma_{s,1}$ is negative. This can be seen from the sign of $\delta(d^g B^2)/\delta\Sigma_{s,1}$ which is positive. For a geometry with leakage at its frontiers, the average neutron travels in the direction of leakage. Increasing the transport correction increases the average number of neutrons traveling in the "forward" direction (for the average neutron, this is the direction of leakage). The result is an increase in the effective leakage so that the ratio $\delta(d^g B^2)/\delta\Sigma_{s,1}$ is positive. The negative sign of the ratio $\delta k_{eff}/\delta\Sigma_{s,1}$ implies that an increase in leakage results in a decrease in k_{eff}. This effect can be seen from equation 3.46 and 3.51.

In differentiating the leakage term $\delta(\mathbf{d_0^g B^2})$, we have assumed the buckling coefficient B^2 to be constant. This is due to the physical interpretation of the buckling coefficient B^2. For a system at critical conditions, the relationship between k_{eff} and k_∞ is given as [81]:

$$k_\infty P_{NL}(B^2, L) = 1.0 = k_{eff} \tag{3.54}$$

where P_{NL} is the non-leakage probability of the neutrons dependent on the diffusion length L and the buckling coefficient B^2.[9] If a sensitivity expression for k_{eff} is to be derived, it is clear that one of the three variables appearing on the left hand side of equation 3.54 should be held constant. The diffusion length L is a measure of the average distance which the neutron travels before capture and depends explicitly on the cross sections. However, the buckling coefficient B is a measure of the reactor size (which is assumed to be fixed). Therefore, it is to be anticipated that for a given reactor size, the buckling coefficient B is constant.[10]

3.2.3 Implementation

Computing the sensitivity expression given by equation 3.40 requires the adjoint flux $\phi^\dagger$ corresponding to the differential adjoint of equation 3.43 and the buckling coefficient $\vec{B}^2$. The sensitivity expression is computed in the following way:

1. First a buckling calculation (homogeneous B_0 and B_1 models as well as heterogeneous B_1 models are available in DRAGON [59]) is performed. In case of a heterogeneous calculation, the direction of leakage is to be chosen best representative of the geometry. The buckling value B^2 or in case of a heterogeneous computation, the buckling vector $\vec{B}^2$ and the mixture dependent diffusion coefficients d_M^g are then exported using the **EDI:** module of DRAGON which is responsible for generating two group homogenized cross sections.[11] Here $\vec{B}^2 = \left\langle B_x^2, B_y^2, B_z^2 \right\rangle$ denotes the square of the components of the buckling vector of equation 3.34.

[9] For example, in the case of the homogeneous medium, the one-group diffusion length $L = \sqrt{\frac{D}{\Sigma_a}}$ is defined to be the ratio of the condensed diffusion coefficient D to the condensed absorption cross section Σ_a. The non-leakage probability would then be defined as $P_{NL} = \frac{1}{1+L^2B^2}$ [81].

[10] Note that in many design problems, it is indeed the cell/assembly/reactor size which is to be varied to reach a k_{eff}=1.0.

[11] No condensation in energy should take place.

2. The module **ASM:**, which calculates the collision probability matrix $\mathbf{P}(\mathbf{\Sigma})$, is modified to take as input the **EDI:** output structure and add the mixture dependent product $d_M^{\vec{g}} \cdot \vec{B}^2$ to the mixture absorption and total cross sections available on the library data structure. The buckling vector $\vec{B}^2$ and the mixture diffusion coefficients $d_M^g = d_M^{\vec{g}} \cdot \vec{B}^2 / \sqrt{\vec{B}^2 \cdot \vec{B}^2}$ are stored under the 'MACROLIB' directory of the library linked list structure. The computed collision probabilities correspond to the $\mathbf{P}(\mathbf{\Sigma} + \mathbf{dB^2})$ that appear in equation 3.40.

3. The module **FLU:** (or **SAD:**) is then used to compute the isotropic component of the forward flux ϕ and the adjoint flux $\phi^\dagger = \mathbf{P}^\dagger(\mathbf{\Sigma} + \mathbf{dB^2}) \cdot \psi^\dagger$ corresponding to equations 3.40 and 3.43 respectively. Note that reflective boundary conditions are imposed when computing the collision probabilities $\mathbf{P}(\mathbf{\Sigma} + \mathbf{dB^2})$ in the previous step.

4. The sensitivity expression given in equation 3.47 is then computed by **SNS:** using equations 3.49 or 3.52 to compute the leakage term $\delta_q(\mathbf{dB^2})$ appearing in the sensitivity expression 3.47. It should be noted that the mixture total cross section Σ_M^g should be reconstructed by adding $d_M^g \sqrt{\vec{B}^2 \cdot \vec{B}^2}$ before being used in equations 3.49 and 3.52.

3.3 Application to Uncertainty Analysis

In computing uncertainty contributions using the Sandwich rule given by equation 1.199, the covariance matrix $\mathbf{V}$ that is used must be consistent in both energy meshing and reaction definition with the computed sensitivities. The covariances provided by the SCALE code [42] are given in 44 group format and correspond to covariances for individual channel reactions/partial cross sections (i.e. (n,elastic), (n,inelastic), (n,2n), ...). As discussed in section 2.1.2, the code ANGELO [43] can be used to transform the SCALE 44 group matrices to the WIMS 172-group format. Although covariance matrices processed by ANGELO correspond in energy meshing to the 172-group WIMS format (i.e. 172×172 element covariance matrices), the reactions available on the WIMS libraries (and therefore the sensitivities computed by **SNS:**) differ in definition from the partial cross sections in terms of which the covariance data is available. Therefore, in order to use the covariances processed by ANGELO, either the sensitivities for the partial reactions should be recovered from the lumped computed sensitivities or the covariance data must be lumped into the absorption and scattering reactions equivalent in definition to the reactions available on the WIMS 172-group library. We note that the same restriction applies to covariances processed by NJOY's ERRORR module (we use ERRORR in this work to process JENDL-4 covariances).

In this section we will review the difficulties involved with computing the uncertainty contribution for scattering reactions when using sensitivities that correspond in definition to the WIMS libraries. We will then proceed to discuss some of the current methods for applying available covariance matrices with sensitivities computed from cross sections in the WIMS libraries [55, 56, 54]. After discussing why these approximations fail to

produce realistic results, we will proceed to present our methodology for computing the uncertainty contribution for heavy isotope scattering reactions.

3.3.1 Scattering Uncertainties

An accurate computation of the uncertainty contribution from scattering reactions is interesting not only due to the difficulty of the computation, but also due to the high uncertainties associated with these reactions. In comparison to fission yield, capture or fission reactions, which typically have a high contribution to the uncertainty due to their large sensitivities, heavy isotope (such as ^{238}U) scattering reactions can contribute to the total response uncertainties not necessarily by having a large sensitivity but rather because of the large uncertainties that are associated with these reactions. This can be observed in figure 3.1, where ^{238}U(n,el) and ^{238}U(n,inel) uncertainties in the fast range (groups 1-45 in the WIMS 172-group energy grid) as reported by the recently released SCALE 6 covariances [42], are presented. Here, the uncertainty for ^{238}U(n,inel) is reported to be between 20% to 35% of the cross section value. Although ^{238}U(n,el) is reported to have a lower uncertainty in the fast range, its contribution to the overall uncertainty is through its anti-correlation with (n,inel). This can be observed from the ^{238}U(n,el)-(n,inel) correlation matrix presented in figure 3.2. At high energies, the evaluator uses coupled channels deformed optical models to represent the cross section. In this range, the evaluator encounters a possible set of reactions which are measured experimentally. These reactions include elastic reactions without a compound nucleus formation, direct interactions (the neutron interacts with a nucleon inside the nuclei), elastic and inelastic reactions via compound nucleus formation, as well as capture and fission reactions [84]. The simplest cross section to measure in this range is the total cross section since it can be measured through transparency measurements [85]. The scattering cross section (usually inelastic) is then obtained as the difference between the total cross section and the remaining reactions (see for example [86]), so that elastic and inelastic cross sections are negatively correlated. As a result of this strong and negative correlation, even if the uncertainty of (n,el) reactions is lower than the uncertainty associated with (n,inel), if the sensitivity is at least of the same order of magnitude as the sensitivity of (n,inel),[12] then the reaction (n,el) contributes to the overall uncertainty through its anti-correlation with (n,inel). As a result, the contribution from heavy isotope elastic reactions to the overall uncertainty can be important.

[12]This is indeed the case for problems involving neutron leakage.

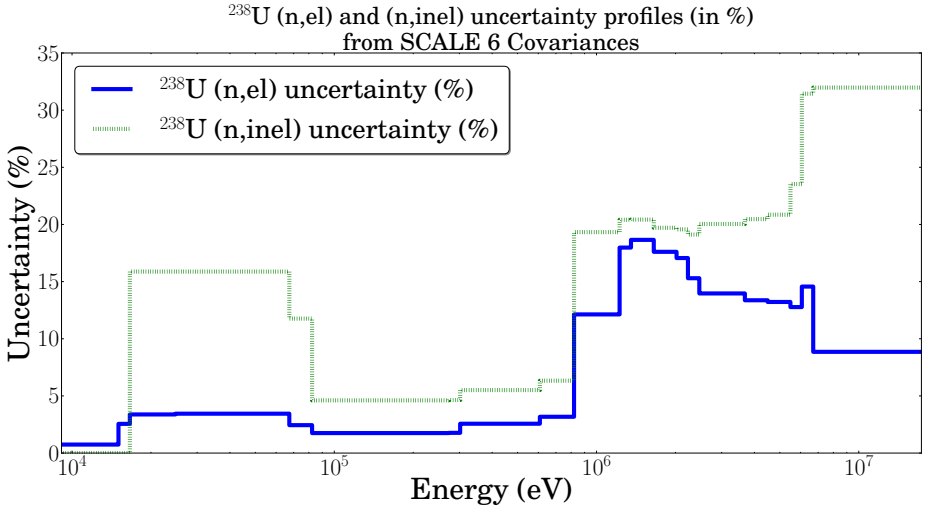

Figure 3.1: Uncertainties (in %) for ^{238}U(n,el) and ^{238}U(n,inel) reactions reconstructed from SCALE6 covariances using ANGELO. Note the high uncertainties reported in the fast range.

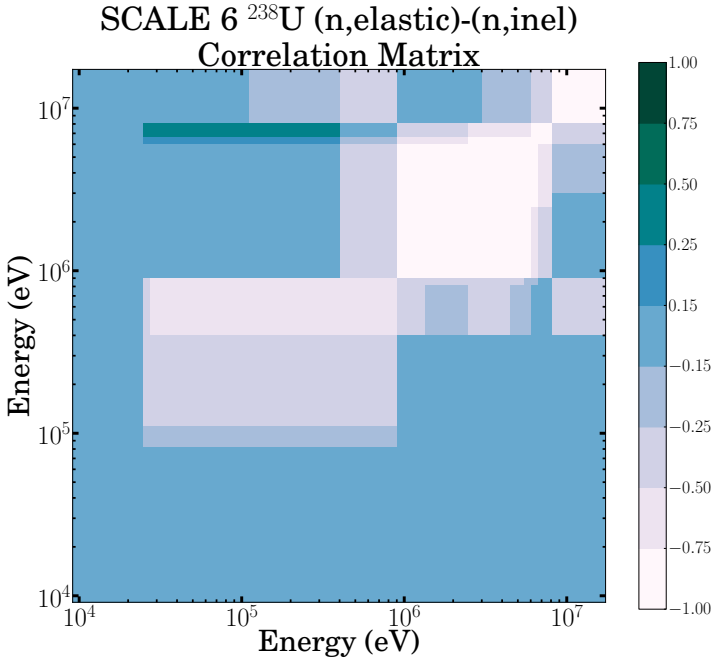

Figure 3.2: (n,el)-(n,inel) Correlation Matrix (fast groups only) reconstructed from SCALE 6 Covariances using ANGELO. Note is the strong anti-correlation reported between elastic and inelastic reactions. **y-axis:** (n,el) - **x-axis:** (n,inel)

Lumped Covariances

As mentioned above, the covariance data used for uncertainty analysis should correspond in definition to the cross sections that were used to compute the sensitivity. In many lattice codes such as DRAGON [59], WIMS [87], HELIOS [88] and CASMO [89], the available cross sections in the library are in the form of lumped reactions. The lumped transfer matrix, and lumped scattering and absorption cross sections available in the WIMS libraries were defined by equations 2.2-2.4 as:

$$\Sigma^{g\to g'}_{(n,SCAT)} = \sigma^{g}_{(n,el)}P^{g\to g'}_{(n,el)} + \sigma^{g}_{(n,inel)}P^{g\to g'}_{(n,inel)} + 2\sigma^{g}_{(n,2n)}P^{g\to g'}_{(n,2n)} + 3\sigma^{g}_{(n,3n)}P^{g\to g'}_{(n,3n)} \tag{3.55}$$

$$\sigma^{g}_{(n,SCAT)} = \sum_{g'=1}^{N_G}\left(\sigma^{g}_{(n,el)}P^{g\to g'}_{(n,el)} + \sigma^{g}_{(n,inel)}P^{g\to g'}_{(n,inel)} + 2\sigma^{g}_{(n,2n)}P^{g\to g'}_{(n,2n)} + ...\right) \tag{3.56}$$

$$\sigma^{g}_{(n,ABS)} = \sum_{x\in(n,abs)}\sigma^{g}_{(n,x)} - \sigma^{g}_{(n,2n)} - 2\sigma^{g}_{(n,3n)} \tag{3.57}$$

where $\sigma^{g}_{(n,SCAT)}$ and $\sigma^{g}_{(n,ABS)}$ are the lumped scattering and absorption cross sections in the energy group g and $P^{g\to g'}_{x}$ is the group to group transfer matrix for reaction type $x \in \{(n,el),(n,inel),(n,2n),..\}$. Except for a few isotopes, only the isotropic component of the scattering matrix $\mathbf{S}_{(n,SCAT)} = (\Sigma^{g\to g'}_{(n,SCAT)})$ is provided in the WIMS libraries [38], so that we limit our discussion here to isotropic scattering. We note that since covariance matrices for secondary angular distributions are not currently available in most evaluations,[13] matrices corresponding to the transport correction cannot be derived. The usual way to account for the contribution of the transport correction to the uncertainty is to assume that the P_1 scattering components have the same uncertainties as the scattering cross section.

A covariance matrix corresponding to the lumped scattering cross section given by equation 3.56 can be constructed by [90]:

$$COV(\sigma^{g}_{(n,SCAT)},\sigma^{g'}_{(n,SCAT)}) = \sum_{x}\sum_{y}\frac{\sigma^{g}_{(n,x)}}{\sigma^{g}_{(n,SCAT)}}COV(\sigma^{g}_{(n,x)},\sigma^{g'}_{(n,y)})\frac{\sigma^{g'}_{(n,y)}}{\sigma^{g'}_{(n,SCAT)}} \tag{3.58}$$

where the summation indices x and y refer to the individual channel reactions $x,y \in \{(n,el),(n,inel),(n,2n),(n,3n)\}$. An expression similar to 3.58 can also be derived for the absorption cross section defined by equation 3.57. We constructed these covariances [90] in application to nuclear data uncertainty propagation using the total cross section and its uncertainties. Similar covariances have since been constructed at VTT [55, 56] and applied to nuclear data sensitivity and uncertainty analysis using perturbation theory with the code CASMO-4. However, while the methodology of VTT works well for absorption reactions, it does not lead to accurate results when the uncertainty for scattering reactions are considered.

[13] The TENDL evaluation provides this data.

Difficulties in Computing the Uncertainty Contribution for Scattering Reactions

Let us consider the sensitivity formula for k_{eff} given by equation 3.47. In this case, the group sensitivity $S^g_{keff,(n,SCAT)}$ to the scattering cross section is defined as the difference between the gain term $G_{g,(n,SCAT)}$ (which represents the gained neutron importance from the scattering reaction) and the loss term $L_{g,(n,SCAT)}$ (which represents the loss in neutron importance due to scattering interactions). Ignoring the fission source normalization appearing in equation 3.47, we have:[14]

$$\text{Loss term: } L^{g,(n,SCAT)}_{k_{eff}} = k_{eff} \sum_{j \in M} V_j \left(\phi^{\dagger}_{j,g} N_I \sigma^g_{I,(n,SCAT)} \phi_{j,g} - \phi^{\dagger}_{j,g} \frac{k_{eff} B^2}{3\Sigma^g_M} \frac{N_I \sigma^g_{I,(n,SCAT)}}{\Sigma^g_M} \phi_{j,g} \right) \tag{3.59}$$

$$\text{Gain term: } G^{g,(n,SCAT)}_{k_{eff}} = k_{eff} \sum_{j \in M} \sum_{g'=1}^{N_G} V_j \phi^{\dagger}_{j,g} \Sigma^{g' \to g}_{I,(n,SCAT)} \phi_{j,g'} \tag{3.60}$$

$$\text{Sensitivity: } S^{g,(n,SCAT)}_{k_{eff}} = G^{g,(n,SCAT)}_{k_{eff}} - L^{g,(n,SCAT)}_{k_{eff}} \tag{3.61}$$

where for simplicity, in computing the leakage contribution that appears in equation 3.59, we have used equation 3.39 to define the diffusion coefficient. Here, the summation index $j \in M$ appearing in equations 3.59 and 3.60 represents summation over all the regions j that are composed of the mixture M, V_j is the volume of region j, $\phi_{j,g}$ and $\phi^{\dagger}_{j,g}$ are the flux and adjoint in region j and group g, Σ^g_M is the macroscopic total cross section for mixture M and N_I is the isotopic density of isotope $I \in M$. The lumped components of the scattering matrix $\Sigma^{g \to g'}_{I,(n,SCAT)}$ and the lumped scattering cross section $\sigma^g_{I,(n,SCAT)}$ were defined by equations 3.55 and 3.56 respectively.

We can imagine the chain rule approach for recovering the sensitivities corresponding to the partial cross sections appearing in equation 2.3. The application of the chain rule to the loss term $L^{g,(n,SCAT)}_{k_{eff}}$ is mathematically valid. The chain rule can therefore be applied to the loss term $L^{g,(n,SCAT)}_{k_{eff}}$ to recover the partial loss term $L^{g,x}_{k_{eff}}$ for the partial cross sections $x \in \{(n,el),(n,inel),(n,2n),...\}$. i.e.

$$L^{g,(n,x)}_{k_{eff}} = L^{g,(n,SCAT)}_{k_{eff}} \cdot \frac{\sigma^g_{(n,x)}}{\sigma^g_{(n,SCAT)}} \tag{3.62}$$

However, computation of the partial cross section for the gain term is not evident as it requires the application of the chain rule *before* the group collapsing (i.e. prior to the summation over the index g' appearing in equation 3.60) so that the partial gain term $G_{g,x}$ for reaction type x is defined as:

$$G^{g,(n,x)}_{k_{eff}} = k_{eff} \sum_{g'=1}^{N_G} \sum_{j \in M} V_j \sum_{g'} \phi^{\dagger}_{j,g} N_I \sigma^{g'}_{I,x} P^{g' \to g}_{x} \phi_{j,g'} \tag{3.63}$$

[14]Note that we have associated the leakage term as a loss for computational purposes only. The contribution of this term to the sensitivity is positive.

Here lies the difficulty associated with recovering partial cross section sensitivities from the computed sensitivity to the lumped scattering cross section. As the form of the group to group transfer function $P_x^{g' \to g}$ varies greatly with the reaction type $x \in \{(n, el), (n, inel), ...\}$, recovering the partial sensitivity requires the application of the chain rule to the gain term of the sensitivity before the collapse of the gain term (before computing the summation over g' appearing in equation 3.63). This can be done by writing out the GAIN matrix in its entirety[15] but would somewhat defeat the purpose of performing the sensitivity computation inside the code. As a result, the practitioner is forced to resort to assumptions regarding the form of the scattering matrix.

We will briefly discuss three approximations that we have seen used by other codes [55, 56, 54] when computing the uncertainty contribution from scattering cross sections using WIMS libraries and SCALE covariances.

3.3.2 Current Approximations for Computing Scattering Uncertainties

- The approximation used by version 1.0 of the Canadian code DINASOUR [54] is to assign the scattering sensitivity component as the contribution due to elastic scattering. This is accurate for ^{1}H (the only possible scattering interaction is via elastic), and is a very good approximation for ^{16}O (where the primary mode of scattering interaction is elastic). However, it does not lead to realistic values when computing scattering reactions for heavy isotopes. In reflected lattices, heavy isotope elastic scattering outside of the resonance region is generally negligible (in the resonance region, the principle component of the sensitivity is due to spectral fine structure effects which were discussed in section 3.1). Therefore, since the uncertainty for elastic scattering is lower than the uncertainty for inelastic, assigning the scattering sensitivity as elastic tends to greatly underestimate the resultant uncertainty contribution from scattering sensitivities.

- A more profound methodology to incorporate the currently available covariance data for use with the sensitivities computed in terms of lumped reactions is to construct covariance matrices corresponding in definition to the lumped reactions. Such matrices can be constructed using equation 3.58. In [55, 56], the covariance matrices for the lumped scattering cross section is applied to the scattering sensitivity $S_{k_{eff}}^{(n,SCAT)} = G_{k_{eff}}^{(n,SCAT)} - L_{k_{eff}}^{(n,SCAT)}$ after computing the sum over the incident energies g' appearing in equation 3.60. This is equivalent to assuming that the chain rule applies to the gain term $G_{k_{eff}}^{g,(n,SCAT)}$ defined in equation 3.63, i.e.:

$$G_{k_{eff}}^{g,(n,x)} = G_{k_{eff}}^{g,(n,SCAT)} \cdot \frac{\sigma_{(n,x)}^{g}}{\sigma_{(n,scat)}^{g}} \tag{3.64}$$

  However, we can see why equation 3.64 does not lead to reliable results. The expression ignores all information regarding the form of the group to group transfer

[15] We provide this matrix in the **SNS:** output file.

matrices $P_{(n,x)}^{g' \to g}$ which appear in equation 3.56 (^{238}U transfer matrices for elastic and inelastic scattering can be observed in figure 3.3). As a result, the scattering sensitivity is weighted unevenly if equation 3.64 is used.

- Rather than using lumped covariance data, Version 2.0 of DINASOUR uses the output of the NJOY GROUPR module to compute the sensitivity $\frac{\partial \sigma_{(n,SCAT)}^{g}}{\partial \sigma_{(n,x)}^{g}}$ for the partial cross section $x \in \{(n,el),(n,inel),(n,2n),...\}$. It then applies the computed sensitivities to the lumped scattering matrix $\mathbf{S}_{(n,SCAT)}$ available in the WIMS libraries and performs direct perturbations to compute sensitivity to partial cross sections or statistical sampling of the cross sections to compute the response uncertainty. This methodology is once again equivalent to applying the chain rule given by equation 3.64 to the lumped gain term, so that it will not produce reliable results when computing the uncertainty contribution from scattering cross sections.

Figure 3.3: Elastic and Inelastic elastic scattering Group to Group transfer matrices for ^{238}U (from JEFF 3.1) for the fast groups of the WIMS 172-group library. Only groups 1 (E=19.6403 MeV) to group 45 (E=11.1378 keV) are shown.

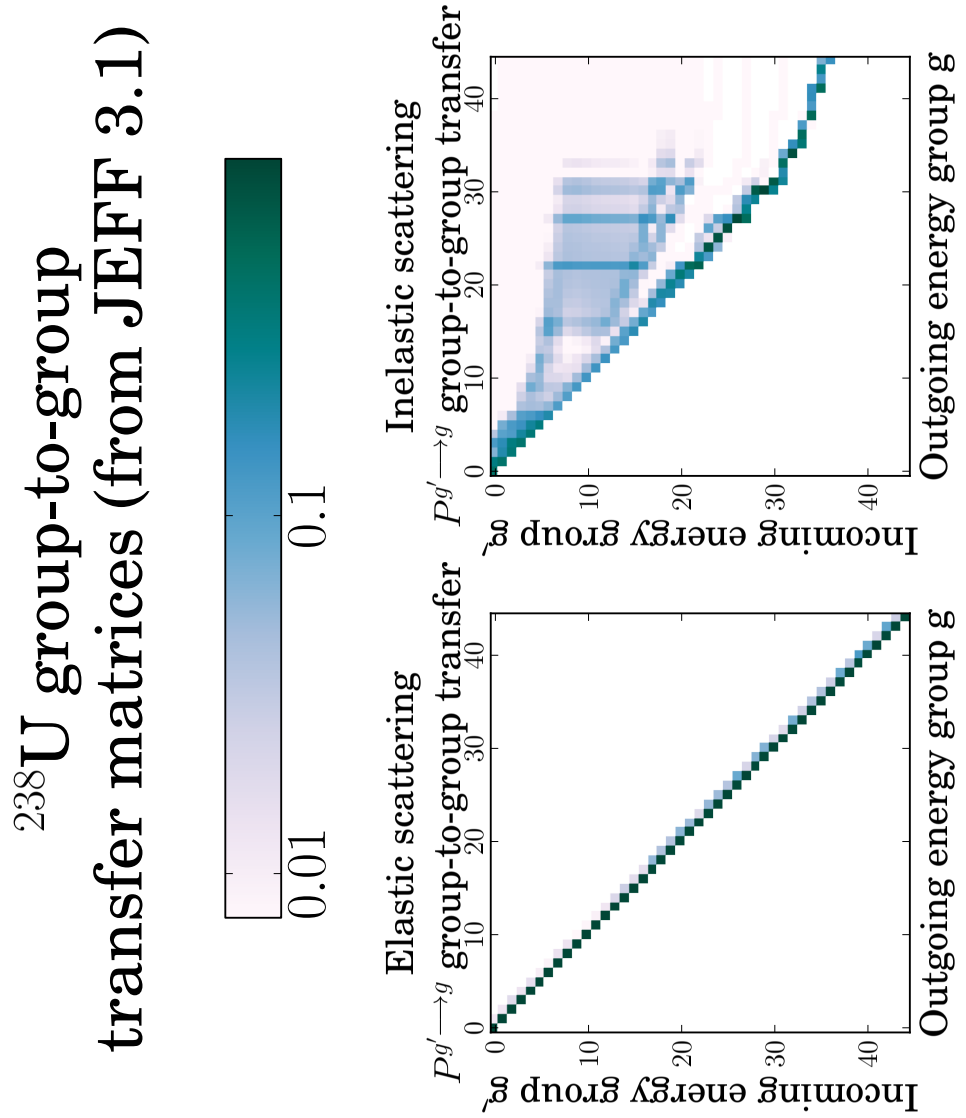

3.3.3 Our Approximation for Reflected Lattices

Figure 3.3 presents the group to group transfer matrices for ^{238}U(n,el) and (n,inel). We note the diagonal nature of the transfer matrix for elastic scattering, and the dense nature of the matrix for inelastic scattering. For the case where scattering is isotropic, the elastic scattering energy transfer function $P_{(n,el)}(E' \to E)$ has the form given by equation 1.66 as:

$$P_{(n,el)}(E' \to E) = \begin{cases} \frac{1}{(1-\alpha)E'} & E \leq E' \leq E/\alpha \\ 0 & \text{else} \end{cases} \tag{3.65}$$

where $\alpha = \left(\frac{A-1}{A+1}\right)^2$, and A is the atomic number of the isotope. A well known phenomena is the decrease in the energy bandwidth $E' \in [E, E/\alpha]$ with increasing mass number. Examining figure 3.3 suggests the assumption:

$$\Sigma^{g' \to g}_{(n,elastic)} \equiv \sigma^{g}_{(n,elastic)} \delta^{g'}_{g} \tag{3.66}$$

to be valid for fast groups. Here $\delta^{g'}_{g}$ is the Kronecker delta function. Equation 3.66 is valid for heavy isotopes since the atomic mass of the target nuclei is large enough that the energy bandwidth $E' \in [E, E/\alpha]$ falls within the energy group. As a result, the elastic scattering transfer matrix is diagonal. Additionally, assuming that the only components of the scattering matrix $S_{(n,SCAT)}$ (whose components were given by equation 3.55) are elastic and inelastic reactions, the problem is further simplified. In this case, it can be observed that the elastic scattering loss and gain terms of equation 1.194 are equal and cancel out, so that the heavy isotope scattering sensitivity can be effectively assigned as inelastic scattering.

Indeed, for reflected lattices, the problem of computing accurately the uncertainty contribution from isotope scattering reactions is quite simple (so far, the only cases we have seen considered by [55, 56, 54] are reflected lattices). The explanation for our approximation given by equation 3.66 is as such:

> As observed from the diagonal nature of the heavy isotope elastic scattering group to group transfer matrix (presented for ^{238}U in figure 3.3), heavy isotope elastic interactions contribute to the scattering sensitivity not by changing the neutron's energy, but rather its direction. For the reflected lattices, particularly those being considered in [55, 56, 54], the reflective nature of the boundary condition along with the small pitch length of the lattice[16] promotes flux isotropy. If the flux is isotropic, the resultant change in the neutron's direction does not have a great effect on the neutron's importance (which is identical for all neutron directions). Hence, in reflected lattices (or in general, when the flux is isotropic), the sensitivity to elastic scattering in the fast groups for heavy isotopes is negligible.

Implementing equation 3.66 for reflective lattices is simple; we do this by assigning the scattering sensitivity for heavy isotopes computed by **SNS:** as the contribution from inelastic scattering. To highlight this point, let us consider the GEN III 9.8% enriched Pu

[16] In comparison to the neutron's mean free path.

MOX pin-cell, the description of which is available under Exercise I.1 of the OECD's Uncertainty Analysis in Modeling (UAM) Benchmark [103]. This is one of the benchmarks considered and presented by Pusa in [56]. Given the harder flux spectrum associated with MOX fuel, ^{238}U(n,inel) cross section is an important contributor to the overall k_{eff} uncertainty. The study of this benchmark not only permits us to quantify the errors introduced by using the approximation suggested above, but also to examine the accuracy of the sensitivities computed by the module **SNS:** for reflected geometries.

UAM GEN III MOX Lattice Cell at 9.8% enriched Pu

We will now consider the 9.8% enriched GEN-III MOX lattice pin-cell outlined under the lattice physics phase of the UAM benchmarks [103]. The cell has a pitch of 1.262 cm, with a pin radius of 0.4126 cm.

Table 3.1 presents the explicit k_{eff} sensitivities and the corresponding reaction uncertainty contributions to the k_{eff} computed by CASMO-4 and SCALE/TSUNAMI 2D along with our results obtained from DRAGON **SNS:**. The CASMO-4 and SCALE/TSUNAMI 2D results have been reproduced from [55]. All presented results have been computed using the ENDF B/VI evaluation. The columns appearing under the heading sensitivity report the integrated k_{eff} sensitivity (in %/%) of the reaction appearing in the table. They represent the % change in k_{eff} from a 1% uniform perturbation in the cross section. The columns appearing under the $\frac{\Delta k}{k}$ report the (%) contribution to the k_{eff} uncertainty for each reaction pair.

The first observation regarding the comparison provided in table 3.1 is the observed differences in the ^{238}U(n,SCAT) sensitivity. The ^{238}U(n,SCAT) sensitivity that is reported by DRAGON is 23% larger[17] in magnitude than the TSUNAMI 2D results reported by [55]. To investigate this discrepancy, we constructed a model with SCALE/TSUNAMI-3D, the results of which are presented in table 3.2. In this table we note that the ^{238}U(n,SCAT) explicit sensitivities computed by DRAGON differ by 5% from the sensitivity reported by SCALE/TSUNAMI-3D. As an additional verification, we have also computed the implicit ^{238}U(n,SCAT) using the DRAGON sensitivities along with our analytical approximation given by equations 3.32 and equation 3.19 (note that this sensitivity is not computed by CASMO-4). As observed in table 3.2, our implicit component for ^{238}U(n,SCAT) differs by 14% from the SCALE/TSUNAMI 3D sensitivity. A comparison plot between the DRAGON computed and the SCALE/TSUNAMI-3D computed *complete* scattering sensitivity (implicit + explicit) can be observed in figure 3.4. The dotted green line presents the ^{238}U(n,el) sensitivity computed by SCALE/TSUNAMI-3D in 238-group format. The dotted red curve presents the SCALE/TSUNAMI-3D ^{238}U(n,inel) sensitivity. The grey curve presents the SCALE/TSUNAMI-3D ^{238}U(n,el) sensitivity collapsed to the WIMS 172-group mesh using the procedure described in section 3.1.4. We note the good agreement between the DRAGON results (blue curve) and the SCALE/TSUNAMI-3D (dotted green and red curves). Without having a more detailed sensitivity profile for the sensitivities reported by [55], we can assume that the

[17] % differences are given relative to SCALE/TSUNAMI-3D results.

23% difference in ^{238}U(n,SCAT) sensitivity observed between our DRAGON computed sensitivity with the TSUNAMI-2D ^{238}U(n,SCAT) reported by [55] is due to underlying differences in the model. Finally, we note the negligible value of ^{238}U(n,el) sensitivity outside of the resonance region (observed by the dotted green curve) and the dominant behaviour of ^{238}U (n,inel) in the fast range (dotted red curve 3.4), both confirming our approximation for the diagonal form of the heavy isotope elastic scattering matrix.

	Explicit Sensitivity (%/%)		
Reaction	**DRAGON** (this work)	CASMO†	TSUNAMI-2D†
^{239}Pu $\bar{\nu}$-$\bar{\nu}$	$7.224 * 10^{-1}$	$7.212 * 10^{-1}$	$7.251 * 10^{-1}$
^{238}U σ_{scat}-σ_{scat}	$-1.84 * 10^{-2}$	$-1.591 * 10^{-2}$	$-1.494 * 10^{-2}$
^{238}U σ_c-σ_c	$-1.802 * 10^{-1}$	$-1.963 * 10^{-1}$	$-1.611 * 10^{-1}$
^{242}Pu σ_c-σ_c	$\mathbf{-1.528 * 10^{-2}}$	$\mathbf{-2.339 * 10^{-2}}$	$\mathbf{-1.557 * 10^{-2}}$
^{239}Pu σ_f-σ_f	$3.60 * 10^{-1}$	$3.619 * 10^{-1}$	$3.596 * 10^{-1}$
^{239}Pu σ_c-σ_c	$-1.997 * 10^{-1}$	$-1.974 * 10^{-1}$	$-2.004 * 10^{-1}$
^{240}Pu σ_c-σ_c	$-1.115 * 10^{-1}$	$-1.104 * 10^{-1}$	$-1.058 * 10^{-1}$
^{238}U $\bar{\nu}$-$\bar{\nu}$	$8.277 * 10^{-2}$	$8.333 * 10^{-2}$	$8.165 * 10^{-2}$
	Contribution to $\frac{\Delta k}{k}$ (%)		
Reaction	**DRAGON** (this work)	CASMO†	TSUNAMI-2D†
^{239}Pu $\bar{\nu}$-$\bar{\nu}$	$7.282 * 10^{-1}$	$7.273 * 10^{-1}$	$7.311 * 10^{-1}$
^{238}U σ_{scat}-σ_{scat}	$\mathbf{2.90 * 10^{-1}}$	$\mathbf{9.952 * 10^{-2}}$	$\mathbf{2.721 * 10^{-1}}$
^{238}U σ_c-σ_c	$2.384 * 10^{-1}$	$2.457 * 10^{-1}$	$2.078 * 10^{-1}$
^{242}Pu σ_c-σ_c	$1.36 * 10^{-1}$	$\mathbf{2.339 * 10^{-1}}$	$1.359 * 10^{-1}$
^{239}Pu σ_f-σ_f	$2.232 * 10^{-1}$	$2.236 * 10^{-1}$	$2.204 * 10^{-1}$
^{239}Pu σ_c-σ_c	$1.928 * 10^{-1}$	$1.960 * 10^{-1}$	$1.928 * 10^{-1}$
^{239}Pu σ_c-σ_f	$1.576 * 10^{-1}$	$1.555 * 10^{-1}$	$1.582 * 10^{-1}$
^{240}Pu σ_c-σ_c	$1.519 * 10^{-1}$	$1.549 * 10^{-1}$	$1.459 * 10^{-1}$
^{238}U $\bar{\nu}$-$\bar{\nu}$	$9.677 * 10^{-2}$	$9.668 * 10^{-2}$	$9.534 * 10^{-2}$

Table 3.1: Scattering k_{eff} sensitivity and uncertainty contributions for the reflected 9.8% MOX fuel pin-cell. Benchmark description in reference [103].
†: reproduced from [55]
DRAGON computation in the 172-group ENDF B/VI (this work). TSUNAMI-2D computation performed in the 238-groups using the ENDF B/VI (reproduced from [55]). CASMO-4 computation performed in 70 groups with the ENDF B/VI evaluation (reproduced from [55]). Note the differences observed for the ^{238}U $\sigma_{scat} - \sigma_{scat}$ uncertainty contribution predicted by CASMO-4 resulting from the application of the chain-rule to the scattering sensitivity. Also note the good comparison between the DRAGON computed ^{238}U $\sigma_{scat} - \sigma_{scat}$ uncertainty and that of SCALE/TSUNAMI-2D confirming our approximation for the diagonal form of heavy isotope elastic scattering matrix.

^{238}U scattering implicit and explicit sensitivities			
DRAGON (ENDF B/VI)		SCALE 5/TSUNAMI-3D (ENDF B/VI)	
Implicit	Explicit	Implicit	Explicit
$2.12 * 10^{-2}$	$-1.84 * 10^{-2}$	$1.86 * 10^{-2}$	$-1.75 * 10^{-2}$

Table 3.2: Comparison of implicit & explicit ^{238}U scattering sensitivities computed from DRAGON **SAD:/SNS:** with the analytical approximation given by equations 3.32 and 3.19, and the sensitivities computed by SCALE5/TSUNAMI-3D. Both computations have been performed using ENDF B/VI. Note the good comparison between the DRAGON explicit values (5% difference relative to SCALE/TSUNAMI-3D and the computed implicit values (14% difference relative to SCALE/TSUNAMI-3D).

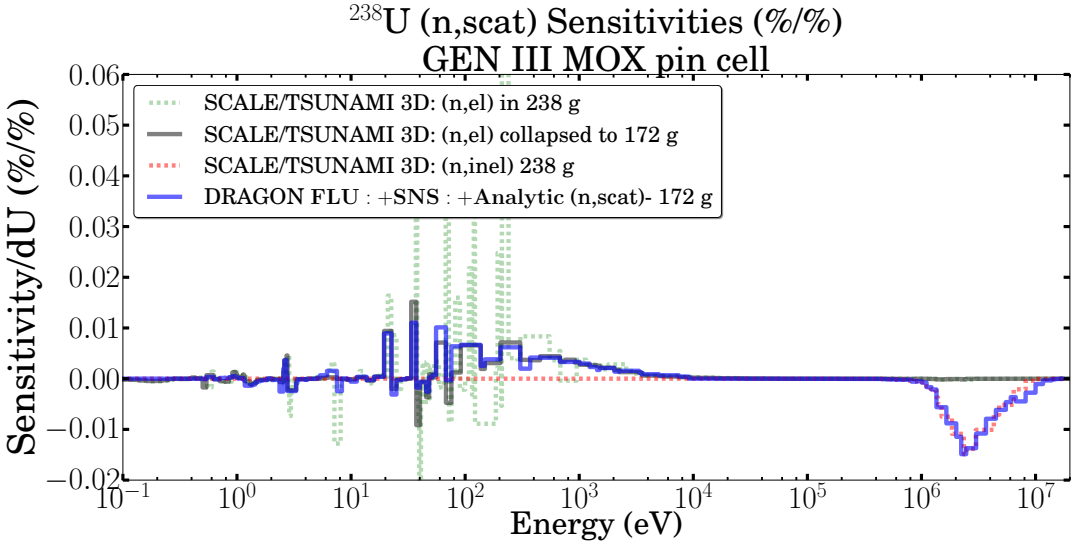

Figure 3.4: ^{238}U **complete (implicit+explicit)** scattering sensitivities for the GEN III MOX fuel pin cell. Note the good agreement between the DRAGON **SNS:** profile (blue curve) with the SCALE/TSUNAMI-3D profile (grey and red curves). The sensitivities in the resonance region are implicit sensitivities to ^{238}U(n,el) cross section.

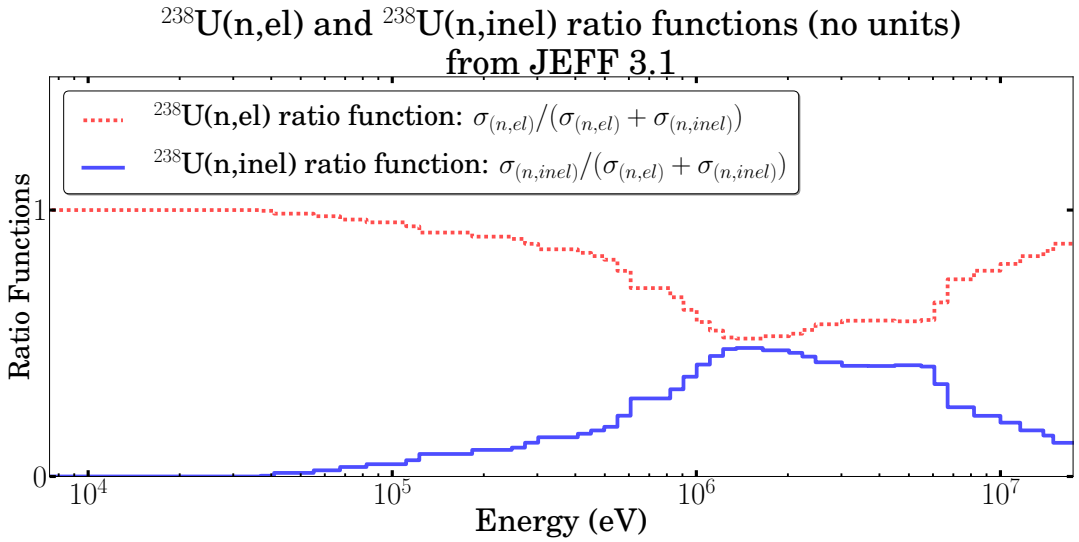

Figure 3.5: ^{238}U elastic ratio function $\sigma_{(n,el)}/(\sigma_{(n,el)}+\sigma_{(n,inel)})$ and inelastic ratio functions $\sigma_{(n,inel)}/(\sigma_{(n,el)}+\sigma_{(n,inel)})$ computed from JEFF 3.1.
Note the dominant (n,el) cross section value in comparison to (n,inel) in the fast range.

Next, we note that as observed from Table 3.1, despite the good agreement between the computed ^{238}U lumped/total scattering sensitivities by CASMO-4 and by TSUNAMI-2D, the approach suggested by [55, 56] does not lead to an accurate value for the uncertainty contribution from ^{238}U scattering. This is due to the application of the chain rule to the gain term of the sensitivity [55, 56]. To understand the underlying physics/error compensations involved by assuming this approximation, we have attempted to reproduce the computation performed by CASMO-4 by applying the chain rule to the sensitivities computed by DRAGON. This is equivalent to applying the lumped covariance matrix to the scattering cross section. To do this, we define the elastic and inelastic scattering sensitivities $S^{(n,el)}_{k_{eff}}$ and $S^{(n,inel)}_{k_{eff}}$, in terms of the lumped scattering sensitivity $S^{(n,scat)}_{k_{eff}}$ as:

$$S^{g,(n,el)}_{k_{eff}} = S^{g,(n,scat)}_{k_{eff}} \cdot \frac{\sigma^g_{(n,el)}}{\sigma^g_{(n,scat)}} = S^{g,(n,scat)}_{k_{eff}} \cdot \frac{\sigma^g_{(n,el)}}{\sigma^g_{(n,el)} + \sigma^g_{(n,inel)}} \tag{3.67}$$

$$S^{g,(n,inel)}_{k_{eff}} = S^{g,(n,scat)}_{k_{eff}} \cdot \frac{\sigma^g_{(n,inel)}}{\sigma^g_{(n,scat)}} = S^{g,(n,scat)}_{k_{eff}} \cdot \frac{\sigma^g_{(n,inel)}}{\sigma^g_{(n,el)} + \sigma^g_{(n,inel)}} \tag{3.68}$$

where the second equalities have been obtained by assuming that the only components of the scattering cross section are elastic and inelastic (i.e. ignoring (n,2n), (n,3n), ...). We note that (n,2n), (n,3n),... reactions have generally low sensitivities in thermal systems. Table 3.3 shows why applying the chain rule to the scattering sensitivity is dangerous. At high energies, the value of the cross section for elastic and inelastic scattering is of the same order of magnitude (see figure 3.5). However, the form of their group to group transfer matrices are very different. Application of the chain-rule to the total scattering sensitivity results in splitting the lumped/total scattering sensitivity between the two reactions based on the ratios of the cross sections $\sigma_{(n,el)}/(\sigma_{(n,el)} + \sigma_{(n,inel)})$ and

$\sigma_{(n,inel)}/(\sigma_{(n,el)} + \sigma_{(n,inel)})$ while ignoring any information in regards to the form of the group to group transfer matrices. These ratio functions can be observed in figure 3.5. In reality it is the form of the group-to-group matrices that dictates the sensitivity (the sensitivity is the difference between the neutron importance gained after the collision and the importance lost from the collision) and not the ratio of the cross sections. At high energies, where the contribution to the scattering sensitivity is primarily due to inelastic scattering (observed earlier in figure 3.4), application of the chain rule results in a false decomposition/weighting with artificially assigning the majority of the scattering sensitivity as elastic. As a result, the inelastic scattering reaction sensitivity is under-estimated, and the elastic scattering reaction sensitivity is over-estimated. The scattering uncertainty contribution computed using the chain rule is observed to be approximately half of the ^{238}U(n,scat) uncertainty that is compute by TSUNAMI-2D or by DRAGON. This is due to the cancellation of errors resulting from the strong anti-correlation that exists between the two scattering reactions, and the inaccurate computation of the contribution of this anti-correlation, which is approximately half of the k_{eff} uncertainty contribution from ^{238}U(n,SCAT).

Table 3.3 reports the resulting sensitivities and uncertainty contributions that one would obtain by using the chain approximation for the scattering sensitivity. For example, we see that ^{238}U elastic scattering reactions which should not have a major contribution at high energies in reflected lattices (observed earlier in figure 3.4) are assigned a higher sensitivity (in magnitude) than the inelastic reaction. The correlation between the two reaction is over estimated as a result, and the contribution from inelastic reactions is under-estimated. The computed uncertainty (127 pcm) reported in table 3.3 differs by approximately 20% from the uncertainty reported by [56] (observed in table 3.1 to be 99 pcm). This difference is due to the discrepancy between the scattering sensitivity computed by DRAGON and the scattering sensitivity computed by CASMO-4 (which differ by 16%).

REACTION	Sensitivity (%)	Uncertainty (pcm)
^{238}U (n,el)-(n,el)	$-1.11 * 10^{-2}$	124
^{238}U (n,inel)-(n,inel)	$-7.0 * 10^{-3}$	130
^{238}U (n,el)-(n,inel)	-	-179
Lumped/Total scattering	$-1.84 * 10^{-2}$	127

Table 3.3: Example of applying the chain-rule to ^{238}U lumped/total scattering cross section. Sensitivities have been computed by applying the chain-rule formula (see equations 3.67-3.68) to the DRAGON **SNS:** computed lumped scattering sensitivity. ANGELO processed covariance matrices from the SCALE 6 library have been used in the uncertainty analysis. Note the over prediction of the elastic sensitivity and the resulting large contribution of the anti-correlation between (n,el) and (n,inel). As a result, applying the chain rule results in a poorly computed scattering uncertainty of 127 pcm (99 pcm from CASMO-4) in comparison to 290 pcm (DRAGON **SAD:/SNS:**) or 272 pcm (TSUNAMI 2D).

The next observed discrepancy in table 3.2 is for ^{242}Pu (n,capture); the sensitivity re-

ported for the capture of ^{242}Pu by CASMO-4 is approximately 50% larger (in magnitude) than the sensitivity computed by either TSUNAMI-2D or DRAGON. The explanation of this discrepancy this is reported in [55, 56] to be due to differences in the self-shielded cross section that is computed by CASMO-4 in comparison to SCALE/TSUNAMI-2D and our DRAGON results.

For all three codes, the sensitivities are in good agreement. We note that in reflected pin cell problems, the flux is isotropic so that deviations between the computed sensitivities are generally low.

3.3.4 Our Approximation for Cases Involving Neutron Leakage

Equation 3.66 is equally applicable for cases involving neutron leakage. We will present two methods for computing heavy isotope scattering sensitivities: the first requires access to partial cross section data and is aimed to recover the elastic and inelastic scattering sensitivities from the computed lumped scattering sensitivity, the second method avoids the requirement of having access to partial cross section data by using lumped covariance matrices.

Uncertainty Propagation with Partial Cross Section Data

Assuming that the only components of the scattering cross section/matrix are (n,el) and (n,inel), we have from substitution of equation 3.66 into equation 3.61:

$$S_{keff}^{g,(n,SCAT)} = G_{keff}^{g,(n,SCAT)} - L_{keff}^{g,(n,SCAT)} = k_{eff} \sum_{j \in M} V_j \left(\sum_{g'} \phi_{j,g}^{\dagger} S_{I,(n,inel)}^{g' \to g} \phi_{j,g'} - {\phi^{\dagger}}_{g} N_I \sigma_{I,(n,inel)}^{g} \phi_{j,g} + {\phi^{\dagger}}_{j,g} \frac{k_{eff} B^2}{3\Sigma_M^g} \frac{N_i \sigma_{I,(n,scat)}^{g}}{\Sigma_M^g} \phi_{j,g} \right) \tag{3.69}$$

where $S_{I,(n,inel)}^{g' \to g}$ is the (n,inel) scattering matrix. Equation 3.69 presents a way for extracting the partial cross section sensitivities from the computed total scattering sensitivities. In the case where neutron leakage is not present, equation 3.69 reduces to the assumption introduced in the previous section, i.e. heavy isotope scattering sensitivities at high energies are due to inelastic scattering. As discussed in the previous section, for pin-cell problems, this is indeed the case and the approximation is valid. In the case where neutron leakage is present (this is the case where heavy isotope elastic scattering reactions are most visible), the partial elastic cross section sensitivity is given by:

$$S_{keff}^{g,(n,el)} = V_j {\phi^{\dagger}}_{j,g} \frac{k_{eff} B^2}{3\Sigma_M^g} \frac{N_i \sigma_{I,(n,el)}^{g}}{\Sigma_M^g} \phi_{j,g} \tag{3.70}$$

the sensitivity to the partial inelastic cross section can then be retrieved by substracting the total scattering sensitivity from the partial elastic sensitivity $S_{keff}^{(n,el)}$ which was computed by equation 3.70, i.e.

$$S_{keff}^{(n,inel)} = S_{keff}^{(n,SCAT)} - S_{keff}^{(n,el)} \tag{3.71}$$

Note that at no point are the components of the inelastic scattering matrix $S^{g'\to g}_{I,(n,inel)}$ required. To compute the partial cross section sensitivities from equation 3.70 and 3.71 requires access to partial cross section data from which the multi-group library (in this case the 172-group WIMS library) was constructed.

Uncertainty Propagation with Lumped Covariance Matrices

Another option for computing scattering uncertainty contributions that avoids the requirement of having access to the partial cross section data is to use lumped covariance matrices. Such matrices can be constructed using the expression given by equation 3.58. As seen from equation 3.69, the inelastic terms must be treated seperately. The covariance between the lumped scattering cross section and inelastic scattering cross section can be computed by [90]:

$$COV\left(\sigma^{g}_{(n,SCAT)},\sigma^{g'}_{(n,inel)}\right)=\sum_{x\in\{(n,el),(n,inel)\}}\frac{\sigma^{g}_{(n,x)}}{\sigma^{g}_{(n,SCAT)}}COV\left(\sigma^{g}_{(n,x)},\sigma^{g'}_{(n,inel)}\right) \tag{3.72}$$

We can then define an equivalent gain term $\tilde{G}_g$ which can be considered as purely originating from inelastic scattering:

$$\begin{aligned}\tilde{G}^{g,(n,inel)}_{k_{eff}} &\equiv k_{eff}\sum_{j\in M}V_j\left(\sum_{g'}\phi^{\dagger}_{j,g}S^{g'\to g}_{I,(n,SCAT)}\phi_{j,g'}-{\phi^{\dagger}}_{j,g}N_I\sigma^{g}_{I,(n,SCAT)}\phi_{j,g}\right)\\ &= k_{eff}\sum_{j\in M}V_j\left(\sum_{g'}\phi^{\dagger}_{j,g}S^{g'\to g}_{I,(n,inel)}\phi_{j,g'}-{\phi^{\dagger}}_{j,g}N_I\sigma^{g}_{I,(n,inel)}\phi_{j,g}\right)\end{aligned} \tag{3.73}$$

where the second equality was obtained by virtue of the approximation given by equation 3.66. An equivalent loss term can also be defined as:[18]

$$\tilde{L}^{g,(n,SCAT)}_{k_{eff}}\equiv-\sum_{j\in M}{\phi^{\dagger}}_{j,g}\frac{k_{eff}B^2}{3\Sigma^{g}_{M}}\frac{N_i\sigma^{g}_{I,(n,SCAT)}}{\Sigma^{g}}\phi_{j,g} \tag{3.74}$$

which can be associated with the lumped scattering matrix. This is equivalent to applying the chain rule of equation 3.62 to the loss terms. We note that the total scattering sensitivity $S^{g,(n,SCAT)}_{k_{eff}}=\tilde{G}^{g,(n,inel)}_{k_{eff}}-\tilde{L}^{g,(n,SCAT)}_{k_{eff}}$ remains invariant. The response uncertainty $\sigma^{\mathbf{2}}_{\mathbf{scat}}$ from scattering cross section uncertainties can be computed as:

$$\begin{aligned}\sigma^{\mathbf{2}}_{\mathbf{scat}}=\sum_{g=1}^{N_G}\sum_{g'=1}^{N_G}\Big(&\tilde{L}^{g,(n,SCAT)}_{k_{eff}}\cdot COV(\sigma^{g}_{(n,SCAT)},\sigma^{g'}_{(n,SCAT)})\cdot\tilde{L}^{g',(n,SCAT)}_{k_{eff}}\\ &-2\tilde{G}^{g,(n,inel)}_{k_{eff}}\cdot COV(\sigma^{g}_{(n,inel)},\sigma^{g'}_{(n,SCAT)})\cdot\tilde{L}^{g',(n,SCAT)}_{k_{eff}}\\ &+\tilde{G}^{g,(n,inel)}_{k_{eff}}\cdot COV(\sigma^{g}_{(n,inel)},\sigma^{g'}_{(n,inel)})\cdot\tilde{G}^{g',(n,inel)}_{k_{eff}}\Big)\end{aligned} \tag{3.75}$$

[18]Note that we associate this term to losses for computational purposes only. In reality, the term has a positive contribution to the sensitivity.

Equation 3.75 presents a simple method for the computation of the uncertainty from the scattering cross section without requiring knowledge of the partial cross sections. Once covariance matrices are computed from equations 3.58 and 3.72, the uncertainty can be calculated using equation 3.75. The only requirement for this approach is that the equivalent loss term $\tilde{\mathbf{L}}$ (which represents the contribution to the sensitivity from the leakage term $\delta(d_g B^2)$) and the equivalent gain term $\tilde{\mathbf{G}}$ are stored during the process of sensitivity analysis.[19] We note that while this approach leads to results consistent with those computed by using partial cross sections, information relating to the origin of the uncertainties is lost. As one of the principle applications of nuclear data uncertainty propagation is to provide meaningful feedback to evaluators, experimentalists, etc., we do not recommend this approach and suggest for partial cross sections contributions to be computed by using equations 3.70 and 3.71.

Figures 3.6 and 3.11 present the correlation matrix for ^{238}U(n,SCAT)-(n,SCAT) and ^{238}U(n,SCAT)-(n,inel) computed from equations 3.58 and 3.72. The cross section values that appear in equations 3.58 and 3.72 have been taken from JEFF 3.1 evaluation, processed into 172-group by the NJOY code. To read and manipulate the covariances, we use our set of PYTHON libaries, which contain modules capable of reading, writing and creating NJOY GENDF format files (see section 2.8.3 of the previous chapter). The matrices are then stored in NJOY ERRORR format for use. After the sensitivities have been computed by DRAGON, the sensitivity to the partial (n,el) and (n,inel) cross sections is computed by using equations 3.70 and 3.71. The uncertainty can be computed either by using the sandwich rule with the computed partial cross sections or by using the lumped covariance matrices presented above. The two methods are equivalent and give identical results that are also consistent with SCALE/TSUNAMI 3D.

3.3.5 Limitations of Our Approximation

First, as we mentioned it several times over the course of this section, the solution we propose is only applicable to heavy isotope scattering reactions. However, while reactions such as ^{1}H(n,el) and ^{16}O(n,el) may have a noticable contribution to the uncertainty due to their high sensitivities, heavy isotope scattering reactions can be great contributors to the uncertainty due to the high uncertainties associated with these isotopes. An accurate computation of the uncertainty contribution from these uncertainties is valuable as they can provide guidelines for future experiments and measurements (i.e. their uncertainties can actually be improved through integral experiments and data adjustment).

Next, the approximation 3.66 ignores the effect of group transfer due to elastic scattering. For heavy isotopes, this does not have a large effect. The key point is that the contribution from elastic reactions is not due to the differences in the importance of neutrons resulting from the energy loss of the elastic collision (as for heavy isotopes, the energy loss from the elastic collision is not large), but rather from the importance gained from the resultant change in the neutron's direction following the elastic collision.

[19] These are stored under 'CORSIGS' and 'GTERM' on the **SNS:** LCM object

Finally, we note that our assumption also ignores the contribution of (n,2n) and (n,3n) reactions. In thermal systems, contribution from these reactions to the total uncertainty is small so that they do not play a major role in the obtained uncertainty for k_{eff}.[20] For example, for the thermal systems considered in [103], the k_{eff} sensitivity of these reactions as computed by SCALE/TSUNAMI-3D is an order of magnitude smaller than the sensitivity of (n,inel). Therefore, in thermal systems, the corresponding uncertainty contribution from these reactions is computed to be a few pcm of the overall k_{eff} uncertainty, so that our assumption of ignoring these reactions is not presumed to lead to large errors in the computed partial sensitivity and uncertainty contributions.[21]

[20]Note that this is not true in the case of evolution/burn up computations where these reactions will dictate the density of child nuclei. Contribution from these reactions to the overall uncertainty in this case is due to the uncertainty on the density of the child nuclei and not related to the current application.

[21]For the benchmarks considered in chapter 4, this error is of the order of 1% of the computed sensitivity.

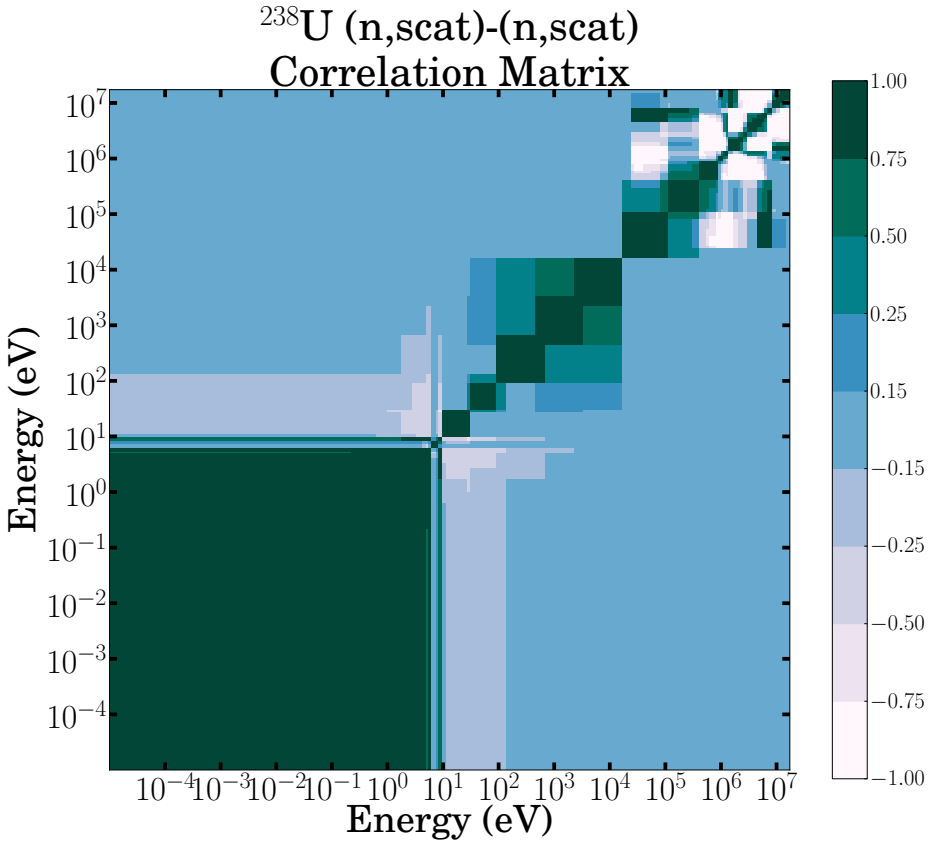

Figure 3.6: SCALE 6 ^{238}U (n,SCAT)-(n,SCAT) lumped scattering correlation matrix. Constructed from SCALE 6 covariances and JEFF 3.1 cross section values

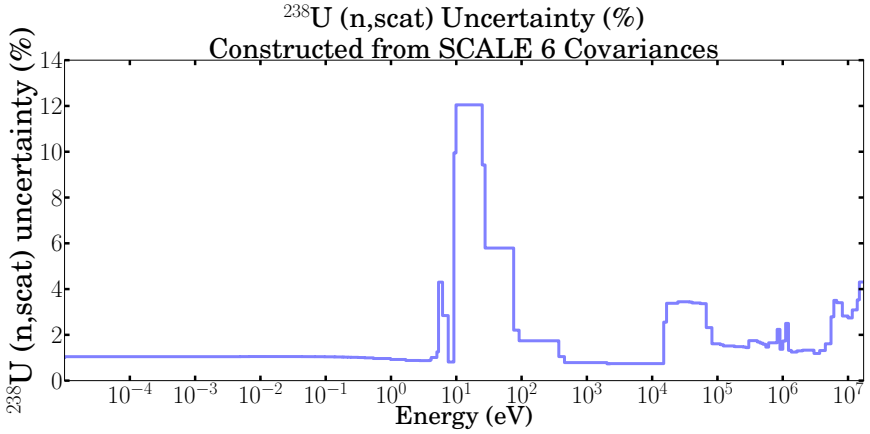

Figure 3.7: Uncertainty (%) for the ^{238}U(n,SCAT) cross section constructed from SCALE 6 covariances and JEFF 3.1

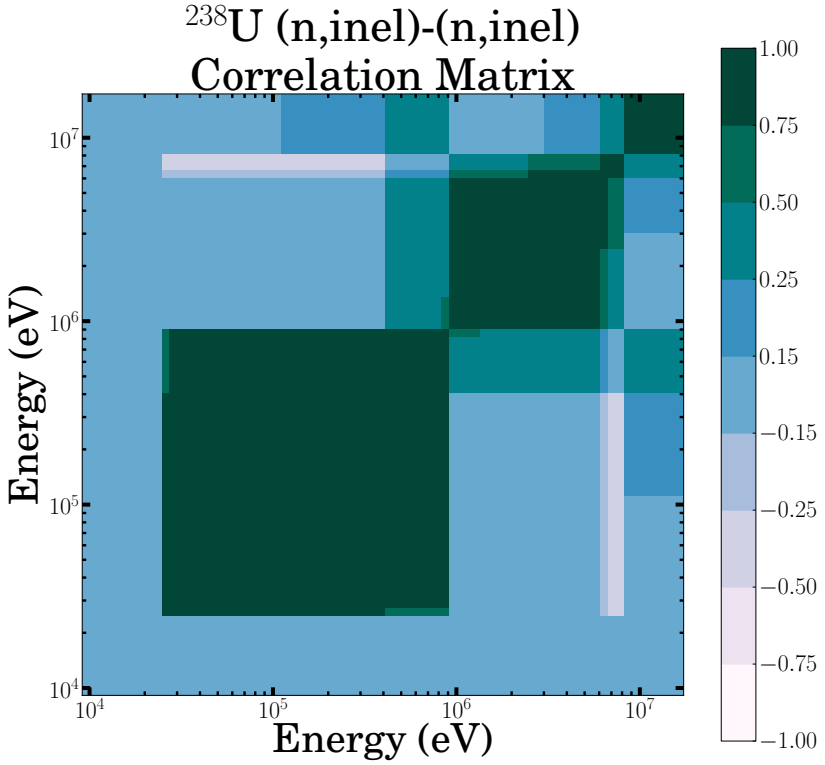

Figure 3.8: ^{238}U(n,inel)-(n,inel) correlation matrix from SCALE 6 Covariances

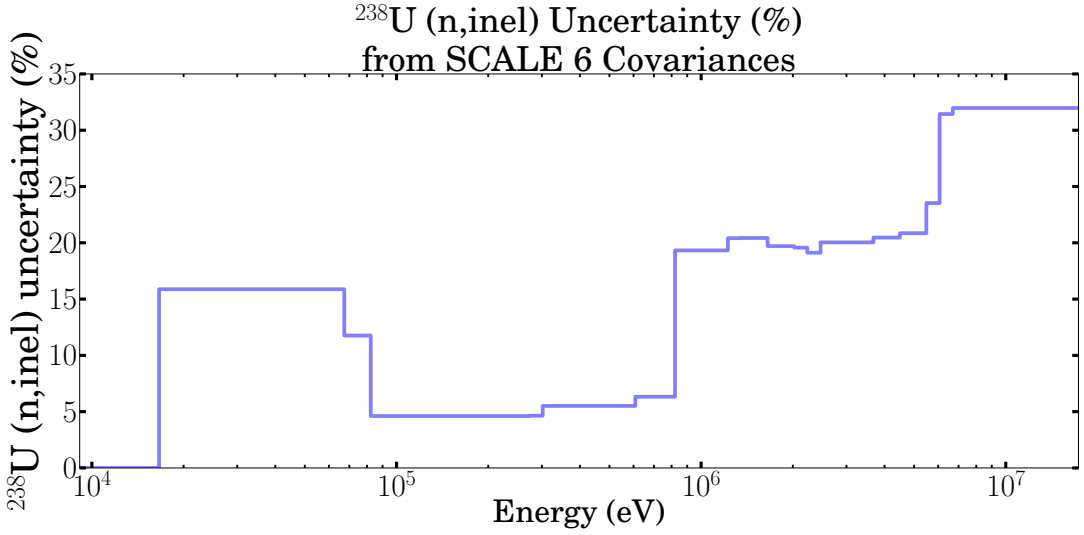

Figure 3.9: ^{238}U(n,inel) uncertainty(%) from SCALE 6 Covariances

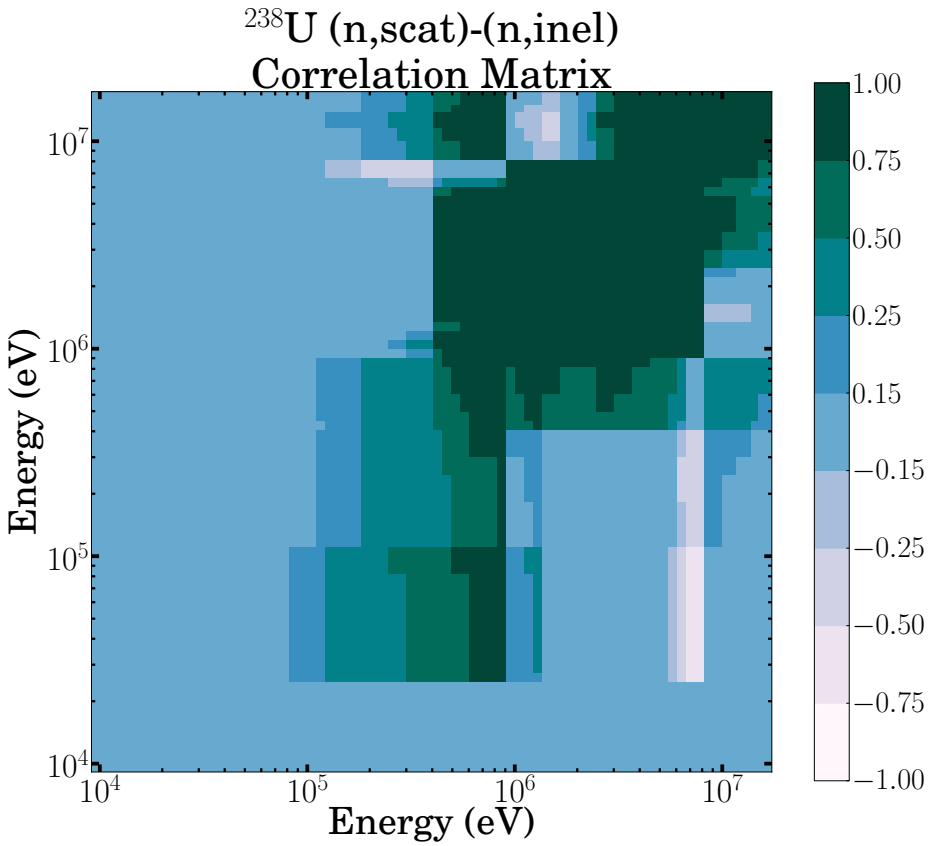

Figure 3.10: ^{238}U(n,SCAT)-(n,inel) correlation matrix for groups 1-45 of the WIMS 172-group library. Constructed from SCALE 6 covariances and JEFF 3.1 cross section values.

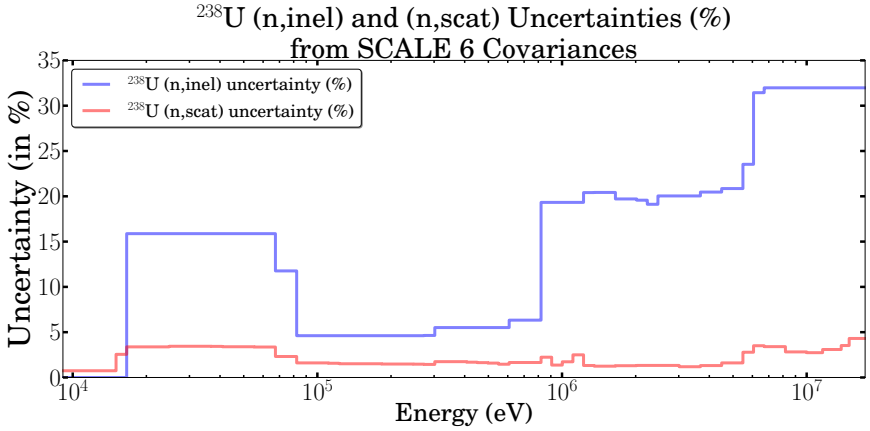

Figure 3.11: ^{238}U(n,SCAT)-(n,inel) correlation matrix for groups 1-45 of the WIMS 172-group library. Constructed from SCALE 6 covariances and JEFF 3.1 cross section values.

Chapter 4

Results and Verification

The reference set of benchmarks in our community is the OECD Uncertainty Analysis in Modelling (UAM) benchmark, which sets out goals and guidelines for developers [103]. Contained in the benchmark description manual are exercises that address sensitivity and uncertainty analysis for pin cell, assembly, core computations and evolution/burn-up calculations. Here, a number of different core designs covering a wide range of spectra and isotopes exist for analysis. Most relevant to the lattice code DRAGON and the CP method are pin cell, assembly, and burn-up computations.

The set of benchmarks contained in Exercise I.1 and I.2 of the UAM benchmarks [103] provide a good verification for the methodology and tools that we have presented in chapter 2. In these two exercises, reflected pin-cell and assembly problems are specified.[1] Participants can provide their results for response uncertainties for homogenized two-group cross sections and critical, and verify their results. Solutions to a number of these benchmarks are already available from participants who used deterministic and Monte Carlo methods for sensitivity analysis and uncertainty propagation.

Relevant to the first two exercises of the UAM benchmarks, the recently published literature shows good agreement between different methods of nuclear data uncertainty propagation, and where available, sensitivity analysis [104, 54, 55, 56, 108]. In the thermal systems studied in the UAM Benchmarks, heavy isotope capture, fission yield and fission cross sections usually have the largest contributions to the response uncertainty, primarily because of their high sensitivities. However, conservative estimates of nuclear data uncertainties are reported by most evaluations to be within the 1-5% range for the major actinides ^{238}U and ^{235}U. Their low uncertainties make improving their cross section values through integral experiments and data adjustment more difficult.

A second group of cross sections whose uncertainty can also contribute to the overall performance parameter are heavy isotope scattering reactions. An example of this is ^{238}U(n,inel) cross section which is reported to have an uncertainty of 20-35% of its

[1] For example, in chapter 3, we provided comparisons between our DRAGON sensitivities and uncertainties and those computed by CASMO-4 and SCALE/TSUNAMI-2D which were reported in [55]. The three solutions were in good agreement not only demonstrating the capacity of our tools but also this conclusion.

value and also to be strongly anti-correlated with ^{238}U(n,el) (see figures 3.1-3.2). An uncertainty analysis for these reactions is also more pragmatic since, given their high uncertainties, their values can actually be improved through integral experiments and data adjustment. However, an accurate computation of the sensitivity for these reactions is more difficult as, unlike absorption and fission sensitivities, the scattering sensitivity expressions depend on the anisotropic flux moments and are more sensitive to the accuracy of the transport computation.[2]

As we will demonstrate shortly, the current methodology available in the code DRAGON [24, 34, 108] does not permit for an accurate computation of scattering sensitivities. This was the underlying reason for the developments introduced in chapter 3. In this chapter we will provide a verification for the developments made in chapter 2 and 3 by presenting our results of the Phase III of the OECD Uncertainty Analysis and Criticality Safety Assessment (UACSA) Benchmark [105, 106, 107]. Currently, we are not aware of a deterministic solution to these benchmarks.[3]

The primary aim of the Expert Group from proposing this benchmark was to study the underlying differences between methods/codes used for sensitivity and uncertainty analysis. The principle requirement of the benchmark is an accurate computation of the scattering sensitivities [107]. The greatest discrepancies amongst benchmark participants were observed for ^{238}U and ^{16}O scattering sensitivities. Therefore, the expert group focused on these two sensitivities in the benchmark summary [107]. One of the conclusions reached by the UACSA Expert Group was that ^{238}U(n,SCAT) and ^{16}O(n,SCAT) sensitivities require improvement. Additionally, a large component of the k_{eff} uncertainty for these benchmarks is also due to ^{238}U(n,SCAT) uncertainties, making an accurate computation of its uncertainty contribution even more necessary.

As a consequence, in this chapter we will study three benchmarks proposed by the Expert group. These benchmarks involve three models: a critical sphere of Uranium Fluoride, a 3D light water MOX fuel lattice at its critical height, and a 3-D small MOX core surrounded by a light water reflector. From a computational point of view, the proposed benchmarks involve three processes:

- A large component of the ^{238}U elastic scattering sensitivity is in the resonance region where implicit effects occur.
- The proposed benchmarks involve geometries where neutron leakage occurs. As a result, scattering reactions gain a new significance due to their competing role with leakage.
- Due to neutron leakage, a new importance is given to scattering reactions, and

[2]At the time of the original development with GPT in DRAGON [24, 34], scattering sensitivities were the most discrepant reported values. Since then, further studies of sensitivity analysis in application to the reflected pin-cell problems in the UAM benchmark [108] highlighted further discrepancies.

[3]Note that a perturbation theory approach with DRAGON-4 using the Method of Characteristics (MOC) was attempted for this benchmark in [109]. However, as the sensitivity computation was being performed in P_0, most of the computed scattering sensitivities are one order of magnitude smaller than the values predicted by SCALE/TSUNAMI-3D.

their role in the compensation of errors becomes more pronounced. An accurate computation of this error compensation is difficult due to the different formats associated with the WIMS libraries and the currently available covariance data. An accurate computation of this uncertainty is not currently possible by codes such as CASMO-4 and DINASOUR [55, 56, 54].

4.1 2% Enriched UF_4 Sphere

This benchmark represents a slightly enriched (2%) sphere of polyethylene. The radius of the sphere is 36 cm. The atomic densities are given in Table 4.1.

2% enriched sphere	
Isotope	Density (atms/barn-cm)
^{235}U	$1.3303 * 10^{-4}$
^{238}U	$6.4370 * 10^{-3}$
H	$3.9097 * 10^{-2}$
C	$1.8797 * 10^{-2}$
F	$2.6280 * 10^{-2}$

Table 4.1: Atomic densities for the 2% UF_4 bare sphere. Reproduced from [106].

4.1.1 Scattering Sensitivities

Table 4.2 presents k_{eff} *integrated* scattering sensitivities for the five isotopes present in the geometry. The values provided in the table represent a % change in k_{eff} resulting from a 1% uniform perturbation in the scattering cross section of the isotope. The columns of the table report the integrated scattering sensitivity of the isotope (in %) as obtained from the different transport computations. The sensitivities appearing in the first column labeled k_{eff} are computed by using the scalar flux ϕ and $\phi^\dagger$ in the sensitivity expression that was obtained from the assumption that the resulting perturbation in the CP matrix can be effectively represented by adding an isotropic source to the in-group scattering term (see equations 1.188 -1.190). The scalar flux ϕ and the adjoint $\phi^\dagger$ have been obtained from DRAGON **FLU:** using a k_{eff} search. The sensitivities in this column present the current approach for computing sensitivities in DRAGON [24, 108, 110]. We will refer to these sensitivities as DRAGON-K (DR-K). The second column presents sensitivities computed by using a B_0 homogeneous leakage model (DR-B_0) and the sensitivity expression we introduced in chapter 3 by treating leakage as a standard cross section (see equations 3.47 and 3.49). The column labeled SCALE P_0 presents results obtained from SCALE6/TSUNAMI-1D by using the flux and adjoint from a P_0 discrete ordinates solution (S6-P_0). The column labeled DRAGON B_1 reports sensitivities that have been computed by using a Homogeneous B_1 leakage model with DRAGON (DR-B_1) and by computing the leakage sensitivity using the transport corrected diffusion coefficient (see 3.47 and 3.52). The column labeled SCALE P_1 presents sensitivities obtained by SCALE/TSUNAMI-1D from a discrete ordinate P_1 solution (S6-P_1); these will be our

reference results.

We note the good agreement between DR-B_1 and S6-P_1. Even for ^{235}U, which has a small sensitivity component of the order of 10^{-4}, our DR-B_1 computed sensitivity is within 8% of the reference S6-P_1 result. This shows the validity of our leakage model.

	Explicit Scattering Sensitivities (%/%)					
Isotope	DRAGON k_{eff}	DRAGON B_0	SCALE P_0	DRAGON B_1	SCALE P_1	Relative Error (%)
^{1}H	$3.17 * 10^{-1}$	$3.55 * 10^{-1}$	$3.21 * 10^{-1}$	$3.82 * 10^{-1}$	$3.76 * 10^{-1}$	-1
^{12}C	$5.70 * 10^{-3}$	$2.50 * 10^{-2}$	$1.55 * 10^{-3}$	$3.32 * 10^{-2}$	$3.17 * 10^{-2}$	-4
^{19}F	$9.47 * 10^{-3}$	$4.73 * 10^{-2}$	$2.96 * 10^{-2}$	$5.71 * 10^{-2}$	$5.58 * 10^{-2}$	-2
^{238}U	$5.24 * 10^{-3}$	$2.18 * 10^{-2}$	$1.55 * 10^{-2}$	$2.94 * 10^{-2}$	$2.80 * 10^{-2}$	-5
^{235}U	$9.27 * 10^{-5}$	$4.07 * 10^{-4}$	$3.61 * 10^{-4}$	$5.22 * 10^{-4}$	$5.63 * 10^{-4}$	8

Table 4.2: Comparison of explicit scattering sensitivities for the 2% enriched UF_4 sphere. The relative error (in %) reports the difference between DRAGON B_1 relative to the SCALE P_1.
DRAGON k_{eff} (DR-K): sensitivities obtained by using the flux and adjoint from a DRAGON k_{eff} search.
DRAGON B_0 (DR-B_0): sensitivities obtained by using the flux and adjoint from DRAGON by using a homogeneous B_0-buckling search (see equations 3.47 and 3.49).
DRAGON B_1 (DR-B_1): sensitivities obtained by using the flux and adjoint from DRAGON by using a homogeneous B_1-buckling search(see equations 3.47 and 3.52) .
SCALE P_0 (S6-P_0): SCALE/TSUNAMI-1D sensitivities from a discrete ordinates P_0 solution.
SCALE P_1 (S6-P_1): SCALE/TSUNAMI-1D sensitivities from a discrete ordinates P_1 solution.

B_0-DRAGON Sensitivities

Next, we see that the DR-B_0 values appearing in the table are more comparable to the DR-B_1 and S6-P_1 (our reference results) than the S6-P_0 results. This may seem surprising given that the sensitivities appearing in both columns originate from the scalar flux and adjoint solutions to Boltzmann equations where scattering anisotropy is ignored and only the zeroth Legendre component of the flux and adjoint are solved for (i.e. the scalar flux). However, we note that in the B_N formalism, the higher order flux moments are coupled in terms of a lower diagonal matrix (see section 3.2.1). Thus, computing a higher flux moment does not influence the previous solution. In the CP formalism, we note that when solving for the scalar flux, the only assumption that was made was that scattering anisotropy could be effectively ignored. Therefore the scalar flux obtained from a CP solution corresponds to the actual scalar flux of a system where scattering anisotropy does not exist (i.e. the zeroth term in the infinite Legendre expansion of the flux). Contrary to the B_N formalism, in the P_N formalism [83], computation of higher order flux moments affect the previous lower order solution. Therefore, the DR-B_0 sensitivities are in better agreement with the DR-B_1 sensitivities because the scalar flux obtained from a CP or a

B_0 solution is more accurate than the scalar flux obtained from a P_0 solution.[4]

Next, we observe that the DR-K sensitivities are lower than all other sensitivities reported in table 4.2. This was the main motivation behind the developments we presented in chapter 3. Even though the DR-K sensitivities were computed by using the flux and adjoint originating from a transport corrected CP solution, the resulting sensitivities are less accurate than the S6-P_0 sensitivities. The reason for this has to do with how we arrived at the perturbation expressions for reactivity. In order to avoid computing the perturbation of the Collision Probability matrix, we assumed that the perturbation in our system, $\delta\mathbf{\Sigma}$, can be effectively represented by adding the isotropic source $\delta\mathbf{\Sigma}\phi(\vec{r}, E)$ to the in-group scattering source (see equations 1.187-1.188). Assuming a perturbation of this form permitted us to approximate the perturbation in the CP matrix in terms of a linear perturbation in the total cross section. However, perturbations that affect the angular flux, or current, can not be represented by such a source. Therefore, the resultant DR-K perturbation expressions do not capture the components of the sensitivity arising from such perturbations.

To study this effect, we can consider three different components of the DR-B_1 sensitivity expression that we arrived at by using the buckling approximation and treating leakage as a standard cross section (see equations 3.46, 3.44, 3.49). In the sensitivity expression for the scattering cross section we can isolate the terms:

- Energy gain/loss defined as the difference $\left\langle \phi^\dagger, k_{eff}\left(\delta_q\mathbf{S} - \delta_q\mathbf{\Sigma}\right)\cdot\phi \right\rangle$ where $q = \sigma_{(n,SCAT)}$. This term accounts for the net importance gained from the neutron after the scattering collision (its sign is usually positive for thermal systems).

- The isotropic component of the leakage term $\left\langle \phi^\dagger, \frac{qk_{eff}B^2}{3(\mathbf{\Sigma}-\mathbf{\Sigma}_{\mathbf{s},\mathbf{1}})}\frac{\delta_q\mathbf{\Sigma}}{(\mathbf{\Sigma}-\mathbf{\Sigma}_{\mathbf{s},\mathbf{1}})}\phi \right\rangle$, i.e. the net importance gained from the neutron's change in direction following the scattering collision.[5]

- Scattering anisotropy approximated from the transport correction as $-k_{eff}\left\langle \phi^\dagger, \frac{qB^2\delta_q(\mathbf{\Sigma}_{\mathbf{s},\mathbf{1}})}{3(\mathbf{\Sigma}-\mathbf{\Sigma}_{\mathbf{s},\mathbf{1}})^2}\phi \right\rangle$ (see equations 3.51-3.52).

The three components of the scattering sensitivities are presented in table 4.3 for DR-B_1 sensitivities. Also reported in the table are integrated sensitivities (%/%) for the DR-K and DR-B_1 approach. The first column GAIN/LOSS (GL) refers to the energy gain/loss component of the sensitivity. The column named STREAMING (ST) presents the contribution of the streaming/neutron leakage term to the integrated DR-B_1 sensitivity, and the last column reports the contribution of the transport correction (TR) to the integrated DR-B_1 sensitivity. The values are given in terms of the percentage contribution to the DR-B_1 integrated sensitivity. The values appearing in the parenthesis are the absolute contribution to the DR-B_1 integrated sensitivity (in %/%).

[4]Indeed, the differences observed in the B_0 sensitivities and the B_1 sensitivities highlight the effect of scattering and flux anisotropy in the system. Since the leakage is underestimated with a B_0 model [83]-scattering sensitivities in the fast range (which compete with leakage) are also underestimated.

[5]Note that for computational purposes, this term is assigned as a loss term. In the sensitivity formulas, its sign is positive.

	Integrated Sensitivities (%/%)		Sensitivity Decomposition† (% of B_1)		
Isotope	DRAGON k_{eff}	DRAGON B_1	GAIN/LOSS	STREAMING	TR
^{1}H	$3.17 * 10^{-1}$	$3.82 * 10^{-1}$	82% $(3.15 * 10^{-1})$	23% $(8.60 * 10^{-2})$	-5 % $(-1.8 * 10^{-2})$
^{12}C	$5.70 * 10^{-3}$	$3.32 * 10^{-2}$	18% $(5.90 * 10^{-3})$	82% $(2.73 * 10^{-2})$	0 % (0.0)
^{19}F	$9.47 * 10^{-3}$	$5.71 * 10^{-2}$	20% $(1.13 * 10^{-2})$	80% $(4.58 * 10^{-2})$	0 % (0.0)
^{238}U	$5.24 * 10^{-3}$	$2.94 * 10^{-2}$	36 % $(5.98 * 10^{-3})$	83% $(2.29 * 10^{-2})$	-19 % $(-5.2 * 10^{-3})$
^{235}U	$9.27 * 10^{-5}$	$5.22 * 10^{-4}$	22% $(9.25 * 10^{-5})$	79% $(4.10 * 10^{-4})$	0 % (0.0)

Table 4.3: Decomposition of the Integrated Sensitivities computed by DRAGON **SNS:** †: Sensitivity decomposition % (absolute value %/%) of the DRAGON results from a B_1 leakage model with transport correction.

For example, we see from table 4.3 that the largest component for the ^{1}H integrated scattering sensitivity is the GL term. This shows the role that ^{1}H plays as a neutron moderator. The GL contribution is positive because an increase in ^{1}H(n,el) cross section results in an increase in the thermal neutron population thereby increasing fission.[6]

Also observed from 4.3 is that the ST contribution to the scattering sensitivity of all elements other than ^{1}H is larger than GL. The ST and TR components can not be computed in the DR-K approach. Comparison of DR-K and GL verifies that the DR-K can only predict the sensitivity component due to energy gain and loss. This limitation of the DR-K approach is constraining when the uncertainty contribution from scattering reactions is important (which is the case for the UACSA benchmarks being studied).

Figures 4.1 presents the ^{1}H(n,el) sensitivity profile. The scattering sensitivity is important over the entire spectrum given Hydrogen's efficiency to moderate neutrons. The DR-K profile appears in gray and effectively shows the GL profile. We observe that at high energies, where neutrons are more prone to leakage, streaming effects become important. This can be seen by comparing the DR-K, with DR-B_1 and S6-P_1. The effect can be seen in figures 4.2, 4.3, and 4.4 for ^{12}C, ^{19}F and ^{238}U scattering sensitivities.

[6]Note that this is true for thermal systems.

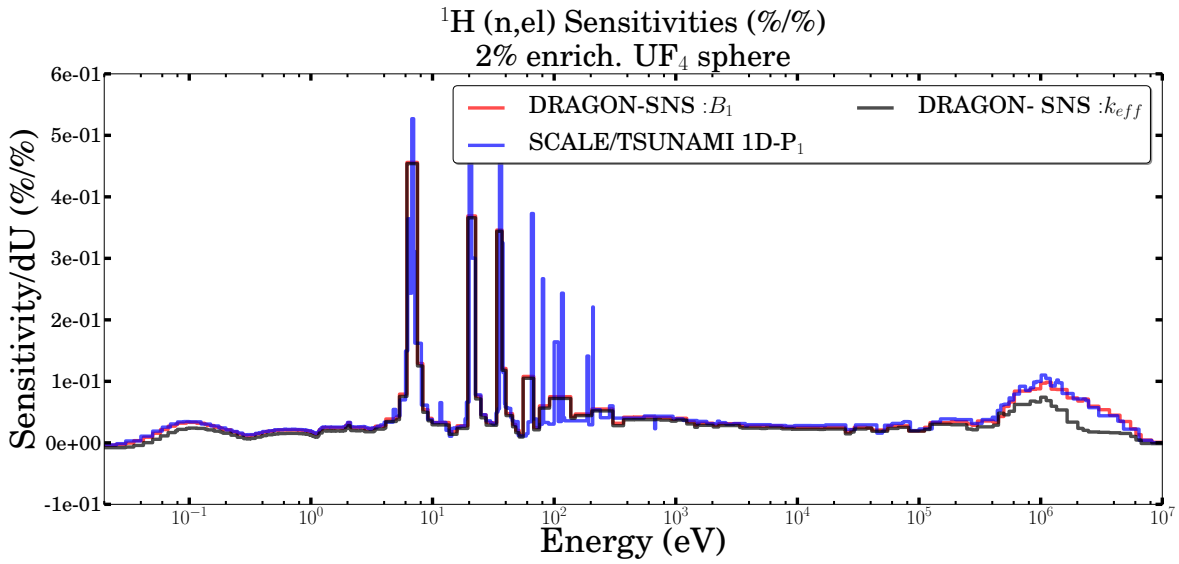

Figure 4.1: Comparison of ^{1}H(n,el) sensitivity for the UF_4 sphere. Note the differences at high energy between the gray curve and the two other curves, that result from streaming effects that are not captured by the DRAGON-k_{eff} (DR-K) approach.

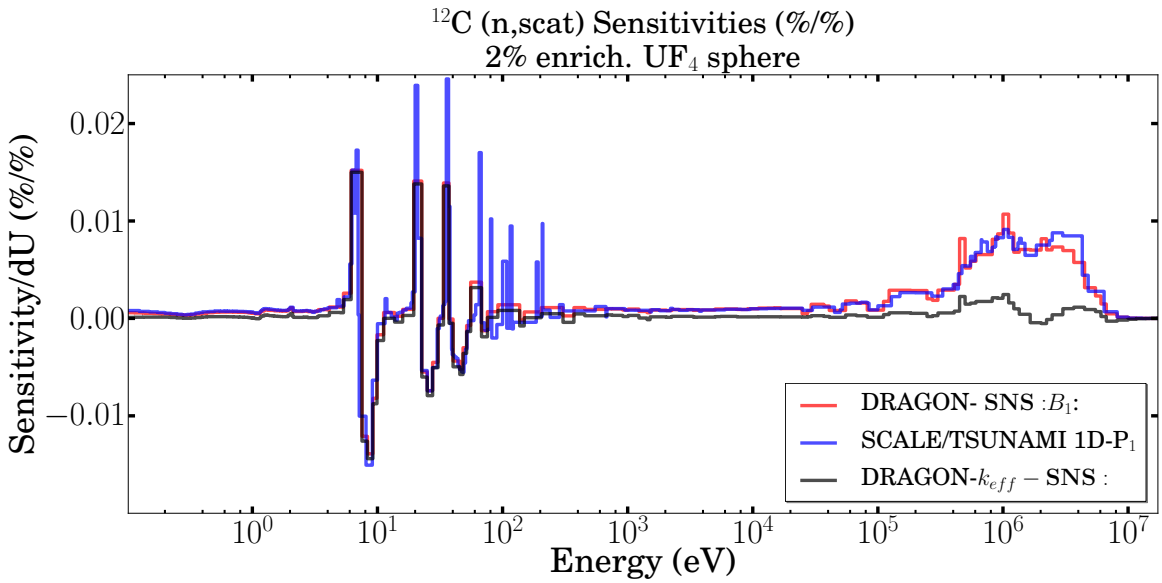

Figure 4.2: Comparison of the ^{12}C(n,SCAT) sensitivity for the UF_4 sphere. Note the differences at high energy between the gray curve and the two other curves, that result from streaming effects that are not captured by the DRAGON-k_{eff} (DR-K) approach. The differences between the DRAGON-B_1 profile and SCALE6/TSUNAMI-1D profile stem from anisotropy.

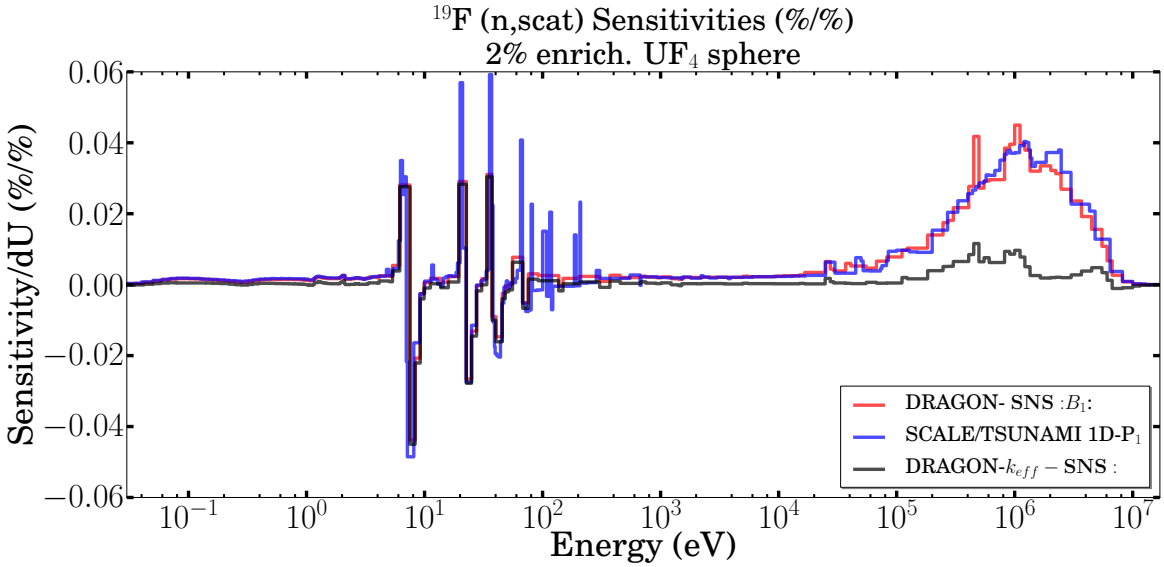

Figure 4.3: Comparison of ^{19}F(n,SCAT) sensitivity for the UF_4 sphere.

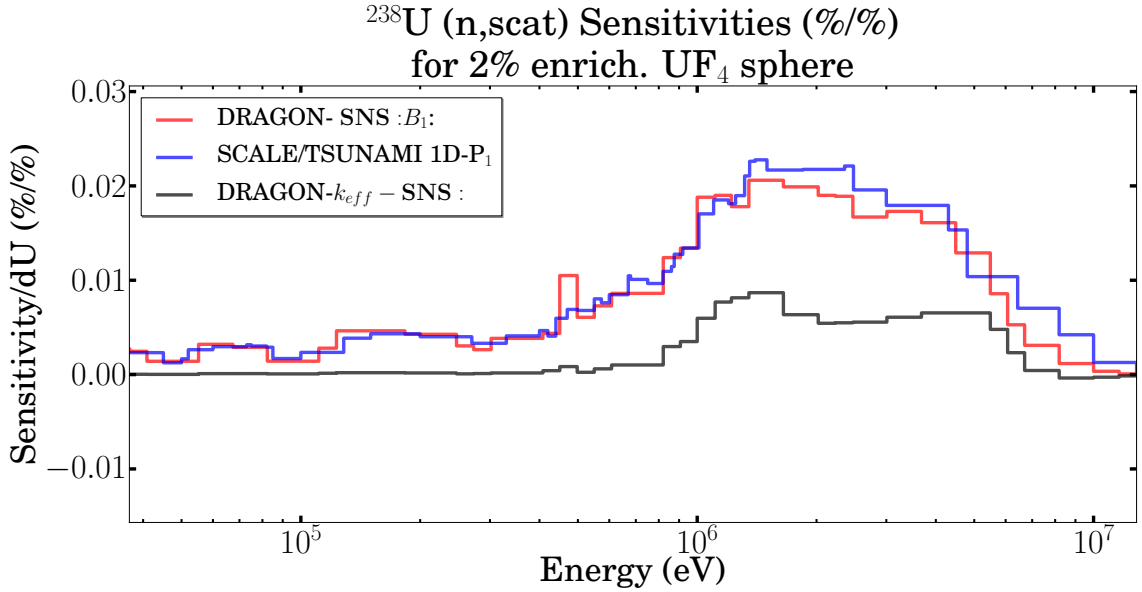

Figure 4.4: Comparison of ^{238}U(n,SCAT) sensitivity for the UF_4 sphere.

Integrated Sensitivities

The main goal of this study is the computation of k_{eff} sensitivities to multi-group cross sections for the purpose of nuclear data uncertainty propagation with DRAGON. This requires the computation of sensitivity profiles for use with the sandwich formula (see equation 1.199).

Table 4.4 presents the DR-K, DR-B_1 and S6-P_1 integrated sensitivities (in %/%). The column labeled relative error presents the difference (in %) between the DR-B1 results and the S6-P_1 results. Comparing the DR-K column with the DR-B_1 column, we observe that absorption and fission sensitivities are not affected by leakage as their sensitivities essentially rely on the scalar flux. The last column in the table presents the error (in %) between the DR-B_1 sensitivities relative to the S6-P_1 sensitivities. We note the good agreement between the presented values. The 9.18% error associated with ^{238}U absorption cross section is due to underlying differences in the self shielded multi-group cross sections and will be discussed in the next section. The row labeled TOTAL reports the sum of the absorption, scattering and fission sensitivities. This sensitivity is called the total sensitivity as it represents the % change in k_{eff} from a 1% perturbation in the atomic density of the isotope.

For ^{238}U, the error in the capture sensitivity is the largest component of the error in the total sensitivity. This is principally due to differences in the self-shielding computation between the two codes. Note that the sensitivities are often of opposite signs, making the total sensitivity usually smaller, and its error more difficult to interpret. The total sensitivity is therefore not an optimal parameter for comparison when performing code-verification.

		Explicit Integrated Sensitivities (%/%)			
	Reaction	DRAGON **SNS:** k_{eff}	DRAGON **SNS:** B_1	SCALE P_1	Rel. Error† (%)
^{19}F	(n,ABS)	$-5.99 * 10^{-3}$	$-5.76 * 10^{-3}$	$-5.39 * 10^{-3}$	6.8 %
	(n,SCAT)	$9.47 * 10^{-3}$	$5.71 * 10^{-2}$	$5.58 * 10^{-2}$	2.2 %
	TOTAL	$3.48 * 10^{-3}$	$5.13 * 10^{-2}$	$5.04 * 10^{-2}$	1.7 %
^{235}U	(n,capture)	$-1.11 * 10^{-1}$	$-1.12 * 10^{-1}$	$-1.12 * 10^{-1}$	0.1 %
	(n,scat)	$9.27 * 10^{-5}$	$5.18 * 10^{-4}$	$5.63 * 10^{-4}$	7.98 %
	(n,f)	$3.69 * 10^{-1}$	$3.65 * 10^{-1}$	$3.66 * 10^{-1}$	0.3 %
	$\bar{\nu}$	$9.49 * 10^{-1}$	$9.49 * 10^{-1}$	$9.49 * 10^{-1}$	0.02 %
	TOTAL	$2.59 * 10^{-1}$	$2.53 * 10^{-1}$	$2.54 * 10^{-1}$	0.3%
^{238}U	(n,capture)	$-3.29 * 10^{-1}$	$-3.32 * 10^{-1}$	$-3.04 * 10^{-1}$	9.18 %
	(n,scat)	$5.24 * 10^{-3}$	$2.74 * 10^{-2}$	$2.80 * 10^{-2}$	2.07 %
	(n,f)	$3.34 * 10^{-2}$	$3.40 * 10^{-2}$	$3.44 * 10^{-2}$	1.14 %
	$\bar{\nu}$	$5.13 * 10^{-2}$	$5.07 * 10^{-2}$	$5.06 * 10^{-2}$	0.3 %
	TOTAL	$-2.96 * 10^{-1}$	$-2.70 * 10^{-1}$	$-2.42 * 10^{-1}$	12 %
^{1}H	(n,γ)	$-1.01 * 10^{-1}$	$-1.02 * 10^{-1}$	$-1.01 * 10^{-1}$	0.6 %
	(n,scat)	$3.17 * 10^{-1}$	$3.82 * 10^{-1}$	$3.76 * 10^{-1}$	1.62 %
	TOTAL	$2.16 * 10^{-1}$	$2.81 * 10^{-1}$	$2.75 * 10^{-1}$	2.21 %
^{12}C	(n,capture)	$-7.05 * 10^{-4}$	$-6.75 * 10^{-4}$	$-6.55 * 10^{-4}$	3.0%
	(n,scat)	$4.87 * 10^{-3}$	$3.32 * 10^{-2}$	$3.17 * 10^{-2}$	4.0%
	TOTAL	$4.16 * 10^{-3}$	$3.25 * 10^{-2}$	$3.11 * 10^{-2}$	4.5%

Table 4.4: Comparison of DRAGON explicit integrated sensitivities (%/%) with SCALE 6 /TSUNAMI-1D
† Relative Difference between the DRAGON **SNS:** B_1 (DR-B_1) results relative to the SCALE6/TSUNAMI-1D results.
Note the underestimated scattering sensitivities obtained from the DR-K approach and the good comparison between the DR-B_1 and S6-P_1 sensitivities.

4.1.2 Implicit Sensitivities

The sensitivities presented in the previous section were explicit sensitivities. They represented a % change in k_{eff} resulting from a 1% change in the self-shielded multi-group cross section. In this section, we will present our results for implicit scattering sensitivities. These sensitivities were computed according to the algorithm outlined in section 3.1.3. The implicit sensitivity accounts for the contribution to the sensitivity from the perturbation in the multi-group cross section resulting from a perturbation in the fine flux.

In the case of ^{238}U (n,γ), an increase in the absorption cross section leads to a higher depression in the fine flux. Since the self shielded multi-group cross section is generated by weighting the absorption cross section with the fine flux, the effect is a net reduction in the absorption rate (i.e. a positive sensitivity). Therefore, the implicit component and the explicit component of the ^{238}U(n,γ) sensitivity have opposite signs. As a result, accounting for the implicit effect decreases the absorption sensitivity, and ignoring the implicit absorption sensitivity leads to an over-estimation of the computed ^{238}U(n,γ) uncertainty contribution.

Unlike absorption, taking into account the implicit component of the ^{238}U(n,el) reaction leads to an increase in its uncertainty so that neglecting the implicit effect would under-estimate the ^{238}U(n,el) uncertainty contribution. This is most likely the reason why the Expert Group decided to consider this sensitivity in [107]. The ^{1}H(n,el) implicit sensitivity was also presented in [107] so that we present this sensitivity as an additional verification. The remaining implicit sensitivities are lower than 1-5% (in magnitude) of the corresponding explicit component and have not been considered in this study. We note that in this benchmark, the contribution of the implicit sensitivity to the total k_{eff} uncertainty from ^{238}U nuclear data uncertainties is 42 pcm when computed by using the DR-B_1 sensitivities and the analytical approximation. The contribution of the implicit sensitivity to the computed uncertainty is 40 pcm when using SCALE6/TSUNAMI-1D.[7]

^{238}U (n,el) Implicit Sensitivity

Of course the reason why we introduced our analytic approximation in section 3.1.3 was that we did not wish to repeat the self shielding computation 47 times per isotope.[8] The analytical approximation of section 3.1.3 requires one forward flux solution, one adjoint solution, and 47 cross section *interpolations* over the estimated dilution factor, and provides a good estimate for the implicit sensitivity in homogeneous systems.

Table 4.5 presents implicit scattering cross section sensitivities calculated for the 2% enriched UF_4 sphere using three different computational schemes as well as reference results obtained by SCALE/TSUNAMI-1D. The values reported in this table represent the contribution to the k_{eff} sensitivity from perturbations in the multi-group cross sections resulting from perturbations in the fine flux. The first column presents the implicit

[7]The covariance data source here are the 44 group SCALE6 covariance library. The contribution of the implicit sensitivity for capture was computed by SCALE to be 12 pcm, with the contribution from the correlation between the two being negligible.

[8]The number 47 corresponds to the number of resonance groups in the WIMS 172 group library

sensitivity computed by the analytical approximation. The second columns presents the implicit sensitivity computed from performing 47 self shielding computations using perturbed libraries, and the chain rule expansion law given by equation 3.19. This computational approach is feasible for large cases since the self shielding computation for these cases accounts for only a fraction of the computation time.[9] This approach requires one flux solution, one adjoint solution and 47 DRAGON self shielding computations. The third column presents sensitivities we obtained from complete simulations by perturbing the cross section and performing a k_{eff} search. This approach requires 47 DRAGON simulations. We note the good agreement between all three computation routes. However, our implicit sensitivities are 22% greater than those reported by SCALE/TSUNAMI-3D.

	Implicit Scattering Sensitivities (%/%)			
	DRAGON			SCALE
Isotope	ANALYTIC + **SNS:**	47 **SHI:** + **SNS:**	DIRECT 47 simulations	/TSUNAMI 1D[109]
^{238}U	$2.65 * 10^{-2}$	$2.55 * 10^{-2}$	$2.59 * 10^{-2}$	$2.16 * 10^{-2}$
^{1}H	-$2.99 * 10^{-2}$	$-2.95 * 10^{-2}$	$-2.94 * 10^{-2}$	$-3.01 * 10^{-2}$
^{19}F	-$4.21 * 10^{-3}$	$-4.22 * 10^{-3}$	$-4.27 * 10^{-3}$	$-3.67 * 10^{-3}$

Table 4.5: Implicit scattering sensitivities for the 2% enriched UF_4 sphere. SCALE/TSUANMI results are reproduced from the model supplied in [109]. Note the good comparison between the three DRAGON methods.

Figure 4.5 presents a comparison between the implicit sensitivity computed with DRAGON using the analytical approximation (red curve), the implicit sensitivities computed using DINASOUR (dotted purple curve), and implicit sensitivities computed by SCALE6/TSUNAMI-1D (blue curve). Provided in the figure is also the SCALE6/TSUNAMI-1D sensitivity collapsed from 238 groups to 172 groups (green curve). The DINASOUR sensitivities have been provided by McMaster University using our input model. DINASOUR perturbs the multi-group parameters in the WIMS library according to the Narrow Resonance Approximation (NRA). It then proceeds to compute the sensitivity by performing direct DRAGON simulations using the perturbed WIMS libraries.

From figure 4.5, we see that the largest observed differences between the sensitivity profiles are in the first few resonances. The observed differences are due to the approximation used for the fine flux as well as differences in the energy mesh used by the codes. The first few resonances of ^{238}U are wide so that the neutron energy loss from the elastic collision with ^{238}U can be effectively ignored (the neutron energy after the collision remains under the resonance). A better approximation in this range is the Wide Resonance Approximation (WRA) where the scattering cross section of the resonance isotope is ignored [20]. The analytical approximation we used (see equation 3.21) is based on the Intermediate Resonance Approximation (IRA). In the IRA, the scattering cross section of the resonant isotope is given a lower weighting in fine flux than when using the NRA (see

[9]Computing the CP matrix is the most computationally intensive part of the calculation

equation 3.21).[10] As a result, the k_{eff} sensitivity to the heavy isotope scattering cross section (in this case ^{238}U) vary based on the specific formalism used. A good example of this is the 6.7 eV resonance of ^{238}U which is wide so that the scattering cross section has little impact on the fine-flux. The SCALE 238-group energy grid is fine enough to capture this effect, as observed in figure 4.5.

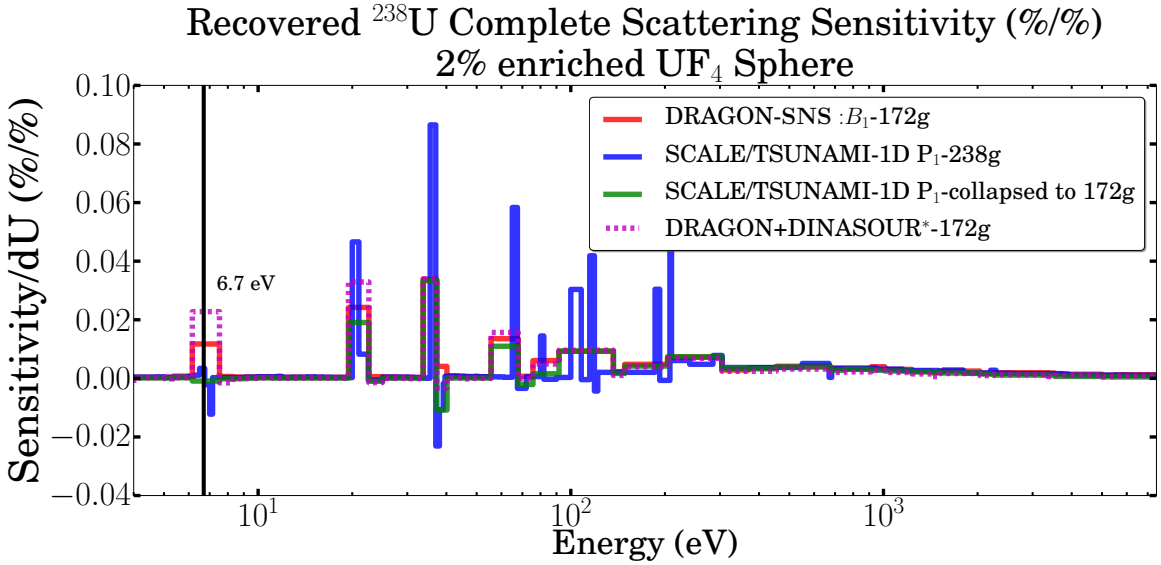

Figure 4.5: Comparison of ^{238}U implicit scattering sensitivities in the resonance region.

Note the differences in the epithermal regions between DINASOUR (NRA), DRAGON-**SNS:** (IRA), and SCALE/TSUNAMI-1D which has a fine enough energy grid thereby avoiding the IRA/NRA approximations in the first few resonances.

For the implicit scattering sensitivities presented in table 3.19, the multi-group cross section that has the highest contribution to the implicit effect is ^{238}U(n,γ). The implicit sensitivity for ^{238}U scattering is positive since an increase in the scattering cross section of ^{238}U results in neutrons being more often scattered out of the resonance thereby reducing the absorption rate.

The implicit sensitivity for the other isotopes $k \neq^{238}$U is negative. An increase in the potential scattering cross sections of isotopes $k \neq^{238}$U results in an increase in the dilution factor (the resonant isotope ^{238}U becomes more dilute). Correspondingly, the flux depression due to the resonances of ^{238}U is decreased (i.e. the flux approaches the $1/E$ asymptotic shape). The result is an overall net increase in the multi-group absorption cross section of ^{238}U, and therefore a net increase in the ^{238}U absorption rate.

For ^{1}H(n,scat), the negative component of the implicit sensitivity from the analytical model (DR-B_1) is plotted in figure 4.7 and compared with results provided from

[10] For ^{238}U, the intermediate resonance factor is reported in the WIMS libraries to have a value $\lambda = 0.2$ [38].

SCALE/TSUNAMI1-D. We note the good agreement between the two computational routes.

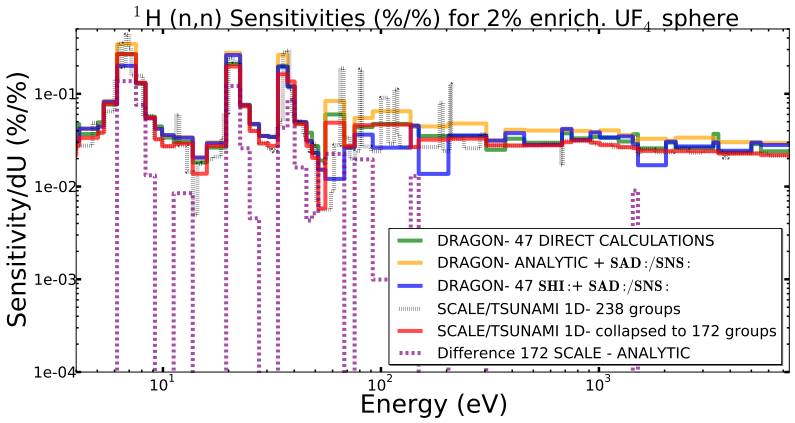

Figure 4.6: Positive component of ^{1}H elastic scattering cross section sensitivity (%/%). 47 direct simulations with DRAGON (green curve); DRAGON-**SNS:** B_1 explicit sensitivities from one **SHI:** computation and the analytical approximation (orange curve); 47 **SHI:** computations (blue curve); SCALE6/TSUNAMI 1D implicit sensitivity in 238-groups (dotted black curve);SCALE6/TSUNAMI 1D implicit sensitivity collapsed to 172-groups (red curve); difference between SCALE6/TSUNAMI-3D collapsed to 172 groups and the analytical model (dotted purple).

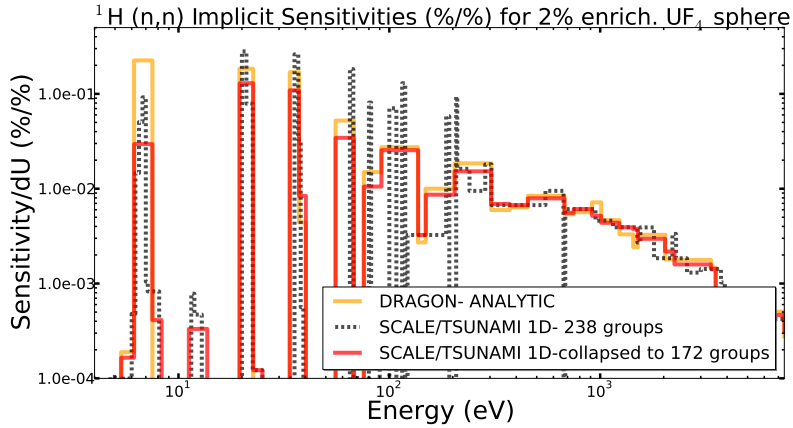

Figure 4.7: Negative component of the ^{1}H (n,scat) implicit sensitivity in the resonance region. One **SHI:** and the analytical approximation (orange curve); 238-group SCALE/TSUANMI 1D implicit sensitivity profile (black dotted); SCALE/TSUNAMI-1D implicit sensitivity collapsed to the 172 group WIMS energy grid.

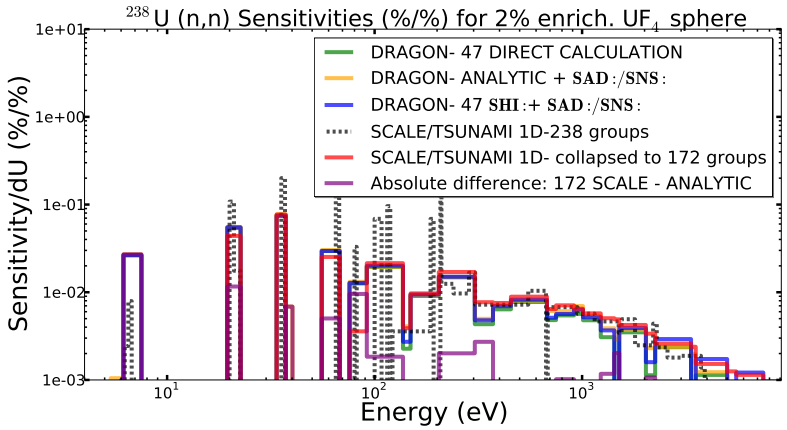

Figure 4.8: **Positive component** of ^{238}U elastic scattering cross section sensitivity (%/%) in the resonance region. 47 direct computations w/ DRAGON (green curve); one **SHI:** computation along with the analytical approximation 3.19 and 3.20 and **SNS:** (orange curve); 47 **SHI:** and equation 3.20 with **SNS:** (blue curve); SCALE/TSUNAMI-1D implicit sensitivity in 238 groups (dotted black curve); SCALE/TSUNAMI-1D implicit sensitivity collapsed to 172 groups (red curve); Difference between the SCALE/TSUNAMI-1D implicit sensitivity collapsed to 172 groups and the analytical model.

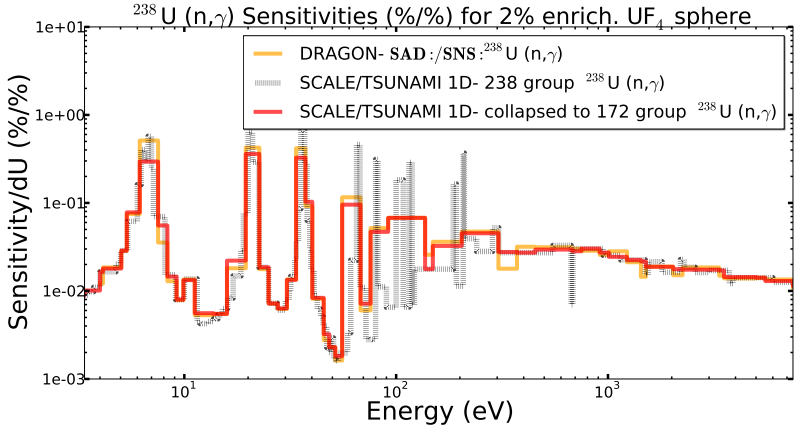

Figure 4.9: **Negative** component of the ^{238} (n,γ) **explicit** sensitivity profiles (%/%) in the resonance region. 172 group DRAGON **SNS:** capture sensitivity profile (orange line); 238 SCALE/TSUNAMI 1D **SNS:** capture sensitivity profile (dotted black); SCALE/TSUNAMI 1D capture sensitivity collapsed to the 172 group WIMS energy grid.

4.1.3 Uncertainty Propagation

Table 4.6 presents the ^{238}U cross section uncertainty contributions obtained from the DRAGON **SNS:** explicit sensitivities. Also provided in the table are reference results computed by SCALE/TSUNAMI-1D. The nuclear data uncertainty source we use in this section is the 44-group covariance matrices released with the SCALE 6 library and processed by ANGELO to the WIMS 172-group energy grid. The first two columns appearing in the table report (in %/%) the DR-B_1 and S6-P_1 integrated explicit sensitivities. The second two columns report the contribution to the k_{eff} uncertainty (in pcm) from the specified reaction pair.

From table 4.6, we observe that despite the small sensitivity of ^{238}U(n,inel), its k_{eff} uncertainty contribution is greater than 50% of the total k_{eff} uncertainty from ^{238}U nuclear data uncertainties. We also observe the negative correlation reported between (n,el)-(n,inel), that accounts for more than half of the (n,inel)-(n,inel) uncertainty. Both of these points highlight the importance of an accurate computation of scattering sensitivities. A DR-K approach predicts ^{238}U(n,inel)-(n,inel) k_{eff}-uncertainty contribution to be 45 pcm. This value is lower by a factor of 5 from the 254 pcm uncertainty contribution which is predicted by SCALE/TSUNAMI-1D and the 243 pcm uncertainty contribution computed by the DR-B_1 approach. The DR-K approach also ignores the contribution from ^{238}U(n,el) and the correlation between ^{238}U(n,el)-(n,inel). However, the total uncertainty computed by the DR-K approach leads to 414 pcm which is very close to the TSUNAMI-1D P_1 predicted value of 460pcm. The reason for this is that the capture cross section is the largest contributor to the uncertainty, which the DR-K approach computes accurately.

The k_{eff} uncertainty contributions from the ^{235}U nuclear data uncertainties are presented in table 4.7. The dominant contributor is the $\bar{\nu}$ uncertainties which have a large contribution given their high sensitivities (sum of all the $\bar{\nu}$ sensitivities should equal to unity). The uncertainties obtained by using the DR-B_1 explicit sensitivities are in good agreement with the SCALE6/TSUNAMI-1D results (S6-P_1).

Uncertainty contributions for ^{1}H and ^{19}F obtained from the explicit sensitivities computed by DR-B_1 and the uncertainties predicted by TSUNAMI-1D are presented in tables 4.8 and 4.9. Since the computed sensitivities were in good agreement, the computed uncertainties are identical. For ^{19}F, we have divided the (n,el) and (n,inel) sensitivities using the partial reaction law that we used for heavy isotope scattering. While in this case, this approach seems to lead to comparable values with S6-P_1, it is not recommended for use with non-heavy isotopes such as ^{12}C and ^{19}F.

When computing the k_{eff} uncertainty contribution from ^{12}C and ^{19}F scattering reactions, neither the chain-rule nor our approximation of no out-group elastic scattering (see equation 3.66) is valid. Therefore we cannot compute the uncertainty contribution from these isotopes. We note that in thermal systems, the uncertainty contribution from the isotopes of medium range atomic masses is usually lower than the contribution from heavy isotopes.

^{238}U Nuclear Data		Comparison of ^{238}U k_{eff} Sensitivity and Uncertainties			
		Sensitivity (%/%)		Uncertainty (pcm)	
REACTION	REACTION	DRAGON **SNS:**	SCALE / TSUNAMI 1D-P1	DRAGON **SNS:**	SCALE / TSUNAMI 1D-P1
(n,capture)	(n,capture)	$-3.3 * 10^{-1}$	$-3.04 * 10^{-1}$	435	408
(n,inel)	(n,inel)	$1.4 * 10^{-2}$	$1.4 * 10^{-2}$	254	243
(n,el)	(n,inel)	-	-	-138	-138
$\bar{\nu}$	$\bar{\nu}$	$5.0 * 10^{-2}$	$5.1 * 10^{-2}$	59	59
(n,el)	(n,el)	$1.6 * 10^{-2}$	$1.3 * 10^{-2}$	41	42
(n,f)	(n,f)	$3.4 * 10^{-2}$	$3.4 * 10^{-2}$	18	18
(n,el)	(n,capture)	-	-	-18	-16
(n,f)	(n,capture)	-	-	2	3
(n,el)	(n,f)	-	-	-2	-2
(n,2n)	(n,2n)	-	$1.042 * 10^{-3}$	-	1
Total Uncertainty Contribution (in pcm)				**490**	**460**

Table 4.6: Comparison of the computed uncertainty contributions, (in pcm), due to ^{238}U cross section uncertainties for the 2% enriched UF_4 sphere. DRAGON computations are obtained using a B_1 homogeneous leakage model. Note that explicit sensitivities are presented. The nuclear data uncertainty source used are the SCALE 6 Covariances.

^{235}U Nuclear Data		Comparison of ^{235}U k_{eff} Sensitivity and Uncertainties			
		Sensitivity (%/%)		Uncertainty (pcm)	
REACTION	REACTION	DRAGON **SNS:**	SCALE / TSUNAMI 1D-P1	DRAGON **SNS:**	SCALE / TSUNAMI 1D-P1
$\bar{\nu}$	$\bar{\nu}$	$9.5 * 10^{-1}$	$9.5 * 10^{-1}$	285	285
(n,capture)	(n,capture)	$-1.1 * 10^{-1}$	$-1.12 * 10^{-1}$	160	159
(n,f)	(n,capture)	-	-	124	124
(n,f)	(n,f)	$3.6 * 10^{-1}$	$3.66 * 10^{-1}$	122	122
(n,el)	(n,capture)	-	-	5	5
(n,el)	(n,f)	-	-	-4	-4
(n,inel)	(n,inel)	$2.3 * 10^{-4}$	$2.42 * 10^{-4}$	1	2
(n,el)	(n,inel)	-	-	-1	-1
(n,el)	(n,el)	$2.9 * 10^{-4}$	$3.0 * 10^{-4}$	1	1
Total Uncertainty Contribution (in pcm)				**370**	**369**

Table 4.7: Comparison of the computed uncertainty contributions, (in pcm), due to ^{235}U cross section uncertainties for the 2% enriched UF_4 sphere. DRAGON computations are obtained using a B_1 homogeneous leakage model. Note that explicit sensitivities are presented. The nuclear data uncertainty source used are the SCALE 6 Covariances.

^{1}H Nuclear Data		Comparison of ^{1}H k_{eff} Sensitivity and Uncertainties			
		Sensitivity (%/%)		Uncertainty (pcm)	
REACTION	REACTION	DRAGON **SNS:**	SCALE / TSUNAMI 1D-P1	DRAGON **SNS:**	SCALE / TSUNAMI 1D-P1
(n,el)	(n,el)	$3.8 * 10^{-1}$	$3.8 * 10^{-1}$	133	133
(n,capture)	(n,capture)	$-1.0 * 10^{-1}$	$-1.0 * 10^{-1}$	5	5
Total Uncertainty Contribution (in pcm)				**143**	**141**

Table 4.8: Uncertainties in (in pcm) due to ^{1}H cross section uncertainties for the 2% enriched UF_4 sphere. DRAGON computations are obtained using a B_1 homogeneous leakage model. Note that explicit sensitivities are presented. The nuclear data uncertainty source used are the SCALE 6 Covariances. Note the good comparison between the DR-B_1 and S6-P_1 computed uncertainty contributions.

^{19}F Nuclear Data		Comparison of ^{19}F k_{eff} Sensitivity and Uncertainties			
		Sensitivity (%/%)		Uncertainty (pcm)	
REACTION	REACTION	DRAGON **SNS:**	SCALE / TSUNAMI 1D-P1	DRAGON **SNS:**	SCALE / TSUNAMI 1D-P1
(n,el)	(n,el)	$3.12 * 10^{-2}$	$3.76 * 10^{-2}$	120	151
(n,inel)	(n,inel)	$2.5 * 10^{-2}$	$1.76 * 10^{-2}$	151	123
(n,el)	(n,inel)	-	-	-95	-128
(n,α)	(n,α)	$-2.81 * 10^{-3}$	$-2.81 * 10^{-3}$	192	189
Total Uncertainty Contribution (in pcm)				**215**	**198**

Table 4.9: Uncertainties in (in pcm) due to ^{19}F cross section uncertainties for the 2% enriched UF_4 sphere. DRAGON computations are obtained using a B_1 homogeneous leakage model. Note that explicit sensitivities are presented. The nuclear data uncertainty source used are the SCALE 6 Covariances. The uncertainty has been computed by applying the approximation introduced for heavy isotopes (no energy loss accompanied from elastic scattering). **This approximation should not be applied to non-heavy nuclides such as ^{19}F.**

Comparison of Approximations for Computing Heavy Isotope Scattering Cross Section Uncertainties

One of the primary efforts made by developers performing nuclear data uncertainty propagation is incorporating the currently available covariance data to their specific code. For users of the WIMS libraries, the main issue is the difference in definition that exists between the cross sections provided in the WIMS libraries in terms of which the sensitivities are computed by codes such as DRAGON, CASMO-4, or DINASOUR, and the partial cross section data in terms of which covariance matrices, coming from experiences and evaluations, are currently available (see section 3.3). We provided an example of our solution to this problem for reflected pin-cells in chapter 3. We have also seen in this section that, for ^{238}U, the contribution from the elastic and inelastic reactions is important to the overall uncertainty.

In section 3.3.4, we provided a comparison between our approximation for computing the scattering sensitivity & uncertainty and the chain-rule approximation. For example, we showed in chapter 3 that, in reflected lattices, the small pitch length and the reflective boundary conditions promote flux isotropy. In this case the sensitivity of ^{238}U(n,el) is negligible and the uncertainty can be computed by simply assigning the obtained scattering sensitivity as the sensitivity of ^{238}U(n,inel). This was the approximation that we used for reflected pin-cells in section 3.3.3.

In table 4.6, when reporting the ^{238}U uncertainty contributions, we observed that the ^{238}U(n,el) scattering cross section can have a non-negligible contribution to the overall uncertainty by its anti-correlation with the ^{238}U(n,inel). Since current codes such as CASMO-4 and DINASOUR, that use the WIMS libraries cannot capture this effect properly, we decided to quantify the errors in the computed scattering uncertainty contribution that are associated from the use of these codes.

To perform this computation, we mimic the sensitivity and uncertainty results that would be computed from codes such as DINASOUR or CASMO-4; we do this by applying the chain rule to the DR-B_1 lumped/total scattering sensitivity. Note that we do not use the code CASMO-4 or DINASOUR to perform this computation. However, we can assume that if the mentioned codes are capable of computing accurately the ^{238}U(n,SCAT) sensitivity (lumped scattering sensitivity), then they will arrive at the partial sensitivities ^{238}U(n,el) and ^{238}U(n,inel) similar to what we present here.

McMaster University has provided us with sensitivities for ^{238}U(n,el) and ^{238}U(n,inel), as computed by their code DINASOUR from our input model. Figure 4.10 presents the sensitivity profile for the lumped scattering reaction as computed by SCALE/TSUNAMI-1D (black curve), DR-B_1 (orange curve) and the code DINASOUR (blue curve). Given the direct perturbation/simulation nature of the code, the results obtained by DINASOUR can be considered as exact to the limit of a k_{eff} sensitivity computation with DRAGON.[11] Note the good agreement between the sensitivity profiles computed by all

[11]Note that the question of precision is always a limiting factor in direct perturbation methods. For example, sensitivity computations for reactivity worths of small samples are difficult without using an

three codes.

Next, in figure 4.11 and 4.12, we present the k_{eff} sensitivity to ^{238}U(n,inel) and ^{238}U(n,el) as computed by applying our approximation of heavy isotope diagonal scattering matrix (orange curve) and the chain-rule approximation (dotted red curve). We note the agreement of our predicted sensitivities with those from DINASOUR for both reactions when applying the chain-rule to the scattering sensitivity. We also observe that, for both reactions, the sensitivity profiles computed in this way are very different, with the chain-rule approach underestimating the (n,inel) sensitivity and overestimating the ^{238}U(n,el) sensitivity.

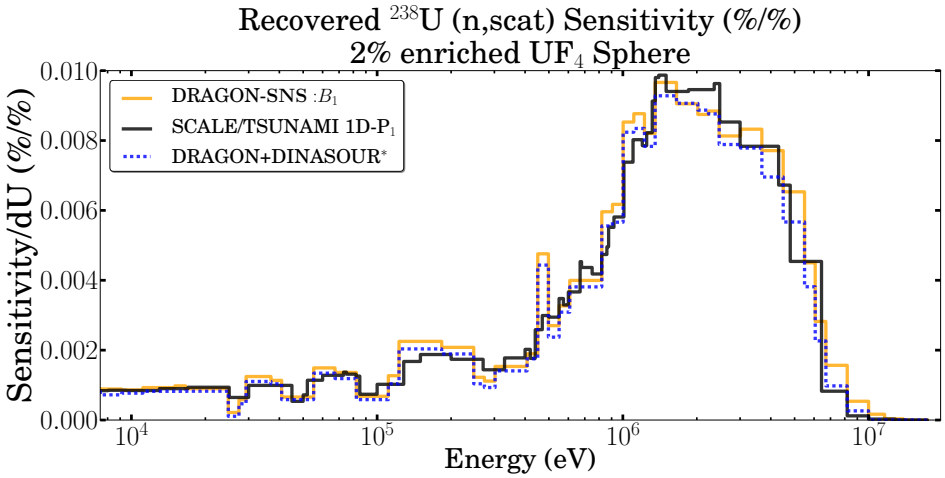

Figure 4.10: Comparison of the k_{eff} sensitivity profiles for the ^{238}U lumped scattering reaction. DRAGON-**SNS:** B_1 solution obtained using the ENDF B/VI (orange curve). SCALE/TSUNAMI-1D P_1 solution obtained using the ENDF B/VI evaluation (black curve). DRAGON+DINASOUR* results supplied by McMaster University using our input model and ENDF B/VII evaluation (blue dotted curve). Note the good comparison between all three computational schemes.

exact perturbation approach.

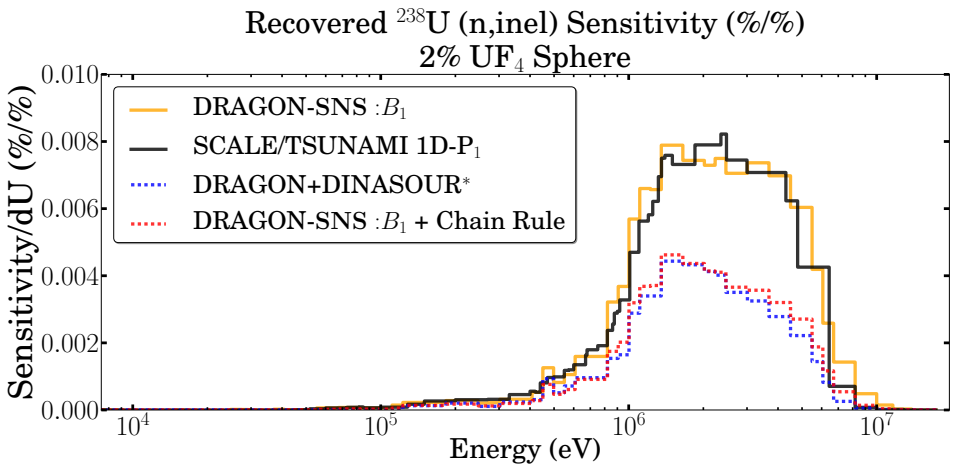

Figure 4.11: Comparison of the k_{eff} ^{238}U (n,inel) sensitivity profiles for the UF_4 sphere. DRAGON-**SNS:** B_1 solution obtained using the ENDF B/VI (orange curve). SCALE/TSUNAMI-1D P_1 solution obtained using the ENDF B/VI evaluation (black curve). DRAGON+DINASOUR* results supplied by McMaster University using our input model and ENDF B/VII evaluation(dotted blue curve). DRAGON-**SNS:** B_1+ Chain rule obtained by applying the chain rule to the **SNS:** computed sensitivity (dotted black curve). Note the good comparison between DRAGON-**SNS:** B_1 with the reference solution SCALE/TSUNAMI-1D P_1 and the poorly computed sensitivity resulting from applying the chain rule.

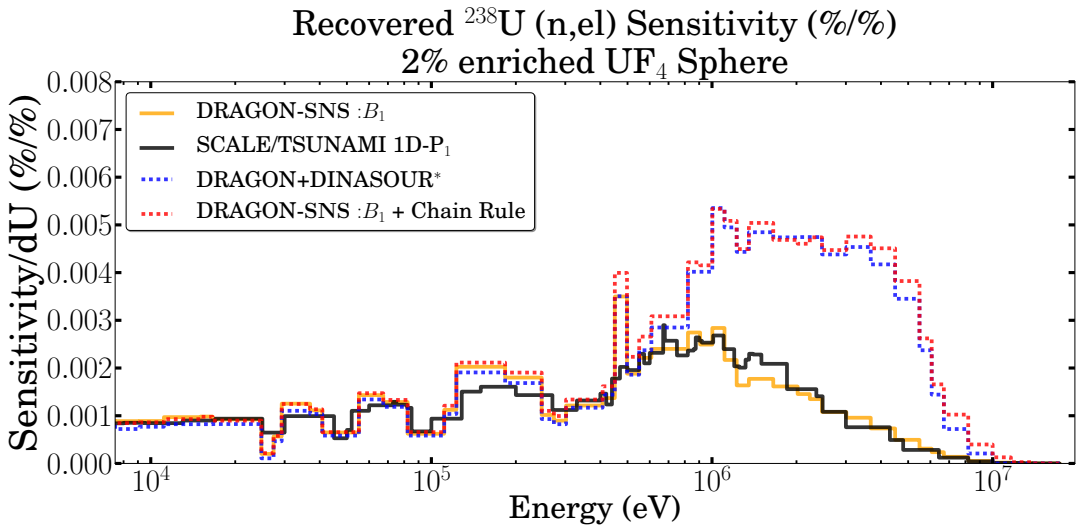

Figure 4.12: Comparison of the k_{eff} ^{238}U (n,el) sensitivity profiles for the UF_4 sphere. DRAGON-**SNS:** B_1 solution obtained using the ENDF B/VI (orange curve). SCALE/TSUNAMI-1D P_1 solution obtained using the ENDF B/VI evaluation (black curve). DRAGON+DINASOUR* results supplied by McMaster University using our input model and ENDF B/VII evaluation (dotted blue curve). DRAGON-**SNS:** B_1+ Chain rule obtained by applying the chain rule to the **SNS:** computed sensitivity (dotted red curve). Note the good comparison between DRAGON-**SNS:** B_1 with the reference solution SCALE/TSUNAMI-1D P_1 and the poorly computed sensitivity resulting from applying the chain rule.

Table 4.10 presents comparison for the retrieved partial ^{238}U(n,el) and ^{238}U(n,inel) cross section sensitivities and their uncertainty contributions computed by applying three various approximations to the DR-B_1 sensitivities, as well as sensitivities and uncertainty contributions reported by SCALE/TSUNAMI-1D. The columns appearing in the table are as follows:

- SCALE: this column presents results obtained using SCALE/TSUNAMI-1D with the P_1 approximation.
- A.1: This column partial cross section sensitivities/uncertainties retrieved from the DR-B_1 **SNS:** explicit sensitivities using the approximation introduced in this work (see equations 3.66 and 3.70-3.71).
- A.2: This column presents partial cross section sensitivities/uncertainties obtained using our approximation introduced in section 3.3.3 for reflected pin-cells which consists of assigning the lumped scattering sensitivity in the fast energy range as the sensitivity to the inelastic cross section.
- A.3: This column presents our results obtained by applying the chain rule to the lumped scattering cross section (see equations 3.67-3.68). It reports the sensitivity & uncertainty that would be predicted by codes such as CASMO-4 and DINASOUR [55, 56, 54].

^{238}**U**	k_{eff} Sensitivity (%)				k_{eff} uncertainty (pcm)			
Reaction	SCALE$^{\diamond}$	A.1*	A.2†	A.3‡	SCALE$^{\diamond}$	A.1*	A.2†	A.3‡
el-el	$1.26 * 10^{-2}$	$1.56 * 10^{-2}$	$5.72 * 10^{-3}$	$2.16 * 10^{-2}$	42	41	4	128
inel-inel	$1.42 * 10^{-2}$	$1.38 * 10^{-2}$	$2.90 * 10^{-2}$	$7.8 * 10^{-3}$	243	254	310	133
el-inel	-	-	-	-	-138	-138	0	-183
^{238}U (n,scat) TOTAL Uncertainty (pcm)					204	217	310	24

Table 4.10: Comparison of various approximations for retrieving partial cross section sensitivities.
SCALE$^{\diamond}$: Results from SCALE/TSUNAMI-1D P1 (S6-P_1).
A.1*: Approximation used in this work and given by equation 3.70 and 3.71 (DR-B_1).
A.2†: Approximation used in this work for application to *reflected* pin-cells.
A.3‡: Approximation used by CASMO-4 [55] and DINASOUR [54] of applying the chain-rule to the scattering cross section. All DRAGON computations have been performed using the DR-B_1 sensitivities (A.1, A.2, and A.3).

Comparing the values provided in table 4.10, we observe the following points:

- A.2: Assigning the scattering sensitivity at high energies as the sensitivity of inelastic scattering results in an over-estimation of the k_{eff} uncertainty by 22% of the DR-B_1 uncertainty contribution (reported in A.1) and 27% of the reference S6-P_1 uncertainty contribution. More importantly, since the elastic cross section is set to zero within this range, the approximation will miss the contribution from the anti-correlation between the two reactions, which has a value larger than 50% of the uncertainty contribution coming from the inelastic cross section. As a result, this approximation overestimates the total contribution of scattering reactions to the k_{eff} uncertainty by 43% of our computed value, and 52% of the value computed by the reference code SCALE/TSUNAMI-1D.

- A.3: Application of the chain rule to the scattering sensitivity results in an over estimation of the elastic sensitivity by 38% of the elastic sensitivity reported by A.1 (DR-B_1) and 71% of the elastic sensitivity computed by S6-P_1. As a result, the chain rule approximation over estimates the contribution from the elastic cross section by some 212% of the DR-B_1 value (A.1) and the S6-P_1 value (SCALE). The approximation also underestimates the inelastic component of the sensitivity by 43% of the DR-B_1 value (A.1) and 45% of the sensitivity computed by SCALE/TSUNAMI-1D. This results in an underestimation of the inelastic contribution to the uncertainty. The uncertainty contribution is over-estimated by 47% of the DR-B_1 computed contribution (A.1) 45% of the S6-P_1 computed contribution. Similarly, since the sensitivities for the ^{238}U(n,el) and ^{238}U(n,inel) reactions differ greatly, the contribution from the anti-correlation between the elastic and inelastic is also over estimated by some 32% of the DR-B_1 or S6-P_1 values. As a result of these differences, the resultant contribution from ^{238}U scattering reactions to the k_{eff} uncertainty is underestimated by approximately one order of magnitude.

Uncertainty Analysis with Lumped Covariances

In [56], Pusa attempts to avoid the intermediate step of computing partial cross section sensitivities by constructing covariance matrices which correspond to the lumped/total scattering cross section defined in the WIMS libraries. As the application is equivalent to assuming that the chain rule applies to the total/lumped scattering cross section, the results obtained by CASMO-4 are not comparable with the computed sensitivities by SCALE/TSUNAMI-2D. The conclusion then reached in [56] is that "it is not possible to perform S&U analysis with respect to the total scattering cross-section in a manner that would produce results consistent with the approach where sensitivities are computed with respect to individual scattering reactions."

We think that it could serve of benefit to provide results using lumped scattering covariance matrices. Here, the key point when constructing the lumped scattering matrix is that the covariance as well as the correlation between the lumped scattering reaction and inelastic scattering should be computed and stored (see equation 3.72).

Table 4.11 presents the uncertainty contribution from the lumped covariance matrices we have constructed. The values appearing in the table are in percent contribution to the total variance with the absolute contribution to the variance reported in the parenthesis. We see that the obtained scattering uncertainty is identical to the approach where partial cross sections are used (217 pcm in table 4.10). While the computed contribution from the scattering cross section uncertainty using this methodology is as accurate as our approach using partial cross sections, information regarding the origin of the uncertainties are lost. For this reason, throughout the remainder of this work, when reporting uncertainty contributions, we will use the approach of partial reactions rather than using our lumped covariance matrices.

We note the good agreement between the computed value of 217 pcm in table 4.10 and the computed value of 216 pcm in this computation. Also, note the error cancellation

between the two reactions which becomes more pronounced. After the computation of the lumped covariance matrix and its correlation with inelastic scattering, this computation will not require knowledge of the partial cross section data.

^{238}U Scattering	% Contribution to the total variance	
REACTION	LOSS (n,scat)	GAIN (n,inel)
LOSS (n,scat)	0.65 % $(2.63 * 10^{-8})$	32.52 % $(1.54 * 10^{-6})$
GAIN (n,inel)	32.52 % $(1.524 * 10^{-6})$	34.39 % $(1.61 * 10^{-6})$
	Variance	$4.69 * 10^{-6}$
	Contribution to Uncertainty (pcm)	**216**

Table 4.11: Computation of ^{238}U(n,SCAT) uncertainty contribution using lumped covariances. The reported values are % of the variance. Absolute values are reported in parenthesis. The computation has been performed using DR-B_1 sensitivities and lumped covariance matrices constructed from the ANGELO processed SCALE-6 covariances.

4.2 MOX Lattice at Critical Height

The previous benchmark provided an example where, due to competition with leakage, a large component of the scattering sensitivities was composed of the streaming term (ST). However, the spectrum was thermal so that anisotropic effects did not have a major contribution to the sensitivity. This benchmark involves the variation of the cell pitch for MOX lattices and provides a study for scattering sensitivities in configurations where scattering anisotropy is important. Since our solution with DRAGON is a CP solution[12] for the scalar flux, with transport corrected isotropic source, capturing the effect of anisotropy is difficult.

4.2.1 Benchmark Description

The geometry for this benchmark corresponds to an infinite x-y configuration of pin cells at critical heights (z-axis). The cell corresponding to the reference case can be observed in figure 4.13. The material composition is given in table 4.12. The participants are asked to provide k_{eff} sensitivity results for ten different lattice pitches. The pitch values can be observed in table 4.13. The goal of the benchmark [105] is to study the variation of the implicit sensitivity with the moderator volume, and the effect of leakage on the resultant sensitivities.

Modeling

The typical approach to model this problem with SCALE is to model the cell in 3-D. Using SCALE6/TSUNAMI-3D (S6-P_1), and the model provided in [109], for each pitch, we have varied the cell height until critical conditions are reached. The k_{eff} and critical heights computed with SCALE6/TSUNAMI-3D are reported in table 4.13.

Our approach to this problem with DRAGON has been to model the lattice in 2-D and use a heterogeneous B_1 leakage model with leakage specified in the z-axial direction (DR-B_1). The critical height can then be computed in terms of the computed buckling coefficient B_z. For instance, in the mono-energetic case, the relationship between the critical height H_z for a rectangular parallelepiped with z-axial leakage is given by [81]:

$$H_z = \sqrt{\frac{\pi^2}{B_z^2}} - 2d \tag{4.1}$$

where the factor $2d$ appearing in the above equation represents the linear extrapolation distance [81] subtracted from both sides of the lattice (hence the factor 2). The linear extrapolation distance d is related to the mono-group diffusion coefficient D as [81]:

$$d = 0.73 \cdot 3 \cdot D \tag{4.2}$$

[12]Note that this is true for all CP computations with DRAGON including the: DR-K, DR-B_0 and DR-B_1 approaches.

Here the one-group diffusion coefficient D is computed by the **EDI:** module of DRAGON [59] which uses the computed flux of the critical cell (in 172-group energy) as the weighting function to compute the diffusion coefficient D.

Table 4.13 reports the computed critical heights as a function of the cell pitch (cm) as computed from equations 4.1-4.2. The DRAGON computed buckling coefficient and diffusion cross section are also provided. We note the good comparison between the computed critical heights by two codes (10% maximum difference).

Computational Times

For this model, the computational time for computing the flux, adjoint and sensitivities with DRAGON is 10 seconds when performing the computation on a 64 bit 2.2 GHz PC. The computation time for the 3-D cell when using SCALE/TSUNAMI-3D is approximately 20 minutes (with a 0.1% statistical error on the computed sensitivities).

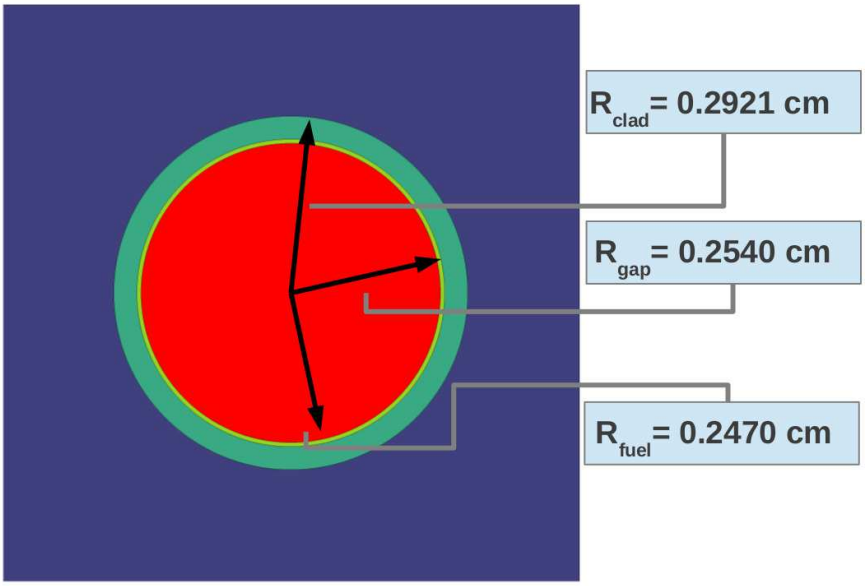

Figure 4.13: MOX lattice dimensions for the reference case (pitch=0.9525 cm).

	Isotopic Densities (atoms/barn-cm)			
Isotope	Fuel	Clad	Moderator	Void
^{238}Pu	$7.3857 * 10^{-6}$	-	-	-
^{239}Pu	$4.2019 * 10^{-3}$	-	-	-
^{240}Pu	$5.6060 * 10^{-4}$	-	-	-
^{241}Pu	$8.7523 * 10^{-5}$	-	-	-
^{242}Pu	$1.6972 * 10^{-5}$	-	-	-
^{235}U	$1.2223 * 10^{-4}$	-	-	-
^{238}U	$1.6876 * 10^{-2}$	-	-	-
^{241}Am	$3.4258 * 10^{-5}$	-	-	-
^{16}O	$4.3713 * 10^{-2}$	-	$3.3680 * 10^{-2}$	$1.0000 * 10^{-6}$
^{1}H	-	-	$6.6733 * 10^{-2}$	-
^{52}Fe	-	$5.5330 * 10^{-2}$	-	-
Cr	-	$1.4394 * 10^{-2}$	-	-
Ni	-	$1.0161 * 10^{-2}$	-	-
Mo	-	$2.1168 * 10^{-3}$	-	-
Mn	-	$1.6935 * 10^{-3}$	-	-
C	-	$6.7739 * 10^{-5}$	-	-
Si	-	$8.4673 * 10^{-4}$	-	-

Table 4.12: Atomic Densities (atoms/barn-cm) for the MOX lattice and core benchmark. Reproduced from [106].

	DRAGON			SCALE/TSUNAMI 3D P_1	
Lattice Pitch (cm)	Buckling B_z^2 (cm^{-2})	Diffusion Coefficient (cm) D	Critical Height (cm)	k_{eff}	Critical Height (cm)
0.586	$8.16 * 10^{-3}$	1.14	30	0.99144	28
0.60	$8.25 * 10^{-3}$	1.14	30	0.99476	28
0.66	$8.82 * 10^{-3}$	1.15	29	0.9975	27
0.73	$9.93 * 10^{-3}$	1.16	27	0.9968	25
0.9525*	$1.45 * 10^{-2}$	1.13	21	0.99831	20
1.05	$1.59 * 10^{-2}$	1.12	20	0.995	18
1.15	$1.69 * 10^{-2}$	1.10	20	0.968	18

Table 4.13: Pitch Variation of the MOX fuel lattice. * reference case
SCALE/TSUNAMI-3D model taken from [109]. Note that the DR-B_1 k_{eff} is 1.0 by definition of the buckling search.

4.2.2 Results

Scattering Anisotropy

Table 4.14 presents the decomposition of the ^{238}U(n,SCAT) DR-B_1 sensitivity into its components of energy GAIN/LOSS (GL), STREAMING (ST), and Transport Correction (TR). Also presented in the table is reference S6-P_1 sensitivities. First, we note that had we used the DR-K approach, we would need to model the cell in 3-D. The results from the DR-K approach would be similar in value to the contribution of the GL column (this is the only term that the DR-K approach is computing). Since we can assume that the ^{238}U(n,el) group to group matrix is diagonal, the GL term represents the importance gained from the energy loss of the neutron after the ^{238}U(n,inel) reaction. For the first two lattice pitches appearing in the table (pitch=0.586 cm and 0.60 cm), the GL component has a slightly negative sign. ^{238}U fast fission in these two geometries accounts for 10% of the total fission rate and ^{238}U(n,inel) competes with ^{238}U(n,f). With the softening of the flux that is accompanied with increasing pitch, thermal fission with ^{239}Pu increases and energy loss from ^{238}U(n,inel) scattering becomes a gain in neutron importance so that the GL component becomes positive.

We also observe that the GL term only accounts for a small part of the ^{238}U(n,SCAT) sensitivity, with the majority of the sensitivity contribution coming from the streaming term ST and scattering anisotropy TR. The DR-K approach is not able to account for these two components and would greatly underestimate the sensitivity. The column labeled as Relative Error reports (in %) the difference between the DR-B_1 computation relative to the S6-P_1 computation.

Next we note that the DR-B_1 sensitivities are slightly larger than the S6-P_1 sensitivities. The reason for this is anisotropy (approximately half of the given error) as well as differences in the computed explicit sensitivity profile in the resonance region due to differences in the energy meshing. This second source of differences has little impact in the final uncertainty given the low uncertainties of ^{238}U(n,el) reported in the resonance region. Also, the main component of the sensitivity in this region is implicit sensitivity which is discussed in the next section.

Next we observe from table 4.14 that at low pitches, where flux anisotropy is the strongest, the TR contribution to the ^{238}U(n,SCAT) sensitivity is also the highest. The largest component of the computed TR component is due to elastic scattering anisotropy.[13] Figure 4.14 presents a comparison of the transport corrected DR-B_1 ^{238}U(n,el) sensitivity profile (in green), the DR-B_1 non-transport corrected sensitivity (dotted red), and the S6-P_1 ^{238}U(n,el) sensitivity profile (in blue). We see the efficiency of the transport correction to capture the effect of anisotropy. The correction works well when the matrix is diagonal and the collision only serves to change the neutron's direction. This is the case for ^{238}U(n,el) and can be observed from the good comparison between the DR-B_1 (green) and the S6-P_1 (blue) curves.

[13] From approximately 100 keV, l-wave interaction becomes possible with the nuclei, so that elastic scattering reaction is no longer required to be isotropic in the Center of Mass frame.

However, a transport correction will not be as effective when the P_1 matrix is dense. This can be seen by comparing the obtained sensitivity expressions which account for leakage and scattering anisotropy when using the transport corrected diffusion cross section (see equations 3.47 and 3.52) with sensitivity expressions for a discrete ordinates code where angular flux moments are used in the sensitivity formulas (see for example the SUSD3D sensitivity expressions given by equation 2.17). We see that in equation 2.17, the scattering sensitivity is defined as a gain term involving the product of the flux moments, summed over the out-going group energies of the scattered neutron. The sensitivity expressions for leakage when using the transport corrected definition of the diffusion coefficient (see equations 3.47 and 3.47) account for scattering anisotropy by subtracting the transport correction from the in-group component of the scattering source, i.e. the gained importance from the energy loss of the neutron following the scattering collision is ignored. In cases where the scattering reaction does not reduce the neutron's energy (such as ^{238}U(n,el)) the transport correction works well.

Figure 4.15 presents the ^{238}U(n,inel) scattering profile for the MOX lattice at 0.586 cm pitch computed by the DR-B_1 approach (green curve) and reference S6-P_1 sensitivities (blue curve). Given the small cell pitch, the system is undermoderated. Therefore, the neutron makes several collisions before being slowed down to thermal energies. Anisotropy effects play an important role here as the neutron can exit and enter the cell several times before being absorbed. When energy loss is coupled with the inelastic scattering reaction, a transport correction will not capture the gain/loss associated with the anisotropic inelastic reaction. We believe this to be the main reason for the differences observed between the two profiles.

With the increase in moderator volume that is accompanied with increasing pitch, the average number of collisions made by the neutron also decreases. A neutron that has an inelastic interaction in the fuel, will most likely exit the fuel and enter the moderator where it can be slowed down to thermal energies and may return to the fuel where it can induce a fission. As a result, the profile for the inelastic reaction converges to the spectrum for fission neutrons (the fast neutrons available in the fuel). This can be seen from figure 4.16, where the ^{238}U(n,inel) sensitivity as computed by DR-B_1 and S6-P_1 sensitivity, for the lattice pitch=1.15 cm is presented.

^{238}**U(n,SCAT)**	Decomposition (% of DR-B_1)			DR-B_1	S6-P_1	Relative
Pitch (cm)	GL (%)	ST (%)	TR (%)	Sensitivity (%/%)	Sensitivity (%/%)	Error (%)
0.586	-5	147	-42	$4.54 * 10^{-2}$	$4.18 * 10^{-2}$	-8 %
0.6	-1	135	-35	$4.33 * 10^{-2}$	$4.02 * 10^{-2}$	-8 %
0.66	12	120	-32	$3.70 * 10^{-2}$	$3.65 * 10^{-2}$	-1 %
0.73	22	137	-25	$3.34 * 10^{-2}$	$3.33 * 10^{-2}$	0 %
0.9525	34	91	-25	$2.65 * 10^{-2}$	$2.53 * 10^{-2}$	-5 %
1.05	36	89	-25	$2.34 * 10^{-2}$	$2.22 * 10^{-2}$	-5 %
1.15	37	113	-24	$2.04 * 10^{-2}$	$1.93 * 10^{-2}$	-6 %

Table 4.14: Comparison of ^{238}U(n,SCAT) Integrated **Explicit** k_{eff} Sensitivities (%/%) as a function of lattice pitch.
DR-B_1: Integrated k_{eff} sensitivities (%/%) from DRAGON **SNS:** with a heterogeneous B_1 leakage model with z-axial leakage.
S6-P_1: Integrated k_{eff} sensitivities (%/%) from SCALE6/TSUNAMI-3D.
GL: (%) contribution of the GAIN/LOSS term to the DR-B_1 integrated sensitivity.
ST: (%) contribution of the STREAMING term to the DR-B_1 integrated sensitivity.
TR: (%) contribution of the Transport Correction term to the DR-B_1 integrated sensitivity.
Re. Err.: Relative Error (in %) between DR-B_1 and S6-P_1. Error computed relative to S6-P_1.
Note the importance of scattering anisotropy on the computed sensitivity, the importance of the streaming term (ST), and the low error reported between the two reactions.

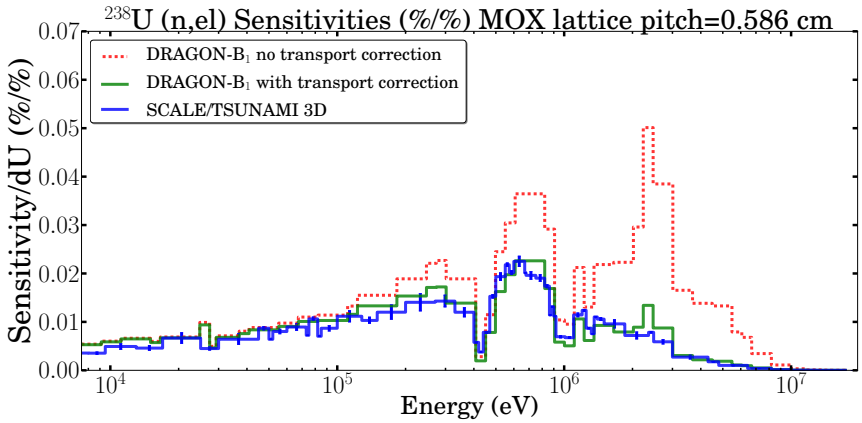

Figure 4.14: Comparison of ^{238}U (n,el) sensitivity for MOX lattice at pitch=0.586 cm.

DRAGON-B_1 **SNS:** with no transport correction (dotted red). DRAGON B_1 (DR-B_1) with transport correction (green). SCALE6/TSUNAMI-3D P_1 (S6-P_1) sensitivities. (in blue).
Note the negative effect of the transport correction on the scattering sensitivity and the efficiency of the transport correction when applied to ^{238}U (n,el).

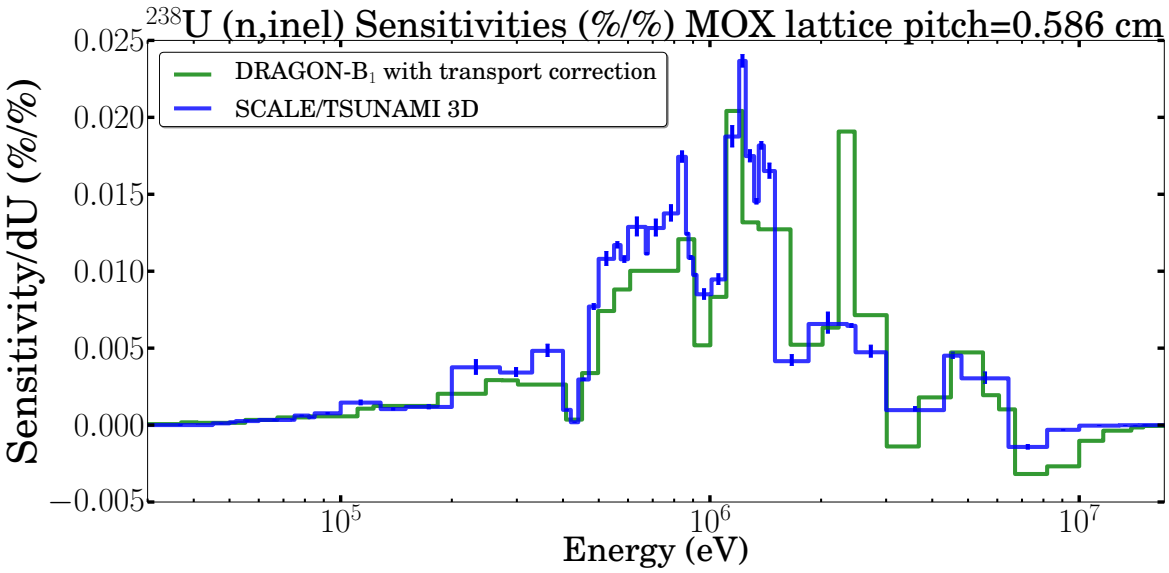

Figure 4.15: Comparison of ^{238}U (n,inel) sensitivity for MOX lattice at pitch=0.586 cm.

DRAGON B_1 with transport correction (green). SCALE6/TSUNAMI-3D P_1 (blue).
Note the differences between the two profiles due to the non-diagonal form of the ^{238}U(n,inel) P_1 matrix which a transport correction cannot capture, and flux anisotropy.

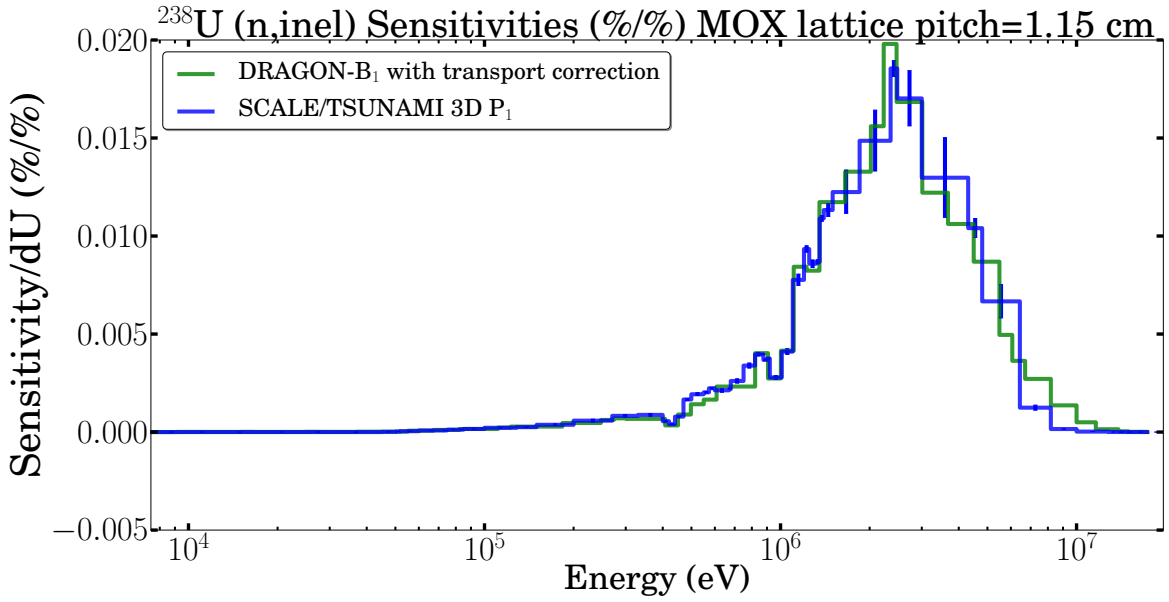

Figure 4.16: Comparison of ^{238}U (n,inel) sensitivity for MOX lattice at pitch=1.15 cm.

DRAGON B_1: DR-B_1 (green). SCALE6/TSUNAMI-3D: S6-P_1 (blue).
Note the good agreement between the two profiles in the absence of anisotropic interactions in the fuel.

The effect observed for ^{238}U(n,inel) anisotropy can also be observed for the sensitivities of ^{16}O(n,SCAT) in the moderator and ^{1}H(n,el). Tables 4.15 and 4.16 report the decompositions of the DR-B_1 scattering sensitivities as well as reference S6-P_1 results. We first observe that both of these reactions have a large component of the scattering sensitivity composed of the importance gained from the neutron's loss of energy following the scattering interaction. This component to the sensitivity is presented in the GL (in % of the DR-B_1 sensitivity). Anisotropy for these reactions is also important as observed from the TR column in the table accounting for the negative contribution of the transport correction. However, neglected in the TR column is the importance gained following the neutron's loss in energy after the (anisotropic) scattering reaction.[14] Given that the ^{16}O(n,SCAT) P_1 matrix is dense, we can expect the GL term associated with this component would be of the same order (though smaller given the forward direction of scattering) as the GL term for the DR-B_1 sensitivity reported in table 4.16. However, we cannot compute GL component for the anisotropic scattering component of the sensitivity as angular fluxes are not computed by DRAGON. We believe this partly explains the observed difference in the Relative Error column. We also believe that in this case, the $\mathbf{dB^2}$ approximation may not be accurate enough to capture effects of anisotropy. With light isotopes, the trend seems to be that whenever anisotropy is high (or the contribution from the transport correction is high), the agreement between the two codes is reduced. For ^{1}H (see table 4.16), although the same error exists from using the transport correction and the buckling approximation, the GL component from the scalar flux is dominant (larger than TR by a factor of 2). This is why the computed relative differences are lower than for ^{16}O(n,SCAT) in the moderator. To verify this point and track down the exact source of error, would require a direct perturbation approach with a 3-D DRAGON lattice. Given the lower contribution to the k_{eff} uncertainty from these reactions, we have not yet performed this computation.[15]

The sensitivity profiles for ^{16}O(n,SCAT) and ^{1}H(n,el) in the moderator computed by DR-B_1 and S6-P_1 are presented in figures 4.17 and 4.19. For ^{16}O in the moderator, we observe from figure 4.17 that the two profiles are not comparable at high energies, with the DR-B_1 approach underestimating the sensitivity. We cannot currently comment on the comparison between the ^{1}H profiles.[16]

Table 4.17 reports the decomposition of the DR-B_1 sensitivity for ^{16}O in the fuel. We note that anisotropic scattering interactions are not observed to have a large effect in the fuel, with the largest component of the sensitivity being leakage term (ST). The ^{16}O(n,SCAT) profiles for ^{16}O in the fuel are plotted in figure 4.18. Observed is the relatively poor comparison at 430 keV. This can be related to the fact that the P_1 coefficient of the ^{16}O scattering cross section (which has a large resonance at this energy) changes signs as a function of the scattering angle at 430 eV. This effect cannot be captured with a transport correction.[17]

[14] Note that for these two isotopes, the anisotropy is in the Laboratory Frame.

[15] The difference between our computed ^{16}O scattering uncertainty contribution with the S6-P_1 approach is approximately 80 pcm.

[16] Note that the statistical error is being reported by S6-P_1 as 0.1%

[17] Correspondence with Dr. G. Rimpault.

^{16}**O(n,SCAT) in H_2O**	Decomposition (% of DR-B_1)			DR-B_1	S6-P_1	Relative Error (%)
Pitch (cm)	GL (%)	ST (%)	TR (%)	Sensitivity (%/%)	Sensitivity (%/%)	
0.586	73	90	-63	$6.34 * 10^{-3}$	$1.57 * 10^{-2}$	60 %
0.6	74	88	-61	$7.28 * 10^{-3}$	$1.76 * 10^{-2}$	59 %
0.66	76	78	-54	$1.11 * 10^{-2}$	$2.57 * 10^{-2}$	57 %
0.73	77	71	-48	$1.54 * 10^{-2}$	$3.44 * 10^{-2}$	55 %
0.9525	79	61	-40	$2.72 * 10^{-2}$	$5.64 * 10^{-2}$	52 %
1.05	78	60	-39	$3.02 * 10^{-2}$	$6.33 * 10^{-2}$	52 %
1.15	78	60	-38	$3.23 * 10^{-2}$	$6.80 * 10^{-2}$	53 %

Table 4.15: Comparison of ^{16}O(n,SCAT) in H_2O: Integrated **Explicit** k_{eff} Sensitivities (%/%) as a function of lattice pitch.
DR-B_1: Integrated k_{eff} sensitivities (%/%) from DRAGON **SNS:** with a heterogeneous B_1 leakage model with z-axial leakage.
S6-P_1: Integrated k_{eff} sensitivities (%/%) from SCALE6/TSUNAMI-3D.
GL: (%) contribution of the GAIN/LOSS term to the DR-B_1 integrated sensitivity.
ST: (%) contribution of the STREAMING term to the DR-B_1 integrated sensitivity.
TR: (%) contribution of the Transport Correction term to the DR-B_1 integrated sensitivity.
Relative Error (in %) between DR-B_1 and S6-P_1 is computed relative to S6-P_1.

^{1}**H(n,el)**	Decomposition (% of DR-B_1)			DR-B_1	S6-P_1	Relative Error (%)
Pitch (cm)	GL (%)	ST (%)	TR (%)	Sensitivity (%/%)	Sensitivity (%/%)	
0.586	161	12	-72	$9.61 * 10^{-2}$	$1.27 * 10^{-1}$	24 %
0.6	158	11	-69	$1.13 * 10^{-1}$	$1.42 * 10^{-1}$	21 %
0.66	146	9	-56	$1.89 * 10^{-1}$	$2.27 * 10^{-1}$	17 %
0.73	142	8	-50	$2.70 * 10^{-1}$	$3.16 * 10^{-1}$	15 %
0.9525	146	8	-54	$4.21 * 10^{-1}$	$4.83 * 10^{-1}$	13 %
1.05	149	9	-57	$4.44 * 10^{-1}$	$5.13 * 10^{-1}$	13 %
1.15	151	9	-60	$4.61 * 10^{-1}$	$5.05 * 10^{-1}$	9 %

Table 4.16: Comparison of ^{1}H(n,el) Integrated **Explicit** k_{eff} Sensitivities (%/%) as a function of lattice pitch. DR-B_1: Integrated k_{eff} sensitivities (%/%) from DRAGON **SNS:** with a heterogeneous B_1 leakage model with z-axial leakage.
S6-P_1: Integrated k_{eff} sensitivities (%/%) from SCALE6/TSUNAMI-3D.
GL: (%) contribution of the GAIN/LOSS term to the DR-B_1 integrated sensitivity.
ST: (%) contribution of the STREAMING term to the DR-B_1 integrated sensitivity.
TR: (%) contribution of the Transport Correction term to the DR-B_1 integrated sensitivity.
Relative Error: Relative Error (in %) between DR-B_1 and S6-P_1. Error computed relative to S6-P_1.

^{16}O(n,SCAT) in Fuel	Decomposition (% of DR-B_1)			DR-B_1	S6-P_1	Relative Error (%)
Pitch (cm)	GL (%)	ST (%)	TR (%)	Sensitivity (%/%)	Sensitivity (%/%)	
0.586	17	98	-15	$5.43 * 10^{-2}$	$5.00 * 10^{-2}$	-9 %
0.6	18	97	-15	$4.99 * 10^{-2}$	$4.55 * 10^{-2}$	-10 %
0.66	20	95	-15	$3.79 * 10^{-2}$	$3.55 * 10^{-2}$	-7 %
0.73	23	92	-15	$3.12 * 10^{-2}$	$2.94 * 10^{-2}$	-6 %
0.9525	27	87	-15	$2.22 * 10^{-2}$	$2.00 * 10^{-2}$	-11 %
1.05	28	86	-15	$1.93 * 10^{-2}$	$1.71 * 10^{-2}$	-13 %
1.15	29	86	-15	$1.67 * 10^{-2}$	$1.46 * 10^{-2}$	-14 %

Table 4.17: Comparison of ^{16}O(n,SCAT) in the fuel: Integrated **Explicit** k_{eff} Sensitivities (%/%) as a function of lattice pitch.
DR-B_1: Integrated k_{eff} sensitivities (%/%) from DRAGON **SNS:** with a heterogeneous B_1 leakage model with z-axial leakage.
S6-P_1: Integrated k_{eff} sensitivities (%/%) from SCALE6/TSUNAMI-3D.
GL: (%) contribution of the GAIN/LOSS term to the DR-B_1 integrated sensitivity.
ST: (%) contribution of the STREAMING term to the DR-B_1 integrated sensitivity.
TR: (%) contribution of the Transport Correction term to the DR-B_1 integrated sensitivity.
Relative Error: Relative Error (in %) between DR-B_1 and S6-P_1. Error computed relative to S6-P_1.

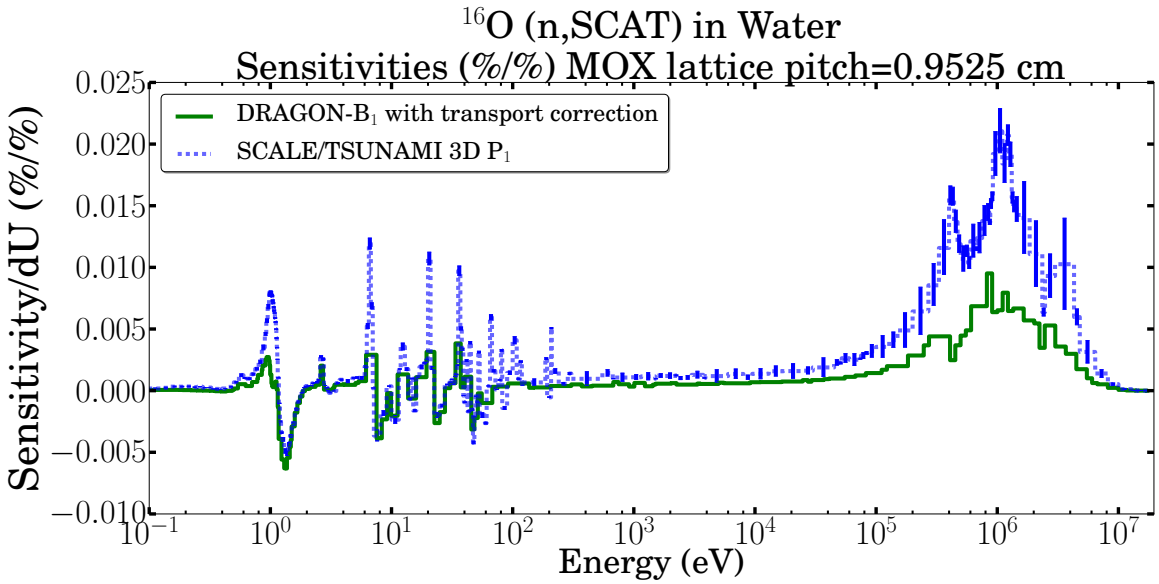

Figure 4.17: Comparison of ^{16}O(n,scat) in H_2O sensitivity profiles for MOX lattice at pitch=0.9525 cm. DRAGON B_1 with transport correction sensitivity profile (green). SCALE6/TSUNAMI-3D P_1 sensitivity profile (blue). Note the poor comparison between the two profiles arising from anisotropic effects.

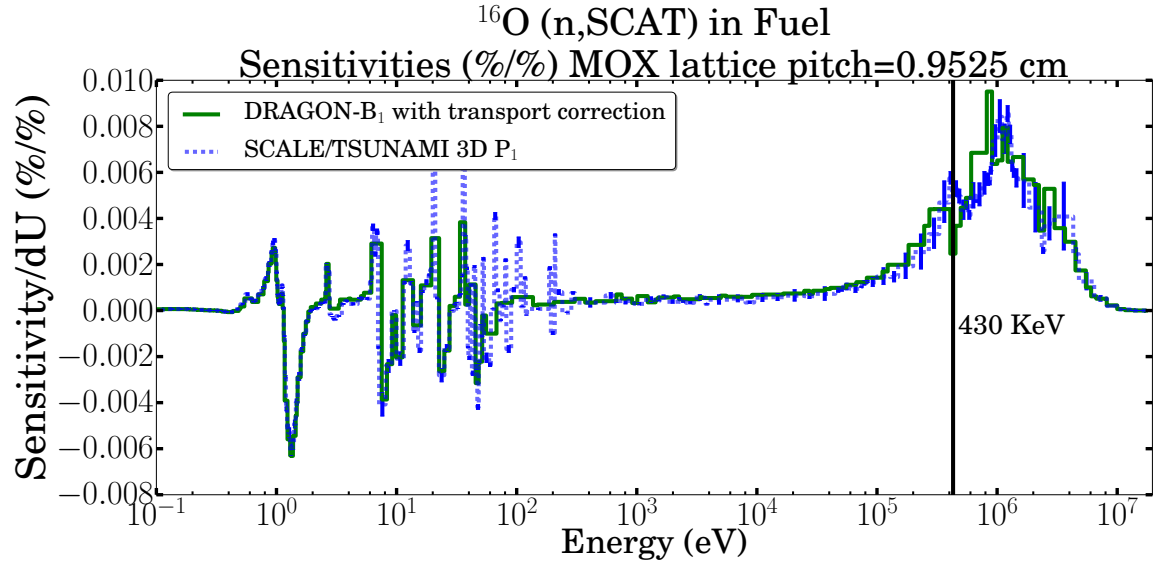

Figure 4.18: Comparison of ^{16}O(n,scat) in the fuel sensitivity profile for MOX lattice at pitch=0.9525 cm. DRAGON B_1 with transport correction (green). SCALE6/TSUNAMI-3D P_1 (blue). Note the effect of the resonance at 430 keV.

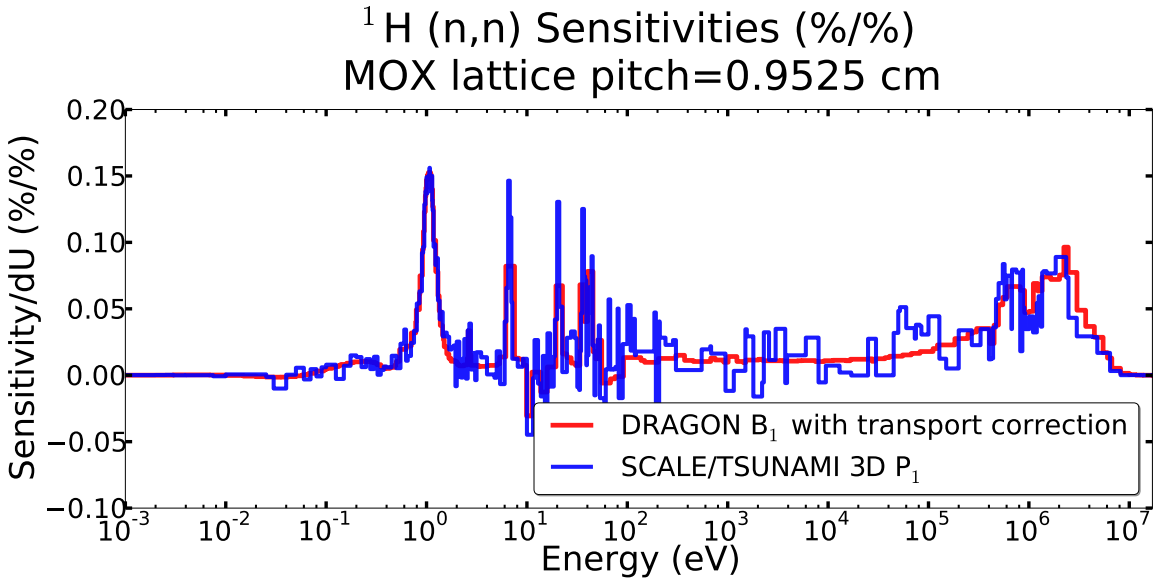

Figure 4.19: comparision of ^{1}H(n,el) sensitivity for MOX lattice at pitch=0.9525 cm. DRAGON B_1 with transport correction (green). SCALE6/TSUNAMI-3D P_1 (blue).

4.2.3 Integrated Sensitivities

Table 4.18 presents our integrated explicit sensitivities (DR-B_1) and the sensitivities computed by SCALE6/TSUNAMI-3D using P_1 expansion for the angular flux (S6-P_1). We have provided sensitivities for the main isotopes present in the fuel and the moderator. We note that for ^{238}U and ^{242}Pu, the observed differences between the absorption cross section sensitivities are largest. These two isotopes are also the isotopes which are the most self-shielded. The observed differences in the computed absorption sensitivities highlight the underlying differences in the self-shielded multi-group cross sections from the different approaches to self-shielding used by the codes.

Integrated Explicit Sensitivities (%/%) at pitch = 0.9525 cm				
Isotope	Reaction	DR-B_1	S6-P_1	Rel. Error (%)
^{239}Pu	(n,ABS)	$-2.63 * 10^{-1}$	$-2.62 * 10^{-1}$	-0.5
	(n,SCAT)	$4.69 * 10^{-3}$	$4.62 * 10^{-3}$	-1.2
	(n, f)	$3.93 * 10^{-1}$	$3.92 * 10^{-1}$	-0.3
	(n,$\bar{\nu}$)	$9.24 * 10^{-1}$	$9.20 * 10^{-1}$	-0.4
	TOTAL	$1.35 * 10^{-1}$	$1.35 * 10^{-1}$	-0.2
^{238}U	(n,ABS)	$-7.61 * 10^{-2}$	$-6.62 * 10^{-2}$	-15.0
	(n,SCAT)	$2.65 * 10^{-2}$	$2.53 * 10^{-2}$	-4.7
	(n, f)	$1.88 * 10^{-2}$	$2.04 * 10^{-2}$	7.9
	(n,$\bar{\nu}$)	$2.68 * 10^{-2}$	$2.94 * 10^{-2}$	9.0
	TOTAL	$-2.94 * 10^{-2}$	$-2.04 * 10^{-2}$	-44.3
^{240}Pu	(n,ABS)	$-6.76 * 10^{-2}$	$-6.32 * 10^{-2}$	-7.1
	(n,SCAT)	$7.5 * 10^{-4}$	$9.02 * 10^{-4}$	16.9
	(n, f)	$3.63 * 10^{-3}$	$3.89 * 10^{-3}$	6.9
	(n,$\bar{\nu}$)	$5.14 * 10^{-3}$	$5.53 * 10^{-3}$	6.9
	TOTAL	$-6.33 * 10^{-2}$	$-5.84 * 10^{-2}$	-8.4
^{241}Pu	(n,ABS)	$-5.09 * 10^{-3}$	$-5.01 * 10^{-3}$	-1.6
	(n,SCAT)	$1.12 * 10^{-4}$	$1.05 * 10^{-4}$	-6.7
	(n, f)	$1.29 * 10^{-2}$	$1.32 * 10^{-2}$	2.4
	(n,$\bar{\nu}$)	$2.81 * 10^{-2}$	$2.84 * 10^{-2}$	1.3
	TOTAL	$7.93 * 10^{-3}$	$8.32 * 10^{-3}$	4.7
^{242}Pu	(n,ABS)	$-2.01 * 10^{-3}$	$-2.51 * 10^{-3}$	19.8
	(n,SCAT)	$2.47 * 10^{-5}$	$1.26 * 10^{-5}$	-96.2
	(n, f)	$8.85 * 10^{-5}$	$9.47 * 10^{-5}$	6.6
	(n,$\bar{\nu}$)	$1.24 * 10^{-4}$	$1.33 * 10^{-4}$	7.2
	TOTAL	$-1.89 * 10^{-3}$	$-2.40 * 10^{-3}$	21.2
^{16}O in Fuel	(n,ABS)	$-6.39 * 10^{-4}$	$-8.48 * 10^{-4}$	24.6
	(n,SCAT)	$2.22 * 10^{-2}$	$2.00 * 10^{-2}$	-11.2
	TOTAL	$2.16 * 10^{-2}$	$1.91 * 10^{-2}$	-12.8
^{16}O in Water	(n,ABS)	$-1.44 * 10^{-3}$	$-1.90 * 10^{-3}$	24.2
	(n,SCAT)	$2.72 * 10^{-2}$	$5.70 * 10^{-2}$	52.2
	TOTAL	$2.58 * 10^{-2}$	$5.51 * 10^{-2}$	53.2
^{1}H	(n,ABS)	$-2.06 * 10^{-2}$	$-1.97 * 10^{-2}$	-4.9
	(n,SCAT)	$4.21 * 10^{-1}$	$4.83 * 10^{-1}$	12.9
	TOTAL	$4.0 * 10^{-1}$	$4.64 * 10^{-1}$	13.7

Table 4.18: Comparison of integrated explicit sensitivities (%/%) for the MOX lattice at pitch=0.9525 cm. DR-B_1: DRAGON **SNS:** with a B_1 transport corrected heterogeneous leakage model with z-axial leakage. S6-P_1 : SCALE6/TSUNAMI-3D sensitivities from a P_1 flux and adjoint multi-group Monte-Carlo solution.

Next, we see that for heavy isotope scattering reactions, the largest discrepancy, in relative terms, appears for ^{240}Pu and ^{242}Pu. We note that their sensitivities are small in absolute values so that they do not have a large contribution to the error. To examine the error, we can compare the partial elastic and inelastic reactions sensitivities obtained from the DR-B_1 approach and the S6-P_1 approach. Table 4.19 presents comparisons between DR-B_1 and S6-P_1 integrated elastic scattering sensitivity (in %/%) for ^{238}U and the Plutonium isotopes. The column labeled TR presents the contribution of the transport correction to the elastic sensitivity. We first note that the TR component has a large contribution of elastic sensitivity. Next, note that the elastic sensitivity is computed to be within 20% for the isotopes having sensitivity of the order of 10^{-4}; approximately half of this difference is in the resonance region where group meshing can have an effect on the computed difference (gain-loss) in the sensitivity expressions. The other portion of the difference can be explained from our assumption of the diagonal nature of heavy isotope elastic scattering transfer matrix and anisotropy. For ^{238}U, approximately 10-15 % of the observed error is due to inherent differences in the elastic scattering in the resonance region and 5-10% error which arises from anisotropy. Finally, the large discrepancies observed with ^{240}Pu,^{241}Pu and ^{242}Pu are rather a question of precision.[18]

Explicit component of Integrated Heavy Isotope Elastic Sensitivities (%/%)				
pitch=0.9525 cm	DRAGON DR-B_1		SCALE	Relative
Isotope	TR	Sensitivity (%/%)	Sensitivity (%/%)	Error (%)
^{238}U	-51	$1.32 * 10^{-2}$	$1.1 * 10^{-2}$	-20
^{239}Pu	-58	$2.93 * 10^{-3}$	$2.55 * 10^{-3}$	-15
^{240}Pu	-46	$4.99 * 10^{-4}$	$6.16 * 10^{-4}$	19
^{241}Pu	-61	$6.35 * 10^{-5}$	$1.052 * 10^{-4}$	40
^{242}Pu	-37	$1.71 * 10^{-5}$	$2.14 * 10^{-6}$	-697

Table 4.19: Comparison of the explicit component of heavy isotope **elastic sensitivities** for pitch=0.9525 cm. DR-B_1: Sensitivity computed by DRAGON **SNS:** from a heterogeneous B_1 search. TR: Contribution of the transport correction (%) to the DR-B_1 computed sensitivity

Table 4.20 presents comparisons for the DR-B_1 and S6-P_1 integrated inelastic sensitivities. (n,2n) reactions here account for approximately 1% of the total scattering sensitivity so that they can be effectively neglected. The largest component of the difference between ^{238}U and ^{239}Pu is believed to be from anisotropy of inelastic scattering reactions which cannot be accounted for by a transport correction. The remaining differences in the sensitivities observed for ^{240}Pu, ^{241}Pu, ^{242}Pu are likely numerical and a question of precision. We note that sensitivities at these orders of magnitude do not contribute to the uncertainty.

Finally, we note that the difference between the computed DR-B_1 and the S6-P_1 sensitivity for ^{238}U(n,SCAT) is only 4.7%. We stress that these were the reactions reported by [107] to be the most discrepant (particularly for ^{238}U). Also observed is that the errors between the partial reactions (n,el) and (n,inel) are much higher, but cancel out due to

[18]Note that all the sensitivities computed by DRAGON **SNS:** are in double precision. We believe these limitations are rather due to the precision of the ENDF format (see section 1.2.1).

Integrated Heavy Isotope Inelastic Sensitivities (%/%)			
pitch=0.9525 cm	DRAGON	SCALE	Relative
Isotope	Sensitivity (%/%)	Sensitivity (%/%)	Error (%)
^{238}U	$1.10 * 10^{-2}$	$1.36 * 10^{-2}$	19
^{239}Pu	$2.55 * 10^{-3}$	$1.98 * 10^{-3}$	-29
^{240}Pu	$6.16 * 10^{-4}$	$2.82 * 10^{-4}$	-118
^{241}Pu	$1.05 * 10^{-4}$	$5.06 * 10^{-5}$	-108
^{242}Pu	$2.14 * 10^{-6}$	$1.01 * 10^{-5}$	79

Table 4.20: Comparison of heavy isotope **inelastic sensitivities** for pitch=0.9525 cm. DR-B_1: Sensitivity computed by DRAGON **SNS:** from a heterogeneous B_1 search. TR: Contribution of the transport correction (%) to the DR-B_1 computed sensitivity.

compensation making ^{238}U(n,SCAT) a poor value for benchmarking. As seen shortly, these reactions also have disproportionate contributions to the uncertainty making an accurate computation of their sensitivities even more necessary.

4.2.4 Implicit Sensitivities

In heterogeneous systems, the analytical approximation is limited as it ignores the perturbation $\delta\Sigma_{eff}$ in the effective dilution factor Σ_{eff} (see section 3.1.3). However, it can still be used to predict the implicit effect of an isotope on itself. While this limitation may seem constraining, in the majority of the benchmarks considered by the UACSA Expert Group, the isotope whose implicit sensitivity had the largest impact on the computed uncertainty was ^{238}U(n,el) [107]. As the principle isotope which contributes to the implicit sensitivity is ^{238}U(n,γ), the analytical approximation can be used to estimate the implicit sensitivity for ^{238}U(n,el). Table 4.21 presents the implicit component of the ^{238}U(n,el) sensitivity computed by using the analytical approximation with the DR-B_1 explicit sensitivities as well as reference results from the SCALE6/TSUNAMI-3D code (S6-P_1). We note the good comparison between the computed values. Similar to the sphere problem of the previous section, the ^{238}U (n,scat) implicit sensitivity is positive due to the increase in the flux depression that is accompanied from an increase in the scattering cross section of ^{238}U (i.e. the scattering reaction helps removing the neutrons under the resonances). With the increase in the moderator volume (increase in pitch), the probability for a neutron born in the fuel to have a collision in the moderator, and be slowed down to thermal energies where it can induce fission, increases. Accompanied with decreasing pitch is the reduction in the absorption rate in the unresolved region where the resonances are narrow and the scattering reaction is effective in removing neutrons under the resonance. Therefore the implicit sensitivity also decreases with increasing pitch. Figure 4.20 presents the scattering sensitivity profiles for ^{238}U(n,el) in the resonance region. The orange curve presents results obtained from the analytical approximation (equation 3.31). The blue curve presents results obtained from 47 self shielding calculation and equation 3.19. For both cases, the dominant contributor to the scattering sensitivity is the capture cross section of ^{238}U (ie. $G^{238U}_{R,(n,\gamma)}$ in equation 3.19). A direct perturbation approach to sensitivity in DRAGON would be expected to produce results comparable to this curve. The dips in

Lattice pitch (cm)	^{238}U (n,n) Implicit Scattering Sensitivities (%/%)		
	DRAGON **SNS:** + ANALYTIC	SCALE/TSUNAMI 3D [109]	Rel. Err.
0.586	$1.71 * 10^{-2}$	$1.60 * 10^{-2}$	-6.9%
0.60	$1.77 * 10^{-2}$	$1.59 * 10^{-2}$	-11%
0.66	$1.71 * 10^{-2}$	$1.45 * 10^{-2}$	-18%
0.73	$1.52 * 10^{-2}$	$1.26 * 10^{-2}$	-20%
0.9525*	$9.14 * 10^{-3}$	$8.3 * 10^{-2}$	-10%
1.05	$7.6 * 10^{-3}$	$7.1 * 10^{-2}$	7%
1.15	$6.9 * 10^{-3}$	$6.2 * 10^{-2}$	10%

Table 4.21: ^{238}U Implicit scattering sensitivities as a function of varying pitch for the MOX lattice. SCALE/TSUNAMI 3D results are reproduced from [109]. DRAGON **SNS:** ANALYTIC computation has been performed from equations 3.31-3.32 and 3.19. * reference case.

the blue curve are due to numerical errors introduced when reading the perturbed cross sections from the DRAGLIB after the self shielding calculation. To read the perturbed cross sections, we use the FORTRAN 77 modules of the GANLIB driver [60] that we compiled as a dynamic library for use with PYTHON. This error is to be expected with FORTRAN when subtracting two similar real numbers in single precision. The dotted black curve presents SCALE/TSUNAMI-3D sensitivities in the SCALE 238-group energy grid. The red curve presents the SCALE/TSUNAMI-3D sensitivities collapsed to the WIMS 172-group energy grid by using the procedure discussed in section 3.1.4. We note the good comparison between the three implicit sensitivities. Differences at low energy most likely stem from our neglect of the contribution from ^{240} Pu (n,γ) in the analytical approximation ($G_{R,x}^{238U}$ of equation 3.19), differences in energy meshing and the self-shielding approach in the two codes (figure 4.21), and differences in the explicit ^{238}U absorption profiles. The explicit absorption profiles are shown in figure 4.21. The general trend between the two sensitivities is that the SCALE predicted absorption sensitivities are slightly lower than those predicted by DRAGON inside the first few resonances.

Prediction of the implicit sensitivities for isotopes $k \neq^{238} U$ requires the computation of the perturbation $\delta\Sigma_e$ in the effective cross section (see equations 3.31-3.32). We have recently seen a publication [110] on the subject outlining recent developments in DRAGON regarding the computation of k_{eff} implicit sensitivities using the Stamm'ler method. We believe that coupling this new module with **SNS:** will not be a difficult task and could allow for a more complete sensitivity analysis package in the code DRAGON.

For this benchmark, the next reaction with the largest implicit sensitivity is ^{1}H(n,el). The implicit sensitivity for this reaction is reported by SCALE/TSUNAMI-3D to be 5% of its explicit sensitivity. Since the cross section for hydrogen is well known (i.e. it has a small uncertainty) the 5% contribution from the implicit sensitivity to the overall uncertainty can be effectively neglected. Similarly, the implicit sensitivity for the remaining isotopes in the benchmark is smaller than 5% of the explicit sensitivity [109] so that the implicit effect can be neglected.

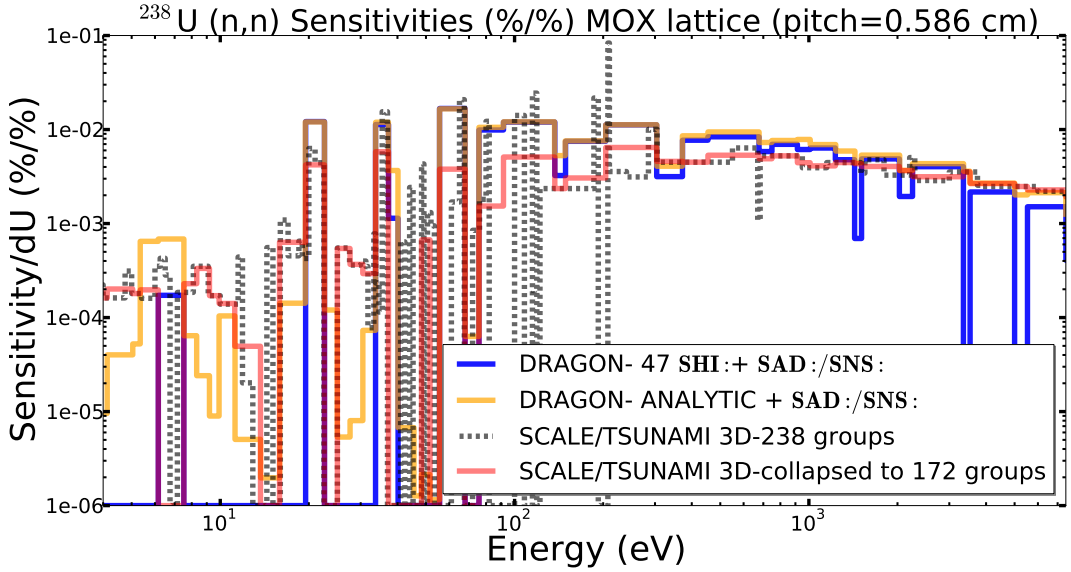

Figure 4.20: Positive component of ^{238}U elastic scattering cross section sensitivity (%/%) in the resonance region: one **SHI:** computation along with equations 3.31-3.32 and 3.19 the explicit sensitivities from **SNS:** (orange curve); 47 **SHI:**, equation 3.19 and the explicit sensitivities from **SNS:** (blue curve), SCALE/TSUNAMI 1D (red curve)

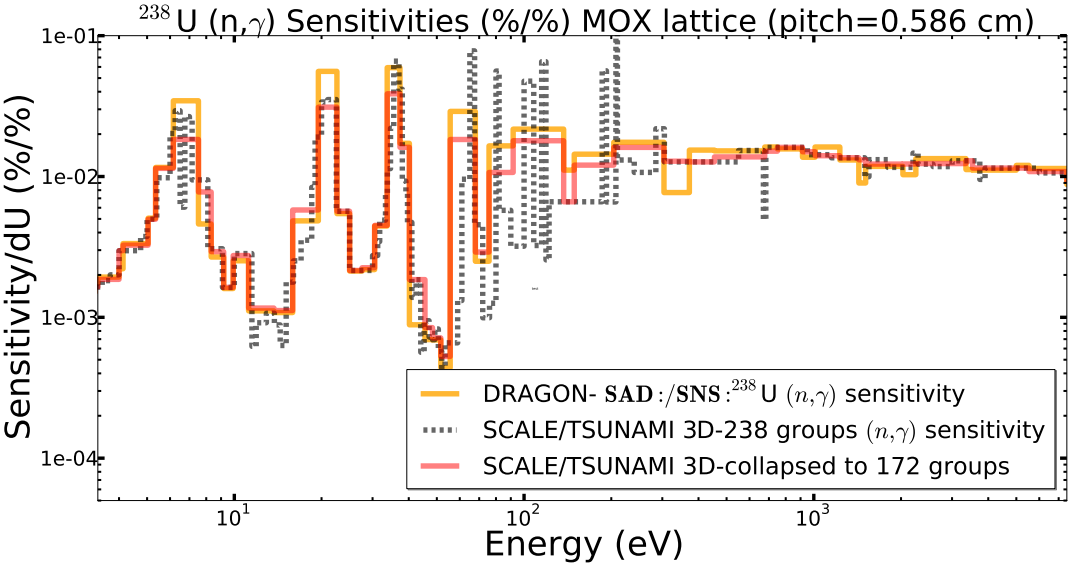

Figure 4.21: Negative component of the ^{238}U (n,γ) **explicit** sensitivity (%/%): 172-group DRAGON **SAD:/SAD:** capture sensitivity profile (orange line), 238 SCALE/TSUNAMI 1D capture sensitivity profile (dotted black), SCALE/TSUNAMI 1D capture sensitivity profile collapsed to the 172-group WIMS energy grid (red curve)

4.2.5 Uncertainty Analysis

Table 4.22 presents the variation of ^{238}U reaction integrated sensitivities (in %/%) as a function of increasing pitch computed from the DR-B_1 approach and the S6-P_1 approach. The relative error reports the difference between the DR-B_1 sensitivities relative to the S6-P_1 sensitivities. Table 4.23 presents reaction pair uncertainty contributions to the k_{eff} uncertainty (in pcm) as a function of increasing pitch.

From table 4.23, we see that the uncertainty contribution for capture reaction decreases as a function of increasing pitch. This can be expected by observing the decrease in the capture sensitivity that is accompanied with increasing pitch. Next, we note that while the error in the absorption sensitivities (table 4.22) is increasing with increasing pitch, the estimated errors in the uncertainties are roughly constant for the more thermal spectra (pitches = 0.73 - 1.05 cm). This is because the largest components of the error in the absorption sensitivities are observed in the first few resonances appearing in the epithermal region. The cross sections in this region are well known and have a low uncertainty, so that the increasing difference in the sensitivities does not have a great impact on the computed uncertainties. At pitch=1.05 cm, the largest contribution to the 82 pcm (n,capture)-(n,capture) uncertainty is from the absorption cross sections in the epithermal region where the sensitivity differences are the largest, resulting in the 33.2% error in the computed uncertainties.

Next, we note the importance of (n,inel) reactions given that they always appear amongst the top contributors to the uncertainty. We also note that their contribution to the uncertainty is increasing with pitch (see table 4.23) even though their sensitivities remain relatively constant (see table 4.22). This can be understood better by discussing the sensitivity profiles of ^{238}U. We see from table 4.14 that, with increasing pitch, the GL component of the sensitivity begins to account for a larger part of the scattering sensitivity. This term is due to ^{238}U(n,inel) (elastic reactions do not slow down neutrons). As the spectrum shifts to a thermal spectrum, the inelastic sensitivity profile approaches the fission source (see figures 4.15 and 4.16). The uncertainty reported for ^{238}U(n,inel) however is higher in this range (see figure 3.9) thereby increasing the ^{238}U(n,inel) contribution to the k_{eff} uncertainty.

Also observed in table 4.23 is the decreasing contribution of ^{238}U(n,f) and ^{238}U(n,$\bar{\nu}$) with increasing pitch/moderation from the reduced fast fission rate. Finally we note that, except for the first two cases where the largest difference is due to differences in the capture cross sections, our computed uncertainties in all remaining cases are approximately within 10% of the uncertainty computed by SCALE6. We also observe from table 4.23 the importance of the negative correlation between ^{238}U(n,inel) and ^{238}U(n,el), which helps in reducing the computed uncertainty for all pitches. Computation of the uncertainty contribution from these reactions is not possible with the DR-K approach.

Similarly, table 4.25 presents uncertainty contributions for ^{239}Pu reactions. Our ^{239}Pu computed uncertainty contributions are in good agreement with values predicted by SCALE/TSUNAMI-3D, primarily due to the $\bar{\nu}$ uncertainty which is being conservatively

reported here. As a result, the underlying comparisons between other contributors are lost when only the error on the isotope's total contribution to the uncertainty is examined. The highest discrepancy here is noticed for inelastic reactions, where the sensitivity is low (order of 10^{-3}) and typically difficult to be compared. We also note that the uncertainty is observed to increase with increasing pitch due to the increase in the thermal fission of ^{239}Pu, and ^{239}Pu $\bar{\nu}$ uncertainties.

^{238}U Explicit Sensitivities (%/%) as a function of pitch									
	(n,el)			(n,inel)			(n,γ)		
PITCH (cm)	DRAGON†	SCALE‡	Rel. Error (%)	DRAGON†	SCALE‡	Rel. Error* (%)	DRAGON†	SCALE‡	Rel. Error* (%)
0.586	$3.6*10^{-2}$	$3.0*10^{-2}$	-20	$9.0*10^{-2}$	$1.1*10^{-2}$	16	$-1.4*10^{-1}$	$-1.3*10^{-1}$	-7
0.6	$3.3*10^{-2}$	$2.7*10^{-2}$	-21	$1.0*10^{-2}$	$1.2*10^{-2}$	16	$-1.4*10^{-1}$	$-1.3*10^{-1}$	-8
0.66	$2.4*10^{-2}$	$1.9*10^{-2}$	-29	$1.2*10^{-2}$	$1.3*10^{-2}$	6	$-1.3*10^{-1}$	$-1.2*10^{-1}$	-10
0.73	$1.9*10^{-2}$	$1.6*10^{-2}$	-18	$1.4*10^{-2}$	$1.6*10^{-2}$	14	$-1.2*10^{-1}$	$-1.0*10^{-1}$	-14
0.9525	$1.3*10^{-2}$	$1.0*10^{-2}$	-20	$1.3*10^{-2}$	$1.4*10^{-2}$	3	$-7.6*10^{-2}$	$-6.6*10^{-2}$	-15
1.05	$1.1*10^{-2}$	$9.4*10^{-3}$	-21	$1.2*10^{-2}$	$1.2*10^{-2}$	2	$-6.5*10^{-2}$	$-5.6*10^{-2}$	-15
1.15	$9.7*10^{-3}$	$8.0*10^{-3}$	-21	$1.1*10^{-2}$	$1.1*10^{-2}$	1	$-5.8*10^{-2}$	$-4.8*10^{-2}$	-20
	(n,f)			(n, $\bar{\nu}$)			(n,total)		
PITCH (cm)	DRAGON†	SCALE‡	Rel. Error* (%)	DRAGON†	SCALE‡	Rel. Error* (%)	DRAGON†	SCALE‡	Rel. Error* (%)
0.586	$5.8*10^{-2}$	$6.1*10^{-2}$	4	$8.9*10^{-2}$	$9.4*10^{-2}$	5	$-3.7*10^{-2}$	$-2.9*10^{-2}$	-27
0.6	$5.5*10^{-2}$	$5.7*10^{-2}$	4	$8.4*10^{-2}$	$8.8*10^{-2}$	5	$-4.0*10^{-2}$	$-3.2*10^{-2}$	-27
0.66	$4.3*10^{-2}$	$4.6*10^{-2}$	5	$6.5*10^{-2}$	$6.9*10^{-2}$	6	$-4.8*10^{-2}$	$-3.8*10^{-2}$	-26
0.73	$3.4*10^{-2}$	$3.6*10^{-2}$	6	$5.0*10^{-2}$	$5.4*10^{-2}$	7	$-4.9*10^{-2}$	$-3.3*10^{-2}$	-49
0.9525	$1.9*10^{-2}$	$2.0*10^{-2}$	8	$2.7*10^{-2}$	$2.9*10^{-2}$	9	$-3.1*10^{-2}$	$-2.1*10^{-2}$	-46
1.05	$1.6*10^{-2}$	$1.7*10^{-2}$	8	$2.2*10^{-2}$	$2.4*10^{-2}$	9	$-2.6*10^{-2}$	$-1.8*10^{-2}$	-46
1.15	$1.3*10^{-2}$	$1.4*10^{-2}$	9	$1.8*10^{-2}$	$2.0*10^{-2}$	11	$-2.5*10^{-2}$	$-1.5*10^{-2}$	-62

Table 4.22: Comparison of DR-B_1 and S6-P_1 ^{238}U **explicit** integrated sensitivities.
† DRAGON **SAD:/SNS:** results obtained from a B_1 Heterogeneous buckling search with imposed axial leakage with transport correction.
‡ SCALE6/TSUNAMI 3D results
* Relative Error = $\frac{\text{SCALE from Sensitivity - DRAGON from Sensitivity}}{\text{SCALE from Senstivity}}$

PITCH = 0.586 cm		**Uncertainty (pcm)**			**PITCH = 0.60 cm**		**Uncertainty (pcm)**		
^{238}U Reaction		DRAGON	SCALE	Rel. Diff* (%)	**^{238}U Reaction**		DRAGON	SCALE	Rel. Diff* (%)
(n,capture)	(n,capture)	192	168	-14.6	(n,capture)	(n,capture)	187	172	-8.7
(n,el)	(n,inel)	-137	-134	-2.6	(n,inel)	(n,inel)	141	146	3.5
(n,inel)	(n,inel)	117	115	-1.3	(n,el)	(n,inel)	-146	-145	-0.5
(n, $\bar{\nu}$)	(n, $\bar{\nu}$)	105	110	5.2	(n, $\bar{\nu}$)	(n, $\bar{\nu}$)	98.1	103	5.1
(n,el)	(n,el)	91.6	90.1	-1.6	(n,el)	(n,el)	84.9	80.3	-5.7
(n,f)	(n,f)	30.6	31.9	4.1	(n,f)	(n,f)	28.9	30	3.9
TOTAL		**248**	**212**	**-17**	**TOTAL**		**248**	**218**	**-13.8**
PITCH=0.66 cm		**Uncertainty (pcm)**			**PITCH=0.73 cm**		**Uncertainty (pcm)**		
^{238}U Reaction		DRAGON	SCALE	Rel. Diff* (%)	**^{238}U Reaction**		DRAGON	SCALE	Rel. Diff* (%)
(n,inel)	(n,inel)	201	256	21.4	(n,inel)	(n,inel)	230	256	10
(n,el)	(n,inel)	-154	-156	1.4	(n,el)	(n,inel)	-147	-156	5.3
(n,capture)	(n,capture)	169	132	-28.1	(n,capture)	(n,capture)	151	132	-14.4
(n, $\bar{\nu}$)	(n, $\bar{\nu}$)	75.9	62.6	-21.2	(n,$\bar{\nu}$)	(n,$\bar{\nu}$)	58.5	62.6	6.5
(n,el)	(n,el)	64.8	51.8	-25.1	(n,el)	(n,el)	52.2	51.8	-0.7
(n,f)	(n,f)	22.6	18.8	-20.2	(n,f)	(n,f)	17.7	18.8	5.8
TOTAL		**260**	**256**	**-1.6**	**TOTAL**		**267**	**256**	**-4.3**
PITCH=0.9525 cm		**Uncertainty (pcm)**			**PITCH=1.05 cm**		**Uncertainty (pcm)**		
^{238}U Reaction		DRAGON	SCALE	Rel. Diff* (%)	**^{238}U Reaction**		DRAGON	SCALE	Rel. Diff* (%)
(n,inel)	(n,inel)	226	229	1.2	(n,inel)	(n,inel)	206	200	-2.9
(n,el)	(n,inel)	-118	-117	-1.3	(n,el)	(n,inel)	-105	-99	-5.5
(n,capture)	(n,capture)	97.3	85.3	-14.1	(n,capture)	(n,capture)	82.6	72.2	-14.3
(n, $\bar{\nu}$)	(n, $\bar{\nu}$)	31.3	34.2	8.6	(n,$\bar{\nu}$)	(n,$\bar{\nu}$)	25.6	27.8	8
(n,el)	(n,el)	34.3	32.5	-5.7	(n,el)	(n,el)	29.5	26.8	-10.3
(n,f)	(n,f)	9.84	10.6	7.4	(n,f)	(n,f)	8.11	8.57	5.3
TOTAL		**236**	**220**	**-7.3**	**TOTAL**		**213**	**193**	**-10.4**
PITCH = 1.15 cm		**Uncertainty (pcm)**							
^{238}U Reaction		DRAGON	SCALE	Rel. Diff* (%)					
(n,inel)	(n,inel)	183	183	0					
(n,el)	(n,inel)	-91.4	-87.7	-4.2					
(n,capture)	(n,capture)	73.8	55.4	-33.2					
(n,$\bar{\nu}$)	(n,$\bar{\nu}$)	25.4	27.1	6.1					
(n,el)	(n,el)	21.1	23.6	10.5					
(n,f)	(n,f)	6.75	7.41	8.9					
TOTAL		**178**	**173**	**-2.9**					

Table 4.23: Comparison of predicted ^{238}U uncertainties computed from DR-B$_1$ explicit sensitivities and ^{238}U uncertainties reported from S6-P$_1$. Nuclear data uncertainty source is SCALE6 44 group covariance library.
* Relative Difference with SCALE $\equiv \frac{\text{Uncertainty computed by SCALE-Uncertainty computed DRAGON}}{\text{Uncertainty from SCALE}} * 100.\%$

^{239}Pu Explicit Sensitivities as a function of pitch									
	(n,el)			(n,inel)			(n,γ)		
PITCH (cm)	DRAGON†	SCALE‡	Rel. Error (%)	DRAGON†	SCALE‡	Rel. Error* (%)	DRAGON†	SCALE‡	Rel. Error* (%)
0.586	$7.9 * 10^{-3}$	$6.3 * 10^{-3}$	-24	$1.4 * 10^{-3}$	$1.8 * 10^{-3}$	23	$5.0 * 10^{-1}$	$4.9 * 10^{-1}$	-2
0.6	$7.2 * 10^{-3}$	$6.2 * 10^{-3}$	-17	$1.5 * 10^{-3}$	$2.2 * 10^{-3}$	33	$4.9 * 10^{-1}$	$4.9 * 10^{-1}$	-1
0.66	$5.3 * 10^{-3}$	$4.7 * 10^{-3}$	-12	$1.7 * 10^{-3}$	$2.4 * 10^{-3}$	29	$4.7 * 10^{-1}$	$4.6 * 10^{-1}$	-1
0.73	$4.3 * 10^{-3}$	$3.9 * 10^{-3}$	-11	$1.9 * 10^{-3}$	$2.4 * 10^{-3}$	24	$4.4 * 10^{-1}$	$4.4 * 10^{-1}$	-1
0.9525	$2.9 * 10^{-3}$	$2.6 * 10^{-3}$	-15	$1.7 * 10^{-3}$	$2.0 * 10^{-3}$	12	$3.9 * 10^{-1}$	$3.9 * 10^{-1}$	0
1.05	$2.5 * 10^{-3}$	$2.2 * 10^{-3}$	-16	$1.6 * 10^{-3}$	$1.8 * 10^{-3}$	10	$3.8 * 10^{-1}$	$3.8 * 10^{-1}$	0
1.15	$2.2 * 10^{-3}$	$1.8 * 10^{-3}$	-17	$1.4 * 10^{-3}$	$1.5 * 10^{-3}$	10	$3.8 * 10^{-1}$	$3.8 * 10^{-1}$	0
	(n,γ)			(n,f)			(n,total)		
PITCH (cm)	DRAGON†	SCALE‡	Rel. Error (%)	DRAGON†	SCALE‡	Rel. Error* (%)	DRAGON†	SCALE‡	Rel. Error* (%)
0.586	$-1.5 * 10^{-1}$	$-1.5 * 10^{-1}$	2	$8.3 * 10^{-1}$	$8.3 * 10^{-1}$	-1	$3.6 * 10^{-1}$	$3.5 * 10^{-1}$	-4
0.6	$-1.6 * 10^{-1}$	$-1.6 * 10^{-1}$	0	$8.4 * 10^{-1}$	$8.3 * 10^{-1}$	-1	$3.5 * 10^{-1}$	$3.4 * 10^{-1}$	-2
0.66	$-1.9 * 10^{-1}$	$-1.9 * 10^{-1}$	0	$8.7 * 10^{-1}$	$8.6 * 10^{-1}$	-1	$2.8 * 10^{-1}$	$2.8 * 10^{-1}$	-2
0.73	$-2.2 * 10^{-1}$	$-2.2 * 10^{-1}$	-1	$8.9 * 10^{-1}$	$8.8 * 10^{-1}$	-1	$2.2 * 10^{-1}$	$2.2 * 10^{-1}$	-2
0.9525	$-2.6 * 10^{-1}$	$-2.6 * 10^{-1}$	0	$9.2 * 10^{-1}$	$9.2 * 10^{-1}$	0	$1.3 * 10^{-1}$	$1.3 * 10^{-1}$	0
1.05	$-2.7 * 10^{-1}$	$-2.7 * 10^{-1}$	0	$9.3 * 10^{-1}$	$9.3 * 10^{-1}$	0	$1.2 * 10^{-1}$	$1.2 * 10^{-1}$	0
1.15	$-2.7 * 10^{-1}$	$-2.7 * 10^{-1}$	-1	$9.4 * 10^{-1}$	$9.3 * 10^{-1}$	0	$1.1 * 10^{-1}$	$1.1 * 10^{-1}$	1

Table 4.24: Comparison of ^{239}U DR-B_1 and S6-P_1 **explicit** sensitivities.

† DRAGON **SAD:/SNS:** results obtained from a B_1 Heterogeneous buckling search with imposed axial leakage and with transport correction.

‡ SCALE/TSUNAMI 3D results

* Relative Error = $\frac{\text{SCALE from Sensitivity - DRAGON from Sensitivity}}{\text{SCALE from Senstivity}}$

PITCH = 0.586cm		**Uncertainty (pcm)**			**PITCH = 0.60 cm**		**Uncertainty (pcm)**		
^{239}Pu Reaction		DRAGON	SCALE	Rel. Diff* (%)	**^{239}Pu Reaction**		DRAGON	SCALE	Rel. Diff* (%)
(n, $\bar{\nu}$)	(n, $\bar{\nu}$)	776	767	-1	(n, $\bar{\nu}$)	(n, $\bar{\nu}$)	787	779	-1
(n,f)	(n,f)	259	244	-6	(n,f)	(n,f)	262	248	-6
(n,capture)	(n,capture)	225	226	0	(n,capture)	(n,capture)	211	212	1
(n,f)	(n,capture)	-113	-106	-6	(n,f)	(n,capture)	-110	-105	-5
(n,inel)	(n,inel)	38	56	33	(n,inel)	(n,inel)	37	54	31
(n,el)	(n,el)	33	28	-16	(n,el)	(n,el)	30	25	-16
TOTAL		**846**	**832**	**-2**	**TOTAL**		**853**	**840**	**-2**

PITCH = 0.66 cm		**Uncertainty (pcm)**			**PITCH = 0.73 cm**		**Uncertainty (pcm)**		
^{239}Pu Reaction		DRAGON	SCALE	Rel. Diff* (%)	**^{239}Pu Reaction**		DRAGON	SCALE	Rel. Diff* (%)
(n, $\bar{\nu}$)	(n, $\bar{\nu}$)	831	823	-1	(n, $\bar{\nu}$)	(n, $\bar{\nu}$)	869	860	-1
(n,f)	(n,f)	261	252	-4	(n,f)	(n,f)	254	246	-3
(n,capture)	(n,capture)	191	192	0	(n,capture)	(n,capture)	205	204	-1
(n,f)	(n,capture)	-67	-64	-4	(n,f)	(n,capture)	94	93	-1
(n,inel)	(n,inel)	37	52	29	(n,inel)	(n,inel)	38	50	24
(n,el)	(n,el)	21	19	-13	(n,el)	(n,el)	17	15	-13
TOTAL		**891**	**880**	**-1**	**TOTAL**		**853**	**840**	**-1**

PITCH = 0.9525 cm		**Uncertainty (pcm)**			**PITCH = 1.05 cm**		**Uncertainty (pcm)**		
^{239}Pu Reaction		DRAGON	SCALE	Rel. Diff* (%)	**^{239}Pu Reaction**		DRAGON	SCALE	Rel. Diff* (%)
(n, $\bar{\nu}$)	(n, $\bar{\nu}$)	927	920	-1	(n, $\bar{\nu}$)	(n, $\bar{\nu}$)	939	933	-1
(n,capture)	(n,capture)	263	260	-1	(n,capture)	(n,capture)	277	275	-1
(n,f)	(n,f)	257	251	-2	(n,f)	(n,f)	266	260	-2
(n,f)	(n,capture)	208	205	-2	(n,f)	(n,capture)	229	226	-1
(n,inel)	(n,inel)	34	39	13	(n,inel)	(n,inel)	31	35	11
(n,el)	(n,el)	11	9	-20	(n,el)	(n,el)	10	8	-22
TOTAL		**1001**	**1011**	**1**	**TOTAL**		**1028**	**1033**	**1**

PITCH = 1.15 cm		**Uncertainty (pcm)**		
^{239}Pu Reaction		DRAGON	SCALE	Rel. Diff* (%)
(n, $\bar{\nu}$)	(n, $\bar{\nu}$)	948	942	-1
(n,capture)	(n,capture)	289	286	-1
(n,f)	(n,f)	274	272	-1
(n,f)	(n,capture)	244	242	-1
(n,inel)	(n,inel)	27	30	11
(n,el)	(n,el)	8	7	-24
TOTAL		**1043**	**1050**	**1**

Table 4.25: Comparison of predicted ^{239}Pu uncertainties computed from DR-B_1 explicit sensitivities and uncertainties from S6-P_1. Nuclear data uncertainty source is SCALE6 44 group covariance library.

* Relative Difference with SCALE $\equiv \frac{\text{Uncertainty computed by SCALE-Uncertainty computed DRAGON}}{\text{Uncertainty from SCALE}} * 100.\%$

4.3 MOX Core with Light Water Reflector

4.3.1 Description

This benchmark can be found in the International Criticality Safety Benchmark Evaluation Project handbook (ICSBEP) [111] under MIX-COMP-THERM-001-001. The criticality experiment represents a fast reactor fuel assembly with recycled Plutonium in a shipping cask, in an accident scenario where water fills the cask [106, 107]. The facility consists of an under-moderated configuration of 609 fuel pins with a lattice pitch of 0.9525 cm arranged in a rectangular configuration. The cross sectional lattice configuration (height-width) is 28x22, with an asymmetry in the top row containing only 17 pins. The fuel used is the same mixture of PuO_2 and UO_2 as the previous benchmark. The isotopic composition is given in table 4.12. The fuel pins in the core have a height of 91.44 cm with an aluminum based reflector (nickel, chrome and aluminum) placed at the top and the bottom of the core. Since the core is fairly symmetric, only a quarter of the core consisting of the asymmetry (located at row 11 of the fuel) has been modeled (see figure 4.22).

Modeling

To account for the different capture cross sections, originating from differences in the fine flux that exists between cells in the inner core and cells on the outer periphery near the reflector, self shielding calculations have been performed for each cell "type" separately (see figure 4.22). In total, five cell "types" have been defined representing the corner cells, the cells on the outer edge of the core, the inner cells and two cells in the asymmetrical levels 10 and 11 of the quarter model. Naturally, the thermal component of the flux in the outer cells is higher than in the inner cells due to the increased moderation by the reflector.

In modeling the geometry, we used the **EXCELT:** [59] module of DRAGON for setting up the tracking geometry. This is one of the more widely used modules of DRAGON, that can be used to model 2-D and 3-D non-centered mesh geometries. Such geometries highlight the power of the collision probability method in providing a true representation of a heterogeneous system. During the modeling process, the standard spatial convergence studies have been performed to ensure k_{eff} stability with respect to the meshing. It should be noted that due to the void boundary conditions, the flux has large variation between the inner core (fuel cells) and the boundary (outer edge of the reflector). Since we assume that the flux is constant in each volume, in the case where a large volume size is selected, the number of reflected neutrons towards the fuel region is underestimated substantially (due to the averaged flux over the region). Overcoming this problem requires a fine splitting in the reflector region. The quarter assembly has therefore been modeled using 1154 sub-volumes. Figure 4.22 presents the cross sectional view of the modeled geometry (2D quarter with assembly).

To approximate the buckling coefficient, z-axial buckling was imposed for the model. The sensitivities are then computed using the algorithm outlined in section 3.2.3. This

solution requires two collision probability matrix computations, two flux computations and one adjoint computation.

Computation Time

The entire computation using the methodology presented in chapters 2 & 3 takes approximately 2.5 hours of simulation time on a standard 64 bit PC 2. 2GHz. The uncertainty analysis can be performed in a few seconds using the computed sensitivity profiles.

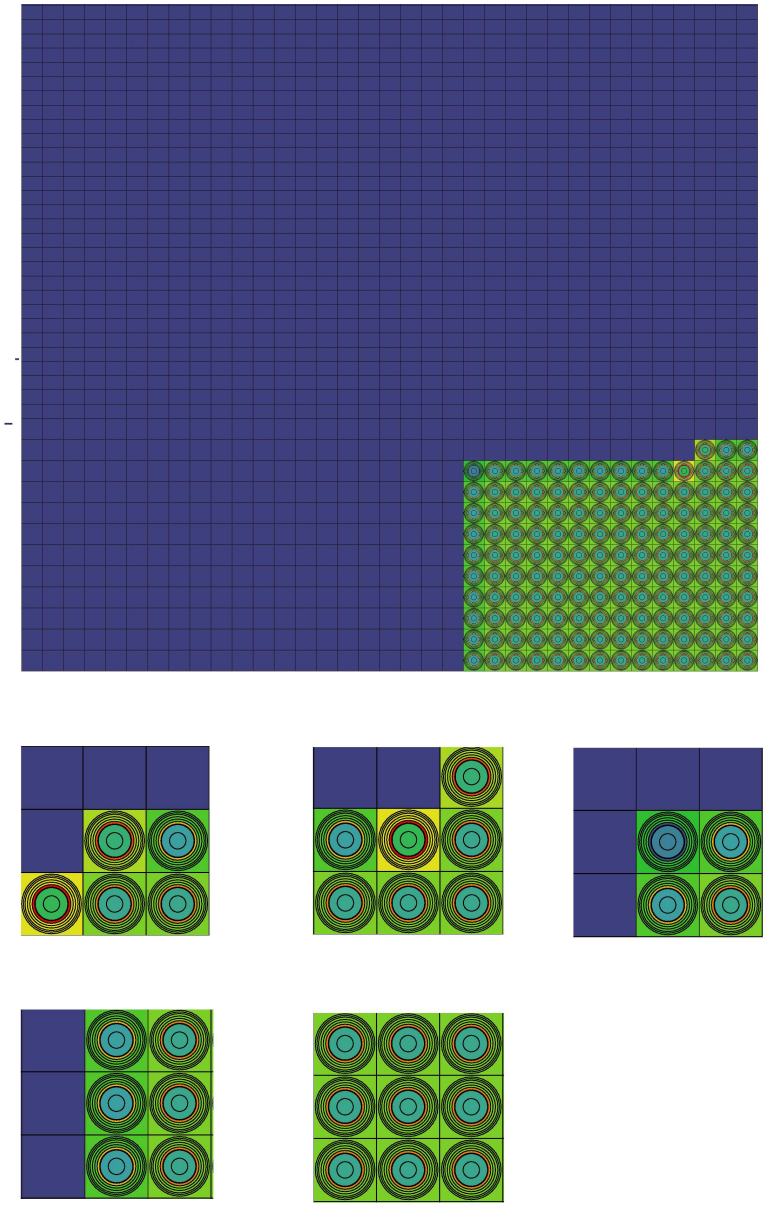

Figure 4.22: Cross sectional view of the quarter core.

SCALE/TSUNAMI-3D model

The IRSN has provided to us sensitivities computed with SCALE5/TSUNAMI-3D using a P_5 expansion of the angular flux (S5-P_5). These results will be our reference results. Details of the IRSN model can be found in [107, 109].

4.3.2 Results

Table 4.26 presents comparisons of integrated sensitivities computed using the DR-B_1 approach with the reference results from SCALE5/TSUNAMI-3D (S5-P_5). We first note their good agreement for the ^{238}U(n,SCAT) sensitivity. The profiles for ^{238}U(n,SCAT) are shown in figure 4.24. In green are sensitivities obtained using the DR-B_1 approach without using a transport correction. In red are results obtained using the DR-B_1 approach with transport corrected total and scattering cross sections. In grey are the reference results obtained with S5-P_5. In dotted blue are the sensitivities computed using the DR-K approach. We see that this last approach greatly underestimates the sensitivity. We also note the good agreement between the transport corrected DR-B_1 approach (red line) and the reference results obtained with S5-P_5.

For this benchmark, we note that a CP solution with a transport correction performs slightly better than a P_1 multi-group Monte-Carlo solution when computing the ^{238}U(n,SCAT) sensitivity. This can be observed by comparing figures 4.23 (reproduced from [109]) with figure 4.24 at high energy. The orange curve in figure 4.23 presents the sensitivity profiles computed with the multi-group Monte-Carlo Criticality Safety code MORET5 [112], with self shielded cross sections obtained with DRAGON4. Similarly, the red curve presents MORET5 sensitivities, with self-shielded cross sections computed using APOLLO2. Both computations are in P_1. The curve in blue represents the SCALE/5-TSUNAMI-3D results obtained by the IRSN [109, 107], also shown in figure 4.24 for comparison with the DR-B_1 approach. We note the good comparison of the DR-B_1 approach at high energies. Differences observed in the resonance region in figure 4.23 between the APOLLO2/MORET5 or DRAGON-4/MORET5 with the SCALE5/TSUNAMI-3D sensitivities arise from the neglect of ^{238}U implicit scattering sensitivities, which are not calculated by the multi-group Monte Carlo approach of MORET5.

For sensitivities in the reflector, we touch at the limitation of the B_N approach. One of the conditions for reformulating the transport problem using the Buckling formalism was that the obtained solution is valid far away from the reflector. When this condition is satisfied, the gradual attenuation of the flux can be captured by the buckling formalism. However, in the reflector, where the flux decreases rapidly over a short distance, the buckling approximation is no longer valid. From the previous benchmark, we observed that the k_{eff} sensitivity of ^{16}O in the moderator could not be effectively computed using a transport correction. In this benchmark, the DRAGON-B_1 computed ^{16}O scattering sensitivity has the highest relative error with respect to the sensitivity computed by SCALE5/TSUNAMI-3D. This is partly due to energy loss from anisotropic scattering reactions, that we cannot account for with a transport correction, and partly due to the poor approximation that the buckling formalism provides in the reflector.

	Sensitivities (%/%)			
	Reaction	SCALE5/TSUNAMI 3D [109]	DRAGON **SNS:** B_1	Rel. Diff (%)
^{238}U	(n,capture)	$-5.88 * 10^{-2}$	$-6.37 * 10^{-2}$	-11.2
	$\bar{\nu}$	$2.53 * 10^{-2}$	$2.38 * 10^{-2}$	6.1
	(n,f)	$1.76 * 10^{-2}$	$1.64 * 10^{-2}$	6.6
	(n,scat)‡	$2.36 * 10^{-2}$	$2.34 * 10^{-2}$	0.5
	(n,inel)	$1.12 * 10^{-2}$	$1.11 * 10^{-2}$	0.7
	(n,el)*	$4.85 * 10^{-3}$	$4.87 * 10^{-3}$	-0.4
	(n,total)	$-2.45 * 10^{-2}$	$-2.78 * 10^{-2}$	-13.6
^{239}Pu	$\bar{\nu}$	$9.25 * 10^{-1}$	$9.28 * 10^{-1}$	-0.3
	(n,f)	$3.84 * 10^{-1}$	$3.89 * 10^{-1}$	-1.2
	(n,capture)	$-2.62 * 10^{-1}$	$-2.61 * 10^{-1}$	0.3
	(n,scat)	$2.89 * 10^{-3}$	$3.01 * 10^{-3}$	-4.1
	(n,el)	$1.59 * 10^{-3}$	$1.11 * 10^{-3}$	29.8
	(n,inel)	$1.25 * 10^{-3}$	$1.89 * 10^{-3}$	-52.0
	(n,total)	$1.25 * 10^{-1}$	$1.30 * 10^{-1}$	-4.4
^{240}Pu	(n,capture)	$-6.12 * 10^{-2}$	$-6.13 * 10^{-2}$	-0.1
	(n,f)	$3.33 * 10^{-3}$	$3.17 * 10^{-3}$	4.7
	$\bar{\nu}$	$4.75 * 10^{-3}$	$4.56 * 10^{-3}$	4.0
	(n,scat)	$3.97 * 10^{-4}$	$3.37 * 10^{-4}$	15.2
	(n,el)	$2.29 * 10^{-4}$	$1.51 * 10^{-4}$	34.1
	(n,inel)	$1.63 * 10^{-4}$	$1.86 * 10^{-4}$	-13.9
	(n,total)	$-5.75 * 10^{-2}$	$-5.78 * 10^{-2}$	-0.4
^{1}H	(n,scat)	$4.17 * 10^{-1}$	$3.59 * 10^{-1}$	13.9
	(n,capture)	$-8.06 * 10^{-2}$	$-6.86 * 10^{-2}$	14.9
	(n,total)	$3.36 * 10^{-1}$	$2.90 * 10^{-1}$	13.6
^{16}O	(n,scat)	$8.77 * 10^{-2}$	$4.55 * 10^{-2}$	48.1
	(n,capture)	$-2.44 * 10^{-3}$	$-2.33 * 10^{-3}$	4.7
	(n,total)	$8.53 * 10^{-2}$	$4.32 * 10^{-2}$	49.4

Table 4.26: Comparison of MOX Core sensitivities (%/%) obtained from DRAGON **SNS:** with B_1 z-axial buckling with a transport correction (DR-B_1) and reference results obtained from SCALE/TSUNAMI 3D provided by IRSN [107, 109]. *: Explicit component of the sensitivity. ‡: Complete (implicit+explicit) component of the sensitivity.

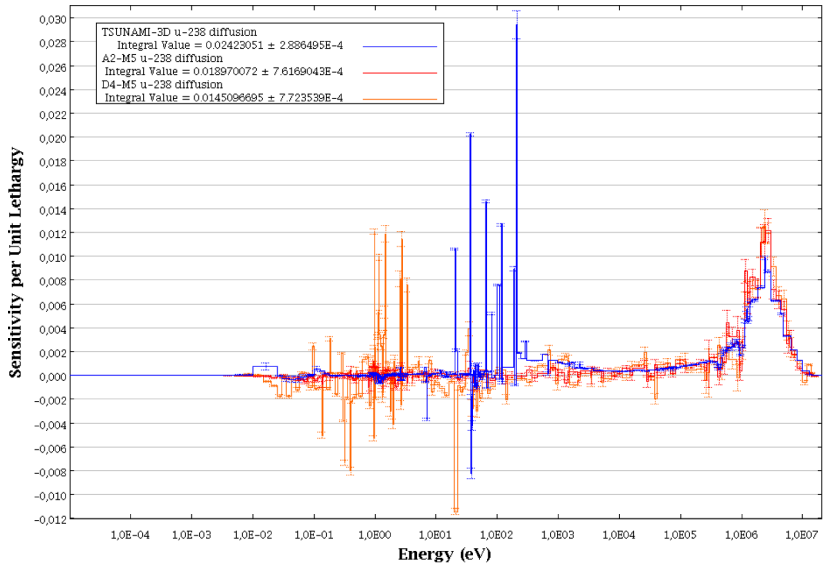

Figure 4.23: MOX core with light water reflector: ^{238}U (n,scat) sensitivity profiles (%/%)/du. **Figure Reproduced from [109]**. APOLLO2/MORET5 (red) P_1: integrated=$0.024 \pm 2.89 * 10^{-4}$ (%/%). DRAGON-4/MORET5 P_1 (orange): integrated $0.019 \pm 7.62 * 10^{-4}$ (%/%). TSUNAMI-3D P_5 (blue): integrated $0.015 \pm 7.72 * 10^{-4}$ (%/%). Note the discrepancy at high energy due to anisotropy.

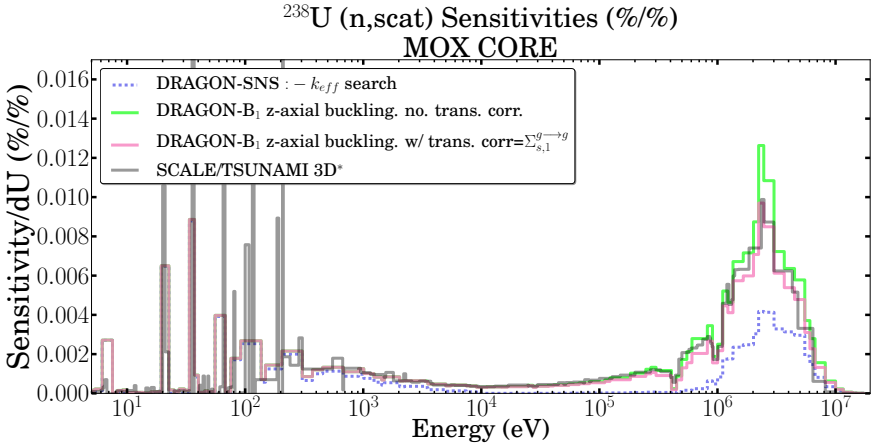

Figure 4.24: MOX core with light water reflector: ^{238}U (n,scat) **complete (explicit + implicit)** sensitivity profile (%/%)/du. SCALE/TSUNAMI 3D* results supplied by the IRSN[107]. Note is the discrepancy at high energy due to anisotropy, and the improved comparison of SCALE/TSUNAMI 3D P_5 with DRAGON **SNS:** B_1 with a transport correction in comparison to APOLLO2/DRAGON-4/MORET5, and the inaccuracy of DR-K approach (dotted blue).

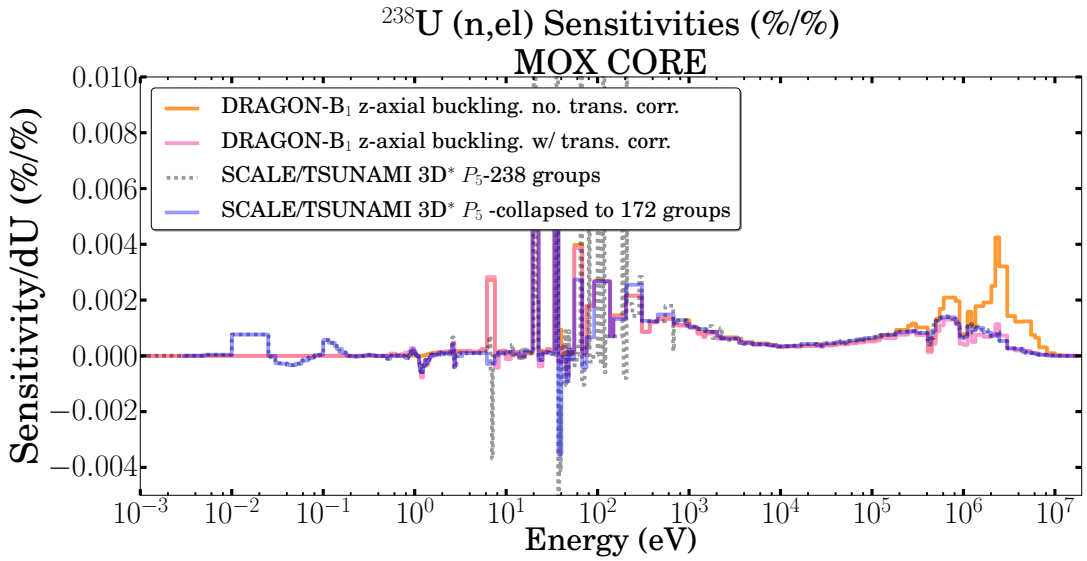

Figure 4.25: MOX core with light water reflector: ^{238}U (n,el) sensitivity profile (%/%)/du. *SCALE/TSUNAMI 3D results supplied by the IRSN[107] Note the effect of the transport correction, and the accuracy of our approximation for retrieving (n,el) partial cross sections.

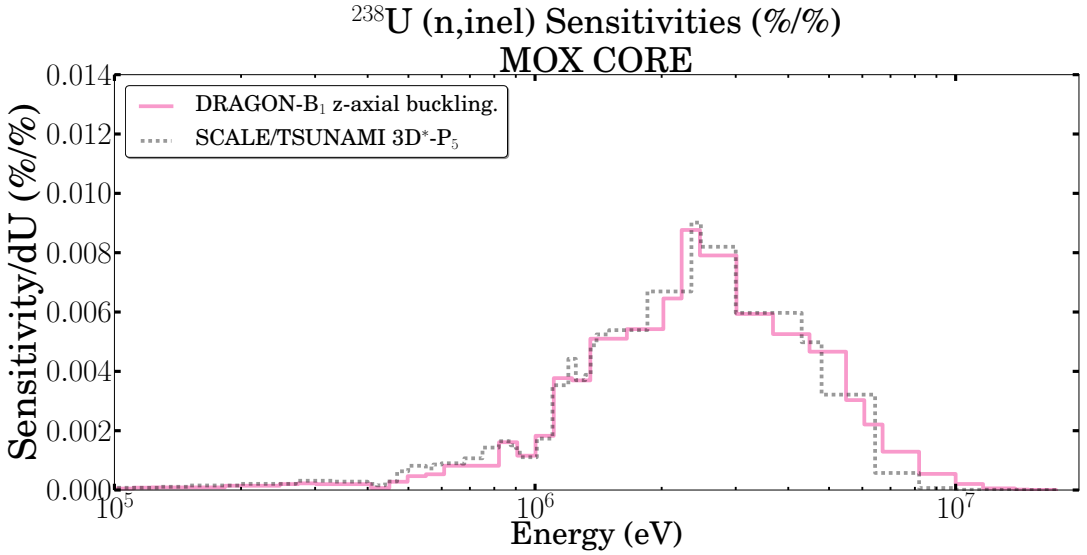

Figure 4.26: MOX core with light water reflector: ^{238}U (n,inel) sensitivity profile (%/%)/du. SCALE/TSUNAMI 3D* results supplied by the IRSN[107]. Note the accuracy of our approximation for retrieving (n,inel) partial cross sections.

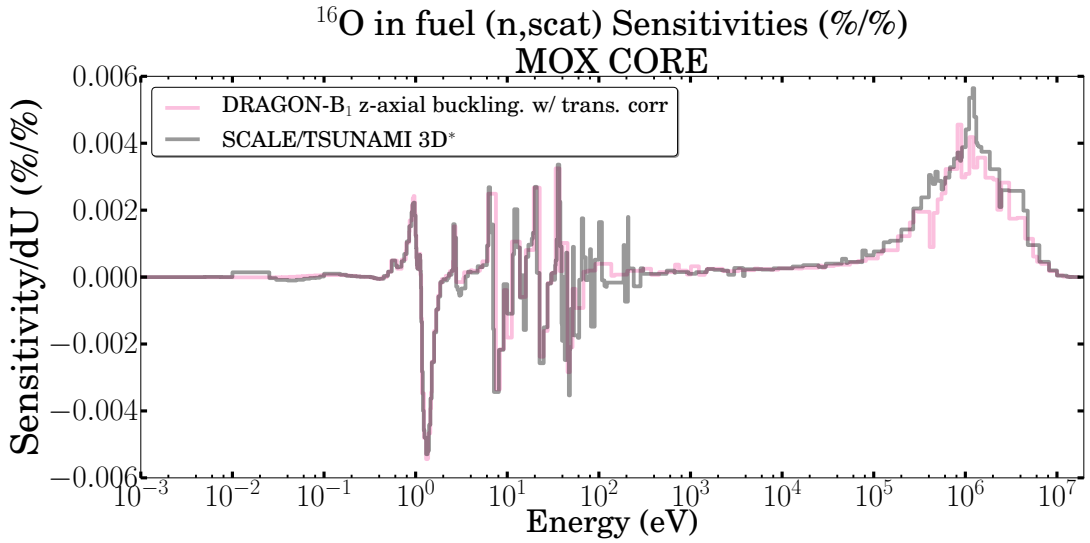

Figure 4.27: MOX core with light water reflector: ^{16}O (n,scat) sensitivity profile (%/%)/du *SCALE/TSUNAMI 3D P_5 results supplied by the IRSN[107] Note the good comparison of DRAGON-B_1 results with SCALE/TSUANMI 3D results for ^{16}O (n,scat) in the fuel where the buckling approximation is valid.

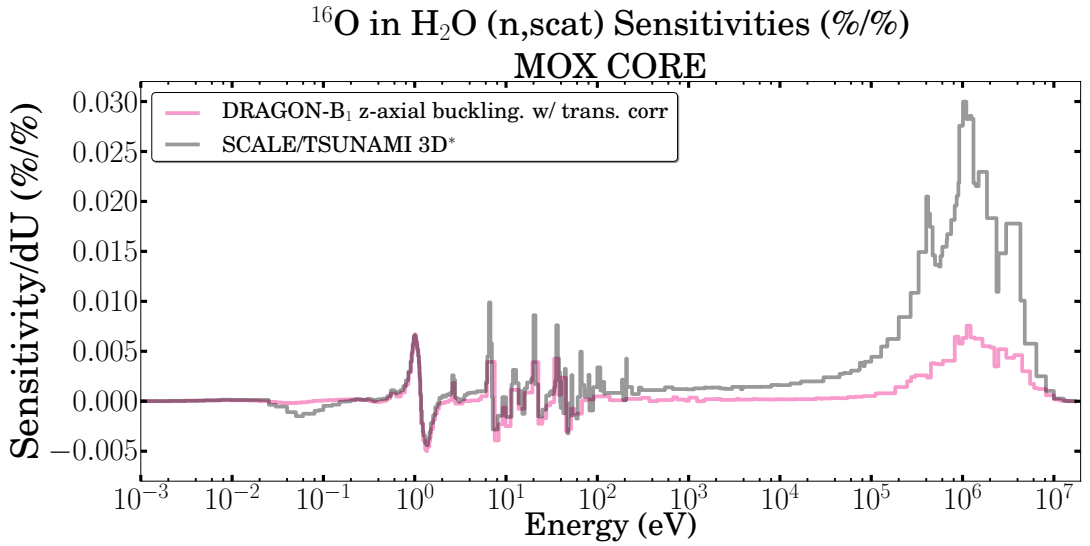

Figure 4.28: MOX core with light water reflector: ^{16}O (n,scat) in H_2O sensitivity profile (%/%)/du. *SCALE/TSUNAMI 3D P_5 results supplied by the IRSN[107] Note the discrepancy between the DR-B_1 and the S5-P_5 results throughout the spectrum due to the inadequacy of the buckling approximation in the light water reflector.

4.3.3 Uncertainty Analysis

Much effort is at present devoted to covariance matrix generation. Different methods have been proposed and are being tested. This results in rather important differences among different covariance matrix evaluations. Despite the fact that cross-section evaluations often differ little as they are generally based on the same set of experimental data, differences in evaluations of cross-section uncertainties can be large. Since the verification of uncertainties is non-trivial, we used three sets of currently available covariance data. In this section, the spread of the uncertainties obtained in this way provides valuable information on the reliability and accuracy of currently available covariance data. In particular the following evaluations were used:

- SCALE-5.1 covariance library evaluation: These covariance files are older, but also very complete. The evaluation covers a large range of isotopes and reactions. The evaluation was originally intended for safety applications, so that the data are intentionally conservative. The resulting uncertainties are therefore generally larger than those based on best-estimate evaluations.

- SCALE-6 covariance library evaluation: These covariance files are more recent than the SCALE 5.1 covariance files, and provide a very complete evaluation based on more modern data. The evaluation includes an ensemble of covariances from various origins: ENDF/B-VI, ENDF/VII, JENDL-3.3 and approximate (low-fidelity) covariances. The assumption here being that since nuclear data evaluations are similar and usually based on the same set of experiments, the covariances taken from one source/evaluation should provide a reasonable representation of uncertainties for the other evaluations. The matrices are intentionally conservative as they were also intended for safety applications.

- JENDL-4.0 evaluation: The Japanese JENDL evaluation has provided covariances matrices in their evaluation files for decades. JENDL-4.0 includes their most recent covariance data released. Covariances matrices exist for fewer isotopes when compared to the SCALE covariance library evaluations, but cover a larger range of reactions.

Tables 4.27 and 4.28 report (in pcm) the ^{238}U and ^{239}Pu reaction contributions to the k_{eff} uncertainty using the three mentioned uncertainty sources. We see that contributions and computed uncertainties differ drastically from one data source to another. For ^{238}U, it can be observed from table 4.27 that even though the computed uncertainty contribution from ^{238}U nuclear data uncertainties as predicted by SCALE5 covariances and JENDL-4 covariances is similar, the reaction contributions as predicted from each evaluation are drastically different. SCALE5 covariances report ^{238}U(n,capture) to be the reaction with the largest uncertainty contribution while SCALE6 and JENDL4 covariances report ^{238}U(n,inel) to be the highest contributor to the uncertainty. Similarly, as observed in table 4.28, the uncertainty data reported by the three evaluations for ^{239}Pu are different, with the SCALE evaluated covariance libraries predicting a total uncertainty approximately 3 times larger than the uncertainty predicted by JENDL 4.0 covariances. The largest difference here is due to the reported ^{239}Pu $\bar{\nu}$ uncertainties which can be observed in figure 4.30. We can conclude that, even with an accurate computation of the

sensitivities, given the differences in the covariance data, the task of predicting a reliable value for the contribution of nuclear data uncertainties to the total k_{eff} uncertainty is difficult.

^{238}U		Contribution to Uncertainty (pcm)		
		SCALE 5 Covariance Library	SCALE 6 Covariance Library	JENDL 4 Covariances
(n,capture)	(n,capture)	121	86	82
(n,inel)	(n,inel)	36	193	98
(n,el)	(n,capture)	-21	6.5	-2.8
(n,el)	(n,inel)	-10	-74	-
(n,f)	(n,f)	9	9	10
(n,f)	(n,capture)	-6	1	0.5
(n,el)	(n,el)	4	15	11
Contribution to k_{eff} uncertainty (pcm)		127	207	128

Table 4.27: Comparison of the ^{238}U uncertainty contributions obtained using SCALE 5, SCALE 6 and JENDL 4 covariance libraries. Note the differences in the predicted reaction uncertainty contributions and total isotope uncertainty contribution to the k_{eff}, that depend greatly on the covariance libraries.

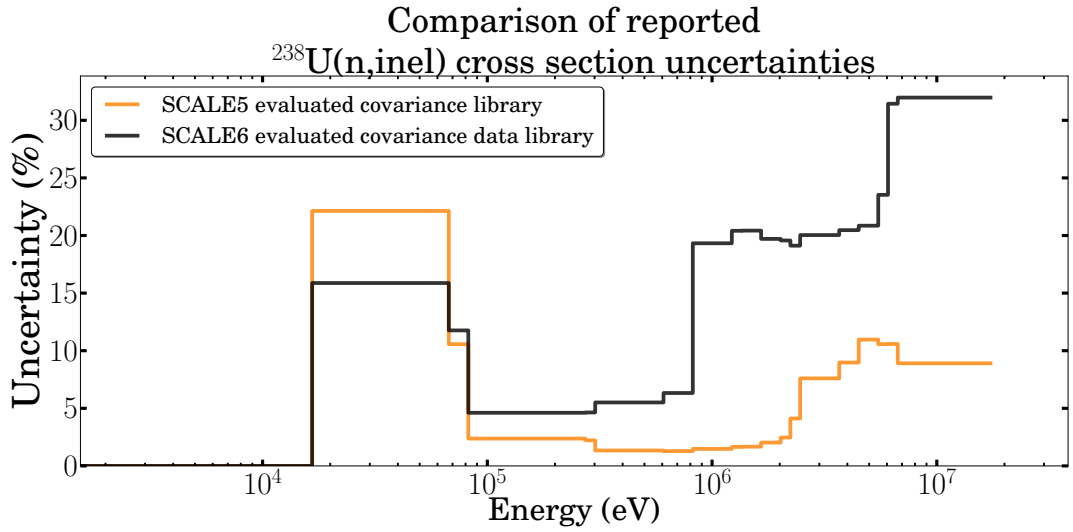

Figure 4.29: Comparison of reported ^{238}U(n,inel) cross section uncertainties. Uncertainty as reported by SCALE-5 evaluated covariance data library (orange curve). Uncertainty as reported by SCALE-6 evaluated covariance data library (black curve). Note the differences in the reported uncertainties at high energies.

^{239}Pu		Contribution to Uncertainty (pcm)		
		SCALE 5 Covariances	SCALE 6 Covariances	JENDL 4 Covariances
$\bar{\nu}$	$\bar{\nu}$	934	933	71
(n,capture)	(n,capture)	666	270	270
(n,f)	(n,f)	510	266	260
(n,f)	(n,capture)	-425	220	-
(n,inel)	(n,inel)	-	21	9
(n,el)	(n,el)	3	5	3
Contribution to the k_{eff} uncertainty (pcm)		1181	1032	381

Table 4.28: Comparison of the ^{239}Pu uncertainty contributions obtained using SCALE 5, SCALE 6 and JENDL 4 covariance libraries. Note the differences in the predicted reaction uncertainty contributions and total isotope uncertainty contribution to the k_{eff}, that depend greatly on the covariance libraries. See figure 4.31 for comparison of the $\bar{\nu}$ sensitivity profiles computed from using DR-B$_1$ and SCALE-5.

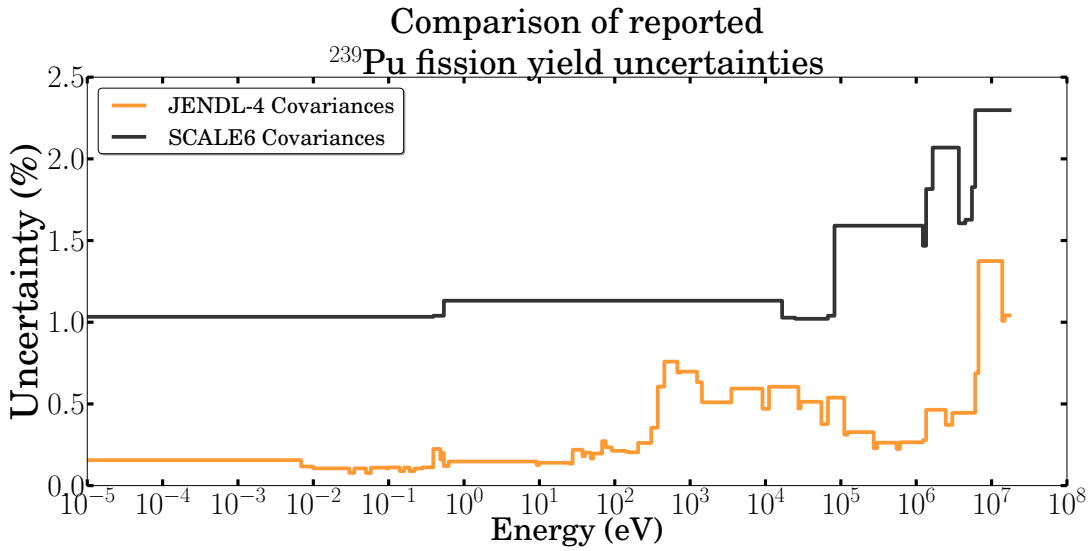

Figure 4.30: Comparison of reported ^{239}Pu $\bar{\nu}$ uncertainties. ^{239}Pu $\bar{\nu}$ uncertainty as reported by JENDL-4 (orange curve), and SCALE 6 evaluated covariance libraries (black curve).

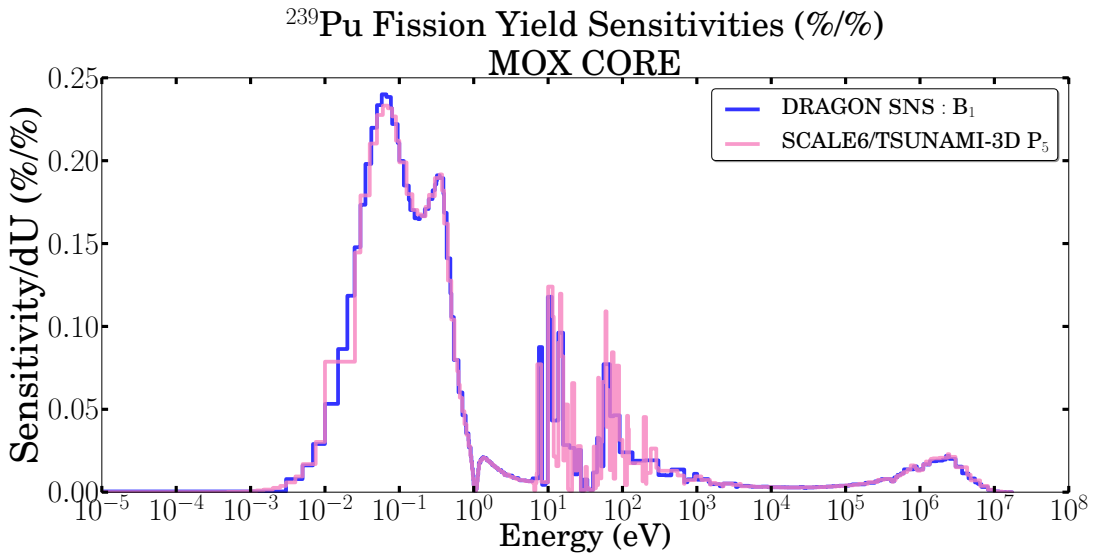

Figure 4.31: Comparison of computed ^{239}Pu $\bar{\nu}$ sensitivity profiles. DR-B_1 $\bar{\nu}$ sensitivity profile (blue). SCALE 5/TSUNAMI-3D $\bar{\nu}$ sensitivity profile (purple). SCALE 5/TSUNAMI-3D results provided by IRSN [106].

DR-K Approach

Finally, we note that if the sensitivities obtained from the DR-K approach are used in the uncertainty analysis, then the contribution from the reaction pairs ^{238}U(n,el)-(n,el) and ^{238}U(n,el)-(n,inel) are completely ignored as the ^{238}U elastic sensitivity would be computed as zero. With the SCALE6 covariances, the contribution of the (n,inel)-(n,inel) reaction pair is computed to be 102 pcm (instead of 193 pcm with DR-B_1), and the total uncertainty due to ^{238}U is computed to be 138 pcm (instead of 207 pcm with DR-B_1).

	Sensitivities (%/%)			
	Reaction	S5-P_5 [109]	DR-B_1	DR-K
^{238}U	(n,scat)	$1.605 * 10^{-2}$	$1.597 * 10^{-2}$	$5.40{*}10^{-3}$
^{239}Pu	(n,scat)	$2.89 * 10^{-3}$	$3.01 * 10^{-3}$	$5.62{*}10^{-4}$
^{240}Pu	(n,scat)	$3.97 * 10^{-4}$	$3.37 * 10^{-4}$	$6.01{*}10^{-5}$
^{1}H	(n,el)	$4.17 * 10^{-1}$	$3.59 * 10^{-1}$	$2.39{*}10^{-1}$
^{16}O	(n,scat)	$8.77 * 10^{-2}$	$4.55 * 10^{-2}$	$6.49{*}10^{-3}$

Table 4.29: Comparison of integrated explicit scattering sensitivities for the MOX core. S5-P_5: SCALE5/TSUNAMI-3D-P_5 sensitivities supplied by the IRSN [109, 107]. DR-B_1: DRAGON **SNS:** sensitivities obtained with a B_1 z-axial leakage model using transport corrected total and scattering cross sections. DR-K: DRAGON **SNS:** sensitivities obtained from the forward and adjoint flux from a k-search. Note the good agreement between S5-P_5 and DR-B_1 integrated sensitivities. Also note that, except for ^{1}H, the DR-K approach underestimates sensitivities by an order of magnitude.

Summary and Conclusion

In this thesis, we presented a comprehensive sensitivity and uncertainty analysis for reactor parameters such as the multiplication factor k_{eff}. We start our analysis at the fundamental step of the physics calculation - the Evaluated Nuclear Data File. By rigorously maintaining the consistency between cross section definitions used for the sensitivity computation and those used in transport computation, we demonstrated that, for the benchmarks considered, conventional deterministic formalisms such as the transport corrected diffusion approximation are sufficient to propagate nuclear-data uncertainties at a level of accuracy comparable to that observed by using state-of-the-art Monte Carlo or deterministic S_N transport tools.[19]

To perform the sensitivity and uncertainty analysis, we used several conventional approximations. Comparison of our methodology and results, with previous attempts at sensitivity and uncertainty analysis performed by other tools [113, 108] demonstrates that the sensitivity can, in some cases, be more affected by the consistency of the cross section data used during the sensitivity computation than by the model approximations. As long as these approximations are applied in a rational manner, and taken into account consistently in the sensitivity and uncertainty analysis, they can be as effective as several more complex and exact methods currently used for sensitivity and uncertainty propagation. We demonstrated this point for the buckling formalism and the analytical formula that we used to compute implicit sensitivities.

Sensitivity coefficients of integral observables on input parameters (such as cross sections) combined with covariance matrices are used to perform error propagation of input parameters. The most difficult sensitivity coefficient to compute is the sensitivity to scattering cross sections, not only because of the arduous task of accurately computing the energy gain and loss difference in the scattering formulas, but also because of the subtle nature that these reactions depend on the transport solution. While poorer agreement was observed for light isotope scattering sensitivity coefficients (particularly ^{16}O), due to the limitations of the transport correction in anisotropic systems, performance parameter uncertainties such as the k_{eff} are generally dominated by cross section uncertainties of heavy isotopes. An accurate computation of scattering sensitivities for heavy isotopes is vital as they can highly contribute to the uncertainty. Additionally, by establishing a consistent link between the cross section data used in the transport and sensitivity code

[19]Indeed, despite the rapid progress in computational power and Monte Carlo methods, deterministic transport codes (such as DRAGON, WIMS, APOLLO) and diffusion theory are still the main tools used by the industry for everyday core and safety computations highlighting the need for upgrading these tools with sensitivity and uncertainty analysis capabilities.

and the cross section data for which nuclear data uncertainties are expressed, we captured the fine role of the compensation of errors in the computation of uncertainties associated with heavy isotope scattering reactions such as, ^{238}U(n,inel) and ^{238}U(n,el).

While not presented in this report, a great part of the developments performed over the course of this study was concentrated on the sensitivity and uncertainty analysis for linear functionals of the flux, using Generalized Perturbation Theory. An example of such a computation for Breeding Ratio responses, as well as uncertainty propagation using the Total Monte Carlo method is provided in the Appendix. We have chosen not to include these results in these pages, as we believe that their true value will be more appreciated when coupled with a 2-group diffusion calculation of a full core, particularly for intended application to integral experiments. Application of sensitivity analysis tools to integral experiments can provide: (i) a validation of the coherence between the microscopic and the integral data, (ii) a qualification of the desired accuracies required for nuclear data, and (iii) if used with diligence, the improvement of the required base data to obtain attainable accuracies.

Finally, we provided a comparison between uncertainties predicted by three of the currently available and widely used nuclear data uncertainty evaluations. By comparing their respective results, we demonstrate that the evaluation of the uncertainty is a non-trivial task even after an accurate computation of the sensitivity. Indeed, the existence of limitations associated with evaluated cross-section data, when applied to designs that operate at different spectra, composition and fuel, is the prime motivation for most nuclear data sensitivity studies, on to which much effort has been recently directed. Many of such inadequacies can be alleviated through the (cautious) use of cross section adjustment techniques. Adjustment by sensitivities and least square procedures incorporate, and are strongly dependent on, the sensitivities. Therefore, a precise computation of sensitivities is vital, as poorly estimated sensitivity can lead to unwanted biases in the adjusted data. The fact that sensitivities to the entire ensemble of data under consideration must be integrated in the adjustment process is more crucial for the adjustment by sensitivities technique.

To summarize, the suite of codes we developed for sensitivity and uncertainty analysis with DRAGON permits for an accurate computation of sensitivities. It also provides a link between the data used in the transport computation and the base nuclear data. A continuation of the work presented in this study could be the application of the developed tools to cross section adjustment techniques, in the frame work of integral experiments. Such an application not only allows the qualification of uncertainties, but when used with caution, it can also provide a means for the improvement of the uncertainty through the amelioration of the cross section data.

Appendix A

Propagation of Nuclear Data Uncertainties in Deterministic Calculations: Application of Generalized Perturbation Theory and the Total Monte Carlo Method to a PWR Burnup Pin-Cell

Presented in the Nuclear Data 2013 International Conference

P. Sabouri[†1], A. Bidaud[†], S. Dabiran[‡], D. Lecarpentier[*], F. Ferragut[†]
[†]: LPSC/IN2P3/CNRS, Grenoble, France
[‡]: McMaster University, Hamilton, Canada
[*]: EDF, Clamart, France

A.1 Abstract

The development of tools for application to nuclear data uncertainty propagation in lattice calculations are presented. The Total Monte Carlo method and the Generalized Perturbation Theory method are used with the code DRAGON to allow propagation of nuclear data uncertainties in transport calculations. Both methods begin the propagation of uncertainties at the most elementary level of the transport calculation - the Evaluated Nuclear Data File. The developed tools are applied to provide estimates for response uncertainties of a PWR cell as a function of burnup.

A.2 Introduction

In recent years, the idea of supplying covariance data along with the Evaluated Nuclear Data File has become more systematic, leading to the inclusion of covariance data for

[1]Corresponding Author

a large number of isotopes in evaluations such as JENDL-4, ENDFB/VII, as well as TENDL. However, in comparison to the number of transport codes available, the number of tools which allow for the use of the provided data to propagate nuclear data uncertainties in transport calculations is limited. Performing such a propagation is often a difficult process, due to the different "definitions" of the neutron cross section which exist along the path of a deterministic calculation, as well as the task of uncertainty propagation itself.

A.3 Methodology

Currently, two major methods are available for uncertainty propagation in reactor calculations. The first method is Generalized Perturbation Theory (GPT) using covariance data in multi-group form along with sensitivity profiles obtained from GPT. The second method is the Total Monte-Carlo method (TMC) developed at NRG [1] requiring hundreds of identical simulations each starting with a unique Evaluated Nuclear Data File. Both methods have been implemented for use with DRAGON 3.06 [2] to allow for nuclear data uncertainty propagation.

Generalized Perturbation Theory

Generalized Perturbation Theory methods provide a rapid and accurate way to calculate sensitivities of responses of the flux to various changes in system conditions. For a linear ratio $R = \frac{\langle \Sigma_x, \phi \rangle}{\langle \Sigma_y, \phi \rangle}$, with Σ_x and Σ_y being arbitary functions and the inner product $\langle\ ,\ \rangle$ representing integration over space and energy, the adjoint fixed source problem is defined as [3]

$$\mathbf{L}^\dagger \Gamma^\dagger = \mathbf{S}^\dagger \Gamma^\dagger + \lambda \mathbf{F}^\dagger \Gamma^\dagger + \frac{\partial R}{\partial \phi} \tag{A.1}$$

where $\mathbf{L}$ is the loss operator of the Boltzmann equation in its differential form, $\mathbf{S}$ and $\mathbf{F}$ correspond to the scattering and fission gain terms of the Boltzmann equation, ϕ corresponds to the neutron flux and $\lambda = \frac{1}{k_{\text{eff}}}$ to the eigen-value of the Boltzmann equation. The sensitivity S_R^α (in %/%) to the nuclear data α may then be calculated as

$$S_\alpha^R = \frac{\alpha}{R}\frac{\partial R}{\partial \alpha} = \frac{\alpha}{R}\left\{ \overbrace{\frac{\partial R}{\partial \alpha}}^{\text{DIRECT}} + \overbrace{\left\langle \Gamma^\dagger, \partial_\alpha (\mathbf{L} - \mathbf{S} - \lambda \mathbf{F})\ \phi \right\rangle}^{\text{INDIRECT}} \right\} \tag{A.2}$$

The first term of Eq. (A.2) is defined as

$$\frac{\partial R}{\partial \alpha} = \frac{\langle \partial_\alpha \Sigma_x, \phi \rangle}{\langle \Sigma_y, \phi \rangle} - R\frac{\langle \partial_\alpha \Sigma_y, \phi \rangle}{\langle \Sigma_y, \phi \rangle}$$

and corresponds to the explicit/direct change in R resulting from the dependence of the functions Σ_x and Σ_y on α. The second term containing the generalized adjoint flux $\Gamma^\dagger$ represents the change in R due to the implicit change of the neutron flux ϕ on the parameter α.

In DRAGON, the flux ϕ is solved by using the Collision Probability (CP) method. The flux ϕ satisfies the integral form of the transport equation [24]

$$(\mathbf{I} - \mathbf{P}(\Sigma_T)\mathbf{S} - \lambda\mathbf{P}(\Sigma_T)\mathbf{F})\phi = 0 \tag{A.3}$$

where the CP matrix $\mathbf{P}(\Sigma_T)$, which may be thought of as the inverse of the loss operator $\mathbf{L}$ of the differential Boltzmann equation, is dense in space and sparse in energy. The adjoint of Eq. (A.3) for the response R is given as [24]

$$(\mathbf{I} - \mathbf{S^T}\mathbf{P^T} - \lambda\mathbf{F^T}\mathbf{P^T})\Gamma^* = \mathbf{P^T}\frac{\partial R}{\partial \phi} \tag{A.4}$$

where $^\mathbf{T}$ represents matrix transposition. Due to the non-commutativity of the CP matrix $\mathbf{P}$ with the operators $\mathbf{F}$ and $\mathbf{S}$, the adjoint of the integral equation Γ^* is not the same as the adjoint of the differential operator $\Gamma^\dagger$. The adjoint equation corresponding to the differential adjoint $\Gamma^\dagger$ can be recovered by multiplying Eq. (A.4) by the collision probability matrix $\mathbf{P}$ so that $\Gamma^\dagger = \mathbf{P}\Gamma^*$. The adjoint of the integral equation satisfies the relation $\Gamma^* = \mathbf{F^T}\Gamma^\dagger$. Ref. [5] interprets the adjoint Γ^* as the importance of the fission source to response R. Table A.1 presents comparisons for the largest sensitivities calculated using DRAGON 3.06 with those obtained from SCALE 6 (explicit contribution) for the breeding ratio $R = \left\langle \Sigma^{238U}_{(n,\gamma)}, \phi \right\rangle / \left\langle \sum_{I\in\text{fissile}} \Sigma^I_{(n,f)}, \phi \right\rangle$ corresponding to a 3.3% enriched PWR pin-cell defined in [103]. A final note should be made in regards to the application

Table A.1: Comparison of integrated sensitivities (%/%) of the Breeding Ratio obtained by SCALE 6 and DRAGON 3.

Reaction	SCALE	DRAGON
^{235}U(n,γ)	1.02	1.02
^{235}U(n,f)	-8.17×10^{-1}	-8.18×10^{-1}
^{238}U(n,f)	-5.11×10^{-2}	-5.14×10^{-2}
^{238}U(n,scat)	1.26×10^{-2}	1.019×10^{-2}
^{1}H(n,γ)	8.10×10^{-3}	-8.25×10^{-3}
^{238}U(n,γ)	2.25×10^{-3}	-1.54×10^{-3}
^{1}H(n,scat)	-1.95×10^{-3}	-1.99×10^{-3}

of GPT methods with CP. Firstly, due to the integral nature of the transport solution, forward and adjoint fluxes for a large range of geometries involving non-centered meshes are available. In particular, one does not need to resort to cylindrization or cartesianization of the geometry as is common with S_N codes. Secondly, the most computationally intensive part of the transport calculation (accounting for between 90% to 97% of the computational time) is spent in the calculation of the CP matrix $\mathbf{P}$. This calculation only needs to be performed once, which makes GPT methods with CP extremely fast in comparison to other methods such as S_N or MOC.

The Total-Monte Carlo Method

The TMC method provides an easy, accurate and flexible way to propagate nuclear data uncertainties. Hundreds of identical simulations are neccessary for each isotope, each starting with a unique ENDF. The Evaluated nuclear data files are provided by NRG using their TALYS code [1]. A multi-group library corresponding to each ENDF is constructed using the NJOY code. A simulation with DRAGON is then performed using the constructed multi-group library. The standard deviation/uncertainty in output parameters due to nuclear data uncertainties may then be calculated. Reference [8] reports convergence of the standard deviation with a negligible skewness for a sample number larger than 200. The data used in this work is ENDF's supplied by NRG with their the TENDL-2011 evaluation [7].

Covariance Data and Multi-Group Covariances

As a result of the multi-group approximation, the continuous spectrum cross sections $\sigma(E)$ are transformed into tabulated sets of multi-group cross section σ^g. The multi-group cross sections $\sigma^g = \int_{E_g}^{E_{g+1}} \sigma(E)\phi(E)dE / \int_{E_g}^{E_{g+1}} \phi(E)dE$ are obtained by averaging the continuous spectrum cross section in the group interval $[E_g, E_{g+1}]$ with the slowing down flux $\phi(E)$. The slowing down flux $\phi(E)$ corresponds to the flux in an infinite homogeneous mixture of the resonant isotope and a moderator with different concentrations of the resonant isotope, at various temperatures. The Narrow Resonance approximation provides a simple analytical formula for the weighting flux given by [9]

$$\phi(E) = \frac{\sigma_p^r + \sigma_0}{\sigma_t^r(E) + \sigma_0} \frac{1}{E} \tag{A.5}$$

where σ_p^r and $\sigma_t^r(E)$ are the potential scattering and total cross section of the resonant isotope, and $\sigma_0 = \frac{N_m}{N_r}\sigma_p^m$ is the product of the ratio of the concentration of the moderator N_i to the concentration of the resonant isotope N_r with σ_p^m being the potential scattering cross section of the moderator. In an infinitely dilute medium ($\sigma_0 \to \infty$), the weighting flux approaches $\phi(E) = \frac{1}{E}$ while for a low dilution of the resonant isotope with the moderator ($\sigma_0 \to 0$), the weighting flux is given by $\phi(E) = \frac{\sigma_p^r}{\sigma_t^r(E)} \frac{1}{E}$. Due to the variation of the weighting flux as a function of dilution, one should expect the uncertainties and covariances corresponding to multi-group cross sections at infinite dilution to be different than those corresponding to finite dilution. A better parameter for disscussion of cross section data in this range is the resonance integral $RI = \int \sigma(E)\phi(E)dE / \int \frac{1}{E}dE$, defined as the absorption cross section leading to the same reaction rate in the resonance had the resonance not been there. At large dilutions (corresponding to low levels of self shielding), the contribution of the cross section $\sigma(E)$ to the resonance integral of Eq. (A.5) is dominated by the largest resonance peaks, so that the uncertainty on the resonance integral is resulting primarily from the uncertainties on the magnitude of the strongest resonances. When self shielding becomes stronger (at low dilutions), due to the strong suppression in the weighting flux of Eq. (A.5) at the resonance, the contribution to the resonance integral uncertainty from the uncertainty of the magnitude of the peaks becomes lower, while the contribution of the uncertainty and correlations of the dips

between the resonances increases. The expected effect observed is an increase in the resonance integral uncertainty with an increase in self shielding (decreasing σ_0) [10].

If the only information in the ENDF file [11] is file 33 (group covariances supplied by the evaluator at infinite dilution), the effect of the variation of the resonance integral uncertainty as a function of dilution is not possible to capture. Furthermore, due to a current limitation in the NJOY ERRORR module [12], even if file 32 (covariances of resonance parameters) is provided, the effect is not possible to capture.

These current limitations are handled by generating covariance matrices from the constructed multi-group libraries produced from the NRG's ENDFs. The covariances are calculated for the temperature and dilution values available on the library. It should be noted that in TENDL-2011, the sampled ENDFs do not contain any covariances between resonance parameters. The uncertainty at infinite dilution is therefore over-estimated with the uncertainty on the resonance integral relatively constant as a function of dilution. For the highest resonances, differences of one order of magnitude in the RI uncertainty are noticed as a function of dilution. Ref. [10] has reported a variation of the resonance integral uncertainty corresponding to two orders of magnitude (decreasing with an increase in dilution) when sampling from the full covariance matrices (with lower resonance peak uncertainties in comparision to the NRG data) provided by ORNL.

A final note should be made in regards to the differences in the definition of cross section reactions between the data normally contained in multi-group libraries and general cross section data (such as those obtained by the NJOY GROUPR module). To reduce unneccessary computational time as well as save storage space, most multi-group libraries (such as the WIMSD4 format [9]) contain data corresponding to lumped reactions. For example, the "absorption" cross section in WIMSD4 format is defined as $\sigma_{ABS} = \sum_{x\in \text{ absorption}} \sigma_x - \sigma_{(n,2n)} - 2 * \sigma_{(n,3n)}$. Lumped covariance matrices corresponding to the absorption cross section can be created by using the procedure outlined in [13].

A.4 Preliminary Results for Evolution Calculations

Table A.2 reports the total uncertainty of isotopic densities N_I due to the nuclear data uncertainties in ^{235}U, ^{238}U, and ^{239}Pu at the end of the cycle for a 3.7% enriched PWR pin cell at a power of 38 kW/kg. The uncertainty of $N_{^{236}U}$ due to the nuclear data

Table A.2: Isotopic density uncertainties (%) for 3.7% enriched PWR cell at 60 GW d T^{-1}.

Isotope	$\sigma(N_I)$	Isotope	$\sigma(N_I)$
^{236}U	1.91%	^{238}Pu	1.40%
^{239}Pu	2.20%	^{240}Pu	1.95%
^{241}Pu	1.66%	^{242}Pu	1.24%
^{237}Np	1.44%	^{242}Am	1.25%

uncertainties of ^{235}U is 1.9% and remains roughly constant as a function of burnup. At the first time step, the uncertainty is the same as that of the capture rate of ^{235}U (i.e. $R = \frac{\left\langle \Sigma^{235}_{(n,\gamma)}, \phi \right\rangle}{\left\langle \sum_{I\in \text{fissile}}, \phi \right\rangle}$) with 60% of the contribution to the variance coming from the

uncertainty on the fission cross section of ^{235}U which has an integrated sensitivity of -0.85 (%/%): 20% of the contribution coming from the uncertainty on capture rate of ^{235}U (having an integrated sensitivity of 1.04%/%) and the remaining 20% from the reported correlation between the capture and fission cross sections. Similarily, the uncertainty of $N_{^{239}Pu}$ at the first time step is identical to the uncertainty of the breeding ratio

$$R = \frac{\left\langle \Sigma^{238}_{(n,\gamma)}, \phi \right\rangle}{\langle \sum_{I \in \text{fissile}}, \phi \rangle}$$

and has a value of 0.93%: 88% of the contribution to the variance is from the uncertainty of the capture cross section of ^{238}U (having an integrated sensitivity of 0.96 %/%) and the remaining 12% from the correlation between the scattering (with an integrated sensitivity of 0.2%/%) and capture.

In general, the uncertainty for a response $R(\bar{N}, \bar{\alpha})$, where $\bar{N} = (N_I)$ is the vector of isotopic densities and $\bar{\alpha} = (\alpha_i)$ is the vector of to the nuclear data parameters, can be calculated by

$$\begin{aligned}(\delta R)^2 = &\sum_{i,j} \frac{\partial R}{\partial \alpha_i} COV(\alpha_i, \alpha_j) \frac{\partial R}{\partial \alpha_j} \\ &+ \sum_{I,J} \frac{\partial R}{\partial N_I} COV(N_I, N_J) \frac{\partial R}{\partial N_J} \\ &+ 2 * \sum_{I,j} \frac{\partial R}{\partial N_I} COV(N_I, \alpha_j) \frac{\partial R}{\partial \alpha_j}\end{aligned} \tag{A.6}$$

where the first term represents the direct contribution to the uncertainty δR due to the uncertainties and correlations of the nuclear data vector $\bar{\alpha}$, the second term accounts for the contribution of the uncertainties and correlations in the isotopic densities $\bar{N}$ (for example, the negative correlation between $N_{^{238}U}$ and $N_{^{239}Pu}$) and the third term represents the contribution from the correlations which exist between the nuclear data and the isotopic densities (for example the negative correlation between the fission of ^{235}U and the density of ^{239}Pu resulting from the constant power constraint). The ideal way to calculate the terms in the above equation is by use of Generalized Perturbation Theory for the coupled Boltzmann and Bateman equations (for instance, as outlined in [5]). Such a formalism is currently under development in DRAGON.

At the start of the cycle, the sensitivities $\frac{\partial R}{\partial N_I}$ for the isotopes not initially existant in the fuel may be small, in which case the second and third terms of Eq. (A.6) can be ignored. In this case the first term of Eq. (A.6) can be calculated by using static GPT calculations at each step. Table A.3 presents comparisons for the uncertainties obtained using static GPT calculations at (ignoring the second and third in Eq. (A.6)) with those obtained by TMC. As seen, with the exception of the computed uncertainty for the Breeding Ratio due to nuclear data uncertainties of ^{238}U , the approximation is valid well until Middle of Life. For the case of ^{238}U, the negative correlations between the atomic densities of ^{238}U and ^{239}Pu, and the negative correlations between the fission of ^{235}U and the number density of ^{239}Pu (as a result of the constant power condition) result in a steady decrease in the breeding ratio uncertainty. The two contributions correspond to the second and third term of Eq. (A.6), respectively. The effect is not

Table A.3: Comparison of Uncertainties obtained for the k_{eff} and Breeding Ratio at BOL, MOL (30 GWdT^{-1}) and EOL (60 GWdT^{-1}).

Material		k_{eff}		Breeding Ratio	
		TMC	GPT	TMC	GPT
BOL	^{235}U	0.48%	0.49%	0.89%	0.86%
BOL	^{238}U	0.34%	0.32%	0.93%	0.97%
MOL	^{235}U	0.23%	0.24%	0.35%	0.39%
MOL	^{238}U	0.34%	0.35%	0.62%	1.02%
MOL	^{239}Pu	0.39%	0.40%	0.38%	0.42%
EOL	^{235}U	0.12%	0.10%	0.07%	0.15%
EOL	^{238}U	0.44%	0.38%	0.27%	1.02%
EOL	^{239}Pu	0.45%	0.59%	0.36%	0.60%

captured resulting in an overestimation of the Breeding Ratio uncertainty. At the End of Life, the correlations of the second and third term of Eq. (A.6) result in a reduction in the overall uncertainty.

A.5 CONCLUSIONS

A consistent methodology for the propagation of nuclear data uncertainties in transport calculations for use with DRAGON using the Total Monte Carlo method and the Generalized Perturbation Theory method has been presented. The two methods were applied to a PWR lattice cell for evolution calculations. The uncertainty propagation starts at the most elementary point of a transport calculation- namely the Evaluated Nuclear Data File. With the exception of the Breeding Ratio uncertainty due to ^{238}U, preliminary results for the evolution of response uncertainties as a function of burnup using GPT are in accordance with those obtained by the Total Monte Carlo method well until MOL. However, ignoring the correlations between nuclide densities and their correlations with the nuclear data results in an overestimation of the uncertainty on the calculated response parameters at the end of life. This shortcoming can be resolved through the implementation of GPT for the coupled Boltzmann and Bateman equations. The effect highlights the contribution of the isotopic density uncertainties and correlations in reducing the total uncertainty for calculated response prameters at the EOL.

The authors are indebted to Dr. D. Rochman (NRG) for having supplied the ENDFs which form the base of this work as well as for the many constructive correspondences

which allowed the use of the provided data.

Bibliography

[1] R. Rochman, *et al.*, J. Korean. Phys. Soc. **59**, 1236, (2011).

[2] G. Marleau, *et al.*, Report IGE-157 (1993).

[3] G. Greenspan, *et al.*, Advc. Nucl. Sci. Tech. **8**, 190, (1980).

[4] T. Courau, *et al.*, Nucl. Sci. Eng **143**, 19, (2003).

[5] G. Greenspan, *et al.*, Advc. Nucl. Sci. Tech. **14**, 210, (1980).

[6] K. Ivanov, *et al.* , Specification of Phase I of OECD LWR UAM, Nuclear Energy Agency, (2011).

[7] ftp://ftp.nrg.edu/pub/wwww/talys/random/random.html.

[8] D. F. da Cruz *et al.*, Proc. of ICAPP 12, 12093 (2012).

[9] WIMS-D LIBRARY UPDATE, IAEA, (2007).

[10] G. Zerovnik, Use of Covariance Matrices for Estimating Uncertainties in Reactor Physics Calculations, Doctoral Dissertation, IJS, (2012).

[11] M. W. Herman, *et al.*, ENDF-6 Formats Manual, (2009).

[12] R. E. MacFarlane, The NJOY Data Processing System, Oak Ridge National Laboratory, (2006).

[13] P. Sabouri, *et al.*, Proc. Physor 2012, **274**, Physor (2012).

Chapter 1

Fondements théoriques

1.1 Données Nucléaires

Les données nucléaires sont à la base de tout calcul de réacteurs. Par conséquent, une bonne connaissance est essentielle dans le calcul de physique des réacteurs. Ces données, présentées sous la forme de sections efficaces nucléaires, décrivent les modes d'interaction possibles pour les neutrons avec des noyaux cibles.

1.2 Matrice de Covariance

Une valeur physique est caractérisée par sa moyenne <q> et la fonction de distribution P(q) qui détermine son incertitude. Quand q est discret, avec un nombre fini de valeurs possibles Q_i et une fonction de distribution de probabilité P(q), la valeur moyenne de q est définie par:

$$< q >= \sum_i q_i P(q_i) \tag{1.1}$$

La précision de q est définie par la différence entre la moyenne et la distribution de la probabilité associée, c'est-à-dire la racine carrée de la variance:

$$\sigma_q^2 = var(q) = (\Delta q)^2 =< (q - < q >)^2 >= \sum_i (\delta q_i)^2 \frac{1}{N} \tag{1.2}$$

où $\delta q_i \equiv q_i - < q >$.

Dans le cas de nombreuses variables, caractérisant la fonction de probabilité $P(\vec{q})$, il est exigé non seulement la connaissance de la moyenne et

de la variance, mais aussi les corrélations entre les échantillons obtenus. Où $\vec{q} = (q_i)_{i=1}^{N}$ est un vecteur composé des n variables q_i. Il est possible pour les variables différentes q_i d'avoir des corrélations entre elles. Ces corrélations sont normalement représentées en notation matricielle par la *matrice de covariance* $\mathbf{V} = (V_{ij})$:

$$\mathbf{V} = \left\langle (\vec{q} - \langle \vec{q} \rangle) \cdot (\vec{q} - \langle \vec{q} \rangle)^T \right\rangle \tag{1.3}$$

où $^{\mathbf{T}}$ représente la transposition vectorielle. Les éléments de la matrice V_{ij} sont définis:

$$V_{ij} = \langle (q_i - \langle q_i \rangle) \cdot (q_j - \langle q_j \rangle) \rangle = \langle \delta q_i \cdot \delta q_j \rangle \tag{1.4}$$

Pour $j = i$, nous avons:

$$V_{ii} = \left\langle \delta {q_i}^2 \right\rangle = var(q_i) \tag{1.5}$$

Les éléments de la matrice de corrélation sont définis comme:

$$C_{ij} = \frac{V_{ij}}{\sqrt{V_{ii} V_{jj}}} = \frac{\langle \delta q_i \cdot \delta q_j \rangle}{\Delta q_i \Delta q_j} \tag{1.6}$$

où $\Delta q_i = \sqrt{V_{ii}}$ est l'écart-type.

1.3 Les Bibliothèques de Sections efficaces et Les Fichiers de Covariance

Les valeurs de section efficace proviennent de mesures physiques ainsi que des modèles physiques. Cependant, avant d'être utilisées dans des calculs, elles doivent être validées. L'objectif du processus de validation est de montrer que les résultats obtenus sont cohérents et complets.

L'évaluation des sections efficaces est réalisée par de nombreux organismes et est présentée sous la forme d'une évaluation de la bibliothèque des sections efficaces, mise à jour périodiquement. Parmi les évaluations récentes, préparées dans les laboratoires différents, nous pouvons citer: ENDF / B-VII (USA), JEFF 3.1 (UE), JENDL 4.0 (Japon), BROND (Russie), CENDL (Chine), et TENDL (Hollande).

1.4 Les Calculs Déterministes

Le transport des neutrons dans un réacteur est un processus de diffusion. Un neutron est né à hautes énergies, se déplace dans le réacteur tout en étant ralenti par des collisions de diffusion élastique et inélastique. Pendant ce temps, le neutron peut être perdu en raison de fuites ou il peut être capturé, ou interagir dans une réaction de production de neutrons tel que (n, 2n), (n, 3n), et de (n, f). Le paramètre d'intérêt pour décrire ce système est le flux de neutrons $\phi(\bar{\rho})$, donné par l'équation de Boltzmann.

1.4.1 Équation de Boltzmann

Dans sa forme intégro-différentielle [8], en supposant que les neutrons sont émis par fission isotrope et que les probabilités d'interaction sont invariantes par rotation, l'équation du transport des neutrons est:

$$\hat{\Omega} \cdot \vec{\nabla}\phi(\vec{r}, \hat{\Omega}, E) + \Sigma(\vec{r}, E)\phi(\vec{r}, \hat{\Omega}, E) = Q(\vec{r}, E, \hat{\Omega}) \tag{1.7}$$

La *source de collision* $Q(\vec{r}, E, \hat{\Omega})$ est définie par:

$$Q(\vec{r}, E, \hat{\Omega}) = \int_{\hat{\Omega}'} d\hat{\Omega}' \int_{E'} dE' q(\vec{r}, \hat{\Omega}' \to \hat{\Omega}, E' \to E) \tag{1.8}$$

où la *densité de collision* $q(\vec{r}, \hat{\Omega} \to \hat{\Omega}, E \to E)$ est:

$$q(\vec{r}, \hat{\Omega}' \to \hat{\Omega}, E' \to E) = \overbrace{\frac{\chi(\vec{r}, E)}{4\pi k_{eff}} \nu(E') \Sigma_f(\vec{r}, E') \phi(\vec{r}, \hat{\Omega}', E')}^{\text{Fission density}} + \overbrace{\Sigma_s(\vec{r}, \hat{\Omega}' \to \hat{\Omega}, E' \to E) \phi(\vec{r}, \hat{\Omega}', E')}^{\text{Scattering density}} \tag{1.9}$$

où :

- $\phi(\vec{r}, \hat{\Omega}, E)$: le flux angulaire de neutrons à $\vec{r}$, dans la direction $\hat{\Omega}$ et à l'énergie E.

- $\Sigma(\vec{r}, E)$: la section efficace macroscopique totale à $\vec{r}$ et énergie E.

- $\Sigma_f(\vec{r}, E')$:

la section efficace macroscopique de fission à $\vec{r}$ et énergie E'.

- ν: le nombre moyen de neutrons produits par fission.

- $\chi(\vec{r}, E)$: le spectre de fission à neutrons à $\vec{r}$ et énergie E; n

- $\Sigma_s(\vec{r}, \hat{\Omega}' \to \hat{\Omega}, E' \to E)$: la section efficace différentielle pour un neutron d'énergie E' et direction $\hat{\Omega}$ de disperser à un neutron à l'énergie $E + dE$ et direction $\hat{\Omega} + d\hat{\Omega}$.

- k_{eff}: le facteur de multiplication effectif.

Équation 1.7 est une équation de conservation. Le terme à gauche représente les neutrons perdus à cause des fuites et des collisions, et le terme à droite représente la source de fission, de diffusion.

1.4.2 L'Anisotropie et la Correction de Transport

La correction de transport est une approximation utilisée pour réduire la dépendance angulaire de la source de collision $Q(\vec{r}, \hat{\Omega}' \to \hat{\Omega}, E' \to E)$. En utilisant la correction de transport, l'équation de Boltzmann devient:

$$\hat{\Omega} \cdot \nabla\phi(\vec{r}, E, \hat{\Omega}) + \bar{\Sigma}(\vec{r}, E)\phi(\vec{r}, E, \hat{\Omega}) = \bar{Q}(\vec{r}, E) \tag{1.10}$$

où [14]:

$$\bar{\Sigma}(\vec{r}, E) = \Sigma(\vec{r}, E) - \Delta\Sigma_{tr}(\vec{r}, E) \tag{1.11}$$

$$\bar{\Sigma}_{s,0}(\vec{r}, E' \to E) = \Sigma_{s,0}(\vec{r}, E' \to E) - \delta(E' - E)\Delta\Sigma_{tr}(\vec{r}, E) \tag{1.12}$$

$$\Delta\Sigma_{tr}(\vec{r}, E) = \int_0^\infty dE' \Sigma_{s,1}(\vec{r}, E \to E') \tag{1.13}$$

L'équation 1.10, prend partiellement en compte l'effet d'anisotropie linéaire de la diffusion. En réduisant la section efficace totale à la section efficace corrigée, définie par l'équation 1.11, la longueur de diffusion du neutron est augmentée. Cela imite l'effet de l'anisotropie linéaire de la diffusion: le neutron diffusé par le choc anisotrope va continuer dans la direction vers

l'avant.

1.4.3 Formulation intégrale

La forme intégrale de l'équation 1.10 est donnée par:

$$\vec{\phi}(\vec{r},E) = \int_{\vec{r'}\in D} \frac{\exp(-\tau(s,E))}{s^2} q(\vec{r'}, E' \to E) d^3\vec{r'} + \int_{\vec{r'}\in \partial D} \frac{\exp(-\tau(s_s,E))}{s_S^2} \left(\hat{\Omega}\cdot\hat{n}_-\right) \phi_-(\vec{r}_S, E, \hat{\Omega}') d^2r' \qquad (1.14)$$

où $\phi_-(\vec{r}, E, \hat{\Omega}')$ est le flux angulaire entrant à la surface ∂D avec l'intérieur normale $\hat{n}_-$.
Le premier terme de l'équation 1.14 représente la contribution de la source de collision q, au flux neutronique à $\vec{r}$. Le deuxième terme est la contribution de tous les neutrons entrants dans la surface ϕ_-.

1.5 Forme Discrétisée

Une solution numérique d'une équation nécessite une discrétisation. En discrétisant l'espace et la surface, et en utilisant l'approximation multigroupe de discrétiser sur l'énergie, l'équation 1.10 devient:

$$\phi_{i,g} = \sum_{\alpha=1}^{N_S} \sum_{\mu=0}^{N_\nu} p_{i\alpha}^{\mu,g} \phi_{-,g}^{\mu,\alpha} + \sum_{j=1}^{N_V} \sum_{g'=1}^{N_G} p_{ij}^{g} Q_{j,g} \qquad (1.15)$$

$$\phi_{+,g}^{\nu,\alpha} = \sum_{\beta=1}^{N_S} \sum_{\mu=0}^{N_\nu} p_{\alpha\beta}^{\nu\mu,g} \phi_{-,g}^{\mu,\beta} + \sum_{g'=1}^{N_G} \sum_{j=1}^{N_V} p_{\alpha j}^{\nu,g} Q_{j,g} \qquad (1.16)$$

avec les probabilités de première collision définies par:

$$p_{ij}^{g} = \frac{1}{V_i} \int_{\vec{r}\in V_i} \int_{\vec{r'}\in V_j} \frac{e^{-\tau^g(s)}}{s^2} d\vec{r'} d\vec{r} \tag{1.17}$$

$$p_{i\alpha}^{\nu,g} = \frac{1}{V_i} \int_{\vec{r'}\in V_i} \int_{S_\alpha} \frac{e^{-\tau^g(s_S)}}{4\pi s_S^2} (\hat{\Omega}\cdot\hat{N}_-)\psi^\nu(\hat{\Omega},\hat{N}_-) d\vec{r'} dA_{S_\alpha} \tag{1.18}$$

$$p_{\alpha i}^{\nu,g} = \frac{4}{S_\alpha} \int_{S_\alpha} \int_{\vec{r}\in V_i} \frac{e^{-\tau^g(s)}}{s^2} (\hat{\Omega}\cdot\hat{N}_+)\psi^\nu(\hat{\Omega},\hat{N}_+) dA_{s_\alpha} d\vec{r} \tag{1.19}$$

$$p_{\alpha\beta}^{\nu\mu,g} = \frac{4}{S_\alpha} \int_{S_\alpha} \int_{S_\beta} \frac{e^{-\tau^g((s_S)}}{4\pi s_S^2} (\hat{\Omega}\cdot\hat{N}_-)(\hat{\Omega}\cdot\hat{N}_+)\psi^\nu(\hat{\Omega},\hat{N}_+)\psi^\mu(\hat{\Omega},\hat{N}_+) dA_{S_\alpha} dA_{S_\beta} \tag{1.20}$$

et $Q_{j,g} = \Sigma_{g'} q_j^{g'\to g}$ est la source de neutrons dans le volume j et le groupe d'énergie g et représente la contribution de la fission et diffusion.

1.5.1 Forme Matricielle

Dans la notation matricielle, les équations 1.15 et 1.16 sont:

$$\vec{\phi} = \mathbf{P_{VS}}\vec{J}_- + \mathbf{P_{VV}}\vec{Q} \tag{1.21}$$

$$\vec{J}_+ = \mathbf{P_{SS}}\vec{J}_- + \mathbf{P_{SV}}\vec{Q} \tag{1.22}$$

où $\vec{J}_+$ and $\vec{J}_-$ sont les courants entrants et sortants. Le flux $\vec{\phi}$ est le vecteur de flux neutronique, et la source $\vec{Q} = (\Sigma_{g'} q_{j,g'\to g})$ est le vecteur source de neutrons dans la région j et dans le groupe d'énergie g.

La Forme Classique

La forme standard de l'équation de transport est le problème de la résolution des valeurs propres généralement écrit comme:

$$(\mathbf{A} - \lambda\mathbf{B})\cdot\vec{\phi} = 0 \tag{1.23}$$

où $\lambda = \frac{1}{k_{eff}}$ et $\mathbf{A}$ and $\mathbf{B}$ sont les opérateurs de l'équation de Boltzmann.

Dans la forme de l'opérateur, nous avons :

$$\vec{\phi} = \mathbf{P}(\mathbf{\Sigma})\,(\mathbf{S} + \lambda\mathbf{F})\,\vec{\phi} \tag{1.24}$$

où $\mathbf{\Sigma} = (\Sigma_g)_i$. On voit que:

$$\tag{1.25}$$

$$\mathbf{A} = \mathbf{I} - \mathbf{P}(\mathbf{\Sigma}) \cdot \mathbf{S} \tag{1.26}$$

$$\mathbf{B} = \mathbf{P}(\mathbf{\Sigma}) \cdot \mathbf{F} \tag{1.27}$$

où $\mathbf{I}$ est la $(N_V \cdot N_G)^2$ matrice identité.

1.6 L'Adjoint Intégral

Le formalisme adjoint est à la base de la méthode de la sensibilité de l'analyse d'incertitude. Pour chaque formulation de l'équation de transport, il existe un flux adjoint correspondant. L'équation adjointe correspondant à l'équation intégrale 1.24 s'écrit:

$$(\mathbf{A}^\dagger - \lambda \mathbf{B}^\dagger) \cdot \vec{\psi}^\dagger = 0 \text{ où} \tag{1.28}$$

$$\mathbf{A}^\dagger = \mathbf{I} - \mathbf{S}^\mathbf{T} \cdot \mathbf{P} \tag{1.29}$$

$$\mathbf{B}^\dagger = \mathbf{F}^\mathbf{T} \cdot \mathbf{P} \tag{1.30}$$

et l'opérateur $^\mathbf{T}$ est la transposition matricielle. $\psi^\dagger$ est également appelé la fonction de l'importance du flux neutronique et est interprétée comme le flux total de neutrons ajouté au réacteur critique à partir d'un flux d'unité de neutrons à la position $(\vec{r}, E)$.

1.7 La Théorie des Perturbations

Une théorie de perturbation formulée en utilisant la formulation intégrale de l'équation de transport présente un intérêt pour deux raisons [15] :

1. La première est la capacité de la formulation intégrale pour calculer des solutions précises dans les systèmes hétérogènes. Cette caractéristique, unique aux formulations intégrales, permet un calcul précis du coefficient de réactivité de petites perturbations insérées dans le coeur.

2. Les perturbations dans les opérateurs, apparaissant dans l'équation de transport intégrale (voir les équations 1.25 - 1.27), sont nonlinéaires par rapport aux perturbations dans les paramètres physiques

sous-jacents. On peut montrer que l'utilisation de la fonction adjoint, pour le système non-perturbé, est plus précise dans sa formulation intégrale de l'équation de transport que dans sa forme intégro-différentielle [26, 15].

1.7.1 Formules de perturbation

Supposons qu'une perturbation $q \to q + \delta q$ dans un paramètre se traduit par la perturbation dans les opérateurs $\mathbf{A}$, $\mathbf{B}$, λ et ϕ selon:

$$\mathbf{A} \to \mathbf{A_p} \equiv \mathbf{A} + \delta\mathbf{A} \tag{1.31}$$
$$\mathbf{B} \to \mathbf{B_p} \equiv \mathbf{B} + \delta\mathbf{B} \tag{1.32}$$
$$\phi \to \phi_p \equiv \phi + \delta\phi \tag{1.33}$$
$$\lambda \to \lambda_p \equiv \lambda + \delta\lambda \tag{1.34}$$

Les équations de Boltzmann pour le système de référence et le système perturbé sont:

$$\text{reference: } \mathbf{A} \cdot \phi = \lambda \mathbf{B} \cdot \phi \tag{1.35}$$
$$\text{perturbé: } \mathbf{A_p} \cdot \phi_p = \lambda_p \mathbf{B}_p \cdot \phi_p \tag{1.36}$$
$$\text{adjoint reference: } \mathbf{A}^\dagger \cdot \psi^\dagger = \lambda \mathbf{B}^\dagger \cdot \psi^\dagger \tag{1.37}$$

Après avoir développé l'équation 1.36, et en négligeant tous les termes d'ordre 2 et supérieurs et en soustrayant de l'équation 1.35, nous avons:

$$(\mathbf{A} - \lambda\mathbf{B}) \cdot \delta\phi + (\delta\mathbf{A} - \lambda\delta\mathbf{B}) \cdot \phi = \delta\lambda \mathbf{B} \cdot \phi \tag{1.38}$$

en utilisant le produit intérieur avec la fonction adjointe $\psi^\dagger$, on obtient:

$$\begin{aligned} \delta\lambda &= \frac{\cancelto{0}{\left\langle (\mathbf{A}^\dagger - \lambda\mathbf{B}^\dagger)\psi^\dagger, \delta\phi \right\rangle}}{\langle \psi^\dagger, \mathbf{B} \cdot \phi \rangle} + \frac{\left\langle \psi^\dagger, (\delta\mathbf{A} - \lambda\delta\mathbf{B}) \cdot \phi \right\rangle}{\langle \psi^\dagger, \mathbf{B} \cdot \phi \rangle} \\ &= \frac{\left\langle \psi^\dagger, (\delta\mathbf{A} - \lambda\delta\mathbf{B}) \cdot \phi \right\rangle}{\langle \psi^\dagger, \mathbf{B} \cdot \phi \rangle} \end{aligned} \tag{1.39}$$

L'équation 1.39 présente la perturbation dans la valeur propre λ en fonction des perturbations dans les opérateurs de l'équation de Boltzmann. Le calcul de la perturbation dans le λ nécessite le flux ϕ, l'adjoint $\psi^\dagger$ et les

perturbations dans les opérateurs $\delta\mathbf{A}$ et $\delta\mathbf{B}$. De cette façon, nous évitons la nécessité pour le calcul de la perturbation $\delta\phi$, qui autrement exigeraient une nouvelle solution de l'équation de transport pour chaque perturbation δq.

1.7.2 Calcul de $\delta\mathbf{A}$ et $\delta\mathbf{B}$

Les opérateurs $\mathbf{A}$ et $\mathbf{B}$ pour la formulation intégrale sont donnés par les équations 1.26 et 1.27:

$$\mathbf{A} = \mathbf{I} - \mathbf{P}(\mathbf{\Sigma})\cdot\mathbf{S} \tag{1.40}$$

$$\mathbf{B} = \mathbf{P}(\mathbf{\Sigma}) \cdot (\overrightarrow{\chi^T} \cdot \overrightarrow{\nu\Sigma_F}) \tag{1.41}$$

Pour utiliser l'équation 1.39 avec l'adjoint intégrante, $\psi^\dagger$ nécessite la connaissance des perturbations dans le opérateurs $\mathbf{A}$ et $\mathbf{B}$. Ces perturbations sont données par:

$$\delta\mathbf{A} = -(\delta\mathbf{P}\cdot\mathbf{S} + \mathbf{P}\cdot\delta\mathbf{S}) \tag{1.42}$$

$$\delta\mathbf{B} = (\delta\mathbf{P}\cdot\mathbf{F} + \mathbf{P}\cdot\delta\mathbf{F}) \tag{1.43}$$

Cependant, nous observons que les perturbations $\delta\mathbf{A}$ et $\delta\mathbf{B}$ dépendent de la perturbation $\delta\mathbf{P}$. Le calcul numérique de cette perturbation est difficile et intensif et n'a pas été considéré dans cette thèse. Une approximation introduite par Takahashi consiste à remplacer la perturbation dans la section totale apparaissant dans l'équation de Boltzmann par une source équivalente dans la section efficace de diffusion.

La forme intégro-différentielle de l'équation de transport est:

$$\left(\hat{\Omega}\cdot\nabla + \mathbf{\Sigma}\right)\phi(\vec{r},\hat{\Omega},E) = (\mathbf{S} + \lambda\mathbf{F})\cdot\phi(\vec{r},E) \tag{1.44}$$

et l'équation intégrale pour le flux est:

$$\vec{\phi} = \mathbf{P}(\mathbf{\Sigma})\cdot(\mathbf{S} + \lambda\mathbf{F})\cdot\vec{\phi} \tag{1.45}$$

maintenant, nous pouvons ajouter $\delta\mathbf{\Sigma}$ pour les deux côtés de l'équation

1.44. L'équation intégro-différentielle et l'équation intégrale sont:

$$\left(\hat{\Omega}\cdot\nabla+\mathbf{\Sigma}+\delta\mathbf{\Sigma}\right)\phi(\vec{r},\hat{\Omega},E)=(\mathbf{S}+\lambda\mathbf{F})\cdot\phi(\vec{r},E)+\delta\mathbf{\Sigma}\cdot\phi(\vec{r},\hat{\Omega},E) \tag{1.46}$$

$$\vec{\phi}(\vec{r},E)=\mathbf{P}(\mathbf{\Sigma}+\delta\mathbf{\Sigma})\cdot(\mathbf{S}+\lambda\mathbf{F})\,\phi(\vec{r},E)+\mathbf{P}(\mathbf{\Sigma})\cdot\delta\mathbf{\Sigma}\cdot\phi(\vec{r},E) \tag{1.47}$$

puisque nous avons ajouté l'opérateur $\delta\mathbf{\Sigma}$ des deux côtés de l'équation, nous voyons que le flux reste inchangé. Si le flux est isotrope, $\phi(\vec{r}\hat{\Omega},E)\simeq\frac{1}{4\pi}\phi(\vec{r},E)$, nous avons[34]:

$$\phi(\vec{r},E)\simeq\mathbf{P}(\mathbf{\Sigma}+\delta\mathbf{\Sigma})\cdot[\mathbf{S}+\lambda\mathbf{F}+\delta\mathbf{\Sigma}]\cdot\phi(\vec{r},E) \tag{1.48}$$

La substitution $\mathbf{P}(\mathbf{\Sigma}+\delta\mathbf{\Sigma})\simeq\mathbf{P}(\mathbf{\Sigma})+\delta\mathbf{P}$ dans 1.48 et, en ignorant le terme de second ordre $\delta\mathbf{P}\cdot\delta\mathbf{\Sigma}$, donne [34]:

$$-\mathbf{P}\cdot\delta\mathbf{\Sigma}\cdot\phi=\delta\mathbf{P}\cdot(\mathbf{S}+\lambda\mathbf{F})\cdot\phi \tag{1.49}$$

L'application à l'expression de perturbation, pour la valeur propre λ apparaissant dans l'équation 1.39, donne:

$$\delta\lambda=\frac{\left\langle\psi^{\dagger},(\delta\mathbf{A}-\lambda\delta\mathbf{B})\phi\right\rangle}{\langle\psi^{\dagger},\mathbf{B}\phi\rangle} \tag{1.50}$$

En substituant les équations 1.42 et 1.43 dans l'équation 1.50 et en utilisant l'approximation donnée par l'équation 1.49 pour $\delta\mathbf{P}\cdot(\mathbf{S}+\lambda\mathbf{F})$, nous avons:

$$\begin{aligned}\delta\lambda&=-\frac{\left\langle\psi^{\dagger},\{\mathbf{P}\cdot(\delta\mathbf{S}+\delta\mathbf{F})+\delta\mathbf{P}\cdot(\mathbf{F}+\mathbf{S})\}\cdot\phi\right\rangle}{\langle\psi^{\dagger},\mathbf{P}(\mathbf{\Sigma})\cdot\mathbf{F}\phi\rangle}\\&=-\frac{\left\langle\mathbf{P^{T}}(\mathbf{\Sigma})\cdot\psi^{\dagger},\{-\delta\mathbf{\Sigma}+\delta\mathbf{F}+\delta\mathbf{S}\}\cdot\phi\right\rangle}{\langle\mathbf{P^{T}}(\mathbf{\Sigma})\cdot\psi^{\dagger},\mathbf{F}\phi\rangle}\\&=\frac{\left\langle\phi^{\dagger},(\delta\mathbf{\Sigma}-\delta\mathbf{S}-\lambda\delta\mathbf{F})\phi\right\rangle}{\langle\phi^{\dagger},\mathbf{F}\phi\rangle}\end{aligned} \tag{1.51}$$

où $\phi^{\dagger}=\mathbf{P}\cdot\psi^{\dagger}$.

1.8 Fonctions de sensibilité

Dans la propagation des incertitudes des données nucléaires, une fonction de sensibilité est une transformation linéaire qui représente la variation relative du paramètre intégral R résultant d'un changement relatif dans les données nucléaires q. Ces fonctions de sensibilité constituent la base de l'approche de la sensibilité pour la propagation des incertitudes. La fonction de sensibilité peut être considérée comme la dérivée de premier ordre ou de la pente de la réponse R par rapport à un changement $\delta q/q$ en q:

$$S_R^q(\bar{\rho}) = \frac{\delta R}{R} / \frac{\delta q(\bar{\rho})}{q(\bar{\rho})} \tag{1.52}$$

où $\bar{\rho}$ est la variable de phase $(\bar{r}, E, \hat{\Omega})$. R est généralement une fonction du flux avec une dépendance non-linéaire sur q. Par conséquent, la fonction de sensibilité S_R^q (en % / %) représente la variation relative de R provenant de petits changements dans q.

1.8.1 Formules de sensibilité pour la réactivité

Dans le cas où le flux est isotrope, la substitution pour $\lambda = \frac{1}{k_{eff}}$ dans l'équation 1.51 donne:

$$\delta(\frac{1}{k_{eff}}) = \frac{\left\langle \phi^\dagger, (\delta\mathbf{\Sigma} - \delta\mathbf{S} - \frac{1}{k_{eff}}\delta\mathbf{F}) \cdot \phi \right\rangle}{\langle \phi^\dagger, \mathbf{F}\phi \rangle} \tag{1.53}$$

car $\delta(\frac{1}{k_{eff}}) = \frac{-\delta k_{eff}}{k_{eff}} \cdot \frac{1}{k_{eff}}$, on a:

$$\frac{\delta k_{eff}}{k_{eff}} = \frac{\left\langle \phi^\dagger, (k_{eff}\delta\mathbf{S} + \delta\mathbf{F} - k_{eff}\delta\mathbf{\Sigma}) \cdot \phi \right\rangle}{\langle \phi^\dagger, \mathbf{F}\phi \rangle} \tag{1.54}$$

en multipliant l'équation 1.54 par $q/\delta q$, on obtient la sensibilité $S_{k_{eff}}^q$, donnée par:

$$S_{keff}^q = \frac{q}{k_{eff}}\frac{\delta k_{eff}}{\delta q} = \frac{\left\langle \phi^\dagger, (\overbrace{qk_{eff}\delta_q\mathbf{S} + q\delta_q\mathbf{F}}^{\text{GAIN}} - \overbrace{qk_{eff}\delta_q\mathbf{\Sigma}}^{\text{LOSS}}) \cdot \phi \right\rangle}{\langle \phi^\dagger, \mathbf{F}\phi \rangle} \tag{1.55}$$

où $q \in \left\{\nu_g, \chi_g, \sigma_{(n,el),g}, \sigma_{(n,inel),g}, \sigma_{(n,f),g}, ...\right\}$ est un paramètre multi-groupe

et $\delta_q \equiv \frac{\partial}{\partial q}$.

1.9 La Propagation d'incertitudes

Les données nucléaires q sont accompagnées des incertitudes et corrélations fournies sous la forme d'une matrice de covariance $\mathbf{V}$, où $\mathbf{V}$ est en unité relative ($(\%)^2$). Nous pouvons donc propager les incertitudes des données de base pour calculer les incertitudes sur le paramètre R. Cela peut être fait par *la loi de propagation des erreurs*:

$$\left(\frac{\Delta R}{R}\right)^2 = \vec{S^T} \cdot \mathbf{V} \cdot \vec{S} = \sum_i \sum_j S_R^{q_i} V_{ij} S_R^{q_j} \tag{1.56}$$

où les sensibilités $S_R^{q_i}$ donnent la variation de la réponse R à une variation de la base de données nucléaires q_i. L'ensemble des coefficients de sensibilité, en fonction de la réaction nucléaire et de l'énergie, est désigné par le vecteur $\vec{S}$. Dans le cas où nous avons un vecteur de réponse R_i, les sensibilités sont exprimées sous forme d'une matrice avec des éléments S_{ij} donnés par [1]:

$$S_{ij} = S_{R_j}^{q_i} = \frac{q_i}{R_j} \frac{\partial R_j}{\partial q_i} \tag{1.57}$$

Chapter 2

Effets de la structure fine du flux

Habituellement, l'analyse de sensibilité et des incertitudes en physique des réacteurs commence par des calculs de transport de neutrons au niveau du groupe, avec une bibliothèque multi-groupe qui a été obtenue pour les hypothèses nécessaires et applicables au système. Cependant, une solution du flux peut être obtenue seulement après que les sections efficaces multi-groupes soient calculées. Cela se fait par le calcul d'autoprotection.

Le calcul d'autoprotection utilise les informations disponibles dans la bibliothèque multi-groupes pour réaliser les sections efficaces multi-groupes représentatives du système. Dans le cas où les méthodes d'équivalence sont utilisées, le calcul d'autoprotection utilise diverses simplifications pour arriver à un principe d'équivalence entre le ralentissement du neutron dans un milieu homogène infini et le ralentissement du flux dans une géométrie hétérogène [73, 21]. Les expressions pour la sensibilité sont ensuite calculées en fonction de ces sections efficaces. Elles représentent la variation en % de la réponse par rapport à une variation uniforme de 1 % de la section efficace autoprotégée.

Dans cette section, nous calculons la sensibilité du paramètre de groupe aux données nucléaires q. Cette sensibilité est appelée la sensibilité implicite [74, 75]. Pour calculer cette sensibilité implicite, nous allons d'abord discuter de la théorie de l'équivalence dans l'application de la cellule de Wigner. Nous présentons alors l'approche de Greenspan [15] pour calculer la perturbation dans le paramètre de groupe. Nous fournissons ensuite une expression analytique pour la perturbation dans le flux que nous utilisons

pour le calcul de la sensibilité implicite dans les géométries homogènes.

2.0.1 La Théorie d'équivalence

Les calculs d'autoprotection, qui utilisent la théorie d'équivalence [21, 73], commencent par les tableaux des sections efficaces en fonction de la température et un facteur de dilution σ_0. Le facteur de dilution σ_0 fournit une mesure de la capacité du modérateur à thermaliser les neutrons. La définition du facteur de dilution dépend des approximations spécifiques qui ont été utilisées pour générer le flux.
Si les résonances sont étroites, le facteur de dilution pour un milieu homogène avec un isotope de résonance est défini comme [19] :

$$\sigma_0 = \sum_{k \neq r} \frac{N_k}{N_r} \sigma_{p,k} \tag{2.1}$$

où N_k est la densité atomique de l'isotope non-résonnant avec la section efficace potentielle $\sigma_{p,k}$ et N_r est la densité atomique de l'isotope de résonance. Les paramètres de groupe sont générés en utilisant le flux de pondération correspondant au ralentissement des neutrons dans un milieu homogène infini composé de l'isotope de résonance et un modérateur. Si les résonances sont étroites, alors le flux dans le milieu homogène est défini comme [38, 19]:

$$\phi^{HOM}(E) = \frac{\sigma_{p,r} + \sigma_0}{\sigma_r(E) + \sigma_0} \frac{1}{E} \tag{2.2}$$

où σ_r et $\sigma_{p,r}$ sont les sections efficaces totale et potentielle de l'isotope avec résonance. L'équation 2.2 suppose que la section efficace de diffusion est dominée par la section efficace potentielle.
Dans les méthodes de la théorie d'équivalence, les expressions de flux, pour une géométrie hétérogène, impliquent souvent des combinaisons linéaires de flux homogène données par l'équation 2.2. Le but des méthodes d'équivalence dans les calculs d'autoprotection est alors de calculer un facteur de dilution σ_0 "meilleur" représentatif de la géométrie. Ce principe est bien illustré en utilisant l'exemple de la cellule de Wigner.

La Cellule de Wigner

On peut imaginer un système constitué de deux volumes, composé d'une région de combustible F immergée dans une région de modérateur M. Le

taux de collision total dans le combustible est donné comme [19, 20]:

$$\Sigma_F(E)\phi_F(E)V_F = P_{F\to F}(E)V_F\int_0^\infty dE'\Sigma_{s,F}(E'\to E)\phi_F(E') + P_{M\to F}(E)V_M\int_0^\infty dE'\Sigma_{s,M}(E'\to E)\phi_M(E') \quad (2.3)$$

où $\Sigma_F = \Sigma_r + \sum_{k\in F}\Sigma_k$ est la section efficace totale du combustible, Σ_r est la section efficace totale de l'isotope r, Σ_k est la section efficace totale de l'isotope $k \neq r$, $\phi_F(E)$ est le flux dans le combustible, V_F est le volume du combustible, $\sigma_{s,F}$ est la section efficace de diffusion du combustible, $\sigma_{s,M}$ est la section efficace de diffusion macroscopique du modérateur, et $P_{F\to F}$ et $P_{M\to F}$ sont les probabilités de collision.

En supposant que la diffusion n'est possible que par des collisions élastiques, les probabilités de transfert d'énergie peuvent être efficacement représentées par la forme $P(E'\to E) = \frac{1}{(1-\alpha_k)}\frac{1}{E}$. En intégrant sur les sections efficaces de diffusion, nous obtenons [19, 20]:

$$\Sigma_F(E)\phi_F(E)V_F = P_{F\to F}(E)V_F\sum_{k\in F}\int_E^{E/\alpha_k}\frac{N_k\sigma_{s,k}(E')\phi_F(E')}{(1-\alpha_k)E'}dE' + P_{M\to F}(E)V_M\sum_{i\in M}\int_E^{E/\alpha_i}\frac{N_k\sigma_{s,i}(E')\phi_M(E')}{(1-\alpha_i)E'}dE' \quad (2.4)$$

où l'indice $k \in F$ est l'isotope dans le combustible et l'indice $i \in M$ est l'isotope dans le modérateur, $\sigma_{s,k}$ et $\sigma_{s,i}$ sont les sections efficaces microscopiques de l'isotope k et i avec les densités N_k et N_i, $\alpha_k = \left(\frac{A_k-1}{1+A_k}\right)^2$, et A_k est le rapport entre le nombre de masse de l'isotope k à la masse de neutrons.

Si la largeur de résonance est petite, les neutrons qui tombent à l'intérieur de la région de résonance viennent de l'extérieur de la résonance où l'interaction est dominée par la section efficace potentielle. En dehors de la résonance, le flux $\phi(E)$ a la forme asymptotique $\frac{C}{E'}$ et la section efficace de diffusion de l'isotope de résonance est égale à la section efficace potentielle $\sigma_{r,p}$. Nous pouvons également supposer que la section efficace du modérateur est constante et dominée par la diffusion potentielle $\sigma_{s,k} = \sigma_{p,k}$. En ignorant la contribution du flux sous la résonance à l'intégrale de l'énergie de

l'équation 2.4, nous avons [19, 20] :

$$\frac{1}{1-\alpha_k}\int_E^{E/\alpha_k} N_k\sigma_{p,k}\phi(E')\frac{dE'}{E'} = N_k\sigma_{p,k}\frac{1}{E} \text{ for } k \neq r \tag{2.5}$$

$$\frac{1}{1-\alpha_k}\int_E^{E/\alpha_r} N_r\sigma_{s,k}(E')\phi(E')\frac{dE'}{E'} = N_k\sigma_{p,k}\frac{1}{E} \text{ for } \text{ for } k = r \tag{2.6}$$

Dans le cas où un seul isotope résonant est considéré, l'équation 2.4 se simplifie en [20]:

$$\Sigma_F(E)\phi_F(E)V_F = \frac{1}{E}\left(P_{F\to F}(E)V_F\Sigma_{p,F} + P_{M\to F}(E)V_M\Sigma_{p,M}\right) \tag{2.7}$$

où $\Sigma_{p,F} = N_r\sigma_{p,r} + \sum_{k\neq r} N_k\sigma_{p,k}$ est la section efficace potentielle du combustible et $\Sigma_{p,M} = \sum_{i\in M} N_i\sigma_{p,i}$ et la section efficace potentielle du modérateur.

Dans le cas où seulement deux régions sont considérées, la relation de réciprocité devient:

$$\frac{P_{M\to F}(E)}{V_F\Sigma_F(E)} = \frac{P_{F\to M}(E)}{V_M\Sigma_M} \tag{2.8}$$

En utilisant la loi de réciprocité ci-dessus, l'équation 2.7 se simplifie en [20]:

$$\phi_F(E) = \frac{1}{E}\left((1 - P_{F\to M}(E))\frac{\Sigma_{p,F}}{\Sigma_M(E)} + P_{F\to M}(E)\right) \tag{2.9}$$

L'équation 2.9 nécessite la connaissance de la probabilité $P_{F\to M}(E)$. Pour la cellule de Wigner, la probabilité $P_{F\to M}$ peut être exprimée comme [78, 20]:

$$\begin{aligned} P_{F\to M}(E) &= \frac{1}{\Sigma_F(E)\bar{l}}\int_0^\infty (1 - \exp(-\Sigma_F(E)l))\, dl \\ &= \frac{1}{\Sigma_F(E)\bar{l} + 1} \end{aligned} \tag{2.10}$$

où $\bar{l} = \frac{4V}{S}$ est la longueur de la corde moyenne dans le combustible de volume V et de surface S. En utilisant l'équation 2.9, le flux $\phi(E)$ se

simplifie en [20]:

$$\phi_F(E) = \frac{1}{E}\frac{\Sigma_{p,F} + 1/\bar{l}}{\Sigma_F(E) + 1/\bar{l}} \tag{2.11}$$

$$= \frac{1}{E}\frac{N_r\sigma_{p,r} + \sum_{k\neq r} N_k\sigma_{p,k} + \Sigma_e}{N_r\sigma_r(E) + \sum_{k\neq r} N_k\sigma_{p,k} + \Sigma_e} \tag{2.12}$$

$$= \frac{1}{E}\frac{\sigma_{p,r} + \overbrace{(\sigma_{0,F} + \Sigma_e/N_r)}^{\sigma_0}}{\sigma_r(E) + \underbrace{(\sigma_{0,F} + \Sigma_e/N_r)}_{\sigma_0}} \tag{2.13}$$

avec $\sigma_{0,F} = \sum_{k\neq r}\frac{N_k}{N_r}\sigma_{p,k}$ et la section efficace d'évasion $\Sigma_e = \frac{1}{\bar{l}}$ définie comme l'inverse de la moyenne longueur de la corde $\bar{l}$.

L'équation 2.13 est remarquablement similaire au flux donné par l'équation 2.2 pour un milieu homogène et infini avec le facteur de dilution $\sigma_0 = \sigma_{0,F} + \Sigma_e/N_R$. Lorsque la longueur moyenne $\bar{l}$ est petite (c'est-à-dire qu'il y a une grande section efficace d'évasion Σ_e), les neutrons du modérateur peuvent facilement atteindre un point à l'intérieur du combustible. Par conséquent, la dépression du flux est minimale.

La plupart des méthodes de l'équivalence représentent la probabilité $P_{F\to M}$ comme une somme d'expressions rationnelles telles que l'équation 2.10. Pour les géométries hétérogènes complexes, chaque formalisme utilise un certain nombre d'hypothèses concernant la forme du flux $\phi_F(E)$ pour arriver à une représentation pour la probabilité $P_{F\to M}(E)$ et la section efficace Σ_e similaires à l'équation 2.9.

Pendant le calcul de $P_{F\to M}(E)$, le choix pour les données nucléaires disponibles est limité aux données disponibles dans la bibliothèque. Ces données comprennent la section efficace potentielle $\sigma_{p,r}$, et la résonance intégrante définie par:

$$I = \frac{\sigma(T,\sigma_0)\sigma_0}{\sigma(T,\sigma_0) + \sigma_0} \tag{2.14}$$

La résonance intégrante I fournit une fonction croissante monotone (en fonction de la dilution) pour laquelle l'interpolation de la dilution et de la température peuvent être effectuées. Si la taille de la résonance est intermédiaire, un facteur $\lambda \in [0,1]$ est disponible [79, 80].

Le facteur λ fournit une mesure de la largeur de la résonance avec $\lambda = 0$ si la résonance est grande, et $\lambda = 1.0$ si la résonance est étroite. Une procédure itérative sur le facteur de dilution σ_0 est effectuée pour arriver à un ensemble des sections efficaces pour tous les isotopes de résonance qui sont présents dans le système.

2.1 L'approche de la dérivation des fonctions composées de Greenspan

Le paramètre multi-groupe $\left\langle \sigma_{x,I}^{HET} \right\rangle$ de l'isotope I pour la géométrie hétérogène peut être exprimé comme:

$$\left\langle \sigma_{x,I}^{HET} \right\rangle = f_x^I(\sigma_0, \sigma_x(E))\sigma_{x,I}^{\infty} \tag{2.15}$$

où $\sigma_{x,I}^{\infty}$ est le paramètre multi-groupe disponible dans la bibliothèque et généré en utilisant le spectre de pondération 1 $/E$. Le facteur f [74] représente l'effet du spectre de neutrons sur les paramètres multi-groupes.

Le changement $\left\langle \sigma_{x,I}^{HET} \right\rangle$, en raison d'un changement dans la donnée nucléaire q, est donné par:

$$\frac{\partial \left\langle \sigma_{x,I}^{HET} \right\rangle}{\partial q} = f_{x,I}\frac{\partial \sigma_{x,I}^{\infty}}{\partial q} + \sigma_{x,I}^{\infty}\frac{df_{x,I}}{dq} \tag{2.16}$$

Si $\left| f_x^I \frac{\partial \sigma_{x,I}^{\infty}}{\partial q} \right| >> \left| \sigma_{x,I}^{\infty} \frac{df_x^I}{dq} \right|$, alors les effets de la structure fine sont négligeables et peuvent être ignorés. Dans ce cas, il existe une relation linéaire entre la section efficace σ_x^{∞} et la section efficace autoprotégée $\left\langle \sigma_{x,I}^{HET} \right\rangle$. Toutefois, dans le cas où $\left| \sigma_{x,I}^{\infty} \frac{df_x^I}{dq} \right|$ n'est pas négligeable, la relation entre la section efficace autoprotégée et la donnée nucléaire q devient plus compliquée. En particulier, comme le facteur f_x^I dépend de tous les constituants de l'ensemble, nous avons [74]:

$$\frac{df_x^I}{dq} = \frac{\partial f_x^I}{\partial \sigma_x^I}\frac{\partial \sigma_x^I}{\partial q} + \sum_{J \neq I}\sum_y \frac{\partial f_x^I}{\partial \sigma_y^J}\frac{\partial \sigma_y^J}{\partial q} \tag{2.17}$$

où J porte sur tous les isotopes autres que I et toutes les réactions x.

Nous notons qu'un changement dans la donnée nucléaire q peut affecter de nombreux facteurs f.

La contribution à la variation résultant dans le paramètre de performance R d'une perturbation dans q peut se faire par différents canaux, y compris toutes les constantes multi-groupes. Par conséquent, $\frac{df}{dq}$ ne peut plus être négligeable. En tenant compte de la contribution possible de tous les canaux, nous arrivons à la forme typique de la sensibilité donnée par [74]:

$$S_{Rq} \equiv \frac{\delta R}{R} / \frac{\delta q}{q}$$

$$\sum_I \sum_x \overbrace{\left[\frac{\delta R}{R} / \frac{\delta \left\langle \sigma_{x,I}^{HET} \right\rangle}{\left\langle \sigma_{x,I}^{HET} \right\rangle}\right]}^{G_{R,x}^I} \overbrace{\left[\frac{\delta \left\langle \sigma_{x,I}^{HET} \right\rangle}{\left\langle \sigma_{x,I}^{HET} \right\rangle} / \frac{\delta q}{q}\right]}^{P_{x,q}^I} = \sum_I \sum_x G_{R,x}^I P_{x,q}^I \tag{2.18}$$

Ici, $G_{R,X}^I$ est le coefficient de sensibilité du R à la constante multi-groupe. C'est précisément ce qui est calculé dans les formules telles que l'équation 1.55 et est souvent désigné comme la sensibilité explicite, car elle ne tient pas compte de tout changement dans le flux. $P_{x,q}^I$ est le coefficient de sensibilité de la constante multi-groupe au paramètre de base q et peut être exprimé par l'équation 2.16, comme [74]:

$$P_{x,q}^I \equiv \frac{\delta \left\langle \sigma_{x,I}^{HET} \right\rangle}{\left\langle \sigma_{x,I}^{HET} \right\rangle} / \frac{\delta q}{q} = \overbrace{\left(f_x^I \frac{\delta \sigma_{x,I}^{\infty}}{\sigma_{x,I}^{HET}}\right) / \left(\frac{\delta q}{q}\right)}^{D_{x,q}^I} + \overbrace{\left(\frac{\delta f_x^I}{f_x^I}\right) / \left(\frac{\delta q}{q}\right)}^{Q_{x,q}^I} \tag{2.19}$$

$$= D_{x,q}^I + Q_{x,q}^I \tag{2.20}$$

où le premier terme $D_{x,q}^I$ compte pour le changement direct dans la section efficace multi-groupe en raison d'un changement dans la donnée nucléaire q. Le deuxième terme $Q_{x,q}^I$, appelé la sensibilité implicite, compte pour la perturbation dans le spectre et est prise en compte par le changement dans le f-facteur δf_x^I.

2.2 L'effet Implicite dans un milieu homogène

Dans un milieu homogène, en supposons que la taille de résonance est intermédiaire nous pouvons exprimer le flux en fonction d'un facteur de dilution σ_0, comme:

$$\phi(E,\sigma_0) = \frac{\lambda\sigma_{p,r} + \sigma_0}{\sigma_a(E) + \lambda\sigma_{s,r}(E) + \lambda\sigma_{p,r} + \sigma_0}\frac{1}{E} \tag{2.21}$$

où $\sigma_a(E)$ est la section efficace d'absorption de l'isotope de résonance et λ est le facteur de Golden-Cohenstein et prend en compte la taille de la résonance [79]. Etant donnée que la section efficace de diffusion est proportionnelle à la section efficace potentielle, une changement uniforme de ϵ % dans la section efficace de diffusion implique un changement de ϵ % dans la section efficace potentielle. On peut imaginer une variation uniforme de la section efficace de diffusion comme:

$$\sigma_{p,r} \to (1+\epsilon)\sigma_{p,r} \;\Rightarrow\; \sigma_{s,r}(E) \to (1+\epsilon)\sigma_{s,r}(E) \tag{2.22}$$

par le mérite de l'équation 2.21, le changement résultant dans le flux est donné par:

$$\begin{aligned}\phi' &= \frac{\lambda\sigma_{p,r} + \sigma_0(1+\epsilon)^{-1}}{(1+\epsilon)^{-1}\sigma_0 + \lambda_r\sigma_{s,r} + \lambda_r\sigma_{p,r} + \sigma_a(1+\epsilon)^{-1}}\frac{1}{E} \\ &\sim \phi(E,\sigma_0')\cdot(1 + \frac{\epsilon\sigma_a}{\sigma_a(E) + \lambda\sigma_{s,r}(E) + \lambda\sigma_{p,r} + \sigma_0'})\frac{1}{E}\end{aligned} \tag{2.23}$$

où $\sigma_0' \equiv (1+\epsilon)^{-1}\sigma_0$, et le valeur pour $I_{a,r}$ est disponible dans la bibliothèque multi-groupe en fonction du facteur de dilution $\sigma_b = \lambda\sigma_{p,r} + \sigma_0$.

Comme observé d'après l'équation 2.23, la perturbation dans le flux peut être prise en compte par interpolation par rapport au facteur de dilution perturbé défini comme suit:

$$\sigma_b' = \frac{\sigma_0}{1+\epsilon} + \lambda\sigma_{p,r} \tag{2.24}$$

Dans un milieu homogène, l'équation 2.21 donne une approximation analytique pour le flux. De même, l'équation 2.23 donne une expression analytique pour la perturbation dans le flux à cause d'une perturbation dans la section efficace potentielle $\sigma_{p,r}$.

De la même manière, une perturbation dans les sections efficaces d'un autre isotope $k \neq r$ dans le système peut être pris en compte en modifiant la section efficace de dilution. En supposant que la taille de la résonance est intermédiaire, le facteur de dilution peut être défini comme : $\sigma_{0,F} = \Sigma_{k \in m} \lambda_k \frac{N_k}{N_r} \sigma_{p,k}$. Par conséquent, une perturbation dans la section efficace de l'isotope $k \neq r$ perturbera la section efficace de dilution de l'isotope r comme:

$$\sigma_b^r \rightarrow \sigma_b^r + \lambda_k \frac{N_k}{N_r} \delta\sigma_{p,k} \tag{2.25}$$

Dans un milieu homogène, les équations 2.24 et 2.25 fournissent une estimation pour la perturbation dans les paramètres multi-groupes $\delta \left\langle \sigma_{x,I}^{HET} \right\rangle / \left\langle \sigma_{x,I}^{HET} \right\rangle$.

Exemple: Sphère de UF $_4$

Le tableau 2.1 présente les sensibilités implicites de la section efficace de diffusion calculées pour une sphère de 2 % enrichi UF_4, en utilisant trois méthodes de calcul différentes, ainsi que les résultats de référence obtenus par SCALE/TSUNAMI-1D. Les valeurs indiquées dans ce tableau représentent la contribution à la sensibilité du k_{eff} aux perturbations dans les sections efficaces multi-groupes résultantes de perturbations du flux.

La première colonne indique la sensibilité implicite calculée par l'approximation analytique présentée ci-dessus. La deuxième colonne indique la sensibilité implicite calculée à partir de l'exécution de 47 calculs d'autoprotection et de l'équation 2.18. Cette approche de calcul est possible pour les grands cas, comme le calcul d'autoprotection pour ces cas ne représente qu'une fraction du temps de calcul. Cette approche nécessite une solution de flux, une solution adjoint et 47 calculs d'autoprotection avec le code DRAGON.

La troisième colonne présente les sensibilités que nous avons obtenues à partir de simulations complètes en perturbant la section efficace et en effectuant un calcul de k_{eff}. Cette approche nécessite 47 simulations de DRAGON. On note la bonne entente entre les trois voies de calcul. Cependant, nos sensibilités implicites sont 22 % supérieures à celles obtenues par SCALE/TSUNAMI-3D.

La figure 2.1 présente une comparaison entre la sensibilité implicite calculée avec DRAGON en utilisant l'approximation analytique (courbe rouge), la sensibilité implicite calculée à l'aide du code DINASOUR (courbe en pointillé violet), et des sensibilités implicites calculées par SCALE6/TSUNAMI-1D (courbe bleue), et la sensibilité calculée à l'aide du SCALE6/TSUNAMI-

	Sensibilités Implicit (%/%)			
	DRAGON			SCALE
Isotope	ANALYTIC + **SNS:**	47 **SHI:** + **SNS:**	DIRECT 47 simulations	/TSUNAMI 1D[109]
^{238}U	$2.65 * 10^{-2}$	$2.55 * 10^{-2}$	$2.59 * 10^{-2}$	$2.16 * 10^{-2}$
^{1}H	$-2.99 * 10^{-2}$	$-2.95 * 10^{-2}$	$-2.94 * 10^{-2}$	$-3.01 * 10^{-2}$
^{19}F	$-4.21 * 10^{-3}$	$-4.22 * 10^{-3}$	$-4.27 * 10^{-3}$	$-3.67 * 10^{-3}$

Table 2.1: Sensibilités implicites pour la diffusion. Résultats SCALE/TSUANMI sont reproduites à partir du modèle fourni dans [109].

1D. Les sensibilités de DINASOUR ont été fournies par l'Université McMaster en utilisant notre modèle d'entrée. DINASOUR perturbe les paramètres multi-groupes dans la bibliothèque WIMS en supposant que les résonances sont étroites. On procède ensuite à un calcul de la sensibilité en effectuant des simulations directes de DRAGON en utilisant les bibliothèques WIMS perturbées.

Sur la figure 2.1, nous voyons que les plus grandes différences observées entre les profils de sensibilité sont dans les premières résonances. Les différences observées sont dues à l'approximation utilisée pour le flux ainsi que des différences dans le maillage de l'énergie utilisée par les codes. Les premières résonances du ^{238}U sont larges de sorte que la perte d'énergie des neutrons à partir de la collision élastique avec ^{238}U peut être efficacement ignorée (l'énergie des neutrons , après la collision reste sous la résonance). Une meilleure approximation dans cette gamme est que la résonance est large [20]. L'approximation analytique que nous avons utilisée (équation 2.21) est basée sur l'approximation que la résonance est intermédiaire (IRA), donc la section efficace de diffusion de l'isotope de résonance a une pondération inférieure que dans le cas où la résonance est étroite (équation 2.21). En conséquence, la sensibilité du k_{eff} à la section efficace de l'isotope lourd (dans ce cas ^{238}U) varie en fonction du formalisme spécifique utilisé.

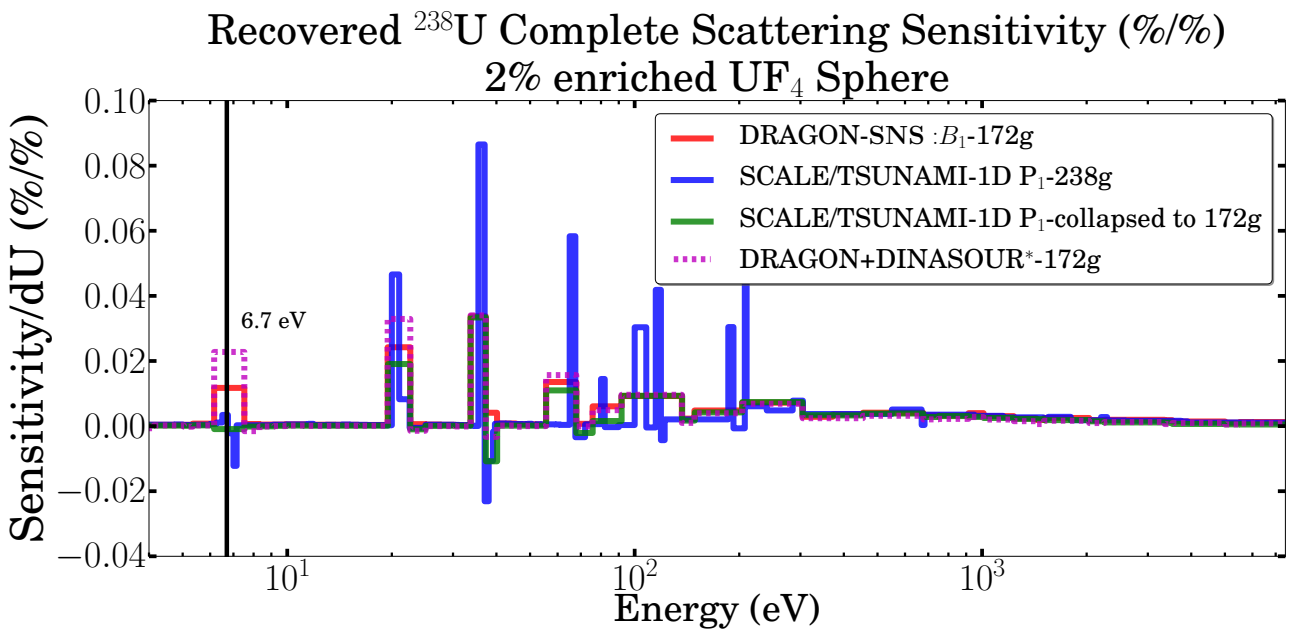

Figure 2.1: Comparaison de sensibilités implicites de ^{238}U(n,el) dans la région de résonance.

Pour les sensibilités implicites de diffusion présentées dans le tableau 2.18, la section efficace qui a la plus forte contribution à l'effet implicite est ^{238}U (n, γ). La sensibilité implicite de diffusion de l'^{238}U est positive comme une augmentation de la section efficace de diffusion de l'^{238}U augmente le nombre de neutrons qui diffusent hors de la résonance.

La sensibilité implicite pour l'autre isotope $k \neq^{238}$U est négative. Une augmentation dans les sections efficaces potentielles des isotopes $k \neq^{238}$U se traduit par une augmentation du facteur de dilution (l'isotope de résonance de l'^{238}U devient plus dilué). En conséquence, la dépression sous la résonance diminue (c'est-à-dire le flux se rapproche de la forme asymptotique $1/E$). Le résultat est une augmentation nette de la section efficace d'absorption multi-groupe de l'^{238}U, et donc une augmentation du taux d'absorption de l'^{238}U.

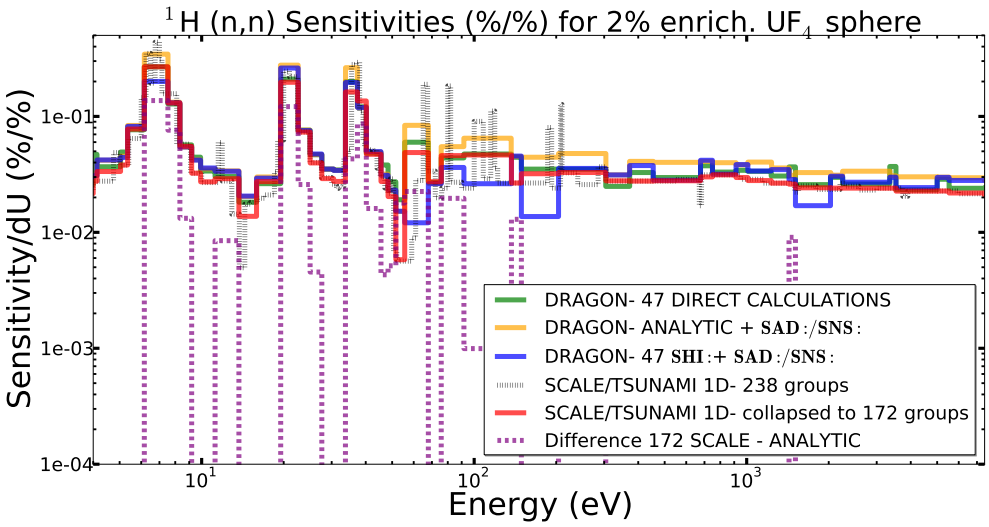

Figure 2.2: composante positive de la sensibilité implicite du k_{eff} pour l' ^{1} H(n,el) (en % / %).

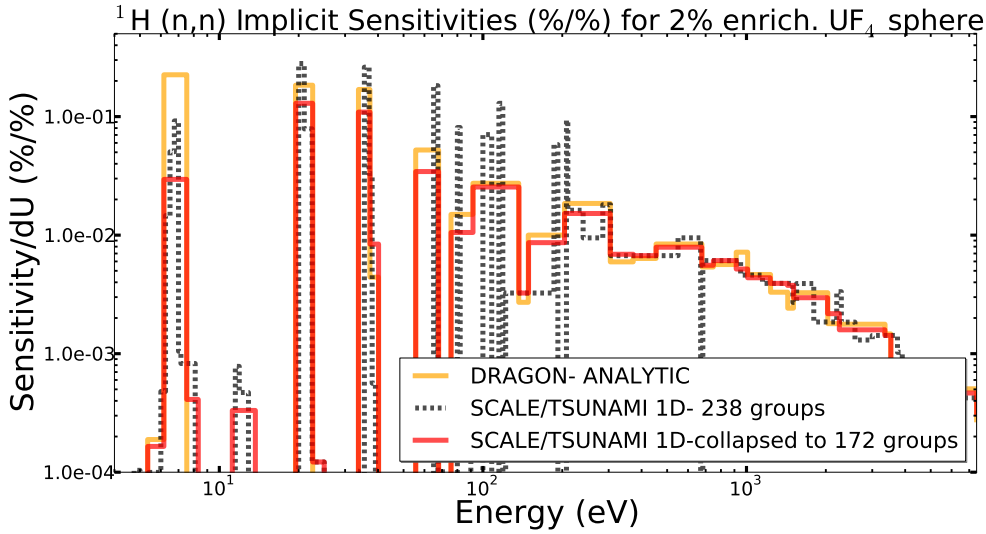

Figure 2.3: composante negatiff de la sensibilité implicite du k_{eff} pour l' ^{1} H(n,el) (en % / %).

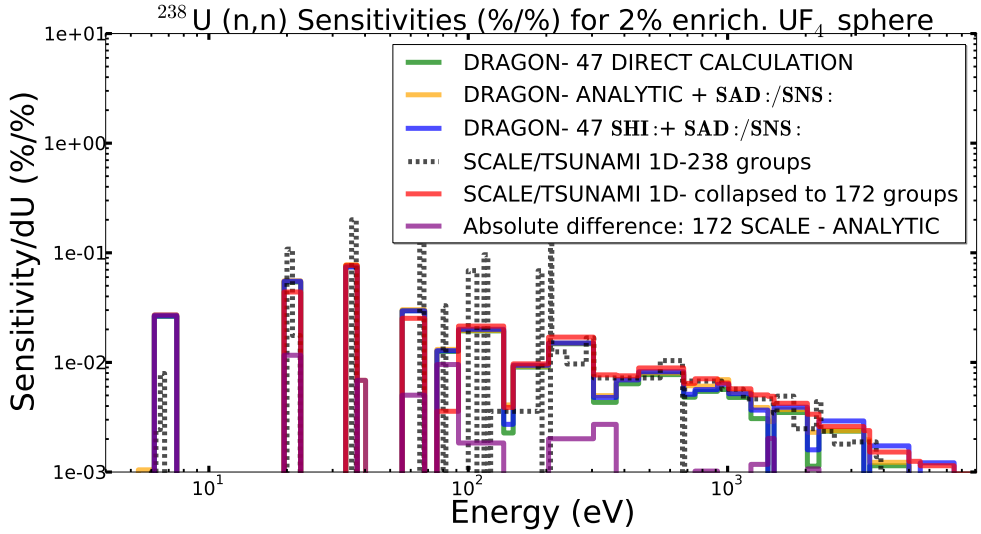

Figure 2.4: composante positive de la sensibilité du k_{eff} pour l'^{238}U U(n,el) dans la région de résonance (en % / %).

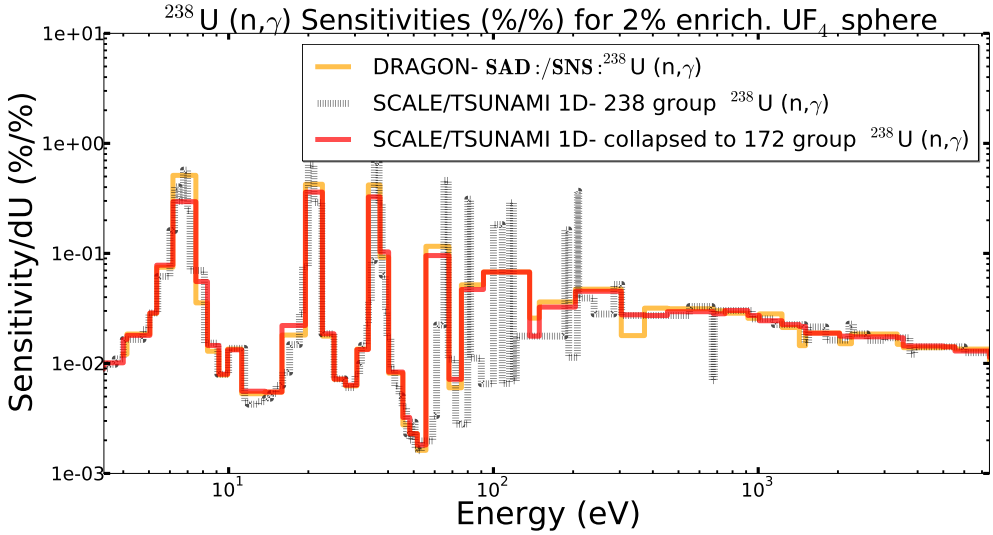

Figure 2.5: composante negatif de la sensibilité du k_{eff} pour l'^{238}U U(n,el) dans la région de résonance (en % / %).

Bibliography

[1] Smith, Donald L. *Probability, statistics, and data uncertainties in nuclear science and technology.* American Nucl. Soc., 1991.

[2] ENDF B/VI Format Manual

[3] WPEC Subgroup #38, " Requirements for a new nuclear data structure Part 1: Vision and Goals", OECD/NEA http://www.oecd-nea.org/science/wpec/sg38/

[4] Nuclear Energy Agency, Experimental Nuclear Reaction Data (EXFOR), http://www.nea.fr/html/dbdata/data/experimental.htm

[5] Kodeli, I., Trkov, A., Capote, R., Nagaya, Y., Maslov, V., "Evaluation of sensitivity coefficients of effective multiplication factor with respect to prompt fission neutron spectrum", *Nuclear Instruments and Methods in Physics Research* A 610 (2009) 540.

[6] Brassart, M., Mounier, C., Dossantos-Uzarralde, P., *Evaluation des matrices de variance-covariance des sections efficaces nucleaires issues du modele optique*, Rapport CEA-R-6042 (2004).

[7] Usachev, L. N. "Perturbation theory for the breeding ratio and for other number ratios pertaining to various reactor processes." *Journal of Nuclear Energy. Parts A/B. Reactor Science and Technology* 18.10 (1964): 571-583.

[8] Davison, Boris, and John Bradbury Sykes. *Neutron transport theory.* Oxford: Clarendon Press, 1957.

[9] Sanchez, R., and Norman J. McCormick. "Review of neutron transport approximations." *Nucl. Sci. Eng.;(United States)* 80.4 (1982).

[10] Ganapol, B. D. *Analytical Benchmarks for Nuclear Engineering Applications: Case Studies in Neutron Transport Theory.* Organisation for Economic Co-operation and Development (2008).

[11] Lewis, Elmer E., and Warren F. Miller Jr. *Computational Methods of Neutron Transport.* Wiley, New York, 1984

[12] Marleau, G. "DRAGON theory manual Part 1: Collision probability calculations." *Report IGE-236 Rev* 1 (2001).

[13] Courant, Richard, and David Hilbert. *Methods of mathematical physics.* Vol. 1. Wiley. com, 2008.

[14] Hebert, Alain. *Applied reactor physics.* Presses international Polytechnique, 2009.

[15] Greenspan, E. H. U. D. "Developments in perturbation theory." *Advances in Nuclear Science and Technology 9* (1976): 181-268.

[16] P. F. Zweifel, Reactor Physics, McGraw Hill Book Company, (1973)

[17] Case, Kenneth M., and Paul F. Zweifel. *Linear transport theory.* Vol. 196. Reading, Mass.: Addison-Wesley, 1967.

[18] Marchuk, Gurii Ivanovich. *Numerical methods for nuclear reactor calculations.* No. 3-4. Consultants Bureau, 1959.

[19] Dresner, Lawrence. *Resonance Absorption in Nuclear Reactors.*, Oak Ridge National Laboratory, 1959.

[20] D. Knott, A. Yamamoto, *Lattice Physics Copmputations* in Handbook of Nuclear Engineering, Vol. III, Springer,

[21] Herbert, A., and G. Marleau. "Generalization of the Stamm'ler method for the self-shielding of resonant isotopes in arbitrary geometries." *Nuclear Science and Engineering*;(United States) 108.3 (1991).

[22] Marleau, G., et al. "Computation of the DP1 collision probabilities for spherical and cylindrical geometries." *Annals of Nuclear Energy* 17.3 (1990): 119-134.

[23] Rudin, Walter. *Principles of Mathematical Analysis.* International Series in Pure& Applied Mathematics, McGraw Hill Book Company, (1976).

[24] Tanguy, Courau. *Application de la theorie des perturbations generalisees aux calculs de cellules utilisant la methode des probabilites de collision*, Thesis (Ph.D.), Ecole Polytechnique de Montreal, 2001.

[25] Lewins, Jeffery. *Importance: the adjoint function.* New York: Pergamon Press, 1965.

[26] McGrath, P. E., and W. K. Foell. Integral Transport Theory Analysis of Central Reactivity Worth Measurements., *Nuclear Science and Engineering* ; (United States) 45.3 (1971) pp. 237-244

[27] Khvedelidze, B.V. *Fredholm theorems for integral equations*, in Hazewinkel, Michiel, Encyclopedia of Mathematics, Springer, ISBN 978-1-55608-010-4, 2001.

[28] Weston Jr, M., ed. *Variational methods in nuclear reactor physics.* Vol. 10. Academic Press, 1974.

[29] Storrer, F., et al. "Heterogeneity calculation for fast reactors by a perturbation method." *Nuclear Science and Engineering* (US) 24 (1966).

[30] Gandini, A. "On the Standard Perturbation Theory." *Nuclear Science and Engineering*, v. 79.4 (1981) pp. 426-430

[31] Pomraning, G. C. "Variational principle for eigenvalue equations." *Journal of Mathematical Physics* 8 (1967): 149.

[32] Kier, P. H., and M. Salvatores. "Effect of local flux distortions on the Doppler effect of small fissile samples." *Nuclear Sciebce Engineering*, v. 53, no. 4, pp. 479-482 53.4 (1974).

[33] Takahashi, H. "Approximation for the Calculation of the Generalized First-Flight Collision Probability", *Nuclear Science and Engineering*, 26: 254-61 (1966). (1966).

[34] Courau, T., and G. Marleau. "Perturbation theory for lattice cell calculations." *Nuclear science and engineering* 143.1 (2003): 19-32.

[35] Courau, T., and G. Marleau. "Calculating Adjoint Fluxes in the Code DRAGON Using the Collision Probability Method." *PHYSOR-2000 International Topical Meeting, Advances in Reactor Physics and Mathematics and Computation into the Next Millennium*, Pittsburgh, PA. 2000.

[36] Courau, T., *Element de transport neutronique: Schema industriel applique aux calculs de reacteurs*, 2008. Cours ENSPG.

[37] I. Kodeli, "Multidimensional Deterministic Nuclear Data Sensitivity and Uncertainty Code System, Method and Application," *Nuclear Science and Engineering*, 2001(138), p. 45-66.

[38] IAEA, *WIMS-D library update : final report of a coordinated research project.* International Atomic Energy Agency, 2007

[39] MacFarlane, R. E., D. W. Muir, and R. M. Boicourt. *The NJOY nuclear data processing system: Volume 1, User's manual.* No. LA-9303-M-Vol. 1. Los Alamos National Lab., NM (USA), 1982.

[40] Chiba, G., *Incorporation of the ERRORJ code into the NJOY code system*

[41] Chiba, G., *ERRORJ Manual*, JNC TN95 20 2003-08, Sept. 2003.

[42] ZZ-SCALE6.0/COVA44G, "A 44-group cross section covariance matrix library retrieved from the scale-6.0 package," NEA Data Bank Code Package USCD 1236/03, 2011.

[43] I. Kodeli, "Manual for ANGELO2 and LAMBDA codes," NEA 1798/03 Package, 2010.

[44] Askew, J.R., Fayers, F. J. Kemshell, P. B., "A General Description of the Code WIMS", *Journal of British Nuclear Energy Society* 5 (1966).

[45] WIMS-D5, *OECD/NEA Data Bank Documentation*, Package ID No. 1507/02 (1998), http://www.nea.fr/html/dbprog/

[46] WIMS Library Update Project, http://www-nds.iaea.org/wimsd/downloads.htm

[47] E. Sartori, "Standard Energy Group Structures of Cross Section Libraries for Reactor Shielding, Reactor Cell and Fusion Neutronics Applications: VITAMIN-J, ECCO-33, ECCO-2000 and XMAS", JEF/DOC-315 Revision 3 - DRAFT (December 11, 1990).

[48] Oak Ridge National Laboratory. *SCALE: A Modular Code System for Performing Standardized Computer Anlyses for Licensing Evaluation,âĂİ ORNL/TM-2005/39, Version 5.1, Vols. I-III, November 2006.*

[49] Oak Ridge National Laboratory. *XSDRNPM: A One-Dimensional Discrete Ordinates Code for Transport Analysis,* ORNL/TM-2005/39, Version 5.1, Vols.II, Book 1, Sect. F3, November 2006.

[50] Oak Ridge National Laboratory. *NEWT: A New Transport Algorithm forTwo-Dimensional Discrete Ordinates Analysis in Non-Othrogonal Geometries,*ORNL/TM-2005/39, Version 5.1, Vols. II, Book 4, Sect. F21, November 2006.

[51] Oak Ridge National Laboratory.*TSUNAMI-1D: Control Module for One-Dimensional Cross-Section Sensitivity and Uncertainty Analysis for Criticality,*ORNL/TM-2005/39, Version 5.1, Vols. I, Book 2, Sect. C8, November 2006.

[52] Oak Ridge National Laboratory. *TSUNAMI-3D: Control Module for Three-Dimensional Cross Section Sensitivity and Uncertainty Analysis for Criticality,* ORNL/TM-2005/39, Version 5.1, Vols. I, Book 2, Sect. C9, November 2006.

[53] B. T. Rearden et al. *Advances in the TSUNAMI Sensitivity and Uncertainty Analysis Codes Beyond SCALE 5,* Oak Ridge National Laboratory manuscript, March 1, 2005.

[54] Ball, Matthew R., *Uncertainty Analysis In Lattice Reactor Physics Calculations* (2012). Open Access Dissertations and Theses. Paper 6565. http://digitalcommons.mcmaster.ca/opendissertations/6565

[55] Pusa, M., "Incorporating Sensitivity and Uncertainty Analysis to a Lattice Physics Code with Application to CASMO-4", *Annals of Nuclear Energy*, 40 (2012), pp. 153-162.

[56] Pusa, M., "Perturbation-theory-based Sensitivity and Uncertainty Analysis in CASMO-4", *Science and Technology of Nuclear Installations*, ID 157029, 2012.

[57] Oak Ridge National Laboratory. *SAMS: sensitivity analysis module in scale,* ORNL/TM-2005/39, Version 5.1, Vols. II, Book 4, Sect. F22, November 2006.

[58] "Scale 6.1 released!", *SCALE Newsletter (2011)*, No. 43, pp. 5

[59] G. Marleau, A. Hebert, R. Roy, *A User Guide for DRAGON 3.06*, Technical Report, IGE-174 Rev. 7, Institut de genie nucleaire, Ecole Polytechnique de Montreal. March, 2008.

[60] R. Roy, A. Hebert, *The GAN Generalized Driver*, Technical Report, IGE-158, Institut de Genie Nucleaire, Ecole Polytechnique de Montreal. March, 2000.

[61] Press, W. H., Flannery, B. P., Teukolsky, S. A., Vetterling, W. T., *Numerical Recipes in Fortran 77: The Art of Scientific Computing*, Cambridge University Press, 1992.

[62] Grasselli, M., Pelinovsky, D., *Numerical Mathematics*, Jones & Bartlett Publishers, 2007.

[63] Sabouri, P., and et. al., "Criticality Safety Assessment Using SUSD3D and DRAGON", *Proceedings of the 20th International Conference on Nuclear Energy for New Europe 2011*, Bovec, Slovenia (2011)

[64] K. Furuta, Y. Oka, S. Kondo, *SUSD: A Computer Code for Cross-Section Sensitivity and Uncertainty Analysis Including Secondary Neutron Energy and Angular Distributions*, Draft of UTNL-R0185 (English Translation, August 1986)

[65] Kodeli, I., *Developpement d'une methodologie pour les analyses de sensibilite et d'incertitude de donnees nucleaire utilisant la theorie des perturbations; application aux reacteurs a fission et a fusion*, HDR Thesis Dissertation, Universite Paris XI (2008).

[66] I. Kodeli, "The SUSD3D Code for Cross-Section Sensitivity and Uncertainty Analysis- Recent Developments", *Transactions of the American Nuclear Society*, Vol. **104**, Hollywood, Florida, June 26-30, 2011.

[67] I. Kodeli, L. Snoj, "Evaluation and Uncertainty Analysis of the Kritz-2 Critical Benchmark Experiments", *Nuclear Science and Engineering*, **171**, 231-238 (2012).

[68] W. A. Rhoades et al., DOORS3.2, *One-, Two-, Three-Dimensional Discrete Ordinates Neutron/Photon Transport Code,* CCC-650,RSICC, Oak Ridge National Laboratory, 1998

[69] R. E. Alcouffe et al., *DANTSYS3.0-A Diffusion Accelerated Neutron-Particle Transport System,* LA-12969-M, Los Alamos National Laboratory, 1995

[70] W. A. Rhoades, R. L. Childs, *TORT-DORT: Two- and Three-Dimensional Discrete Ordinates Transport,* Version 2.7.3, RSIC-CCC, ORNL RSIC, Oak Ridge, TN (1993)

[71] I. Kodeli, *SUSD3D, 1-, 2-, 3-Dimensional Cross Section Sensitivity and Uncertainty Code*, NEA-1628/03,(2008) packages.

[72] Lewins, Jeffery. "Time-dependent variational theory." *Nuclear Science and Engineering* 31 (1968): 160.

[73] M. Livolant, F. Jeanpierre, *Autoprotection des resonances dans les reacteurs nucleaires. Aplication aux isotopes lourds*, CEA-R-4533, Commissariat a l'Energie Atomique (1974)

[74] E. Greenspan, *Sensitvity functions for Uncertainty Analysis*, in Advances in Nuclear Science and Technology, Vol 14., Plenum Press, New York and London.

[75] M. L. Williams, "Eigenvalue Sensitivity theory for resonance-shielded cross sections," *Nuclear Science and Engineering* 2001(138), pp. 177-191

[76] Williams, Mark L. *Perturbation theory for nuclear reactor analysis.* CRC Handbook of Nuclear Reactors Calculations 3 (1986): 63-188.

[77] R. J. J. Stamm'ler and M. J. Abbate, *Methods of Steady State Reactor Physics in Nuclear Design,* Academic Press, London (1983)

[78] Weinberg A. M. , Wigner E. P., *The Physical Theory of Neutron Chain Reactors*, University of Chicago Press, Chicago, 1958.

[79] R. Goldstein, E. R. Cohen, "Theory of Resonance Absorption of Neutrons," *Nuclear Science and Engineering*, 1962(13), pp. 132-140

[80] Y. Ishiguro, H. Takano, "Intermediate Neutron Resonance Absorption with Interference Scattering in Heterogeneous Systems," *Journal of Nuclear Science and Technology*, 1969 (6), pp. 380-389

[81] Glasstone, S., Sesonske, A., *Nuclear Reactor Engineering.*, VN Nostrand Reinhold Company, New York (1963).

[82] A. Hebert, P. Benoist, "A consistent technique for the global homogenization of a pressurized water reactor assembly", *Nuclear Science and Engineering*, 1991 (109), 360-371.

[83] P. Benoist, I. Petrovic, "B_N Theory: Advances and New models for Neutron Leakage Calculations", *Advances in Nuclear Science and Technology*, Vol 24, 1996, Plenum Press, New York.

[84] Suraud, Eric. *Physique des collisions nucleaires.* Hermann, 1998.

[85] Noguere, G., and et. al., "Multi-group covariance matrices for the resolved resonance range of hafnium isotopes," *International Conference on Nuclear Data for Science and Technology*, France, April 22-27, Article 81, 2007.

[86] K. Shibata, O. Iwamoto, T. Nakagawa, N. Iwamoto, A. Ichihara, S. Kunieda, S. Chiba, K. Furutaka, N. Otuka, T. Ohsawa, T. Murata, H. Matsunobu, A. Zukeran, S. Kamada, and J. Katakura: "JENDL-4.0: A New Library for Nuclear Science and Engineering," *Journal of Nuclear Science and Technology*, 48(1), 1-30 (2011).

[87] WIMS9A, "NEW FEATURES", A guide to the New Features of WIMS Version 9A". Serco Assurance, http://www.sercoassurance.com/answers/, 2005

[88] *HELIOS Methods*, Studsvik Scanpower, 2000

[89] J. Rhodes and M. Edenius, *CASMO-4, A fuel Assembly Burnup Program, Users Manual*, 2001

[90] Sabouri, P., Dabiran, S., et. al., "Proposal for the Utilization of the Total Cross Section Covariances and its Correlations with Channel Reactions for Sensitivity and Uncertainty Analysis", *PHYSOR-2012 International Topical Meeting, Advances in Reactor Physics and Mathematics and Computation into the Next Millennium*, Knoxville, TN, USA (2012).

[91] MacFarlane, Robert E. *TRANSX 2: A code for interfacing MATXS cross-section libraries to nuclear transport codes.* Los Alamos National Laboratory, 1992.

[92] Roy, R. "Anisotropic scattering for integral transport codes. Part 2. Cyclic tracking and its application to *xy* lattices." *Annals of Nuclear Energy* 18.9 (1991): 511-524.

[93] IAEA1408/03, WLUP3.0 Package, Sept. 22, 2003

[94] Oak Ridge National Laboratory. *KENO V.a: an improved Monte Carlo criticality program,* ORNL/TM-2005/39, Version 5.1, Vols. II, Book 2, Sect. F11,November 2006.

[95] Marleau, G., Hebert, A., "Solving the multigroup transport equation using the power iteration method," in *Symposium on Reactor Dynamics and Plang Control*, Kingston, Ontario, 1985.

[96] NumPy Community, *NumPy Reference*, Release 1.9.0.dev-9464075, August 2013. http://docs.scipy.org/doc/numpy-dev/numpy-ref.pdf

[97] SciPy Community, *SciPy Reference Guide*, Release 0.13.0.dev-bf605c0, August 2013. http://docs.scipy.org/doc/scipy-dev/scipy-ref.pdf

[98] Hebert, A., Marleau, G., Roy, R., *A Description of the Data Structures for DRAGON 3.06*, IGE-232 Rev. 5, Institut de genie nucleaire, Ecole Polytechnique de Montreal. March, 2008.

[99] Marleau, G., Hebert, A., Roy, R., *A User Guide for DRAGON Version 4*, IGE-294, Institut de genie nucleaire, Ecole Polytechnique de Montreal, 2013.

[100] Toueg, B., *Modelisation des effets d'historique dans un reacteur a eau pressuriee*, Master's Dissertation, Institut de genie nucleaire, Ecole Polytechnique de Montreal, April 2011.

[101] Kloss, G. K., Authomatic C Library Wrapping-Ctypes from the Trenches, *The Python Papers*, Vol. 3, No. 3, 2008.

[102] Koning, Arjan J., Stephane Hilaire, and Marieke C. Duijvestijn. "TALYS: Comprehensive nuclear reaction modeling." *AIP Conference Proceedings.* Vol. 769. 2005.

[103] K. Ivanov, et. al., *Benchmark for Uncertainty Analysis in Modeling for Design, Operation, and Safety Analysis of LWRs, Volume I: Specification and Support Data for Neutronic Cases(Phase I)*, OECD Nuclear Energy Agency, Feb. 2011

[104] Yankov, A., and et. al., "Comparison of XSUSA and "Two-STEP" Approaches for Full-Core Uncertainty Quantification", *Proceedings of the PHYSOR 2012 International Conference*, Knoxville, USA (2012).

[105] Mandate for the OECD/NEA/NSC/WPNCS Expert Group on Uncertainty Analysis for Criticality Safety Assessment, http://www.oecd-nea.org/science/wpncs/UACSA/UACSAMandateII.pdf

[106] T. Ivanovna, "Benchmark Phase III for the Expert Group on Uncertainty Analysis for Criticality Safety Assessment: Computation of k_{eff} Sensitivity Coefficients to Neutron Data", available in http://www.oecd-nea.org/science/wpncs/UACSA/.

[107] Ivanova, T., et al. "OECD/NEA Expert Group on Uncertainty Analysis for Criticality Safety Assessment: Results of Benchmark on Sensitivity Calculation (Phase III)." *PHYSOR 2012 Advances in Reactor Physics* (2012).

[108] Bidaud, A., Marleau, G., "Nuclear Data Uncertainty Analysis using the coupling of DRAGON with SUSD3D", *Proceedings of Computational Methods & Reactor Physics (M& C 2009)*, American Nuclear Society, New York, 2009.

[109] Laville, C., *Etude de Differentes Methodes de Calculs de Coefficients de Sensibilites du K_{EFF} aux Donnees Nucleaires,* Masters Dissertation, Ecole Polytechnique de Montreal (2011)

[110] Dion, M., Marleau, G., "Resonance Self-Shielding Effects on Eigenvalue Sensitivity", *Proceedings in the M&C 2013 International Conference*, Sun Valley, Idaho, May 5-9, 2013.

[111] Briggs, J. Blair, Scott, L., Nouri, A., *The international criticality safety benchmark evaluation project.* Nuclear science and engineering 145.1 (2003): 1-10.

[112] Note DSU/SEC/T/2011-300 - Indice A - *Manuel utilisateur du code MORET 5.A.1*

[113] Bidaud, A., *Analyses de sensibilite et d'incertitude de donnees nucleaires. Contribution a la validation d'une methodologie utilisant la theorie des perturbations; application a un concept innovant: reacteur a sels fondus thorium a spectre epithermique.*, thesis dissertation, Universite Paris 11 (2005).

Abstract

This thesis presents a comprehensive study of sensitivity/uncertainty analysis for reactor performance parameters (e.g. the k_{eff}) to the base nuclear data from which they are computed. The analysis starts at the fundamental step, the Evaluated Nuclear Data File and the uncertainties inherently associated with the data they contain, available in the form of variance/covariance matrices. We show that when a methodical and consistent computation of sensitivity is performed, conventional deterministic formalisms can be sufficient to propagate nuclear data uncertainties with the level of accuracy obtained by the most advanced tools, such as state-of-the-art Monte Carlo codes. By applying our developed methodology to three exercises proposed by the OECD (UACSA Benchmarks), we provide insights of the underlying physical phenomena associated with the used formalisms.

Résumé

Dans cette thèse, nous présentons une étude rigoureuse des barres d'erreurs et des sensibilités de paramètres neutroniques (tels le k_{eff}) aux données nucléaires de base utilisées pour les calculer. Notre étude commence au niveau fondamental, i.e. les fichiers de données ENDF et leurs incertitudes, fournies sous la forme de matrices de variance/covariance, et leur traitement. Lorsqu'un calcul méthodique et consistant des sensibilités est consenti, nous montrons qu'une approche déterministe utilisant des formalismes bien connus est suffisante pour propager les incertitudes des bases de données avec un niveau de précision équivalent à celui des meilleurs outils disponibles sur le marché, comme les codes Monte-Carlo de référence. En appliquant notre méthodologie à trois exercices proposés par l'OCDE, dans le cadre des Benchmarks UACSA, nous donnons des informations, que nous espérons utiles, sur les processus physiques et les hypothèses sous-jacents aux formalismes déterministes utilisés dans cette étude.